# IDENTIFICATION AND CHARACTERIZATION OF MICRORNAS WHICH MODERATE NEUTROPHIL MIGRATION AND ACUTE INFLAMMATION

by

**Alan Yi-Hui Hsu**

**A Dissertation**

*Submitted to the Faculty of Purdue University*

*In Partial Fulfillment of the Requirements for the degree of*

**Doctor of Philosophy**


Department of Biological Sciences

West Lafayette, Indiana

August 2020

## THE PURDUE UNIVERSITY GRADUATE SCHOOL
## STATEMENT OF COMMITTEE APPROVAL

**Dr. Qing Deng, Chair**

Department of Biological Sciences, Purdue University

**Dr. Andrea Kasinski**

Department of Biological Sciences, Purdue University

**Dr. David Umulis**

Department of Agricultural & Biological Engineering, Purdue University

**Dr. Qing Jiang**

Department of Nutritional Science, Purdue University

**Dr. Jun Wan**

Department of Medical and Molecular Genetics, Indiana University

**Dr. Chang Kim**

Department of Pathology, University of Michigan

**Approved by:**

Dr. Janice P. Evans

*Dedicated to my mother; Wen-Jen Hsieh, my father; Eric Hsu, and my wife Jenny Kuo*

# TABLE OF CONTENTS

# LIST OF ABBREVIATIONS

| | |
|---|---|
| AGO | Argonaute |
| Akt | Protein kinase B |
| AO | Acridine Orange |
| ApH | Aphidicolin and hydoxyurea |
| ARG1 | Arginase 1 |
| CCL | CC Motif Chemokine Ligand |
| Cdca8 | Cell Division Cycle Associated 8 |
| Cdk | cyclin dependent kinase |
| CFU | colony stimulating factor |
| CHT | caudal hematopoietic tissue |
| CkII | Casein kinase II |
| CNS | central nervous system |
| CRISPR | Clustered Regularly Interspaced Short Palindromic Repeats |
| Cxcl | CXC Motif Chemokine Ligand |
| Cxcr | CXC Motif Chemokine Receptor |
| DAMP | damage associated molecular pattern |
| DEGs | differentially expressed genes |
| DMSO | Dimethyl sulfoxide |
| Dpf | days post fertilization |
| ef1a | Elongation factor 1alpha 1 |
| ESAM | endothelial cell selective adhesion molecule |
| ESL1 | E-selectin ligand 1 |
| fMLP | N-Formylmethionineleucylphenylalanine |
| Fpr1 | Formyl Peptide Receptor 1 |
| GCSF | granulocyte colony stimulating factor |
| GFP | green fluorescence protein |
| Got2 | GlutamicOxaloacetic Transaminase 2 |
| Gsk3b | Glycogen synthase kinase 3 beta |
| Hpi | hours post infection |
| ICAM | Intercellular Adhesion Molecule |
| IL | Interleukin |
| Inos | (inducible) Nitric oxide synthases |
| IV | intravenous |
| JAM | junctional adhesion molecule |
| kif14 | Kinesin Family Member 14 |
| Kpna | Karyopherin alpha |
| LAD | leukocyte adhesion deficiency |
| LFA1 | Lymphocyte functionassociated antigen 1 |
| LPS | Lipopolysaccharides |

| | |
|---|---|
| LTB4 | Leukotriene B4 |
| lyzC | Lysozyme C |
| Mac1 | Macrophage1 antigen |
| mcm5 | Minichromosome Maintenance Complex Component 5 |
| MCSF | macrophage colony stimulating factor |
| mfap4 | microfibril associated protein 4 |
| microRNA | miRNA (miR) |
| MIF | Macrophage Migration Inhibitory Factor |
| MMP | matrix metalloproteinase |
| Mpeg | The macrophage-expressed gene |
| MPO | myeloperoxidase |
| mpx | myeloperoxidase |
| mRNA | messenger RNA |
| NADPH | nicotinamide adenine dinucleotide phosphate |
| NE | Neutrophil elastase |
| NET | Neutrophil extracellular traps |
| NGAL | Neutrophil gelatinaseassociated lipocalin |
| PAK | Pseudomonas aeruginosa |
| PAK | p21 activating kinase |
| PAMP | Pathogenassociated molecular pattern |
| PBMC | Peripheral blood mononuclear cell |
| PBS | Phosphatebuffered saline |
| PECAM | Platelet endothelial cell adhesion molecule |
| PGK | Phosphoglycerate kinase |
| PI3K | Phosphoinositide 3kinases |
| PMA | Phorbol 12-myristate 13-acetate |
| PRR | Pattern recognition receptor |
| PSGL1 | Pselectin ligand 1 |
| qRTPCR | Quantitative real time polymerase chain reaction |
| RAC2 | Rac Family Small GTPase 2 |
| RFP | Red fluorescence protein |
| ROS | Reaction oxygen species |
| RRE | Rev response element |
| RTPCR | Reverse transcription polymerase chain reaction |
| Shp2 | Src homology region 2 (SH2)containing protein tyrosine phosphatase 2 |
| shRNA | Small hairpin RNA |
| Stat3 | Signal Transducer and Activator Of Transcription 3 |
| SV40 | Simian virus 40 |
| Tet | Tetracyclinecontrolled transcription |
| TGFβ | Transforming growth factor beta |
| TLR | Toll Like Receptor |
| TNFα | Tumor necrosis factor alpha |
| Tunel | Terminal deoxynucleotidyl transferasemediated dUTPbiotin Nick End Labeling |

| | |
|---|---|
| UtrCH | Utrophin |
| UTR | Untranslated region |
| WHIM | Warts; hypogammaglobulinemia infections; myelokathexis |
| WPRE | Woodchuck Hepatitis Virus (WHP) Posttranscriptional Regulatory Element |
| YFP | Yellow fluorescence protein |

# LIST OF FIGURES

# ABSTRACT

Neutrophils are the first cells recruited to an immune stimulus stemming from infection or sterile injuries via a mixture of chemoattractant cues. In addition to eliminating pathogens, neutrophils coordinate the overall inflammation by activating and producing inflammatory signals in the tissue while modulating the activation of other immune cells which in some cases leads to adverse tissue damage. Over amplified or chronic neutrophil recruitment directly leads to autoimmune diseases including rheumatic arthritis, diabetes, neurodegenerative diseases, and cancer. Dampening neutrophil recruitment is a strategy to intervene in neutrophil-orchestrated chronic inflammation. Despite intensive research over the past several decades, clinical studies targeting neutrophil migration have been largely unsuccessful, possibly due to the prominent redundancy of adhesion receptors and chemokines. Additional challenges lie in the balance of dampening detrimental inflammation while preserving immunity. Neutrophils are terminally differentiated cells that are hard to study in cell culture. Mouse models are often used to study hematopoiesis, migration, and chemotaxis of neutrophils but is very labor intensive. To discover novel therapeutic targets that modulate neutrophil migration, we performed a neutrophil-specific microRNA (miRNA) overexpression screen in zebrafish and identified eight miRNAs as potent suppressors of neutrophil migration. We have generated transgenic zebrafish lines that overexpresses these candidate miRNAs where we recapitulated the mitigation in neutrophil motility and chemotaxis to tissue injury or infection. Among those we further characterized two miRNAs which have not been reported to regulate neutrophil migration, namely miR-722 and miR-199.

MiR-722 downregulates the transcript level of *rac2* through binding to the *rac2* 3'UTR. Furthermore, miR-722-overexpressing larvae display improved outcomes in both sterile and bacterial systemic models, which correlates with a robust upregulation of the anti-inflammatory cytokines in the whole larvae and isolated neutrophils. miR-722 protects zebrafish from lethal lipopolysaccharide challenge. In addition, overexpression of mir-722 reduced chemotaxis of human neutrophil like cells, indicating that miR-722 is a potential agent to reduce inflammation in humans.

MiR-199, decreases neutrophil chemotaxis in zebrafish and human neutrophil-like cells. Intriguingly, in terminally differentiated neutrophils, miR-199 alters the cell cycle-related pathways and directly suppresses cyclin-dependent kinase 2 (*cdk2*), whose known activity is restricted to cell cycle progression and cell differentiation. Inhibiting Cdk2, but not DNA replication, disrupts cell polarity and chemotaxis of zebrafish neutrophils without inducing cell death. Human neutrophil-like cells deficient in CDK2 fail to polarize and display altered signaling downstream of the formyl peptide receptor. Chemotaxis of primary human neutrophils is also reduced upon CDK2 inhibition. Furthermore, miR-199 overexpression or CDK2 inhibition significantly improves the outcome of lethal systemic inflammation challenges in zebrafish.

In summary, our results reveal previously unknown functions of these miRNAs, and provide potential avenues to modulate neutrophil migration as well as lead to discoveries of novel factors which can regulate this process. We have also discovered a non-classical role of CDK2 in regulating neutrophil migration which provides directions for alleviating systemic inflammation and a better understanding of neutrophil biology.

# CHAPTER 1. INTRODUCTION

## 1.1 Neutrophils

The innate immune system is comprised of many cell types that maintain immune homeostasis and pathogen clearance along with many other functions. Neutrophils comprise 40%~70% of white blood cells in human circulation (C. Rosales, 2018). The majority of neutrophils and their progenitor cells are stored in the bone marrow where they terminally differentiate, exiting the cell cycle and acquiring the signature of segmented nucleus and large contents of granules (Amulic, Cazalet, Hayes, Metzler, & Zychlinsky, 2012). Neutrophils are retained in the bone marrow by binding of their receptor CXCR4 to the C-X-C-motif chemokine ligand 12 (CXCL12) in the microenvironment. Under inflammatory conditions, neutrophils switch from a CXCR4 to CXCR2 dominate expression. CXCR2, along with CD62L, facilitates neutrophil mobilization out of the bone marrow into circulation in response to immunological cues such as G-CSF, CXCL1/2, or other chemotactic signals (Eash, Greenbaum, Gopalan, & Link, 2010).

Neutrophils directly interact with pathogens and cause inflammation. They are terminally differentiated and reside in the G0 phase of the cell cycle and no longer proliferate or undergo self-expansion. Starting from granulopoiesis, which is the formation of granules and maturation, neutrophils have a limited life span in circulation (<48 hours) (Stoller, 2015). Due to the short life span of terminally differentiated neutrophils, the human body produces on average 100 billion new neutrophils every day to maintain their population (Dancey, Deubelbeiss, Harker, & Finch, 1976). This number can be further increased during inflammation via emergency hematopoiesis (Manz & Boettcher, 2014) to rapidly increase effector neutrophil numbers in blood. To have our body invest so much resources to maintain this neutrophil population showcases the importance of these cells to human health.

After performing immunological functions in the designated tissue or reaching the end of their life span in circulation, neutrophils may either undergo apoptosis and clearance by resident macrophages (efferocytosis) where macrophages then secrete anti-inflammatory signals to dampen further inflammation (Kennedy & DeLeo, 2009). Or neutrophils may also undergo reverse transendothelial migration (Yoo & Huttenlocher, 2011) to migrate back into the

circulation and travel to the liver, where they are processed by macrophage efferocytosis mediated by liver X receptor (LXR) signaling (Hong et al., 2012; N et al., 2009).

Over amplified neutrophilic inflammation is a main driver of the immunopathology underlying a broad range of human diseases, exerting direct effects such as in rheumatic arthritis, and indirect effects observed in diabetes, neurodegenerative diseases, and cancer (Borregaard, 2010; Nathan, 2006). Failing to clear dying or inflammatory neutrophils could lead to chronic inflammation and autoimmune disorders, including cystic fibrosis, atherosclerosis, chronic obstructive pulmonary disease, and rheumatoid arthritis (Amulic et al., 2012). Hence, neutrophil homeostasis and inflammation as well as infiltration and clearance need to be tightly regulated to avoid inflammatory diseases while maintaining immune functions. Striking the balance between neutrophil protection and pathological properties is a difficult balance as introduced below, the same functions which protect humans if left unchecked, may lead to undesirable outcomes and lead to diseases. Current drugs such as corticosteroids and the microtubule destabilization agent colchicine have been used to dampen neutrophilic inflammation but lack neutrophil specificity, and induces adverse side effects (Cocco, Chu, & Pandolfi, 2010). Thus, it is a priority to develop a better understanding of neutrophil signaling in migration and inflammation which will instruct the development of next-generation therapeutics for inflammatory-related diseases.

## 1.2 Neutrophil migration and recruitment

Neutrophils in circulation or migrating out of the bone marrow can rapidly infiltrate into inflamed tissue in response to pathogen infection or sterile tissue inflammation. This process is facilitated by pathogen-associated molecular pattern (PAMP) and damage-associated molecular pattern (DAMP) molecules. These molecules bind to receptors on the neutrophil surface pattern recognition receptor (PRR) to allow the neutrophils to migrate toward this gradient and infiltrate the destination tissue, but there have been reports of other host or pathogen signals which can directly recruit neutrophils as well (M. R. Williams, Azcutia, Newton, Alcaide, & Luscinskas, 2011b; Zeytun, Chaudhary, Pardington, Cary, & Gupta, 2010).

In order to arrive into the inflamed tissue, neutrophils must cross the endothelium layer of the vasculature. This infiltration is a sequential process of rolling on the vessel endothelium, firm

adhesion, followed by trans-endothelial migration through the vessel wall or junction (M. R. Williams et al., 2011b). Inflammatory mediators produced in response to infection or inflammation can activate the endothelial cells, upregulating the expression of E/P-selectin on their surfaces to facilitate binding by neutrophil PSGL-1 (P-selectin ligand 1), L-selectin, and ESL-1 (E-selectin ligand 1) which are expressed constitutively on the neutrophil surface (Bruehl et al., 1997; Steegmaier, Borges, Berger, Schwarz, & Vestweber, 1997). This moderate binding serves to slow down the neutrophils in circulation and cause this "rolling" phenomena. Even though the selectin associated binding is not stable and turn-over is fairly quick, it is sufficient to mediate the attachment of neutrophils to endothelial cells in the bloodstream with shear stress (Pospieszalska & Ley, 2009).

The firm adhesion of neutrophils to endothelial cells is mainly mediated by integrins and their respective ligands. β2 integrins LFA-1 and Mac-1 expressed by neutrophils bind to their ligands, ICAM-1and ICAM-2 on the surface of the activated endothelial cells (Bunting, Harris, McIntyre, Prescott, & Zimmerman, 2002). The selectin-mediated rolling triggers the conformation change of LFA-1 to an active form, and thus, has higher affinity binding to ICAM-1 (Kuwano, Spelten, Zhang, Ley, & Zarbock, 2010). Full activation of LFA-1 results in firm adhesion and requires an additional engagement of chemokine signaling in neutrophils to achieve stationary binding (Zarbock, Deem, Burcin, & Ley, 2007).

Neutrophils migrate through endothelial cells via paracellular routes between cells or transcellular routes where they need to cross an endothelial cell body after firmly attaching to the endothelium. This transmigration process is also facilitated by β2 integrins. Paracellular migration also requires endothelial junction and adhesion molecules including JAM (junctional adhesion molecule), PECAM (platelet endothelial cell adhesion molecule), ESAM (endothelial cell-selective adhesion molecule), CD99, and VE-Cadherin (Allingham, van Buul, & Burridge, 2007; van Buul, Anthony, Fernandez-Borja, Burridge, & Hordijk, 2005; Woodfin et al., 2009) to modify the junctions and allow efficient and easy passage of neutrophils to the target tissue. Though paracellular migration is usually the dominant method, there are some scenarios such as bacterial infection in the CNS which would lead to a transcellular dominant recruitment (Wewer et al., 2011) where the endothelial cell would directly uptake the neutrophil into a vesicle like

structure and traffic it through its cell body via a phagocytosis/exocytosis method (Phillipson, Kaur, Colarusso, Ballantyne, & Kubes, 2008).

After crossing the endothelial layer, neutrophils secrete proteases and matrix metalloproteinase (MMP-8, MMP-9) to break down the extracellular matrix consisting mainly of collagens and laminins. This allows the neutrophils to migrate though the dense extracellular space towards the site of inflammation and follow chemotactic cues which can be of host or pathogen (Kang et al., 2001).

### 1.3 Neutrophil function

After infiltrating the inflamed tissue, neutrophils can perform an array of functions to help contain and limit the infection besides mediating other immune cell recruitment and inflammation. The most predominant function of neutrophils is to directly take up the damaged cells or pathogens though phagocytosis. This is predominantly mediated by the PAMP/DAMP and PRR interactions, where the engulfed cargo is then fused with internal granules or lysosomes and is degraded or killed (Amulic et al., 2012; C. Rosales, 2018).

Neutrophils can secrete a number of cytokines and granules to signal other immune cells or directly work on the microbes. Reaction oxygen species (ROS) can be generated inside the phagosome or secreted extracellularly to directly work on the pathogen while other secreted effectors are mostly packaged inside granules storing volatile effectors possessing anti-microbial capabilities. Neutrophil granules can be categorized into three types; primary, secondary, and tertiary. Primary granules (azurophilic granules) are the largest and first granules to be formed and secreted. They possess specific anti-microbial cargos such as myeloperoxidase (MPO), neutrophil elastase (NE) and other proteins including defensins, lysozyme, and serine proteases (elastase, proteinase 3 and cathepsin G) (Lacy, 2005; Nusse & Lindau, 1988). Secondary granules (or specific granules) are generated and released after primary granules. They are smaller and contain the glycoprotein lactoferrin and other antimicrobial compounds such as NGAL (Faurschou & Borregaard, 2003). Finally, tertiary granules (gelatinase granules) contain proteases such as MMP-9 heparanase, gelatinase, and ARG-1. When neutrophils are activated, granules are able to mobilize and fuse with engulfed phagosomes or exocytose through the

plasma membrane, releasing their compounds into the target tissue resulting in an anti-microbial environment for invading microbes (Borregaard, 2010). However the overactivation and production of granule release "pouring" into the tissue may lead to tissue damage and over inflammation (Potera et al., 2016; J. Wang, 2018).

Besides being the first cells to respond to inflammatory cues by rapidly migrating to the inflamed tissue where they perform the aforementioned functions, neutrophils can also secrete cytokines to recruit other immune cells to induce a more complete immune response. Neutrophils reinforce the immune response by secreting IL-8 to recruit other neutrophils (Scapini et al., 2000) where this recruitment is complemented by a following wave of LTB4 signaling after initial chemotactic signaling where neutrophils can "swarm" - recruitment to a cluster of preexisting neutrophils - to further enhance recruitment robustness (Afonso et al., 2012). Neutrophils can secrete other acute phase pro inflammatory cytokines such as IL-1β and TNF-α to positively feedback and enhance the inflammation response (Sica et al., 1990). Neutrophils can also express chemoattractants including CCL2, CCL3, CCL20, and CCL19 to recruit circulating monocytes (Scapini et al., 2001; Yoshimura & Takahashi, 2007) and activate dendritic cells via CCL3 signaling (Peters et al., 2008). Neutrophils can also bridge the adaptive immune system and assist in lymphocyte priming by secreting IL-12 to aid in T cell differentiation and expansion (Romani et al., 1997) while serving as antigen presenting cells to facilitate T cell clonal expansion (Abdallah, Egan, Butcher, & Denkers, 2011; R. E. Davis, Sharma, Chen, Sundar, & Wilson, 2017). During an acute strong inflammatory signal, too much proinflammatory cytokines might be produced leading to immune hyper-activation termed cytokine storm, which could lead to mass immune cell infiltration, tissue damage, and hypoxia in the micro or organelle level, resulting in disease and pathologies (Bordon et al., 2013; Q. Yang, Ghose, & Ismail, 2013).

Neutrophils have a wide arsenal to combat microbes and facilitate inflammation, but there is one function that is truly unique - neutrophil extracellular traps (NETs). The formation of NETs occurs when neutrophils release their de-condensed chromatin content mixed with anti-microbial agents also found in the granules such as MPO or NE which are also found in the granules in the extracellular space as a fibrous structure that traps and contains the microbes in the surrounding

environment (Fuchs et al., 2007; Urban et al., 2009). This has been an extensive topic of research in recent years as it has been shown that neutrophils can release bits of their chromosomes into NETs while maintaining other cellular functions, this is referred to as vital NETosis (Yipp et al., 2012) in contrast to when the neutrophils release all of their DNA content in suicidal NETosis, though the regulation between the two are not yet clear (de Buhr & von Kockritz-Blickwede, 2016; Jorch & Kubes, 2017). During NETosis the intracellular DNA content along with many ROS producing enzymes are released into the extracellular space, leading to massive inflammation along with the intended original anti-microbial function, which has been shown to lead to extensive tissue damage, and the DNA content may lead to autoimmune pathologies (Gupta & Kaplan, 2016; Lightfoot & Kaplan, 2017; Nakazawa et al., 2017; O'Brien, Biron, & Reichner, 2017).

## 1.4 MicroRNAs in neutrophils

MicroRNAs (miRs) are short (20-22 nucleotides) evolutionary conserved non-coding RNAs which act on their target messenger RNAs (mRNAs) and post-transcriptionally regulate protein synthesis by inhibiting mRNA transcription or marking the mRNA for degradation. (Gurol, Zhou, & Deng, 2016; Winter, Jung, Keller, Gregory, & Diederichs, 2009). Target selectivity is determined by nucleotides 2-8 of the miR sequence termed the “seed sequence” which binds to the 3’ UTR of the mRNA transcript with full or partial complementary. MiR genes, similar to other protein coding genes, are transcriptionally regulated by specific promoters. Once transcribed, the classical miRNA biogenesis pathway includes having the MiR transcribed in the nucleus by RNA polymerase II and cleaved into primary-miR hairpin, followed by processing by Drosha in to pre-miRNA and subsequently exported outside of the nucleus into the cytosol. It is there where the pre-miRNA hairpin terminal loop is cleaved into a mature duplex by Dicer and one miR strand (the mature guide strand miRNA) would be loaded into Argonaute (AGO) proteins where the passenger strand is degraded. This protein along with RISC can target completely or partially complementary mRNA targets (Ha & Kim, 2014) to science the target mRNA through translational repression, mRNA destabilization, or cleavage. As of 2018, more than 2,600 miRs have been identified in humans, where miRs have been implicated in and observed to moderate wide varieties of cellular processes. MiRs fine-tune gene expression and can target many different genes simultaneously resulting in a profound impact on biological

systems. MiRs have been reported to be involved in virtually all biological functions, hence identifying or regulating miRNAs could be a feasible strategy for treating associated diseases or to unveil new methods of fine tuning biological processes (Vidigal & Ventura, 2015).

Recently miRs and anti-miRs have been utilized as strategies to treat human diseases such as ALS, HCV infection, and cancer (Broderick & Zamore, 2011; Christopher et al., 2016). A comprehensive list of miRs expressed in neutrophils has been obtained by cloning (Gantier, 2013) and microarray (Larsen et al., 2013) techniques, but how these miRs interplay in regulating inflammation in neutrophils is still mostly unknown, with the except ion of miR-223 (Johnnidis et al., 2008) and miR-142 (Fan et al., 2014a). With this, it would be an attractive strategy to supplement neutrophils with miRs as therapeutics (Reid et al., 2016) to assess how they might regulate neutrophilic inflammation and possibly be used as a strategy to prevent and treat neutrophil associated inflammatory diseases.

## 1.5 Challenges in neutrophil research

With neutrophil-related research, there are many challenges that can arise due to the nature of neutrophils. Since they are terminally differentiated, neutrophils have a relatively short life span. Hence, this aspect hinders growing them in cell culture and making the stable genetic alterations that are needed to study them. To address this, neutrophil-like cell lines have been used recently in the neutrophil field including the human promyelocytic leukemia HL-60 cells and PLB-985 cells (Pedruzzi, Fay, Elbim, Gaudry, & Gougerot-Pocidalo, 2002; Tucker, Lilly, Heck, & Rado, 1987). Although they can display neutrophil-like morphology and function, these cell lines cannot fully recapitulate the biology of neutrophils. *In vitro* assays using these cell lines are also unable to recapitulate *in vivo* experiments. And since these cells need to be artificially differentiated into neutrophil-like cells, cell differentiation could be adversely effected by gene manipulation prior to differentiation, thus there have been reports using inducible promoters to modulate gene expression post differentiation in HL-60 cells (Hsu et al., 2019a). Moreover, neutrophils themselves consist of a heterogeneous population, suggesting there exist various neutrophil subtypes. Due to this, their distinct roles have not been clearly defined (Christoffersson & Phillipson, 2018; X. Wang, Qiu, Li, Wang, & Yi, 2018).

Mouse models are the most widely used mammalian animal model due to their similarity to humans and their ability to recapitulate certain human diseases. Extensive genetic tools are also available to manipulate the murine genome, either constitutively or conditionally, knocking out, knocking down, or knocking in the genes of interest. However, in neutrophil research, mouse models may not always be suitable. One of the biggest challenges using mouse in neutrophil studies is that the neutrophil numbers in the circulation of mouse is relatively low, 5-10% relative to the total peripheral blood mononuclear cell (PBMC), compared to humans which has a neutrophil composition of 40-70%. This discrepancy can greatly affect phenotypes related to neutrophil function manipulation by not being as robust or detectable. The nature of mouse neutrophils obtained from mouse may also present difficulty in mimicking the human immune response as murine neutrophils do not perform the same as human neutrophils (Mestas & Hughes, 2004).

In the beginning of the 1990s, use of zebrafish as popular model to study neutrophil biology has emerged. In comparison to mouse, the innate immune system of zebrafish is highly conserved with that of humans (Renshaw & Trede, 2012).This includes similarities in terms of their morphology and functions to human neutrophils (Henry, Loynes, Whyte, & Renshaw, 2013). The biggest advantage of using zebrafish as an animal model for studying neutrophils is its property of optical transparency. Real time visualization of neutrophil behavior can easily be captured *in vivo,* something that cannot be achieved in mouse. Zebrafish is also more economical to maintain and due to the high fecundity many offspring are easily obtained. Moreover, during the embryonic period of zebrafish development, only the innate immune system is present, thus zebrafish is an excellent reductionist model. Although the genetic alteration tools for zebrafish are not as established as they are for mouse, established techniques have been engineered to generate constitutive gene manipulation via the Tol2 transposon mediated insertion (Kawakami, 2005) and also through the use of tissue specific manipulation via CRISPR editing (W. Li et al., 2019; W. Zhou, L. Cao, et al., 2018).

In this dissertation we have done the first systemic survey of the function of miRs in regulating neutrophil migration, aiming to identify and characterize microRNAs and anti-microRNAs with therapeutic potentials in restraining neutrophilic inflammation. We then delineated the

downstream targets of these candidate miRNAs to better understand neutrophil biology and shed light on potential avenues for clinical applications to modulate neutrophil migration in hypothesizing to control/fine-tune neutrophilic pathologies. Through this work, we have established miRNA candidates and uncovered their respective mechanisms that could be used to alleviate inflammation and regulate neutrophil migration. Furthermore, what is learned here will contribute to a broader understanding of cell migration, which is fundamental to various homeostatic and pathogenic conditions such as embryogenesis, wound healing, and cancer metastasis.

# CHAPTER 2. DEVELOPMENT AND CHARACTERIZATION OF AN ENDOTOXEMIA MODEL IN ZEBRAFISH

## 2.1 Abstract

Endotoxemia is a condition in which endotoxins enter the blood stream and cause systemic and sometimes lethal inflammation. Zebrafish provides a genetically tractable model organism for studying innate immunity, with additional advantages in live imaging and drug discovery. However, a *bona fide* endotoxemia model has not been established in zebrafish. Here we have developed an acute endotoxemia model in zebrafish by injecting a single dose of LPS directly into the circulation. Hallmarks of human acute endotoxemia, including systemic inflammation, extensive tissue damage, circulation blockade, immune cell mobilization, and emergency hematopoiesis, were recapitulated in this model. Knocking out the adaptor protein Myd88 inhibited systemic inflammation and improved zebrafish survival. In addition, similar alternations of pathways with human acute endotoxemia were detected using global proteomic profiling and MetaCore™ pathway enrichment analysis. Furthermore, treating zebrafish with a protein tyrosine phosphatase, non-receptor type 11 (Shp2) inhibitor decreased systemic inflammation, immune mobilization, tissue damage, and improved survival in the endotoxemia model. Together, we have established and characterized the phenotypic and gene expression changes of a zebrafish endotoxemia model, which is amenable to genetic and pharmacological discoveries that can ultimately lead to a better mechanistic understanding of the dynamics and interplay of the innate immune system.

## 2.2 Introduction

The clinical manifestations associated with gram negative bacterial infection, such as vascular damage and leakage, disseminated intravascular coagulation, tissue hypoxia, systemic inflammation, cytokine storm, and in extreme cases elevation into sepsis (Andreasen et al., 2008; Sam, Sharma, Law, & Ferguson, 1997), is often caused by the presence of bacteria cell wall contents. Principally among these components are endotoxins or Lipopolysaccharides (LPS) (Raetz & Whitfield, 2002), which enter the blood circulation (Munford, 2016). A reductionist approach is taken to obtain a clean understanding of the host response elicited upon recognizing

endotoxins in cell cultures and mouse models, leaving out the complex interactions associated with tissue damage caused by live bacteria (Fink, 2014). Cultured cells offer a potent platform to dissect the signaling pathways activated by a LPS stimulation, but not the interactions of different cell types *in vivo*. Mouse models have offered many significant insights at the whole organism level in response to endotoxemia, yet suffers from the throughput, as well as divergence in the altered pathways (Seok et al., 2013). As such, there is a need to develop other animal models that can complement the cell culture and murine models.

The zebrafish is a fully sequenced model organism (Howe et al., 2013) with a highly conserved innate immune system, including cell types and signaling molecules (Lieschke & Currie, 2007; Stein, Caccamo, Laird, & Leptin, 2007). Zebrafish larvae develop innate immune cells within two days post fertilization while the adaptive immune system is not present until approximately three weeks post fertilization (Novoa & Figueras, 2012; van der Vaart, Spaink, & Meijer, 2012), making it a favorable model to study innate immune dominant responses. The transparent nature of zebrafish larvae allow imaging of dynamic interactions between immune cells and somatic tissues at the whole organism level (Lieschke & Currie, 2007; Sullivan & Kim, 2008). Additional advantages of using zebrafish include high fecundity and ease of gene editing, making it an ideal model for high throughput genetic and compound screening (Takaki, Cosma, Troll, & Ramakrishnan, 2012).

Despite a lack of a complete understanding of the LPS receptor in zebrafish (Sullivan et al., 2009), the downstream immune adaptors, pathways, and general immune response to LPS (Forn-Cuni, Varela, Pereiro, Novoa, & Figueras, 2017; Stein et al., 2007) are highly conserved. It is expected that a zebrafish endotoxemia model will advance our understanding of the initiation and resolution of the systemic inflammation during acute endotoxemia in humans.

LPS has previously been used as an immune-stimulant to cause inflammation in zebrafish larvae and to screen for anti-inflammatory compounds, through injection into the yolk (L. L. Yang et al., 2014) or bathing of the whole larvae. A single injection of 1ng of LPS into the yolk of 3 days post fertilization (dpf) zebrafish larvae caused upregulation of pro-inflammatory cytokines and caused 100% lethality at 24 hours post infection (hpi). The limitation of this approach is a lack of

yolk equivalent tissue in humans and poor physiological conservation (L. L. Yang et al., 2014). The LPS bath model has been used in several studies (Novoa, Bowman, Zon, & Figueras, 2009; Philip, Wang, Mauro, El-Rass, Marshall, Lee, Slutsky, dos Santos, et al., 2017; Sullivan & Kim, 2008), where vascular damage/leakage, tail fin edema, and immune activation were observed. However, the constant presence of LPS in the bath causes an overwhelming systemic inflammation that initiates at the epithelial surface and does not allow for detoxification of LPS and subsequent resolution of the inflammation (Novoa et al., 2009; Philip, Wang, Mauro, El-Rass, Marshall, Lee, Slutsky, dos Santos, et al., 2017; Sullivan & Kim, 2008). The pivotal role of immunostimulant introduction has been previous reported where bacterial injection and emersion caused dysregulation of overlapping but distinct responsive genes (Diaz-Pascual, Ortiz-Severin, Varas, Allende, & Chavez, 2017). Furthermore, an administration route that faithfully mirrors human immune interactions, is necessary to facilitate a true endotoxemia model (Takaki et al., 2012). Hence, a *bona fide* zebrafish endotoxemia model still needs to be developed.

We have designed a 3D printable injection plate to facilitate higher throughput for zebrafish larvae intravenous injection. Delivering LPS into the blood stream leads to acute systemic inflammation that starts to resolve at 24 hpi. Conserved phenotypic and gene expression changes are also observed in our model. Together, we have developed and characterized a zebrafish endotoxemia model that represents the fundamental biological processes of endotoxemia in humans. This model can be used in combination with murine models to fully dissect the molecular mechanisms regulating the magnitude of inflammation and to discover compounds that would mitigate detrimental consequences in the host.

## 2.3 Results

### 2.3.1 Establishment of an endotoxemia model

To efficiently inject LPS through the intravenous (IV) route, we adapted a previously reported method (Benard et al., 2012), and further optimized it by positioning larvae in an injection plate custom made with a 3D printed mold (Fig. 2-1A, B, Fig. 2-2). This plate can hold 20 zebrafish larvae in individual clefts and allows injection of 1-5 dpf zebrafish larvae into any position in the trunk. Utilizing this setup, we were able to inject 3 dpf larvae intravenously at a rate of 150

larvae/hour. With any immune process the dose and duration of challenge greatly dictates the immune response and phenotype (Anel & Kumar, 2005; Redl, Bahrami, Schlag, & Traber, 1993). LPS from *Pseudomonas aeruginosa* was selected because of its virulence in the bath model (Novoa et al., 2009) and in addition, the *Pseudomonas* species are a prevalent cause of infections and acute inflammation in intensive care units (Gotts & Matthay, 2016). Injection of 10 ng, 15 ng, and 25 ng LPS induced a dose dependent mortality ranging from 20% to 60% at 5 days post injection (dpi) (Fig. 2-1C). Control larvae injected with PBS did not show any mortality. As such, a dose of 25 ng, reproducibly causing approximately 50% mortality, was selected for future experiments. At 8 hpi, the majority of LPS injected larvae exhibited pericardial edema and circulation obstruction (Fig. 2-1D, E). However, only a few larvae displayed tail fin abnormalities, in contrast to the observation made when bathing the fish with LPS (Philip, Wang, Mauro, El-Rass, Marshall, Lee, Slutsky, dos Santos, et al., 2017). At 24 hpi, the percent of pericardial edema and circulation obstruction in the LPS injected larvae group decreased, suggesting recovery in some of the larvae that have survived the acute challenge (Fig. 2-1F, G) despite some larvae still having abnormalities. Our model coincides with pulmonary edema and circulatory obstruction which have been reported to be outcomes of acute endotoxemia in humans (Finley, Holliday, Lefcoe, & Duff, 1975; Okamoto, Tamura, & Sawatsubashi, 2016).

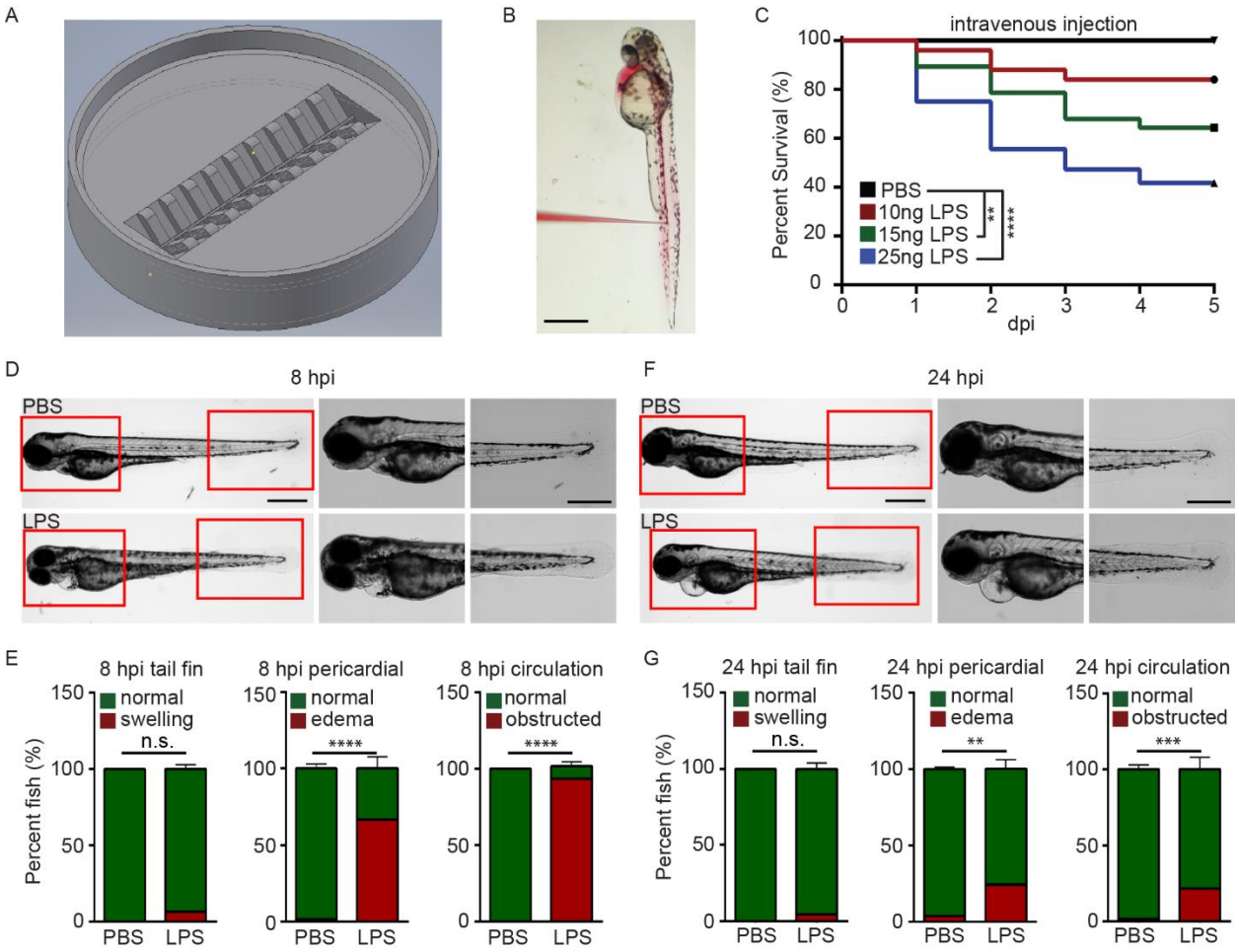


**Figure 2-1 Zebrafish intravenous injection plate design and intravenous LPS injection.**

(A) Illustration of the zebrafish intravenous injection plate. (B) A representative image of zebrafish larvae at 3 dpf injected with PBS containing 1% Phenol Red. Scale bar: 500 μm. (C) Survival curve of zebrafish after PBS or 10, 15, 25 ng LPS intravenous injection. One representative experiment of three independent biological repeats (n>20 each group) is shown. **, p<0.01, ****, p<0.0001, Gehan-Breslow-Wilcoxon test. (D) Representative images of zebrafish larvae injected with PBS or LPS at 8 hpi. Scale bar: 500 μm. Boxed regions of the pericardium and tailfin are enlarged. Scale bar: 200 μm. Images representative of three independent experiments are shown (n=20). (E) Percentage of fish with tailfin edema, pericardial edema, and circulation obstruction in PBS or LPS injected larvae at 8 hpi. Results are presented as mean ± sd. (N = 3 independent experiments with over 20 larvae each/experiment). ***, p<0.001, ****, p<0.0001, Mann–Whitney test. (F, G) Representative images and quantification of inflammatory phenotypes in LPS or PBS injected larvae as (D, E) at 24 hpi.

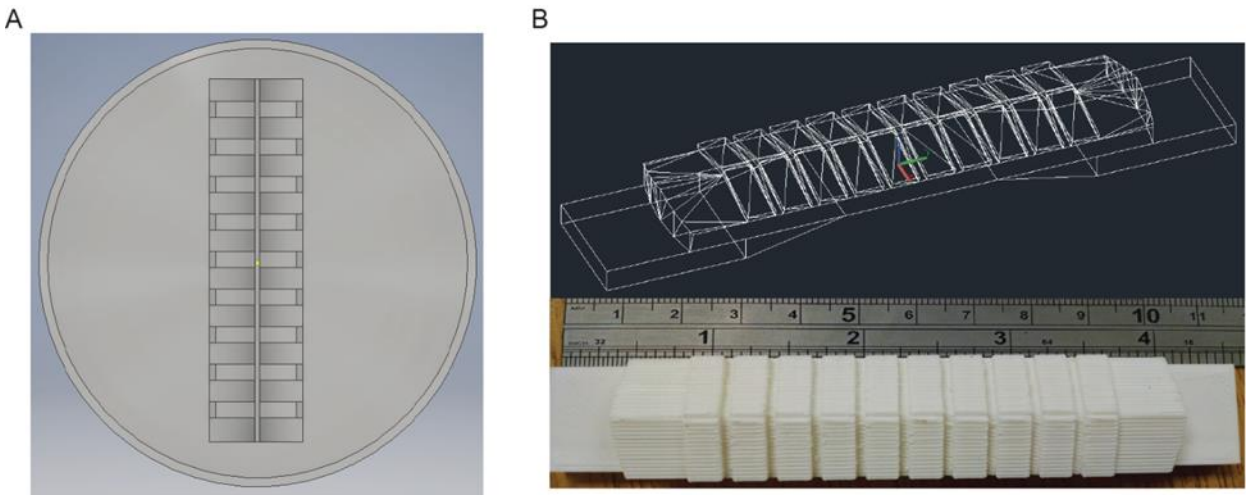


**Figure 2-2 Schematic of Zebrafish intravenous injection plate.**

(A) Overlooking view of zebrafish intravenous injection plate. (B) AutoCAD and a representative image of the mold used to make the injection plate from a 10 cm dish.

### 2.3.2 Systemic NF-κB activation in the endotoxemia model

Systemic inflammation is a hallmark of endotoxemia (Andreasen et al., 2008; Kiers et al., 2017) where multiple receptors are activated and signals converge to activate the NF-κB family of transcription factors (Denlinger et al., 1998; Gaestel, Kotlyarov, & Kracht, 2009). To determine the degree of inflammation in the whole larvae, an NF-κB reporter zebrafish line, *Tg(NF-κB:GFP)* (Kanther et al., 2011), was used, where the transcription of the GFP reporter gene is activated by NF-κB, which has been shown to be a central mediator of most inflammation processes(Taniguchi & Karin, 2018) and is a good indicator of inflammation(Liu, Zhang, Joo, & Sun, 2017). Compared to uninjected or PBS injected controls, LPS injected larvae exhibited an increase in GFP level throughout the body, indicating systemic NF-kB activation. The tail fin region was selected for quantification, where minimal basal auto-fluorescence was present. GFP intensity significantly increased at 8 hpi and 24 hpi in the LPS injected larvae (Fig. 2-3A, B). This is consistent with the time frame in acute human endotoxemia when systemic NF-kB and inflammation was noted (Abraham, 2003). Furthermore, pro-inflammatory cytokine levels and the complement component *c3a* were significantly upregulated at 8 hpi in endotoxemic larvae compared to PBS injected controls (Fig. 2-3C), consistent with previous studies (Fine, 1974; Surbatovic et al., 2015). This upregulation of pro-inflammatory cytokines and complement component persisted at 24 hpi, though the magnitude decreased significantly, while *il10*, a signature anti-inflammatory cytokine, was significantly upregulated (Fig. 2-3D) (Howard, Muchamuel, Andrade, & Menon, 1993), suggesting the initiation of the resolution of the systemic inflammation induced by LPS. The dynamic time course was similar to those observed in mouse and humans (Ertel, Keel, Steckholzer, Ungethum, & Trentz, 1996; Olszyna, Pajkrt, Lauw, van Deventer, & van Der Poll, 2000; Pinsky et al., 1993; H. Wang, Czura, & Tracey, 2004).

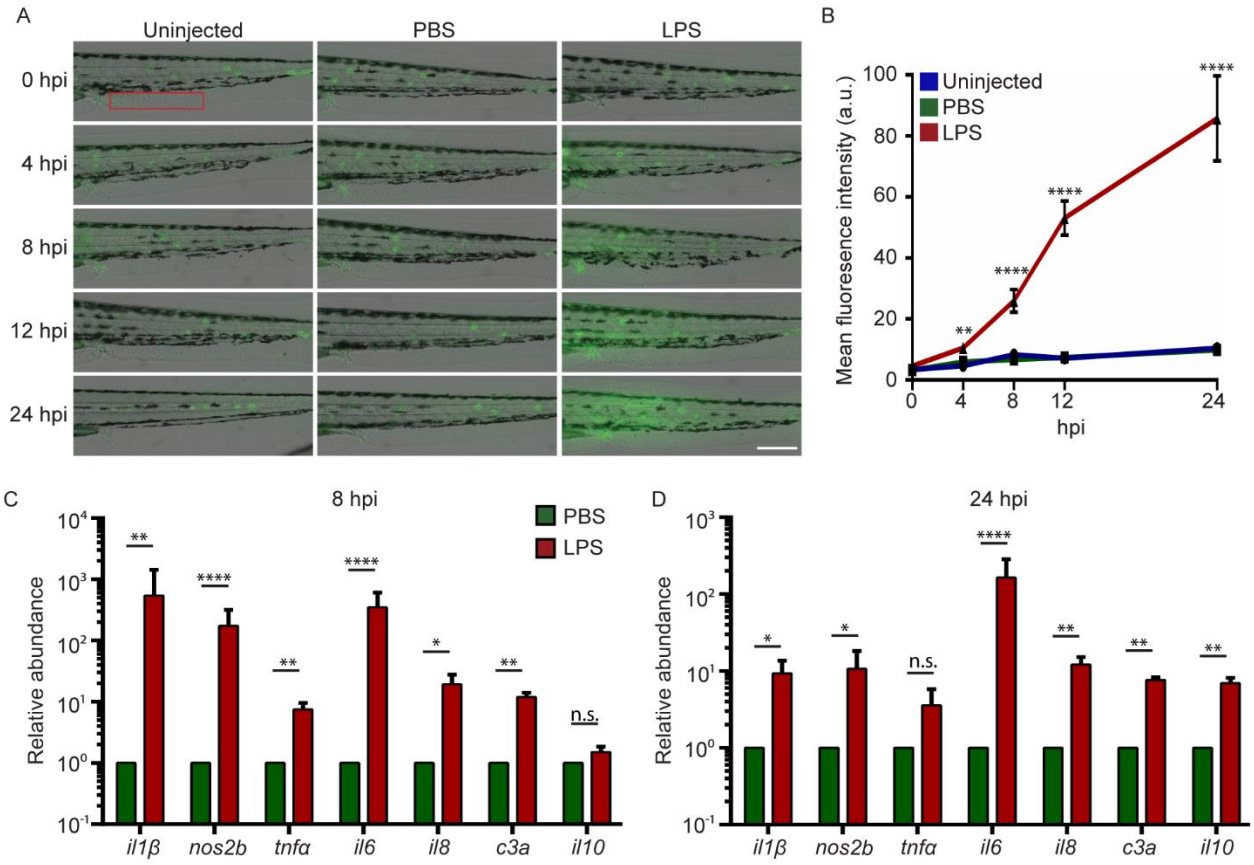


**Figure 2-3 Intravenous LPS activates NF-κB pathway and elicits a systemic immune response**

(A) *Tg(NF:κB:GFP)* larvae were intravenously injected with PBS, LPS, or were uninjected. Representative images of GFP signals at indicated time points post injection. Images representative of three independent experiments shown (n=20). Scale bar: 200 μm. (B) Quantification of the GFP intensity in the caudal fin region (red box in Figure 2-3A. Results are presented as mean ± s.d. (n=3 independent experiments with over 20 larvae each/experiment). **, p<0.01, ****, p<0.0001, Kruskal-Wallis test. (C, D) Transcript levels of genes encoding pro-inflammatory and anti-inflammatory cytokines in whole larvae injected with either PBS or LPS at 8 hpi (C) and 24 hpi (D). Results are normalized to *ef1α* and are presented as mean ±s.d. (n=3 biological repeats with 20 larvae in each group). *, p<0.05, **, p<0.01, ***, p<0.001, ****, p<0.0001, Sidak's multiple comparisons test.

### 2.3.3 Tissue damage in the endotoxemia model

To determine the degree of tissue damage in the live animal, we generated a zebrafish line *Tg(βactin:secA5-YFP)* $^{pu17}$, where AnnexinV tagged with YFP is constitutively produced and secreted (Fig. 2-4A). Apoptotic cells induced with UV are efficiently labeled as originally characterized by van Ham et al. (van Ham, et al. 2010) (Fig. 2-5). LPS injected larvae possessed more AnnexinV puncta in the trunk as well as in the vasculature at 12 and 24 hpi (Fig. 2-4B and C). Two separate approaches, Terminal deoxynucleotidyl transferase-mediated dUTP-biotin Nick End Labeling (TUNEL) (Fig. 2-4D and E), and Acridine Orange (AO) (Fig. 2-4F and G) (Hammerschmidt et al., 1996), staining were used to confirm the results at 24 hpi when the cell death were most prominent. Again, extensive tissue damage, in the vascular tissue and caudal hematopoietic tissue (CHT), the bone marrow equivalent in zebrafish larvae, were observed in the LPS injected group. To further evaluate vascular and cell junction integrity, we measured the mRNA levels of cell junction genes. Occludin members and Claudin-5 genes were significantly downregulated whereas claudin-2 was significantly upregulated at 8 hpi (Fig. 2-4H), suggesting loss of vascular cell junction integrity (Fisher et al., 2012; Philip, Wang, Mauro, El-Rass, Marshall, Lee, Slutsky, dosSantos, et al., 2017). Vascular junction genes returned to physiological levels at 24 hpi (Fig. 2-4I) with higher expression of Occludin family genes which have been shown to facilitate tissue repair (Du et al., 2010). These results faithfully recapitulated tissue damage throughout the body which is another hallmark of endotoxemia (Sam et al., 1997).

**Figure 2-4 LPS induces tissue damage.**

(A) Diagram of the construct used to generate the apoptosis reporter line where a secreted AnnexinV tagged with an YFP protein is driven by the *β-actin* promoter. (B, C) *Tg (β-actin:secANV-YFP)* were injected with PBS or LPS. Representative images (B) and Quantification (C) of the YFP positive foci in trunks at indicated time points post injection. (D, E, F,G) WT zebrafish larvae were injected with PBS or LPS. Representative images (D) and quantification (E) of TUNEL positive cells in the trunk at 24 hpi. Representative images (F) and Quantification (G) of the Acridine Orange positive cells in the trunk at 24 hpi Scale bar: 100μm. Results are presented as mean ± sem. (N = 3 independent experiments with over 20 larvae each/experiment). *, $p<0.05$, ****, $p<0.0001$, Mann–Whitney test. (B,D,F) Images representative of three independent experiments was shown (n=20). (H, I) Transcript levels of genes encoding vascular and cell junction proteins in whole larvae injected with either PBS or LPS at 8 hpi (H) and 24 hpi (I). Results were normalized with *ef1α* and are presented as means±s.d. (N=3 biological repeats with 20 larvae in each group). **, $p<0.01$, ***, $p<0.001$, ****, $p<0.0001$, Sidak's multiple comparisons test.

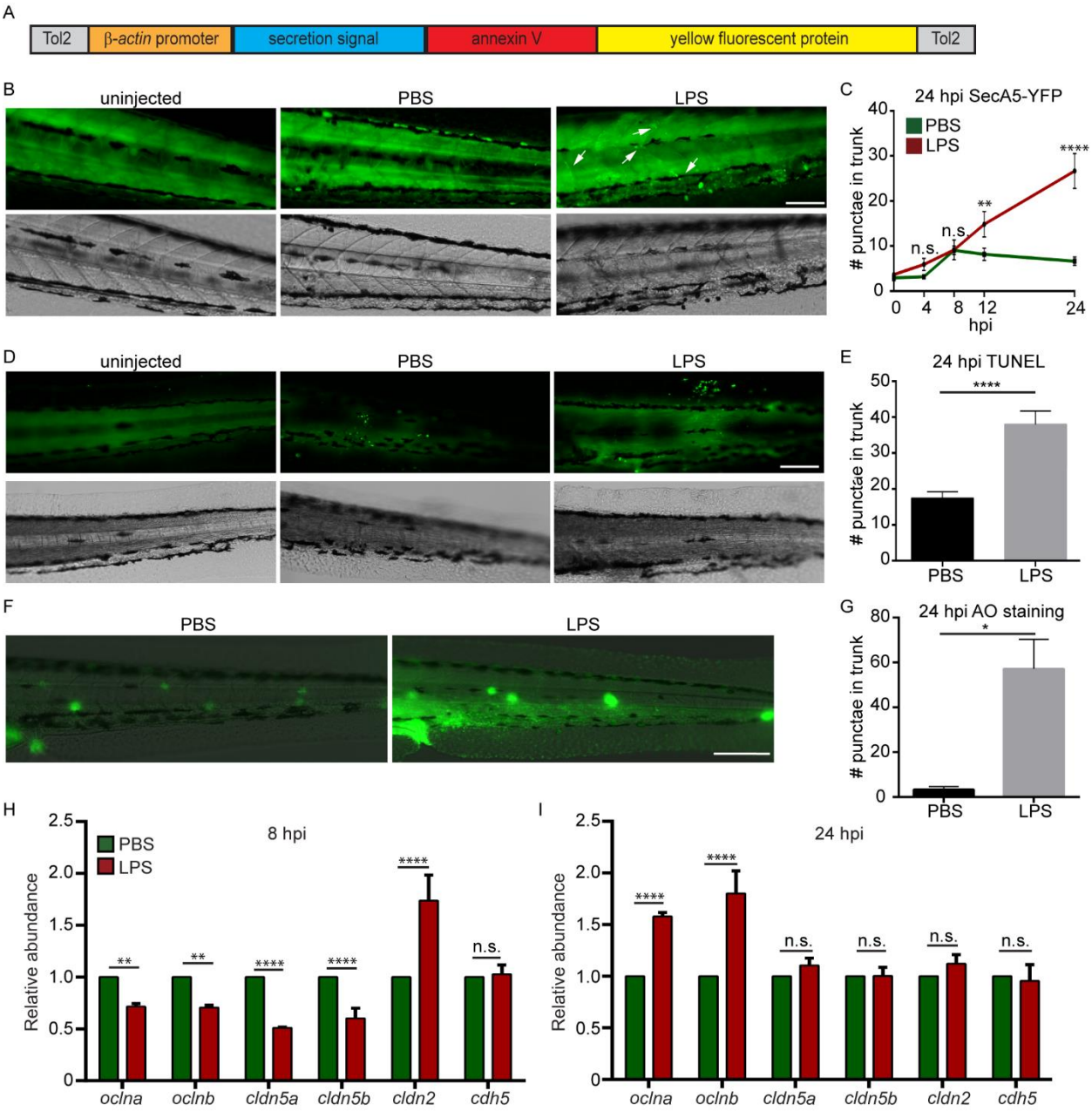
A
Tol2
β-actin promoter
secretion signal
annexin V
yellow fluorescent protein
Tol2
B
uninjected
PBS
LPS
C
24 hpi SecA5-YFP
PBS
LPS
# punctae in trunk
hpi
n.s.
n.s.
**
****
D
uninjected
PBS
LPS
E
24 hpi TUNEL
# punctae in trunk
****
PBS
LPS
F
PBS
LPS
G
24 hpi AO staining
# punctae in trunk
*
PBS
LPS
H
8 hpi
PBS
LPS
Relative abundance
oclna
oclnb
cldn5a
cldn5b
cldn2
cdh5
I
24 hpi
Relative abundance
oclna
oclnb
cldn5a
cldn5b
cldn2
cdh5

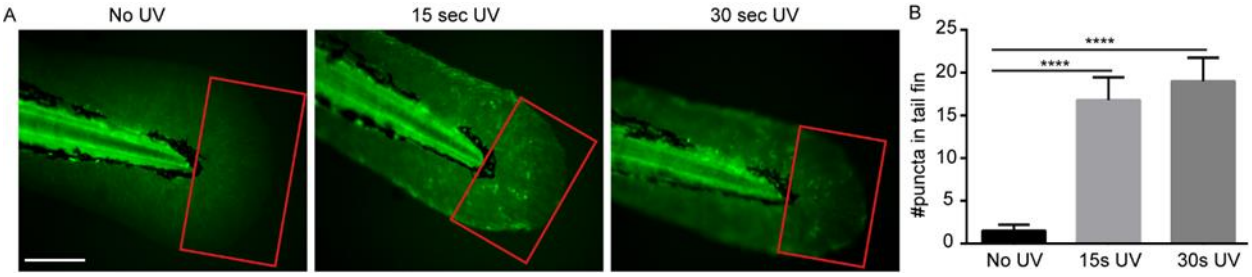


**Figure 2-5 Characterization of *Tg(βactin:secA5-YFP)* line**

(A) *Tg(βactin:secA5-YFP)* larvae at 3 dpf were subjected to either no UV, 15 sec, or 30 sec irradiation. (B) Quantification of puncta in the boxed region in tail fin. Scale bar: 100 µm. Results are presented as mean ± s.d. (N = 3 independent experiments with over 20 larvae each/experiment). ****, $p<0.0001$, Kruskal-Wallis test.

### 2.3.4 Emergency hematopoiesis in the endotoxemia model

As a result of profound inflammation, high levels of acute phase cytokines such as granulocyte and macrophage colony stimulating factors, and TNF-α are released into the circulation that mobilize the myeloid cells out of the bone marrow reservoir and induce a rapid differentiation of common myeloid progenitors to replenish the innate immune cells in a process termed "emergency hematopoiesis/granulopoiesis" (Manz & Boettcher, 2014). This phenomenon has been observed during endotoxemia in humanized mouse models (Skirecki et al., 2015). To determine the kinetics of immune cell mobilization and emergency hematopoiesis, we used a transgenic zebrafish line with macrophages and neutrophils labeled separately, *Tg(mpx:mcherry/mpeg:GFP-H2B)* (Fig. 2-6A) (Yoo, et al 2011, Davis, et al. 2016). Upon the induction of endotoxemia, neutrophils and macrophages mobilized out of the CHT (orange box region) by 2 hpi and entered the vasculature and the trunk tissue. Immune cells continued to mobilize and only scarce amounts of phagocytes resided in the CHT at 12 hpi followed by recovery to normal levels at 24 hpi (Fig. 2-6B, C and D). PBS injection induced a regional inflammatory response which was resolved by 8 hpi and did not induce significant depletion of immune cells in the CHT. For a more quantitative measure in the whole larvae, qRT-PCR for neutrophil (*lyzC*) (C. Hall, Flores, Storm, Crosier, & Crosier, 2007) and macrophage (*mfap4*) (Walton, Cronan, Beerman, & Tobin, 2015), specific genes were performed. Similarly, transient declines in both *lyzC* and *mfap4* were noted from 4-12 hpi, followed by a full recovery at 24 hpi (Fig. 2-6 E and F). Consistently, the hematopoiesis stimulating growth factors, *csf3 (g-csf)* and *csf1 (m-csf)* (Greenbaum & Link, 2011) were upregulated at both 8 and 24 hpi (Fig. 2-6 G and H) as previously reported during emergency hematopoiesis (Panopoulos & Watowich, 2008). This is the first *in vivo* observation of the dynamics of immune cell mobilization and emergency hematopoiesis in the hematopoietic tissue and at the whole organism level during endotoxemia.

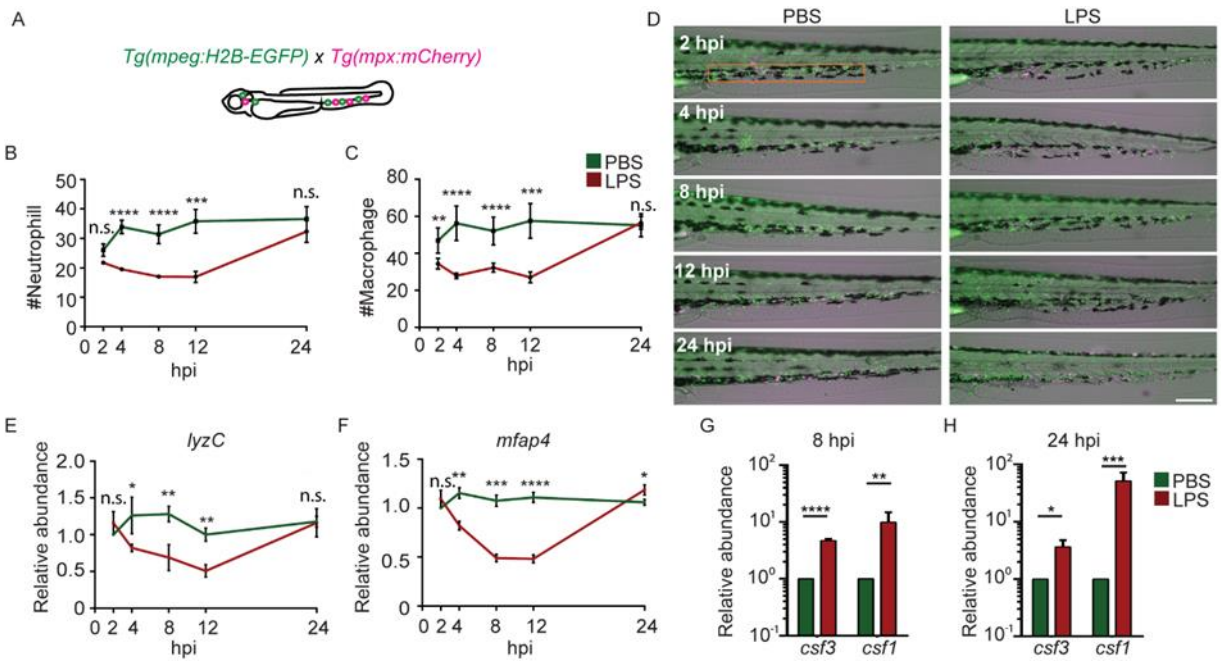


**Figure 2-6 Immune cell mobilization and emergency hematopoiesis induced with LPS injection**

(A). *Tg(mpeg :H2B-GFP)* fish were crossed with *Tg(mpx :mCherry)* label macrophages (green) and neutrophils (red) Quantification of neutrophil (B) and macrophage (C) numbers and representative images (D) in the caudal hematopoietic tissue (orange box) after PBS or LPS injection. Images representative of three independent experiments was shown (n=20). Scale bar: 200 μm. (E, F) mRNA level of *lyzC* (E) and *mfap4* (F) in the whole larvae injected with PBS or LPS. Results were normalized with *ef1α* and are presented as means±s.d. (N = 3 independent experiments with over 20 larvae each/experiment). *, p<0.05, **, p<0.01, ***, p<0.001, ****, p<0.0001, Mann–Whitney test. (G, H) mRNA level of *csf3* and *csf1* in whole larvae injected with PBS or LPS at 8 hpi (G) and 24 hpi (H). Results were normalized with *ef1α* and are presented as means±s.d. (N=3 biological repeats with 20 larvae in each group). *, p<0.05, **, p<0.01, ***, p<0.001, ****, p<0.0001, Mann–Whitney test.

### 2.3.5 Myd88 mediates inflammation in the endotoxemia model

Myd88 is a critical adaptor protein mediating pro-inflammatory signaling downstream of Toll-like receptors via the activation of the NF-κB pathway (Deguine & Barton, 2014). Although the LPS receptor in zebrafish is not clear (Sullivan & Kim, 2008), we next determined whether Myd88 is required for LPS induced systemic inflammation. We utilized the CRISPR/Cas9 system to knock out *myd88* as previously described (Zhou, Pal, Hsu, Theodore Gurol, & Jennifer L. Freeman, 2018) and observed a decrease in baseline NF-κB activity in the uninjected larvae (Fig. 2-7A and B). Disruption of *myd88* reduced NF-κB induced GFP signal intensity in LPS injected larvae at 8 and 24 hpi (Fig. 2-7C and D), which coincides with significantly improved survival rates (Fig. 2-7E), suggesting that MyD88 is a central mediator of inflammation downstream of the LPS receptor in fish, further confirming the conservation of zebrafish and humans (van der Sar et al., 2006).

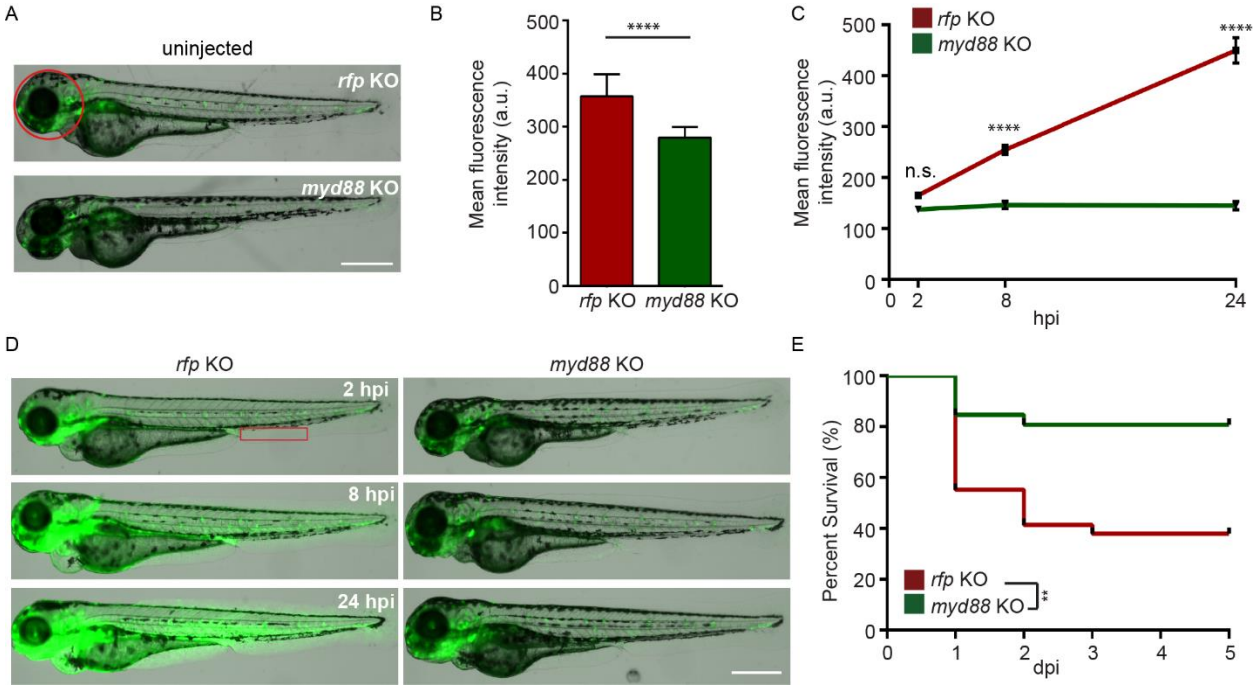


**Figure 2-7 Knock out of MyD88 dampens NF-κB activation and reduced mortality in the zebrafish endotoxemia model**

Zebrafish embryos of *Tg(NF:κB:GFP)* were injected with sgRNA against *myd88* or *rfp* at the single cell stage. (A, B) Representative images (A) and quantification (B) of the GFP intensity in the head (red circle) of uninjected 3dpf larvae. Scale bar: 500 µm. Results are presented as mean ± s.d. (N = 3 independent experiments with over 20 larvae each/experiment). ****, p<0.0001, Mann–Whitney test. (C, D) *myd88* or *rfp* KO larvae were injected with LPS. Quantification of NF-κB activity (C) and representative images (D) of the GFP intensity in the *Tg(NFκB :GFP)* background in the indicated region (red box). Scale bar: 500 µm. Results are presented as mean ± s.d. (N = 3 independent experiments with over 20 larvae each/experiment). ****, p<0.0001, Kruskal-Wallis test. (E) Survival curve of *myd88* or *rpf* KO larvae injected with LPS. One representative experiment of three independent biological repeats (n =20 each group) are shown. **, p<0.01, Gehan-Breslow-Wilcoxon test.

### 2.3.6 Global proteomic profiling in the endotoxemia model

Next we sought to address whether the biological response to endotoxemia in zebrafish larvae would mimic that seen in humans. Larvae were injected with PBS, LPS, or left uninjected, followed by whole larvae proteomic analysis at 8 hpi and 24 hpi. The proteomes of PBS injected larvae and those of uninjected control were found to be similar (raw data uploaded, see methods). Proteins with significant ($p<0.05$) and over 1.5 fold changes among the PBS and the LPS injected groups were converted to the human orthologues and subjected to MetaCore™ pathway enrichment analysis using the Uniprot database. At 8 hpi, many of the enriched pathways were involved in cell mobilization and motility, cell junction alterations, as well as innate immune functions (Fig. 2-8A), suggesting an acute activation of immune cells and inflammation in tissues during endotoxemia (Philip, Wang, Mauro, El-Rass, Marshall, Lee, Slutsky, dos Santos, et al., 2017; Zenker et al., 2014). At 24 hpi, Creb signaling pathways, reverse cholesterol transport, ROS, and Ask1 activation pathways were enriched, showing a more sustained biological response and pathway cross-talk (McGillicuddy et al., 2009; Noh, Park, Cho, & Choi, 2011; W. Wang et al., 2003; Wen, Sakamoto, & Miller, 2010) (Fig. 2-8B). In immune/inflammation related pathways (Fig. 2-8C, and D), pathway enrichments of hematopoiesis and chemotaxis along with inflammation were seen at 8 hpi (Fig. 2-8C). While at 24 hpi, Hmga/b, Il3, and Il6 responses pathways were enriched, which are hallmarks of prolonged over-inflammation (Fig. 2-8D) (Vallieres & Rivest, 1999; Weber et al., 2016; Yanai et al., 2013). To further investigate the dynamics of the individual proteins involved in the inflammation processes, a heat map was generated for both time points (Fig. 2-8E). Upregulation of Gsk3b (Dugo et al., 2007) and downregulation of Stat3 (Murray, 2006) during acute phases of endotoxemia was observed, consistent with their role in promoting inflammation. At 24 hpi, Stat3 and Sod1/2 (Yasui & Baba, 2006) were upregulated possibly to facilitate resolution. Meanwhile immune effector proteins such as Mif were upregulated, suggesting the persistence of systemic inflammation (Bernhagen et al., 1995).

**Figure 2-8 Global proteomics analysis in the zebrafish endotoxemia model**

3 dpf larvae were either injected with PBS or LPS. Samples were flash frozen at 8 hpi and 24 hpi and subjected to proteomics analysis. Proteins with significant difference in expression levels were then subjected to pathway analysis. (A, B) Top ten global enriched pathways at 8hpi (A) and 24hpi (B) in LPS injected larvae compared to that of PBS injected control. (C, D) Top ten immune pathways enriched at 8hpi (C) and 24hpi (D) LPS injected larvae compared to that of PBS injected control. The $-\log_{10}$ p values below the graph were calculated by MetaCore software and indicate the magnitude of alteration of the whole network. (N = 3 independent experiments with over 20 larvae each/experiment). (E) Fold changes of proteins involved in the top 10 enriched immune pathways at 8 hpi and 24 hpi. The heat map presents the relative expression of proteins in LPS injected larvae compared to that of PBS injected control. Three independent experiments are shown.

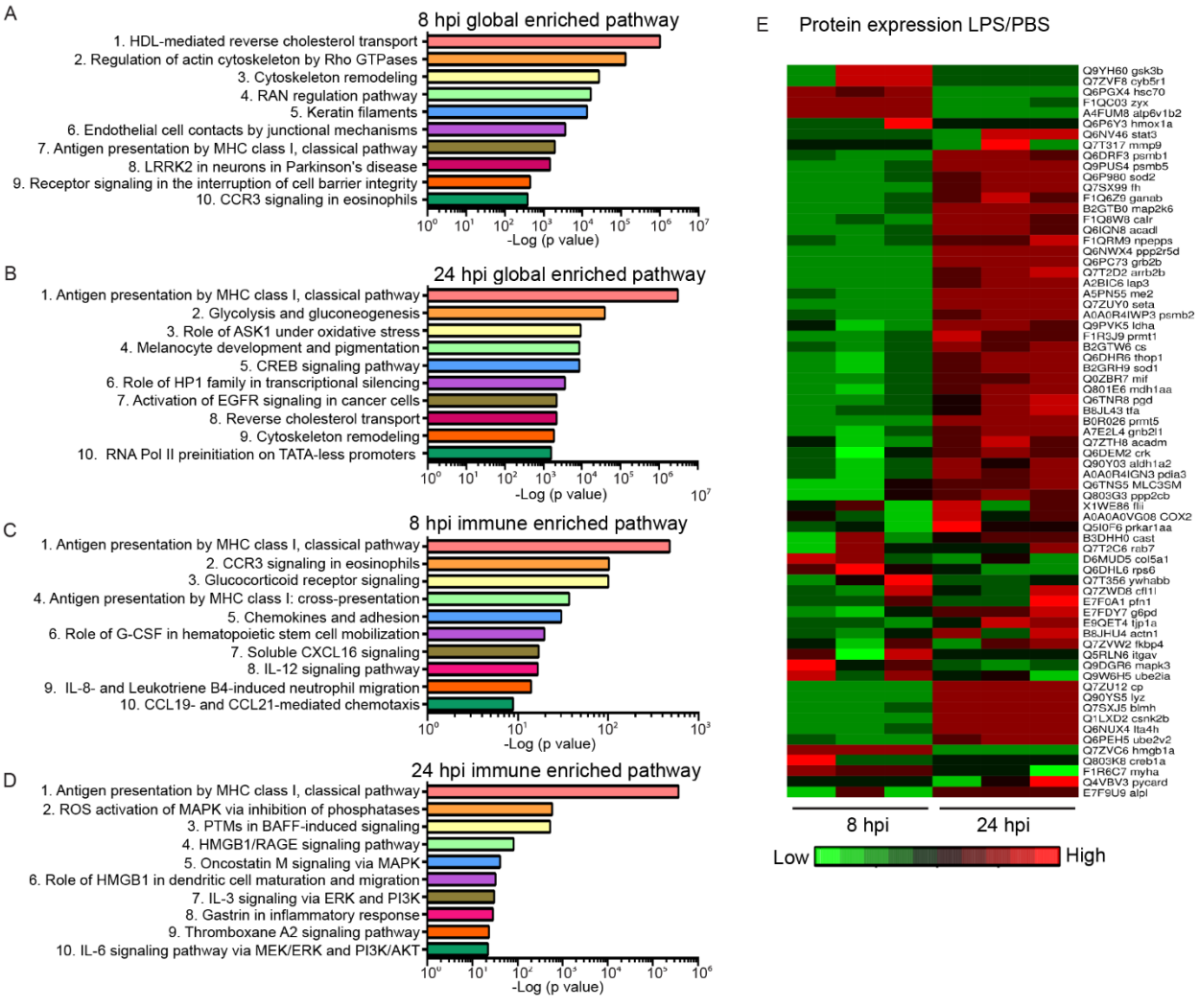
A
8 hpi global enriched pathway
1. HDL-mediated reverse cholesterol transport
2. Regulation of actin cytoskeleton by Rho GTPases
3. Cytoskeleton remodeling
4. RAN regulation pathway
5. Keratin filaments
6. Endothelial cell contacts by junctional mechanisms
7. Antigen presentation by MHC class I, classical pathway
8. LRRK2 in neurons in Parkinson's disease
9. Receptor signaling in the interruption of cell barrier integrity
10. CCR3 signaling in eosinophils
-Log (p value)
B
24 hpi global enriched pathway
1. Antigen presentation by MHC class I, classical pathway
2. Glycolysis and gluconeogenesis
3. Role of ASK1 under oxidative stress
4. Melanocyte development and pigmentation
5. CREB signaling pathway
6. Role of HP1 family in transcriptional silencing
7. Activation of EGFR signaling in cancer cells
8. Reverse cholesterol transport
9. Cytoskeleton remodeling
10. RNA Pol II preinitiation on TATA-less promoters
-Log (p value)
C
8 hpi immune enriched pathway
1. Antigen presentation by MHC class I, classical pathway
2. CCR3 signaling in eosinophils
3. Glucocorticoid receptor signaling
4. Antigen presentation by MHC class I: cross-presentation
5. Chemokines and adhesion
6. Role of G-CSF in hematopoietic stem cell mobilization
7. Soluble CXCL16 signaling
8. IL-12 signaling pathway
9. IL-8- and Leukotriene B4-induced neutrophil migration
10. CCL19- and CCL21-mediated chemotaxis
-Log (p value)
D
24 hpi immune enriched pathway
1. Antigen presentation by MHC class I, classical pathway
2. ROS activation of MAPK via inhibition of phosphatases
3. PTMs in BAFF-induced signaling
4. HMGB1/RAGE signaling pathway
5. Oncostatin M signaling via MAPK
6. Role of HMGB1 in dendritic cell maturation and migration
7. IL-3 signaling via ERK and PI3K
8. Gastrin in inflammatory response
9. Thromboxane A2 signaling pathway
10. IL-6 signaling pathway via MEK/ERK and PI3K/AKT
-Log (p value)
E
Protein expression LPS/PBS
Q9YH60 gsk3b
Q7ZVF8 cyb5r1
Q6PGX4 hsc70
F1QC03 zyx
A4FUM8 atp6v1b2
Q6P6Y3 hmox1a
Q6NV46 stat3
Q7T317 mmp9
Q6DRF3 psmb1
Q9PUS4 psmb5
Q6P980 sod2
Q7SX99 fh
F1Q6Z9 ganab
B2GTB0 map2k6
F1Q8W8 calr
Q6IQN8 acadl
F1QRM9 npepps
Q6NWX4 ppp2r5d
Q6PC73 grb2b
Q7T2D2 arrb2b
A2BIC6 lap3
A5PN55 me2
Q7ZUY0 seta
A0A0R4IWP3 psmb2
Q9PVK5 ldha
F1R3J9 prmt1
B2GTW6 cs
Q6DHR6 thop1
B2GRH9 sod1
Q0ZBR7 mif
Q801E6 mdh1aa
Q6TNR8 pgd
B8JL43 tfa
B0R028 prmt5
A7E2L4 grb2l1
Q7ZTH8 acadm
Q6DEM2 crk
Q90Y03 aldh1a2
A0A0R4IGN3 pdia3
Q6TNS5 MLC3SM
Q803G3 ppp2cb
X1WE86 flii
A0A0A0VG08 COX2
Q5I0F6 prkar1aa
B3DHH0 cast
Q7T2C6 rab7
D6MUD5 col5a1
Q6DHL6 rps6
Q7T356 ywhabb
Q7ZWD8 cfl1l
E7F0A1 pfn1
E7FDY7 g6pd
E9QET4 tjp1a
B8JHU4 actn1
Q7ZVW2 fkbp4
Q5RLN6 itgav
Q9DGR6 mapk3
Q9W6H5 ube2ia
Q7ZU12 cp
Q90YS5 lyz
Q7SXJ5 blmh
Q1LXD2 csnk2b
Q6NUX4 lta4h
Q6PEH5 ube2v2
Q7ZVC6 hmgb1a
Q803K8 creb1a
F1R6C7 myha
Q4VBV3 pycard
E7F9U9 alpl
8 hpi
24 hpi
Low
High

### 2.3.7 Shp2 inhibitor suppresses inflammation in the endotoxemia model

To demonstrate the feasibility of using our model for drug discovery and mechanistic study, two different classes of pharmacological agents were evaluated. Corticosteroids have been extensively used for the suppression of inflammatory responses, including in zebrafish studies (Coutinho & Chapman, 2011; d'Alencon et al., 2010), where a mixture of hydrocortisone and dexamethasone were used (C. J. Hall et al., 2014). We also determined the effect of a previously published protein tyrosine phosphatase inhibitor, the Shp2 (Ptpn11a) inhibitor 11a-1 (Zeng et al. 2014) in our endotoxemia model. Shp2 is required for pro-inflammatory cytokine production, ROS production, and macrophage M1 polarization (X. J. Li et al., 2015; Zhao et al., 2016), but has not been tested as a drug target in endotoxemia. As expected, significant decreases in the NF-κB levels (Fig. 2-9A and B) and mortality (Fig. 2-9C) in LPS injected larvae treated with either the Shp2 inhibitor or corticosteroid were noted. In 11a-1 treated larvae, inflammatory cytokines were decreased whereas anti-inflammatory *il10* was increased at 8 hpi (Fig. 2-9D). Tissue damage was significantly reduced (Fig. 2-9E and F) and the vascular junction genes were preserved at 8 hpi when treated with 11a-1 (Fig. 2-9G). In addition, 11a-1 treatment also preserved the phagocyte numbers in the CHT (Fig. 2-9H, I and J) as well as in the whole larvae (Fig. 2-9K), and mitigated the increase of myelopoiesis stimulating growth factors at 8 hpi (Fig. 2-9L). Together, our finding that corticosteroids can suppress the LPS induced inflammatory responses in the zebrafish endotoxemia model further validated its utility for the discovery of novel therapeutic agents to treat endotoxemia. The observed anti-inflammatory and protective effects by compound 11a-1 in our LPS induced endotoxemia model suggests that Shp2 inhibition may provide a potential strategy for combating endotoxemia.

**Figure 2-9 Shp-2 inhibitor reduces LPS induced systemic inflammation and mortality**

(A, B) Zebrafish embryos of *Tg(NF:κB:GFP)* were treated with DMSO, Shp2 inhibitor (11a-1), or corticosteroids and injected with LPS. Representative images (A) and Quantification (B) of the GFP intensity in the indicated region. Scale bar: 500 μm. Results are presented as mean ± s.d. (N = 3 independent experiments with over 20 larvae each/experiment). ***, p<0.001, ****, p<0.0001, Kruskal-Wallis test. (C) Survival curve LPS injected larvae treated with DMSO,11a-1 or corticosteroid. One representative experiment of three independent biological repeats (n =20 each group) is shown. *, p<0.05, ***, p<0.001, Gehan-Breslow-Wilcoxon test. . (D) Transcript levels of genes encoding pro-inflammatory and anti-inflammatory cytokines in whole larvae treated with DMSO or 11a-1 at 8 hpi. Results were normalized with *ef1α* and are presented as means±s.d. (N=3 biological repeats with 20 larvae in each group). *, p<0.05, **, p<0.01, ****, p<0.0001, Sidak's multiple comparisons test. (E, F) *Tg(β-actin:secANV-YFP)*$^{pu17}$ were treated with DMSO or 11a-1 and injected with LPS. Representative image (E) and quantification (F) of apoptotic cell puncta in the trunk. Scale bar: 200 μm. ****, p<0.0001, Mann–Whitney test. (G) Transcript levels of genes encoding vascular and cell junction proteins in whole larvae at 8 h post LPS injection treated with DMSO or 11a-1. Results were normalized with *ef1α* and are presented as means±s.d. (N=3 biological repeats with 20 larvae in each group). **, p<0.01, ***, p<0.001, Sidak's multiple comparisons test. (H, I, J) *Tg(mpeg :H2B-GFP)* were crossed with *Tg(mpx :mCherry)*, treated with DMSO or 11a-1 and injected with LPS). Representative images (H) and quantification of neutrophil (I) and macrophage (J) numbers in the caudal hematopoietic tissue (orange box). One representative result of three independent experiments was shown (n=20). Scale bar: 200 μm. Results are presented as mean ± s.d. (N = 3 independent experiments with over 20 larvae each/experiment). **, p<0.01, ****, p<0.0001, Mann–Whitney test. (K, L) Transcript levels of genes encoding *lyzC* and *mfap4* (K), *csf3* and *csf1* (L) in whole larvae treated with DMSO or 11a-1 after LPS injection. Results were normalized with *ef1α* and are presented as means±s.d. (N=3 biological repeats with 20 larvae in each group). *, p<0.05, **, p<0.01, ****, p<0.0001, Mann–Whitney test.

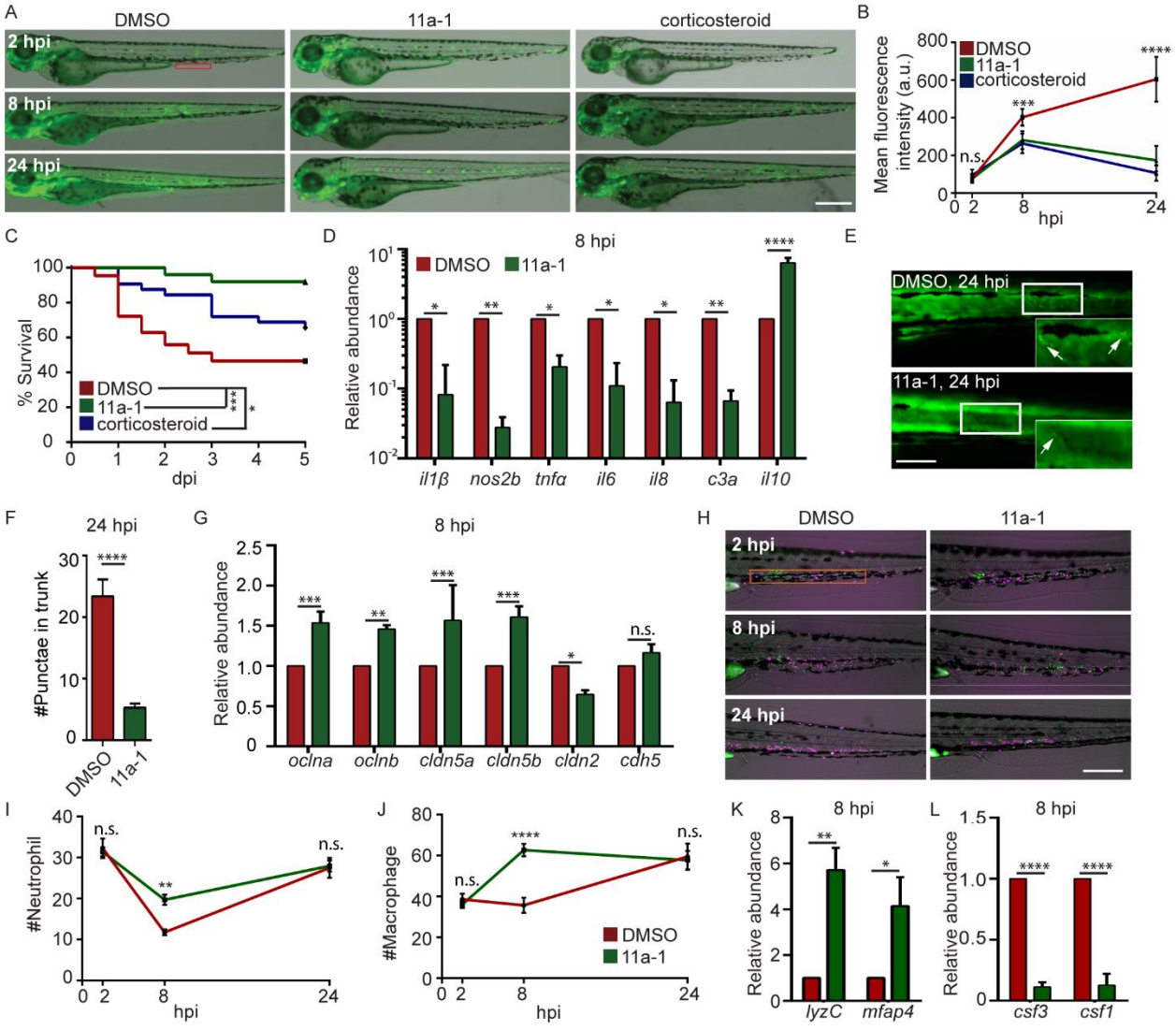
A
DMSO
11a-1
corticosteroid
2 hpi
8 hpi
24 hpi
B
Mean fluorescence intensity (a.u.)
DMSO
11a-1
corticosteroid
n.s.
hpi
C
% Survival
DMSO
11a-1
corticosteroid
dpi
D
8 hpi
Relative abundance
DMSO
11a-1
il1β
nos2b
tnfα
il6
il8
c3a
il10
E
DMSO, 24 hpi
11a-1, 24 hpi
F
24 hpi
#Punctae in trunk
DMSO
11a-1
G
8 hpi
Relative abundance
ocln a
ocln b
cldn5a
cldn5b
cldn2
cdh5
H
DMSO
11a-1
2 hpi
8 hpi
24 hpi
I
#Neutrophil
n.s.
hpi
J
#Macrophage
n.s.
DMSO
11a-1
hpi
K
8 hpi
Relative abundance
lyzC
mfap4
L
8 hpi
Relative abundance
csf3
csf1

## 2.4 Discussion

Here we report a zebrafish endotoxemia model facilitated by intravenous injection of LPS into 3 dpf larvae. Hallmarks of acute endotoxemia, including systemic inflammation, extensive tissue damage, loss of vascular junction integrity, immune cell mobilization, emergency hematopoiesis, and host mortality were observed herein. It is well known that during systemic inflammation neutrophils and macrophages migrate out of the zebrafish caudal hematopoietic tissue, enter the circulation and peripheral tissues and preform immune functions to combat the immunostimulus (Deng, Yoo, Cavnar, Green, & Huttenlocher, 2011b; Mathias et al., 2009). With a single dose of LPS administration, emergency hematopoiesis happened quickly and by 24 hpi, the immune cells in the CHT and the entire larvae were replenished. Therefore, our model provides a great tool in mechanistic studies of emergency hematopoiesis and resolution of the systemic inflammation.
We have reiterated several characteristics of the resolution after systemic inflammation such as elevated *il-10* levels to shift the immune response to anti-inflammation (Fig. 2-3D) (Howard et al., 1993), increased Occludin-5 which facilitate vascular tissue repair (Fig. 2-4I) (Du et al., 2010), upregulated hematopoiesis growth factors to replenish the immune reservoir (Fig. 2-6H) (Panopoulos & Watowich, 2008), while also identifying many proteins associated with inflammation resolution with proteome analysis. With this model, we may be able to further our understanding on the resolution stages of acute endotoxemia.
We were able to recapitulate several previously reported changes in protein abundance associated with endotoxemia in our proteomic results (Kasthuri, Wroblewski, Jilma, Key, & Nelsestuen, 2007; Yilmaz et al., 2016), including proteins and pathways involved in inflammation, vascular and organ damage, hematopoiesis, metabolism, inflammation resolution, and tissue repair. For example, the aspartate aminotransferase Got2 was upregulated at advanced stages of endotoxemia which is closely correlated with liver damage (Faix, 2013; Yokoyama et al., 1995). Hmga2, which is often seen upregulated in human sepsis which has been shown to be involved in immune activator functions and tissue damage, increased over time in our endotoxemia model (H. M. Huang et al., 2017; Lauw et al., 2000). Casein kinase II (CkII) has been reported to be an anti-inflammatory regulator required for anti-inflammatory cytokine production such as Tgf-β (Zdunek, Silbiger, Lei, & Neugarten, 2001) and observed to be downregulated in multiple inflammatory diseases (Singh & Ramji, 2008). Here we observed, for the first time in animal models, an upregulation of Casein kinase II (CkII) at the later stage of

acute endotoxemia, providing supporting evidence that CkII possibly drives the initiation of the resolution response. Another family of proteins that we have linked to endotoxin immune response is the Karyopherin alpha (Kpna) family proteins which have been known to promote inflammation via p65 NF-κB activation (Cai et al., 2016). However we were not able to detect differences in various immediate inflammatory proteins such as Nos2b and Il1b, but were detected to be upregulated at the mRNA level. This could be due to the stringent cut off criteria of our proteomic studies (Diaz-Pascual et al., 2017).

While corticosteroids are often used in a broad spectrum of inflammatory conditions, they come with adverse side effects (Buchman, 2001). As such there is a constant search for specific drugs to treat specific conditions. Shp2 is the first reported oncogenic tyrosine phosphatase that regulates multiple cellular process, including signal transduction, downstream of growth factor receptor signaling, and Schwann cell development (Grossmann, Rosario, Birchmeier, & Birchmeier, 2010; Grossmann et al., 2009). Multiple variants of Shp2 inhibitors are available for treating cancers (Bollu, Mazumdar, Savage, & Brown, 2017), of which TNO155 synthesized by Novartis is currently in phase I clinical trial for lung and head and neck cancer (NCT03114319). In regards to innate immune mediated systemic inflammation, Shp2 is an upstream activator of Akt and Ras pathways (Lauriol, Jaffre, & Kontaridis, 2015; Qu, 2000) which promotes cardiac mitochondria dysfunction in sepsis mouse models (Zang et al., 2012) and exacerbates systemic lupus erythematosus (J. Wang et al., 2016). Shp2 inhibition promotes innate immune cells to shift toward an anti-inflammatory phenotype with more Il10, Stat3 production, and an M2 dominant macrophage phenotype (Tao et al., 2014) (Zhao et al., 2016). Here we utilized a recently developed Shp2 inhibitor 11a-1 (Zeng et al. 2014) and found drastically reduced systemic NF-κB and immune activation with decreased lethality in treated larvae, suggesting a potential role of the Shp2 inhibitor as an anti-inflammatory drug. Although the mechanisms of how Shp2 promotes systemic inflammation in the zebrafish model requires further investigation, this proof of concept demonstrates that our endotoxemia model can be used to test candidate drugs at a whole organism level.

Though LPS has been widely used as an immunostimulant in many fields of studies, the response and tolerance toward LPS varies greatly between species and is also dependent on the routes of administration. Humans have a much lower tolerance than other commonly used model animals (Copeland et al., 2005; Dillingh et al., 2014). It is speculated that mouse have a much higher

tolerance to LPS due to their innate immunoglobulins against LPS. LPS-antibody complexes signal through Fc receptors, enhancing the clearance of LPS by recruited phagocytes (Lehner et al., 2001), or suppressing the signals from TLRs (Ko et al., 2009) which results in divergence from the response in humans (Seok et al., 2013). Zebrafish larvae are also more tolerant to LPS compared to humans (Novoa et al., 2009), possibly due to their aquatic habitats (Lieschke & Currie, 2007) or the identified TLR4 delivering an inhibitory signaling (Sepulcre et al., 2009). In contrast with the murine models, zebrafish larvae younger than two weeks do not have a functional adaptive immune system. These differences may be the reason why LPS induced signaling pathway changes are not entirely conserved among the three species, highlighting the necessity of including multiple animal models. Another very interesting observation is that immunological priming by commensal at early developmental stage shapes inflammatory reactions later on (Galindo-Villegas, Garcia-Moreno, de Oliveira, Meseguer, & Mulero, 2012). Future experiments using germ free technique can be used to determine the effect of the immune priming in our endotoxemia model.

In summary, we provide here an endotoxemic model utilizing the strength of zebrafish larvae which faithfully represents the hallmarks and signatures of acute endotoxemia. We further show that our model can be genetically manipulated to study inflammation and treated with drugs to assess the effect of potential compounds in an endotoxemic scenario. It is our expectation that our newly developed zebrafish endotoxemia model will provide a complementary tool for a full understanding of acute inflammation in humans.

# CHAPTER 3. OVEREXPRESSION OF MICRORNA-722 FINE-TUNES NEUTROPHILIC INFLAMMATION THROUGH INHIBITING RAC2 IN ZEBRAFISH

## 3.1 Abstract

Neutrophilic inflammation is essential for defending against invading pathogens, but can also be detrimental in many clinical settings. The hematopoietic-specific small Rho-GTPase Rac2 regulates multiple pathways that are essential for neutrophil activation, including adhesion, migration, degranulation and production of reactive oxygen species. This study tested the hypothesis that partially suppressing *rac2* in neutrophils with a microRNA would inhibit neutrophil migration and activation, which will reduce the immunological damage caused by systemic inflammation. We have generated a transgenic zebrafish line that over-expresses microRNA-722 (miR-722) in neutrophils. Neutrophil motility and chemotaxis to tissue injury or infection are significantly reduced in this line. MiR-722 downregulates the transcript level of *rac2* through binding to seed match in the *rac2* 3'UTR. Furthermore, miR-722 over-expressing larvae display improved outcomes in both sterile and bacterial systemic models, which correlates with a robust upregulation of the anti-inflammatory cytokines in the whole larvae and isolated neutrophils. Finally, the miR-722 mimics protect zebrafish from lethal LPS challenge. Together, we provide evidence and the mechanism of an anti-inflammatory microRNA that restrains detrimental systemic inflammation.

## 3.2 Introduction

How to dampen immune activation is a major challenge in modern medicine. Neutrophils are the most abundant white blood cells in the circulation and the first line of defense against infections. While essential for battling against pathogens, acute or chronic neutrophil activation drives immunopathology in numerous human diseases, including those directly involving an immune component (such as organ transplantation, sepsis and rheumatoid arthritis) and those that are not obviously linked (such as diabetes, neurodegenerative disease and cancer) (Borregaard, 2010; Nathan, 2006). Neutrophils release toxic granular contents including proteases, as well as extracellular traps and produce a large amount of reactive oxygen species, which help eliminate

the threat of pathogens but can cause detrimental effects on hosts. Recent evidence suggests that neutrophils, in addition to mediating acute inflammation, are a critical regulator of the inflammatory landscape. They live longer than previously recognized (Pillay et al., 2010). In addition, they initiate (Sreeramkumar et al., 2014), disseminate (Woodfin et al., 2011), and critically regulate the magnitude of inflammation (Warnatsch, Ioannou, Wang, & Papayannopoulos, 2015) while bridging innate and adaptive immunity (Abi Abdallah, Egan, Butcher, & Denkers, 2011; Lim et al., 2015) in both sterile inflammation and infection. Thus, a successful strategy to prevent the infiltration of neutrophils is expected to significantly improve inflammatory conditions and reduce the risk of many modern diseases. As such, the microtubule destabilizing agent colchicine, a potent inhibitor for neutrophil motility and activation, is approved for treating acute inflammation in familial Mediterranean fever and gout patients (Cocco et al., 2010). However, colchicine and the broad-spectrum anti-inflammatory agent corticosteroids lack neutrophil specificity and are inevitably accompanied with adverse side effects (Cocco et al., 2010). There is an urgent need to develop anti-neutrophil therapies that would benefit a diverse population suffering from inflammatory ailments.

MicroRNAs are evolutionarily conserved, small non-coding RNAs that post-transcriptionally regulate protein synthesis (Fabian & Sonenberg, 2012). MiR expression is controlled by specific promoters and regulated at the transcriptional and post-transcriptional levels. The initial transcription of long primary transcripts are processed in the nucleus into short ~70 nt precursor miRNA hairpins, and further exported and processed in the cytoplasm into mature ~22 bp miR duplexes, containing both 5p and 3p strands. The duplex is then loaded into Argonaut (AGO) proteins, where the passenger strand is degraded, which allows the guide strand to direct the miR Induced Silencing Complexes to partially complementary target sites (Gurol et al., 2016). Either or both of the 5p and 3p strands can act as the predominant functional strand, depending on the unstable terminus at the 5’ end or other unknown mechanisms. The majority of the microRNAs bind to their target transcript though complementarity in the 3’UTR to suppress gene expression, although in some cases, enhanced target gene expression was observed (Ma et al., 2010). The seed sequence (positions 2-8 of the mature miRNA) is the major determinant of target recognition, although the contribution of other nucleotides cannot be excluded (Helwak, Kudla, Dudnakova, & Tollervey, 2013). As of April 2017, 2588 human mature microRNAs have been

identified, which are implicated in a wide variety of cellular processes and human diseases. MicroRNAs and anti-microRNAs are recent additions to the clinician's arsenal as next generation therapeutics to treat human diseases (Broderick & Zamore, 2011; Hayes, Peruzzi, & Lawler, 2014). Currently, miR-122 antagonists are in clinical trials for chronic hepatitis C infection (RG-101 by Regulus). Extensive effort has been made characterizing inflammation related microRNAs. The microRNA expression profiles in various inflammatory conditions, including sepsis have been documented (Gurol et al., 2016). However, the use of this information is currently limited to establishing microRNAs as biomarkers and diagnostic tools. The biological functions of these microRNAs and their therapeutic potential are merely starting to emerge. The majority of microRNA-inflammation research is restricted to macrophages, with their roles in neutrophils poorly characterized. Human peripheral blood neutrophils (Gantier, 2013; Landgraf et al., 2007; Ward et al., 2011) and activated tissue infiltrating neutrophils (Larsen et al., 2013) express a different profile of microRNAs. It is reasonable to speculate that microRNAs are potent regulators of neutrophil function and inflammation.

In the present study, we aim to identify a microRNA that would restrain hyperactive neutrophilic inflammation and to test its impact in acute systemic inflammation settings. Rac2, a member of the Rho small-GTPase family, is restricted to the hematopoietic lineage, which plays a principal role in regulating the actin cytoskeleton and neutrophil biology. By using neutrophils isolated from *Rac2* knockout mouse (Roberts et al., 1999), in combination with studying a dominant negative form of Rac2 in zebrafish neutrophils in vivo (Deng et al., 2011b), multiple parallel pathways of Rac2 effector functions have been discovered. Rac2 is required for neutrophil motility and chemotaxis by regulating actin polymerization at the leading edge in a positive feedback loop with PI3K (Yoo et al., 2010). Rac2 is required for adhesion and retention of neutrophils in the hematopoietic tissue, yet not required for their release from this tissue (Deng et al., 2011b). In addition, Rac2 is an essential subunit for the phagocyte NADPH oxidase complex, directly interacting with $gp19^{phox}$ and $p67^{phox}$, and is responsible for the generation of super oxide ions during infections (Jonzon & Bindslev, 1991). Furthermore, Rac2 is required for the degranulation of primary granules in neutrophils (Abdel-Latif et al., 2004). It is our expectation that suppressing Rac2 activity in neutrophils will greatly reduce the number of infiltrating neutrophils in the tissue and alleviate patients from over-inflammatory burdens. However,

benefits of Rac2 as therapeutic targets have not been previously explored, probably due to a lack of a Rac2 specific inhibitor as well as the fact that Rac2 deficiency results in primary immune deficiency and poor wound healing (D. A. Williams et al., 2000).

The zebrafish is a fully sequenced vertebrate model organism with a conserved innate immune system (Deng & Huttenlocher, 2012). The ease of genetic manipulation and the optical transparency of zebrafish larvae made them ideal model organisms to observe the behavior of phagocytes in a non-invasive way and to dissect related molecular mechanisms. Here we provide the first microRNA that suppresses the expression of *rac2* and demonstrated that partial *rac2* suppression attenuated the acute lethal inflammation under both sterile and non-sterile conditions.

## 3.3 Results

### 3.3.1 MiR-722 over-expressing neutrophils are defective in motility and chemotaxis.

To test the efficacy of microRNAs as next-generation therapeutics that would restrain neutrophil migration and inflammation, we looked into microRNAs that can suppress *rac2* expression. We performed bioinformatics analysis (TargetScanFish) and identified three microRNAs (miR-194, miR-722 and miR-129) that are predicted to bind to the 3'UTR of both transcript variants of the zebrafish *rac2* gene. miR-722 and miR-129 share the same seed sequence and bind to a perfect seed matching site in the *rac2* 3'UTR with a context + score percentile above 90. MiR-194 binds to a separate site with a partial seed match and a context + score percentile at 69, possibly a weaker regulator of *rac2*. Data compiled from previous microRNA sequencing experiments suggest that miR-722 is intergenic and predominantly produces a mature 3p strand that harbors the *rac2* binding sequence (www.miRbase.org). In contrast, both the mature 5p and 3p strands of miR-129 are detected, which potentially complicates the biological consequence of over-expressing this microRNA. In addition, miR-722 level is below the detection limit by quantitative microRNA RT-PCR in sorted neutrophils. Last but not least, the seed binding sequence is also present in human *RAC2* 3'UTR. Based upon aforementioned reasons, miR-722 was selected for further characterization.

First, we generated a transgenic zebrafish line that over-expresses miR-722 specifically in neutrophils (schematic in Fig. 3-1A). To facilitate the identification and characterization of cells expressing this microRNA, a 206 bp genomic DNA sequence flanking microRNA-722 was cloned into an intron that allows co-expression of miR-722 with a green fluorescent reporter protein, Dendra2. Three founders each of the zebrafish that express the vector control or miR-722 were obtained. We observed specific upregulation of both the precursor and mature forms of miR-722 in the transgenic animals, without alterations in the level of miR-223 or a ubiquitously expressed microRNA let-7e (Fig. 3-1B), confirming that microRNA biogenesis in neutrophils is intact. In addition, similar numbers of neutrophils were present in both lines (Fig. 3-1C), indicating that miR-722 does not impair neutrophil biogenesis or survival. We next examined the recruitment of miR-722 over-expressing neutrophils in two separate acute inflammation models: a localized bacterial infection and tail transection. Significantly fewer neutrophils were recruited in miR-722 over-expressing lines in both incidences (Fig. 3-1D, E). This phenotype was further confirmed in the offspring from separate founders (Fig. 3-1 G, H and I), excluding the positional effect of the random genomic insertion by the tol2 transposon method. Furthermore, the motility of the miR-722 over-expressing neutrophils was significantly hampered (Fig. 3-1F), which phenocopied the Rac2-deficient neutrophils (Deng et al., 2011b; Rosowski, Deng, Keller, & Huttenlocher, 2016), coinciding with the prediction that miR-722 down-regulates *rac2* expression in neutrophil.

**Figure 3-1 Neutrophil recruitment and motility is hindered in miR-722 over-expressing zebrafish line**

(A) A Schematic of Tol2-lyzC:miR-722/Dendra2 plasmid, injected into wild-type AB zebrafish embryos to generate the transgenic line Tg(lyzC:miR-722/Dendra2)pu6 (miR-722). Tg(lyzC:Dendra2)pu7 was generated using the same configuration without the miR-722 insertion (vector). All experiments were performed with F2 larvae at 3dpf. (B) Relative expression level of precursor and mature miR-722, miR-223, and let-7e (normalized to U6 expression) in vector and miR-722 lines determined by RT-qPCR, mean ± s.d. (N = 3 biological repeats with 10 larvae at each time point in each group). P value was calculated with unpaired Student's t-test. (C) Representative images and quantification of total neutrophils in vector and miR-722 lines. One representative result of three independent experiments was shown (n=20). Scale bar: 500 μm. (D) Representative images and quantification of neutrophil recruitment to localized ear infection in vector or miR-722 larvae at 1 hour post infection. The infected ear is indicated with the circle. One representative result of three independent experiments was shown (n=20). P value was calculated with unpaired Student's t-test. Scale bar: 100 μm. (E) Representative images and quantification of neutrophil recruitment to tail transection site in vector or miR-722 larvae at 1 hour post injury. Neutrophils in the boxed region were quantified. One representative result of three independent experiments was shown (n=20). P value was calculated with unpaired Student's t-test. Scale bar: 100 μm. (F) Tracks and quantification of neutrophil motility in vector or miR-722 larvae. Results were pooled from three independent larvae (n=60). P value was calculated with unpaired Student's t-test. Scale bar: 50 μm. Quantification of total number of neutrophils (G), neutrophils recruited to the ear 1 h post P. aeruginosa infection (H) and to the wound 1 hour post tail transection (I). One representative result of three independent experiments was shown (n=20). No statistical difference among the results from separate founders were observed with unpaired one-way ANOVA.

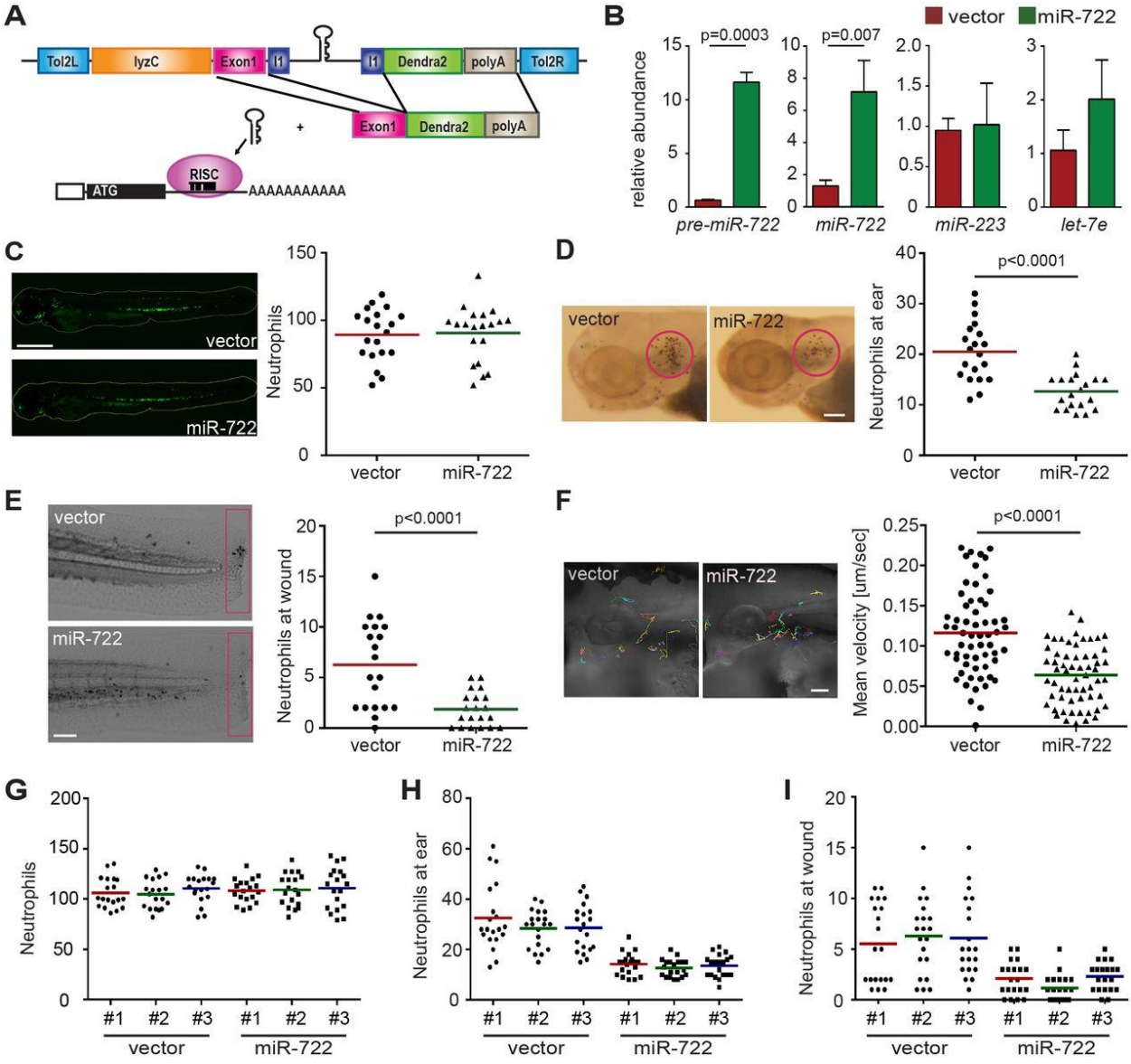
A
Tol2L
lyzC
Exon1
I1
I1
Dendra2
polyA
Tol2R
Exon1
Dendra2
polyA
RISC
ATG
AAAAAAAAAA
B
vector
miR-722
relative abundance
p=0.0003
p=0.007
pre-miR-722
miR-722
miR-223
let-7e
C
vector
miR-722
Neutrophils
vector
miR-722
D
vector
miR-722
p<0.0001
Neutrophils at ear
vector
miR-722
E
vector
miR-722
p<0.0001
Neutrophils at wound
vector
miR-722
F
vector
miR-722
p<0.0001
Mean velocity [um/sec]
vector
miR-722
G
Neutrophils
#1
#2
#3
#1
#2
#3
vector
miR-722
H
Neutrophils at ear
#1
#2
#3
#1
#2
#3
vector
miR-722
I
Neutrophils at wound
#1
#2
#3
#1
#2
#3
vector
miR-722

### 3.3.2 MiR-722 directly suppresses zebrafish *Rac2* expression.

We then confirmed that miR-722 can directly suppress zebrafish *rac2* gene. The zebrafish *rac2* 3'UTRs harbor a miR-722 binding site with perfect seed sequence match (Fig. 3-2A). We performed reporter assays to validate the direct translational suppression by miR-722. Expression of miR-722 significantly suppressed the relative luciferase activity, which was dependent on the seed sequences in zebrafish *rac2* gene (Fig. 3-2B). Since reporter assays are based on enforced microRNA and transcript over-expression that can yield false positive results, we measured the endogenous *rac2* transcript level. In the miR-722 over-expressing zebrafish line, the *rac2* mRNA is significantly reduced (Fig. 3-2C), suggesting a direct destabilization of the *rac2* transcript by miR-722 in neutrophils. Another neutrophil specific gene, lysozyme C, was not altered in the same sample, indicating the specificity of miR-722 towards *rac2*.

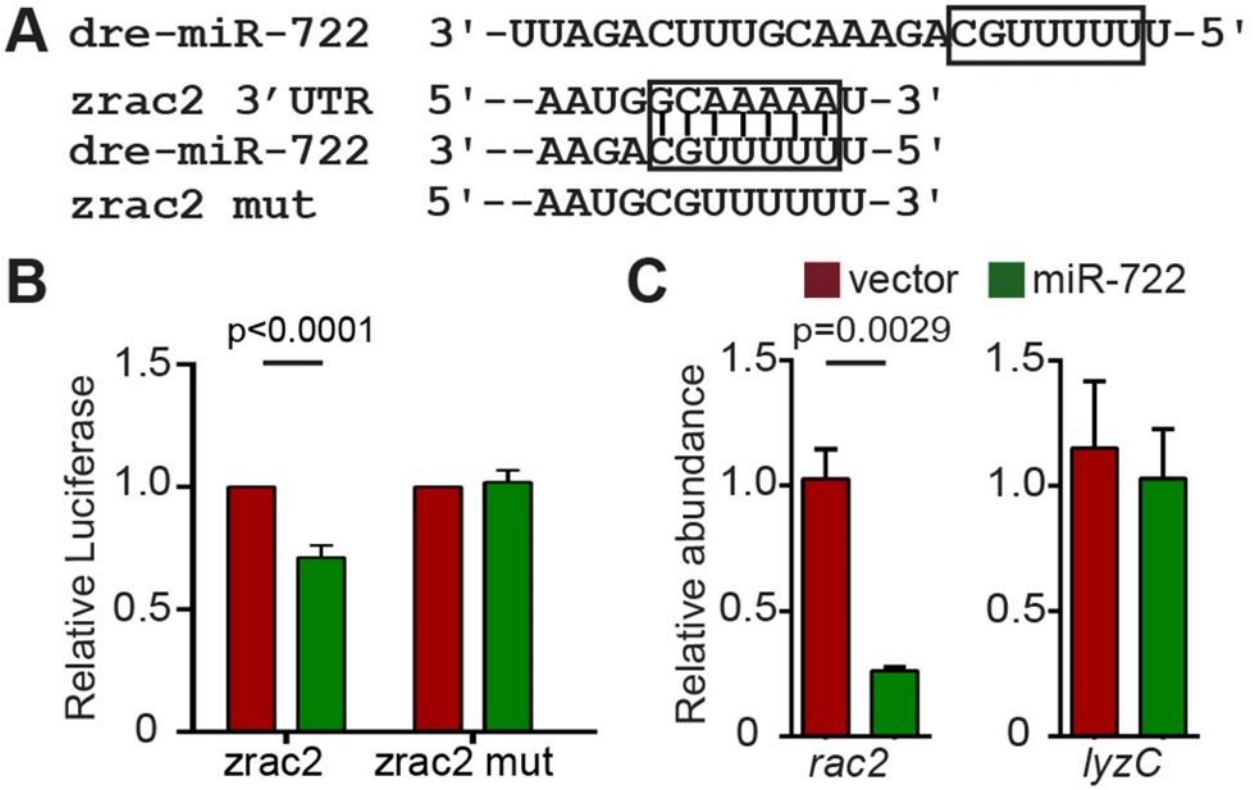


**Figure 3-2 miR-722 down regulates the zebrafish *rac2* transcript through binding to seed complementary sequences in the 3'UTR**

(A) Sequence of miR-722 and zebrafish *rac2* 3'UTRs. The seed sequence and its binding sites in 3'UTRs are boxed. (B) Selective suppression of Renilla luciferase activity by miR-722 through binding to seed sequence in zebrafish *rac2* 3'UTRs. Result was presented as mean ± s.d. (N = 3 independent experiments). P value was calculated with paired Student's t-test. (C) Relative expression level of *rac2* and lyzC mRNA (normalized to ef1a) in vector and miR-722 larvae determined by RT-qPCR. Result was presented as mean ± s.d. (N = 3 independent experiments with over 20 larvae each/experiment). P value was calculated with unpaired Student's t-test.

### 3.3.3 *Rac2* over-expression rescues miR-722 induced phenotypes.

To further validate that *rac2* is a major target of miR-722 in neutrophils, we performed a rescue experiment using a transgenic zebrafish line that over-express zebrafish *rac2* followed by the SV40 3'UTR that is resistant to miR-722 mediated suppression (Deng et al., 2011b). A line that expresses mCherry alone was used as a control. Clutch mates were used in this experiment to minimize the impact of genetic variation in different lines (Fig. 3-3A). Consistent with our data that miR-722 directly downregulates endogenous *rac2* expression, defects in neutrophil motility (Fig. 3-3B) or their recruitment to tissue injury (Fig. 3-3C) or infection (Fig. 3-3D) resulted from miR-722 over-expression were all rescued by *rac2* over-expression, pinpointing *rac2* as a relevant miR-722 target in neutrophils.

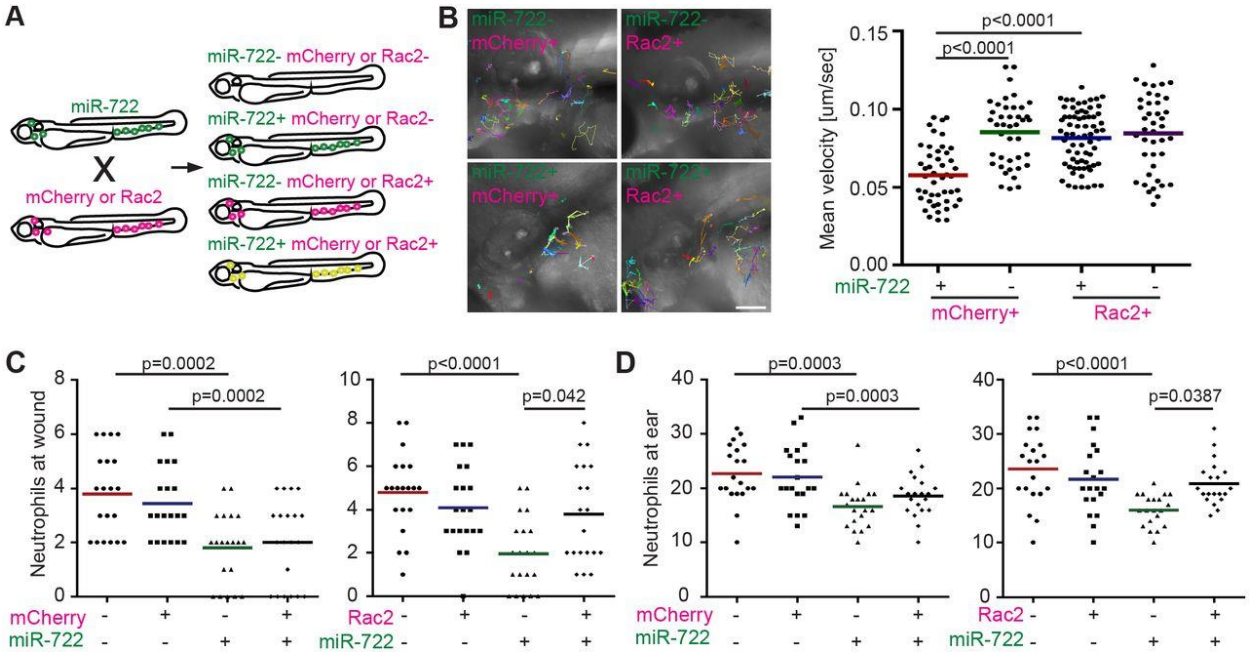


**Figure 3-3 Over-expression of *rac2* rescues neutrophil recruitment in the miR-722 expressing larvae**

(A) Tg(lyzC:miR-722/Dendra2)pu6 was crossed with Tg(mpx:mCherry-2A-*rac2*) (*rac2*) and the offspring were separate into four groups. For control, Tg(lyzC:miR-722/Dendra2)pu6 was crossed with Tg(mpx:mCherry) (mCherry). All experiments were performed with F2 larvae at 3dpf. (B) Tracks and quantification of neutrophil motility in indicated lines. Results were pooled from three independent larvae. P values were calculated with unpaired Student's t-test. Scale bar: 100 μm. Quantification of neutrophil recruitment to tail wounding (C) or localized ear infection (D) in siblings separated into four groups as depicted in (A). One representative experiment of three independent biological repeats were shown (n=20 for each group). P values were calculated with unpaired two-way ANOVA.

### 3.3.4 Neutrophil specific miR-722 over-expression protects zebrafish from lethal systemic inflammation.

Neutrophils are a major cell type which causes tissue damage during severe inflammation. Thus, we tested whether miR-722 over-expressing zebrafish were more resistant to lethal inflammatory challenges, for example, a bacterial systemic infection model using the Gram-negative bacteria *Pseudomonas aeruginosa PAK* strain. The miR-722 over-expressing larvae survived better (Fig. 3-4A), despite the presence of similar bacterial burdens (possibly as a result of intact macrophage functions), excluding the possibility that the miR-722-overexpressing line had increased bactericidal activity (Fig. 3-4B). In addition, in both lines, there was an initial drop of neutrophil number upon infection, which later recovered (Fig. 3-4C). This increased resistance coincided with a more robust upregulation of the anti-inflammatory cytokines, including IL-10 and the TGF-β family members (Fig. 3-4D,E). The pro-inflammatory cytokines, including TNF-α, IL-6 and IL-8, were also induced in the miR-722-overexpressing line, but not significantly. Interestingly, *nos2b*, an important pro-inflammatory gene that produces nitric oxide species, was not highly induced. Similar expression changes of *inos2b*, *il-10* and *tgf-β2* were observed in FACS-isolated neutrophils, consistent with neutrophil-restricted overexpression of miR-722 (Fig. 3-4F). Because zebrafish *nos2b* also harbors miR-722-binding sites, we next examined whether *rac2* overexpression mitigates the protective effect elicited by miR-722. Restoring *rac2* expression in the miR-722-overexpressing line increased susceptibility, to levels comparable to the wild-type larvae, from the acute systemic *Pseudomonas* infection (Fig. 3-4G), suggesting that miR-722 protects zebrafish from lethal inflammatory challenge via the suppression of *rac2*. In wild-type larvae, the endogenous level of miR-722 was not upregulated during systemic inflammation (Fig. 3-4H).

We also developed a sterile systemic inflammation model by injecting lipopolysaccharide (LPS) into the zebrafish intravenously. The vector-control-overexpressing larvae succumbed to overinflammation within 6 days post-injection. In comparison, miR-722-overexpressing larvae survived significantly better (Fig. 3-5A). Similar to the changes observed with bacterial infection, upregulation of the anti-inflammatory cytokines was also observed with sterile inflammation (Fig. 3-5B,C).

**Figure 3-4 The miR-722 over-expression line is more resistant to bacterial induced systemic inflammation**

F2 larvae from Tg(lyzC:miR-722/Dendra2)pu6 (miR-722) and Tg(lyzC:miR-722/Dendra2)pu6 (vector) at 3 dpf were injected intravenously with 1000 CFU of Pseudomonas. (A) Mortality, (B) colony forming unit (CFU) and (C) total neutrophil number in the vector or miR-722 lines were documented till 7 days post infection (dpi). One representative experiment of three biological repeats was shown in (A). (B, C) mean ± s.d. (N = 3 biological repeats with 10 larvae at each time point in each group). P value was calculated with Gehan-Breslow-Wilcoxon test. (D, E) Relative abundance of transcripts of pro-inflammatory and anti-inflammatory cytokines at 0h and 8h post infection (hpi). Result was presented as mean ± s.d. (N = 3 biological repeats with 20 larvae in each group). P value was calculated with one-way ANOVA. (F) Neutrophils were sorted from larvae at 8 hpi and the relative transcript levels of indicated genes were quantified. One representative experiment of two independent biological repeats was shown. P value was calculated with paired Student's t-test. (G) Tg(lyzC:miR-722/Dendra2)pu6 (miR-722) was crossed with Tg(mpx:mCherry-2A-*rac2*) (*rac2*) and the offspring were separate into four groups as in Fig. 3A. Mortality was documented till 7 dpi. One representative experiment of three independent biological repeats (n = 20 each group) were shown. P value was calculated with Gehan-Breslow-Wilcoxon test. (H) Relative expression levels of miR-722 before or after intravenous injection with 25ng of LPS or with 1000 CFU of Pseudomonas, mean ± s.d. (N = 3 biological repeats with 10 larvae at each time point in each group). No statistical differences with unpaired one-way ANOVA.

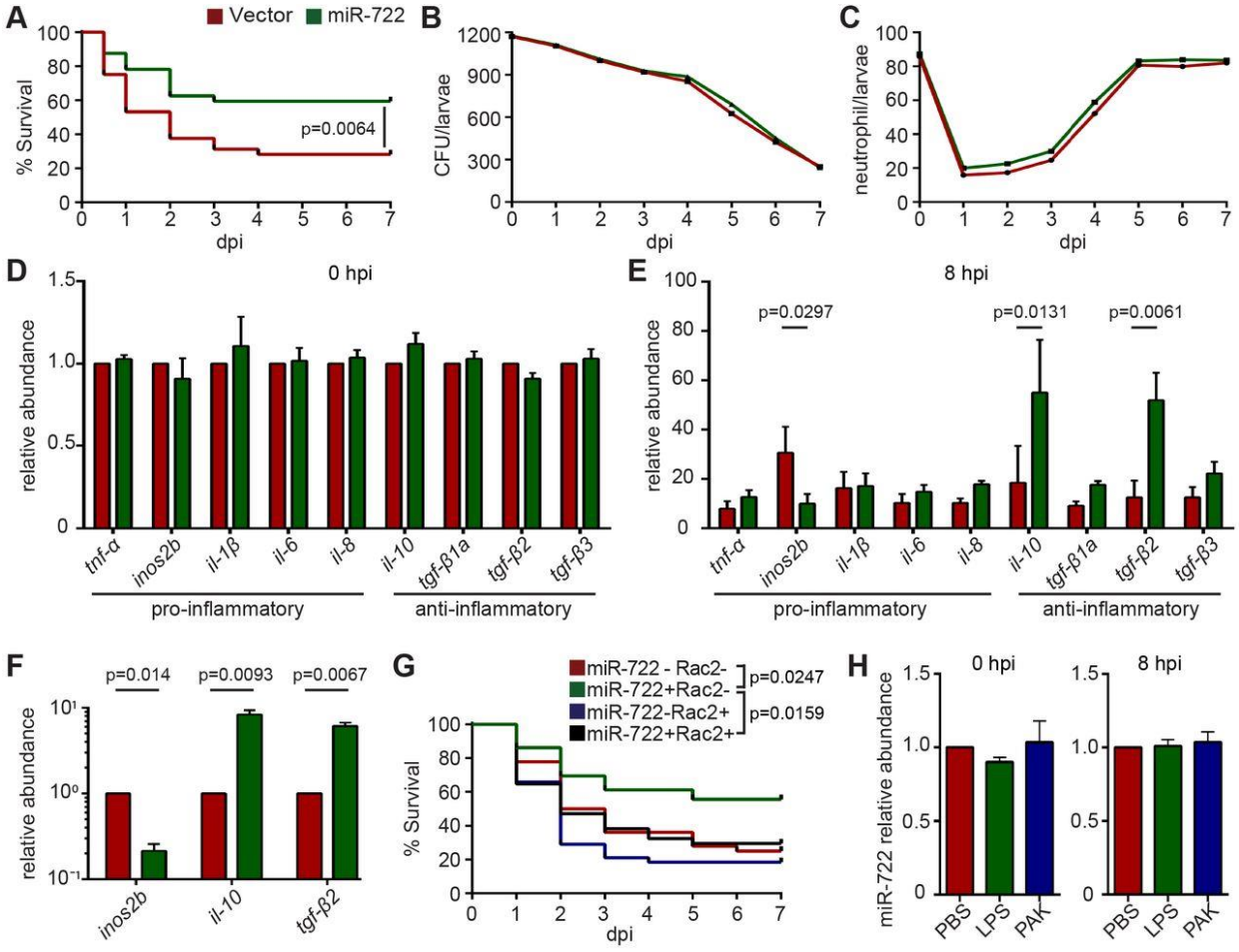
A
Vector
miR-722
% Survival
p=0.0064
dpi
B
CFU/larvae
dpi
C
neutrophil/larvae
dpi
D
0 hpi
relative abundance
tnf-α
inos2b
il-1β
il-6
il-8
il-10
tgf-β1a
tgf-β2
tgf-β3
pro-inflammatory
anti-inflammatory
E
8 hpi
p=0.0297
p=0.0131
p=0.0061
relative abundance
pro-inflammatory
anti-inflammatory
F
p=0.014
p=0.0093
p=0.0067
relative abundance
inos2b
il-10
tgf-β2
G
miR-722 - Rac2-
miR-722+Rac2-
miR-722-Rac2+
miR-722+Rac2+
p=0.0247
p=0.0159
% Survival
dpi
H
0 hpi
8 hpi
miR-722 relative abundance
PBS
LPS
PAK

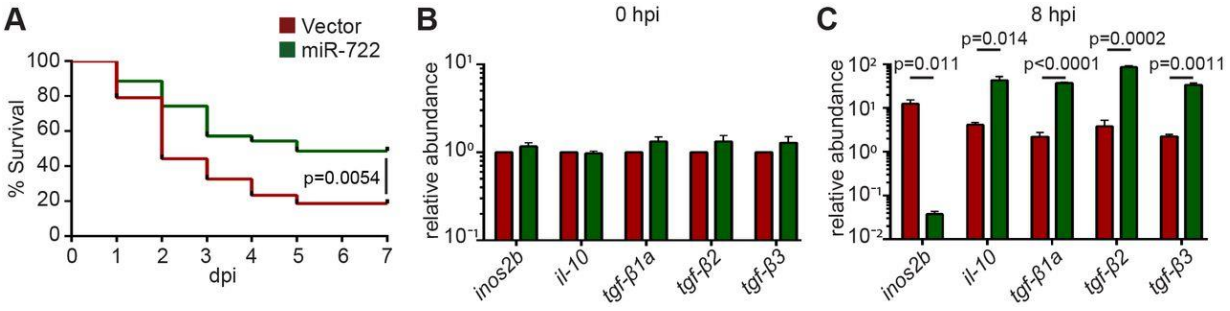


**Figure 3-5 The miR-722 over-expression line is more resistant to sterile systemic inflammation**

F2 larvae at 3 dpf were injected intravenously with 25 ng LPS. (A) Mortality of the vector and miR-722 lines. One representative experiment of three independent biological repeats (n=20 each group) was shown. P value was calculated with Gehan-Breslow-Wilcoxon test. (B-C) Relative abundance of transcripts of pro-inflammatory inos2b and anti-inflammatory cytokines at (B) 0h and (C) 8h post injection (hpi), mean ± s.d. (N = 3 biological repeats with 20 larvae in each group). P value was calculated with one-way ANOVA.

### 3.3.5 MiR-722 mimic protects against sterile inflammation.

Finally, we injected miR-722 mimics into zebrafish embryos at 1-cell stage to deliver miR-722 ubiquitously. As expected, neutrophil recruitment to the injury site was impaired in the larvae receiving miR-722 mimics as compared to the buffer injected while recruitment was more robust in miR-722 inhibitor injected larvae (Fig. 3-6A). We observed significantly increased resistance to lethal LPS challenge in the miR-722 mimic injected larvae, compared with the buffer or the miR-722 inhibitor injected larvae (Fig. 3-6B), suggesting that miR-722 is a potential prophylactic measure in sterile inflammation. MiR-129-5p, which is conserved between zebrafish and human, shares the same seed sequence of miR-722. The seed match is present in the 3'UTRs of both the zebrafish *rac2* and human *RAC2* genes. To test the broader translational value of *rac2* targeting microRNAs, hsa-miR-129-5p mimics were delivered into the zebrafish embryos. Larvae that received the miR-129 mimic were more resistant to LPS challenge than those receiving a non-*rac2*-targeting miR-223 mimic (Fig. 3-6B,C). To demonstrate that the miR-722 mimic also elicits its protective role via inhibiting *rac2* in neutrophils, the mimic was injected into a line that expressed the miR-722 resistant *rac2* in neutrophils. Indeed, the protective role of miR-722 was abrogated in the *rac2* over-expressing line, but not in a line that express the mCherry control in neutrophils (Fig. 3-6D). Taken together, our results suggest that *rac2* inhibiting microRNA mimics can improve the outcome in sterile inflammation.

By contrast, a protective effect from miR-722 mimic in the *Pseudomonas* sepsis model was not observed (Fig. 3-6E). Similar amounts of neutrophils were recruited to localized PAK infection (data not shown). In addition, despite that the anti-inflammatory cytokines were upregulated in infected larvae that received miR-722 mimic, the fold changes were variable between experiments that did not reach statistical significance (Fig. 3-6 F, G). The different host outcome with miR-722 mimic treatment between the sterile and bacterial infection is possibly due to lower than biologically relevant threshold concentration or short-lived effectiveness of the miR-722 mimic to have a sustained effect when battling live organisms that take days to cleared (Fig. 3-4B).

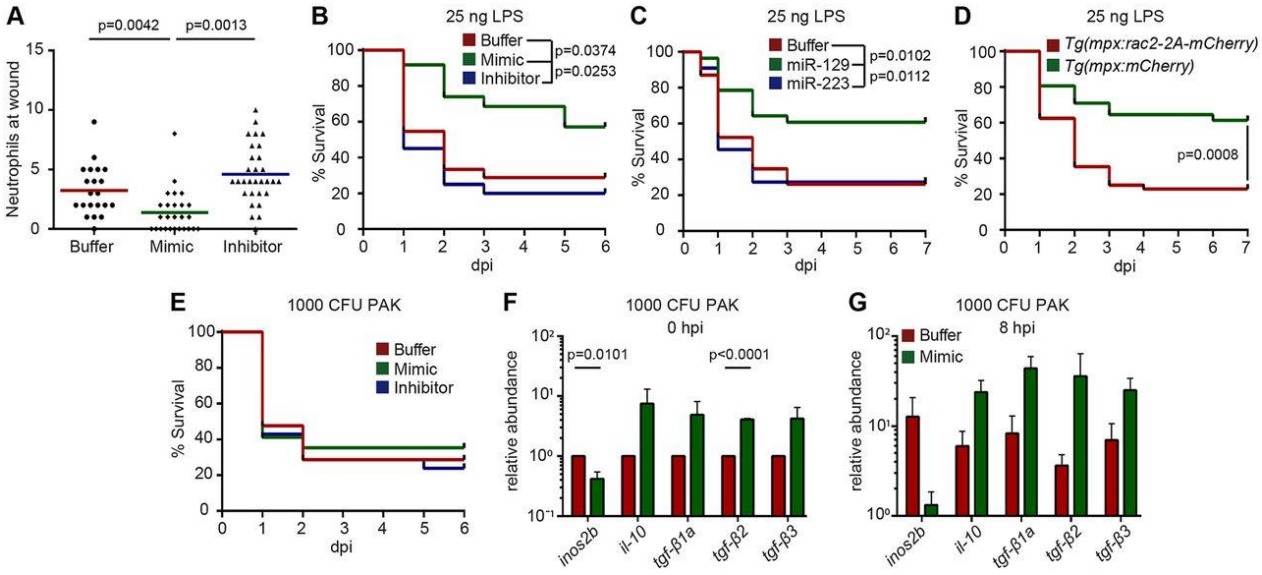


**Figure 3-6 miR-722 mimic reduces neutrophilic inflammation and mortality from systemic LPS challenge**

Embryos were injected with buffer, microRNA mimics, or a miR-722 inhibitor at one-cell stage and experiments were performed with larvae at 2 dpf. (A) Neutrophil recruitment to the injury site at 1 h post tail transection. One representative experiment of three independent biological repeats were shown (n = 20 for each group). P values were calculated with unpaired one-way ANOVA. (B-C) Survival of larvae with (B) buffer, miR-722 mimic, or inhibitor or (C) buffer, miR-129 mimic, or miR-223 mimic upon systemic LPS challenge. One representative experiment of three independent biological repeats (n ≥20 each group) was shown. P values were calculated with Gehan-Breslow-Wilcoxon test. (D) Survival of Tg(mpx:mCherry) and Tg(mpx:mCherry-2A-*rac2*) larvae with miR-722 mimic upon systemic LPS challenge. One representative experiment of three independent biological repeats (n =20 each group) was shown. P value was calculated with Gehan-Breslow-Wilcoxon test. (E) Survival of larvae intravenously injected with PAK at 2 dpf. One representative experiment of three independent biological repeats (n =20 each group) was shown. Not significant as determined with Gehan-Breslow-Wilcoxon test. (F-G) Relative abundance of transcripts of pro-inflammatory inos2b and anti-inflammatory cytokines at (F) 0h and (G) 8h after intravenous injection of 1000 CFU PAK. Results are presented as mean ± s.d. (N = 3 biological repeats with = 20 larvae in each group). P value was calculated with one-way ANOVA.

## 3.4 Discussion

Here we have identified a microRNA, miR-722, that when over-expressed in neutrophils, reduces neutrophil chemotaxis and protects the whole organism from both sterile and non-sterile inflammatory assaults. Our findings are of significant importance as we have identified a leukocyte-specific manner to restrain the systemic inflammatory response and have a direct impact on numerous human diseases, including those directly involving an immune component such as rheumatic arthritis and those that are not obviously linked such as diabetes, neurodegenerative disease and cancer.

Here we have demonstrated that *rac2* is a major target of miR-722 in neutrophils. *Rac2* regulates multiple steps in neutrophil-mediated tissue damage, including reducing neutrophil adhesion to the capillary (causing ischemic damage) and their release of reactive oxygen species and granular contents (major mediators for the secondary organ damage). In light of the detrimental roles neutrophils play, it is not surprising that *rac2* inhibition improves the outcome in our systemic inflammation models. It remains to be determined which is the most critical step in this process. Whether it is myeloipoeisis, neutrophil exit from bone marrow, chemotaxis, adhesion to blood vessel, degranulation or releasing reactive oxygen or nitrile species require further investigation. It certainly is possible that multiple steps have to be spontaneously inhibited to elicit a protective effect in treating undesired inflammation. The therapeutic potential of Rac2 inhibition has not been explored previously, probably due to the difficulty in developing a specific chemical inhibitor for Rac2 that would not inhibit the closely related family member Rac1, which is expressed in all cells and developmentally essential(Duquette & Lamarche-Vane, 2014). Rac1 and Rac2 proteins are very similar in their structure and function, although they harbor different functions in neutrophils (H. Zhang, Sun, Glogauer, & Bokoch, 2009). MicroRNAs can bind to the 3'UTR of their target genes and it is very practical to identify microRNAs that target only *RAC2* but not *RAC1*, making it possible to selectively suppress *RAC2* expression. We have demonstrated that two different *rac2* targeting microRNA mimics are equally potent in zebrafish. Many other microRNAs are predicted to target the *RAC2* gene in humans, but not the *RAC1* gene, for example, miR-6090 and miR-6726 (targetscan), which warrant further characterization.

It is interesting that *Rac2* knockout animals or zebrafish expressing a dominant negative form of Rac2 in neutrophils are more susceptible to infections (Deng et al., 2011b; Roberts et al., 1999; Rosowski et al., 2016). In contrast, miR-722 over-expression in neutrophils protected zebrafish from lethal challenge of *Pseudomonas* infection. This discrepancy is possibly due to the fact that microRNAs are fine-tuners that modulate the protein expression level post transcriptionally. In our study, we observed a partial inhibition of *rac2* expression and impaired/delayed neutrophil chemotaxis. We reasoned that neutrophils still preserve some of the effector functions, yet the magnitude of the inflammation and the bystander tissue damage are decreased which translates into a favorable balance of the pro-inflammatory and anti-inflammatory cytokines that promotes the resolution of inflammation. Along the same line, therapeutic doses and delivery methods of *Rac2* targeting microRNAs have to be carefully determined in humans to elicit the most favorable outcome.

We have selected a clinical strain of *Pseudomonas aeruginosa* for our current study because of its prevalence in human sepsis patients (Gotts & Matthay, 2016) and it is a well characterized systemic infection model in zebrafish (Clatworthy et al., 2009). *Pseudomonas aeruginosa* is an opportunistic pathogen in human, not a natural zebrafish pathogen and it requires a much higher infection dose to cause significant mortality (2000-10000 CFU) in immune competent larvae, compared with natural fish pathogens, such as *Edwardsiella tarda* (van Soest et al., 2011) and *Streptococcus iniae* (Harvie, Green, Neely, & Huttenlocher, 2013). It has long been appreciated that neutrophils cause tissue damage while eliminating bacterial infections (reviewed in (Weiss, 1989)). However, it is difficult to separate these two functions, since similar mechanisms, such as reactive oxygen species, proteases and extracellular traps contribute to both processes. To date, solid evidence that inflammation contributes to mortality in a *Pseudomonas* blood infection model is not available, although it is an attractive hypothesis based on the literature. Our work has associated the improved survival with increased production of anti-inflammatory pre-resolving cytokines, but not with bacterial burden, providing the first evidence that inflammation is relevant to mortality in this model.

There are several recent examples that anti-inflammatory intervention increases zebrafish survival without altering the bacterial burden. The interleukin-1 receptor antagonist anakinra

treatment enhanced zebrafish survival in Shigella flexneri or Burkholderia cenocepacia infection, without affecting the bacterial load (Mazon-Moya et al., 2017; Mesureur et al., 2017). The Myd88 mutant also lived significant longer than the wild-type siblings in Burkholderia cenocepacia infection, with no differences in bacterial burden (Mesureur et al., 2017). In addition to live bacterial infection, we have also used Pseudomonas aeruginosa LPS to induce mortality that is caused by sterile inflammation. We observed similar phenotypes with both live bacteria and a purified bacterial cell wall component, indicating that miR-772 regulates the inflammation process to favor host survival.

So far, reduction of neutrophil numbers has not been associated with increased survival in zebrafish infection models. Several primary neutrophil deficiency models have been established and many are associated with increased susceptibility to infections (reviewed in (Harvie & Huttenlocher, 2015)). In the WHIM and LAD models, neutrophil recruitment to wounding or infection is completely abolished, indicating that neutrophils provide protective immunity and a substantial loss of neutrophil function is detrimental to the host.

A partial reduction of neutrophil number can be achieved by disrupting the GCSFR/Csf3r, using either a morpholino (Liongue, Hall, O'Connell, Crosier, & Ward, 2009) or a recently generated mutant (Pazhakh, Clark, Keightley, & Lieschke, 2017), or with the *Escherichia coli* nitroreductase/metronidazole system (Pisharath, Rhee, Swanson, Leach, & Parsons, 2007).

The GCSFR/Csf3r morphants are more susceptible to *Salmonella* (C. J. Hall et al., 2012) and Chikungunya Virus (Palha et al., 2013). The caveat of this approach is whether GCSFR depletion affects macrophage numbers, especially in older larvae, still needs to be determined. In addition, since Gcsfr-depleted larvae were more susceptible to infection than Runx1-depleted larvae (where both neutrophil and macrophage numbers were reduced) (C. J. Hall et al., 2012), it is possible that GCSFR regulates other aspects of neutrophil biology, not restricted to neutrophil numbers.

The alternative approach for neutrophil depletion using the nitroreductase/ metronidazole system was first performed by Prajsnar *et al* where 50% of neutrophils were depleted without affecting

macrophage numbers (Prajsnar et al., 2012). Although the larvae are more susceptible, neutrophils were discovered as a privileged intraphacyte niche for disseminated *Staphylococcus* infection, highlighting the multifaceted role of this phagocyte. In a more recent study, over 95% depletion of neutrophils did not affect zebrafish survival during *Burkholderia* infection (Mesureur et al., 2017). The caveat of this approach is the risk of non-specific alteration in the immune system caused by un-natural phagocyte death.

Nevertheless, neutrophil depletion has been proven to be beneficial in many murine inflammation models, including infections (reviewed in (Mocsai, 2013)). To be more specific, mouse depleted of FcεRI+ neutrophils were less susceptible to experimental cerebral malaria after infection with *Plasmodium berghei*, without reducing the parasite burden in blood (Porcherie et al., 2011). Our research sets apart from the existing literature that a fine-tuning of neutrophil function, rather than total neutrophil depletion or loss-of-function was achieved.

In summary, we have provided a proof-of-concept strategy in treating conditions in which over-activation of the immune system contributes to disease with microRNAs, particularly those targeting *RAC2* expression. Human neutrophils have an estimated circulatory half-life of up to 90 hours (Pillay et al., 2010; Tak, Tesselaar, Pillay, Borghans, & Koenderman, 2013). Although this measurement may be explained alternatively as the half-life of neutrophil progenitors, a population of older neutrophils survive for several days in the body in other model organisms (Cheretakis, Leung, Sun, Dror, & Glogauer, 2006; Vincent, Chanana, Cronkite, & Joel, 1974). MicroRNAs in human therapeutic settings could at least theoretically be rapid enough to downregulate Rac2 expression in mature neutrophils and/or long-lasting enough to downregulate Rac2 during neutrophil maturation in the bone marrow until their mobilization into the circulation. Due to current technical hurdles that prevent us from effectively delivering miR-772 into neutrophils in the larvae, we have not been able to show the efficacy of miR-722 in treating existing inflammation. Nevertheless, we have demonstrated that miR-722 can be used as a prophylactic measure that alters the overall immune response during systemic inflammation, which may be relevant to conditions in humans such as a means to prevent overt inflammation elicited during organ transplantations. With the combination of a yet-to-be optimized efficient

phagocyte specific delivery system, we provide an alternative concept in restraining unresolving neutrophilic inflammation.

# CHAPTER 4. INDUCIBLE OVEREXPRESSION OF ZEBRAFISH *MICRORNA-722* SUPPRESSES CHEMOTAXIS OF HUMAN NEUTROPHIL LIKE CELLS

## 4.1 Abstract

Neutrophil migration is essential for battling against infections but also drives chronic inflammation. Since primary neutrophils are terminally differentiated and not genetically tractable, leukemia cells such as HL-60 are differentiated into neutrophil-like cells to study mechanisms underlying neutrophil migration. However, constitutive overexpression or inhibition in this cell line does not allow the characterization of the genes that affect the differentiation process. Here we apply the tet-on system to induce the expression of a zebrafish microRNA, *dre*-miR-722, in differentiated HL-60. Overexpression of miR-722 reduced the mRNA level of genes in the chemotaxis and inflammation pathways, including Ras-Related C3 Botulinum Toxin Substrate 2 (RAC2). Consistently, polarization of the actin cytoskeleton, cell migration and generation of the reactive oxygen species are significantly inhibited upon induced miR-722 overexpression. Together, zebrafish miR-722 is a suppressor for migration and signaling in human neutrophil like cells.

## 4.2 Introduction

The neutrophil is the most abundant white blood cell in the circulation and a significant regulator of inflammation. While essential for battling against pathogens, neutrophil activation drives immunopathology in numerous human diseases, including organ transplantation, sepsis, rheumatoid arthritis, diabetes, neurodegenerative disease and cancer (Borregaard, 2010; Nathan, 2006; Soehnlein, Steffens, Hidalgo, & Weber, 2017), although the link of some diseases to the innate immune system is not intuitive. Besides killing pathogens, they communicate with other cells to shape the inflammatory response. For example, neutrophils initiate inflammation by scanning platelets (Sreeramkumar et al., 2014), migrating away from the initial activation site to disseminate inflammation to the lung (Woodfin et al., 2011), priming macrophages by providing DNA in the forms of extracellular traps (Warnatsch et al., 2015) and can directly present antigens to activate T cells (Abi Abdallah et al., 2011; Lim et al., 2015).

Manipulating neutrophil migration and activation is implicated in managing chronic inflammation (Kolaczkowska & Kubes, 2013; Soehnlein et al., 2017). The current challenge in the field is that primary neutrophils are terminally differentiated with a very short life span ex vivo, which excludes the feasibility of genetic manipulation for functional characterization. To model neutrophils, human promyelocytic leukemia HL-60 cells (Pedruzzi et al., 2002) and NB4 cells (Lanotte et al., 1991) are differentiated in culture for 5-7 days into neutrophils-like cells. Gene transduction approaches using either the lenti- or retro-virus are successful in these cell lines, providing a genetically tractable system. However, due to the cell differentiation process, extensive characterization is required to separate the effect of the target genes on cell differentiation and mature cell function. Inducible expression using tet-on (gene expression activated by doxycycline) is widely applied in cancer research and other cell lines. However this technique has not been applied to neutrophil precursor cells.

MicroRNAs (MiRNA) are evolutionarily conserved, non-coding RNAs of ~22 nucleotides that post-transcriptionally regulate gene expression (Fabian & Sonenberg, 2012). miRNAs are master regulators that can simultaneously suppress hundreds of genes and regulate numerous cellular processes and human diseases. miRNA profiles are distinct in human peripheral blood neutrophils (Gantier, 2013; Landgraf et al., 2007; Ward et al., 2011) and activated tissue infiltrating neutrophils (Larsen et al., 2013), suggesting that they are regulated by the inflammation process or tissue environment. On the other hand, only a few miRNAs are functionally characterized in neutrophils (Gurol et al., 2016). In HL-60 cells, miRNA expression changes during cell differentiation (Jian et al., 2011; Kasashima, Nakamura, & Kozu, 2004; Pizzimenti et al., 2009) and after radiation (Liamina et al., 2017) or resveratrol treatment (Ergin, Bozkurt, Cubuk, & Aktas, 2015). Indeed, multiple miRNAs regulate HL-60 growth, differentiation and survival in vitro (Bousquet et al., 2008; H. Chen, Chen, Fang, & Mi, 2010; K. Huang, Dong, Wang, Tian, & Zhang, 2015; Jian et al., 2011; Kawasaki & Taira, 2004; Lin et al., 2015; Sharifi, Salehi, Gheisari, & Kazemi, 2014; Shen et al., 2016; S. L. Wang, Lv, & Cai, 2016; X. S. Wang et al., 2012). On the other hand, reports on how miRNAs regulate differentiated cell function such as migration is scarce. Introduction of synthetic miR-155 and miR-34 mimics into differentiated HL-60 suppressed cell migration but not differentiation (Cao et al., 2017), whereas

depleting miR-155, on the other hand, induced cell differentiation and apoptosis (Liang et al., 2017).

In zebrafish, we have identified a miRNA, miR-722, that when overexpressed in neutrophils, reduces neutrophil chemotaxis and protects the organism from both sterile and non-sterile inflammatory assaults (Hsu et al., 2017a). A hematopoietic specific isoform of the small GTPase, rac2, was identified as a direct target of miR-722. Here, we used the tet-on technique to induce the overexpression of miR-722 in differentiated HL-60 cells and uncovered a similar suppressive function of miR-722 in human neutrophils.

## 4.3 Results

### 4.3.1 Establishing an inducible gene expression system in HL-60

To establish a platform that allows inducible gene expression in HL-60 cells, a lentiviral backbone initially constructed by Dr. David Root (Addgene plasmid # 41395) was selected. It contains all elements to enhance viral production and integration, including a Psi packaging element to facilitate pseudovirus production, RRE and WPRE nuclear exporting elements to enhance integration in the host genome. The puromycin resistant gene and the reverse tetracycline-controlled transactivator is constantly expressed under the control of the PGK promoter. Addition of tetracycline or its close derivative doxycycline induces the binding of the transactivator to the tet responsive element, activating the target gene expression in a dose dependent manner (Figure 4-1A). The microRNA hairpin is cloned into the intron of a fluorescent reporter gene, *Dendra2*. To ensure an effective selection of cells with integration, we measured cell proliferation in the presence of increased doses of puromycin. HL-60 cells treated with 0.5 µg/ml puromycin continued to proliferate for one day before getting killed. Cells treated with 1 or 2 µg/ml puromycin were killed within the first day and continued to die out (Figure 4-1B). Based on this result, we selected the condition of 1 µg/ml puromycin treatment for at least 7 days to ensure the removal of untransduced cells. We then determined the dose of doxycycline differentiated HL-60 cells (dHL-60) can tolerate. Cells at 4 days post-differentiation were treated with increased doses of doxycycline, and cytotoxicity was observed at 3 and 5 µg/ml

concentrations, but not at 1 µg/ml (Figure 4-1C), suggesting that doxycycline at 1 µg/ml is tolerated by dHL-60 cells. Inducible expression of miR-722 in HL-60

We then generated stable HL-60 lines in which the miR-722 or a vector control expression is regulated by the tet responsive element. For simplicity, we refer to them as miR-722 and control lines. After induction, we observed significant increases of the Dendra2 reporter expression with or without DMSO induced differentiation (Figure 4-1D). The experimental flow thus is finalized as depicted in Figure 4-2A. To confirm that miR-722 expression is indeed induced, we quantified the levels of the precursor transcript and the mature microRNA. Since miR-722 is absent in human and HL-60 cells, we detected 10,000 fold increase of the mature miR-722 level in the miR-722 line, but not in the control line (Figure 4-2B). The majority of the cells from both lines expressed a detectable level of the Dendra2 reporter (Figure 4-2C). General microRNA biogenesis was not affected, since the level of two other mature microRNA, MIR-223 and LET7 in dHL-60 was not affected. Additionally, cell viability or differentiation (as measured by surface expression of annexin V binding and CD11b expression) was not affected by overexpression of miR-722 in dHL-60 cells (Figure 4-2C, D).

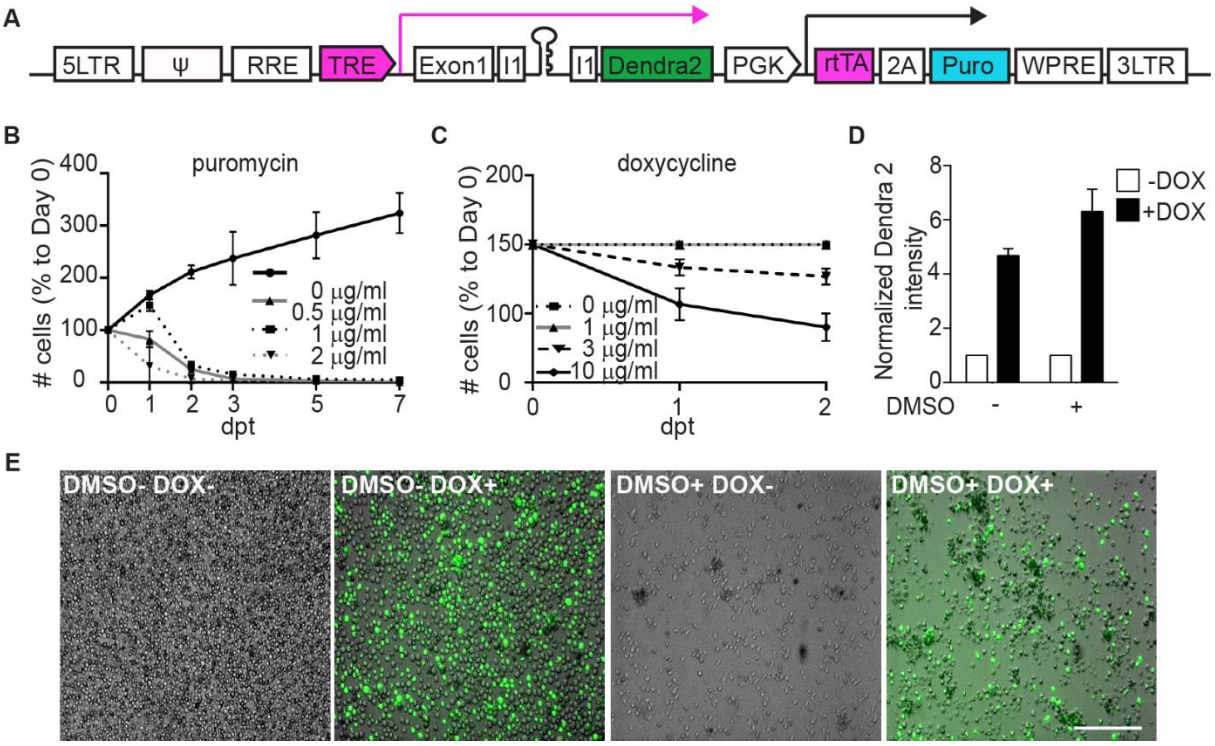


**Figure 4-1 Inducible expression of a miRNA together with a reporter gene in HL-60 cells.**

(A) Schematics of the plix 4.03 vector modified for the inducible expression of a microRNA and a reporter. The miRNA hairpin resides in the intron of the Dendra2 reporter (green) under the control of a doxycycline response element (TRE, magenta and magenta arrow). The puromycin resistant cassette (Puro, cyan) linked with the reverse tetracycline-controlled transactivator (rtTA, magenta) was driven by a constitutively active PGK promoter (black arrow). Flanking elements including the Psi packaging element, REE and WPRE nuclear exporting elements enhance integration in the host genome. (B) Proliferation of HL-60 cells in the presence of the indicated doses of puromycin. Cell numbers were normalized to day 0; dpt: days post treatment. (C) Survival of differentiated HL-60 cells in the presence of the indicated doses of doxycycline starting 4 day post differentiation. Cell numbers were normalized to day 0; dpt, days post treatment. (B, C) Results are averaged of three independent experiments and shown as mean ± s.d.. (D, E) Quantification (D) and representative images (E) of a stable line of HL-60 cells transduced with the construct depicted in (A) with/without differentiation (± DMSO) or induction (± DOX). Scale bar: 200 µm. (D) Mean fluorescence intensity was normalized with cell number and fold increase compared to uninduced controls are shown. Results are presented as mean ± s.d. from three independent experiments. **, $p < 0.01$, ****, $p < 0.0001$, Mann–Whitney test.

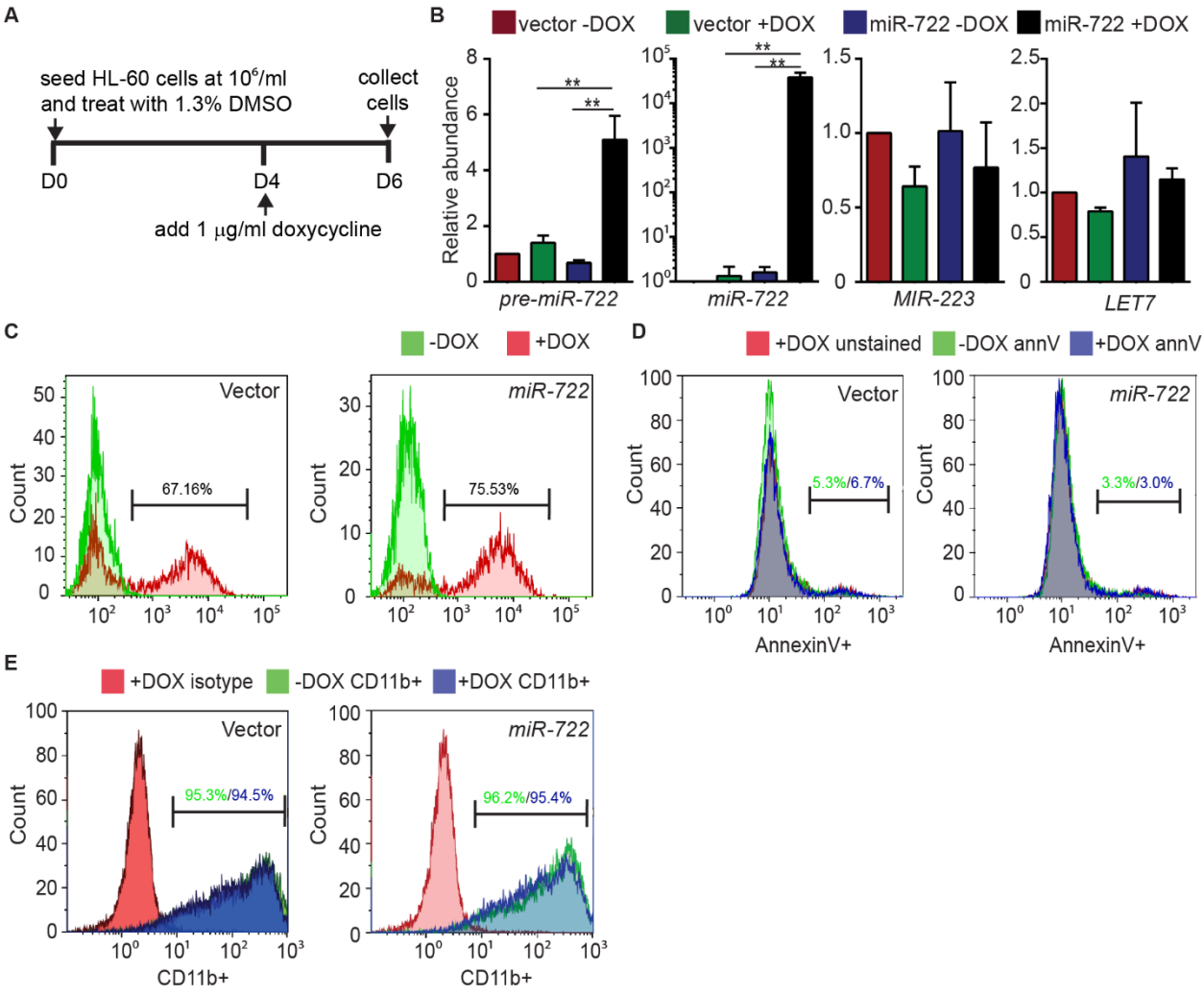


**Figure 4-2 Specific induction of miR-722 does not affect HL-60 differentiation or survival.**

(A) Schematics of the experimental flow for the inducible expression of a microRNA and a reporter. The stable HL-60 cell lines over expressing miR-722 or the vector control were differentiated with 1.3 % DMSO for 6 days and treated with 1 μg/ml doxycycline from day 4 or left untreated. (B) Levels of pre-miR-722, miR-722, MIR-223, and LET7 in vector or miR-722 expressing dHL-60 lines ± doxycycline (DOX). Messenger RNAs were normalized to GAPDH and miRNAs were normalized to U6. Results are presented as mean ± s.d. from three independent experiments. **, $p < 0.01$, Mann–Whitney test. (C, D, E) Histogram of Dendra 2 expression (C), Annexin V staining (D), and CD11b expression (E) of vector and miR-722 expressing dHL-60 with or without DOX. Positive cells are gated based on –DOX (C), unstained (D) or isotype control (E) and percentages of positive cells are labeled in corresponding color. Images are representative of three independent experiments.

### 4.3.2 miR-722 suppresses cell migration and signaling related genes in HL-60

To characterize the signaling pathways that are regulated by miR-722, we performed RNAseq of the miR-722 and the control lines. Since lentiviral mediated DNA integration is random, although with some preferences (Deichmann et al., 2007; Felice et al., 2009), we compared the gene expression changes in both lines ± Dox to minimize the artifact associated with insertion sites. Induction of miR-722 in dHL-60 resulted in significant dis-regulation of transcripts (FDR-adjusted p-value < 0.01 & FC < $-\log_2 1.8$, see Methods for details) as shown in Figure 4-3A. There were more down-regulated differentially expressed genes (DEGs) (n = 1943) identified than up-regulated ones (n = 632), which is consistent with the function of microRNAs as suppressors of gene expression. Among the down-regulated transcripts, the human orthologues of predicted miR-722 targets in zebrafish were significantly enriched (p = 0.003) (Figure 4-3B), while miR-722 targets were depleted in up-regulated gene group (p = 0.031). The results indicate an evolutionary conservation of miR-722 targets. Under the same cutoffs used in comparison in the miR-722 line, no significant dysregulation was identified in the control line ± Dox, where only 15 transcripts had p < 0.01 without multiple-test correction (Figure 4-4). Moreover, fold changes of genes in the control line were presented in a symmetric way between up- and down-regulation. The different patterns between miR-722 and vector suggests that the effect of miR-722 was not due to the reporter gene expression alone. Via enrichment analysis on Gene Ontology and KEGG pathways, we found that the down regulated transcripts were significantly over-represented in pathways regulating cell migration, chemotaxis, signaling and inflammation (Figure 4-3C, D, E and F). To validate the RNAseq results, we quantified the relative expression level of several transcripts in the chemotaxis pathway and indeed all were significantly downregulated upon the induction of miR-722, but not the reporter gene alone (Figure 4-5A). Among the selected genes, the chemokine receptor encoding gene, *Fpr1*, harbors miR-722 binding sites in its 3´UTR and is a potential direct target. Since *rac2* is a direct target of *miR-722* in zebrafish, we tested whether human *RAC2* is also a miR-722 target. We detected significant down regulation of *RAC2* at both the transcript and protein levels upon miR-722 overexpression (Figure 4-5A, B). Indeed, a 7mer-m8 site (complementarity at nt 2-7 and mismatch at nt8) was present in the *RAC2* 3´UTR (Figure 4-5C). In a luciferase reporter assay, specific suppression by miR-722 was observed with the wild-type *RAC2* 3´UTR, but not the mutated 3´UTR lacking the

seed binding site (Figure 4-5D, E), confirming that *RAC2* is a direct target of miR-722 in human cells.

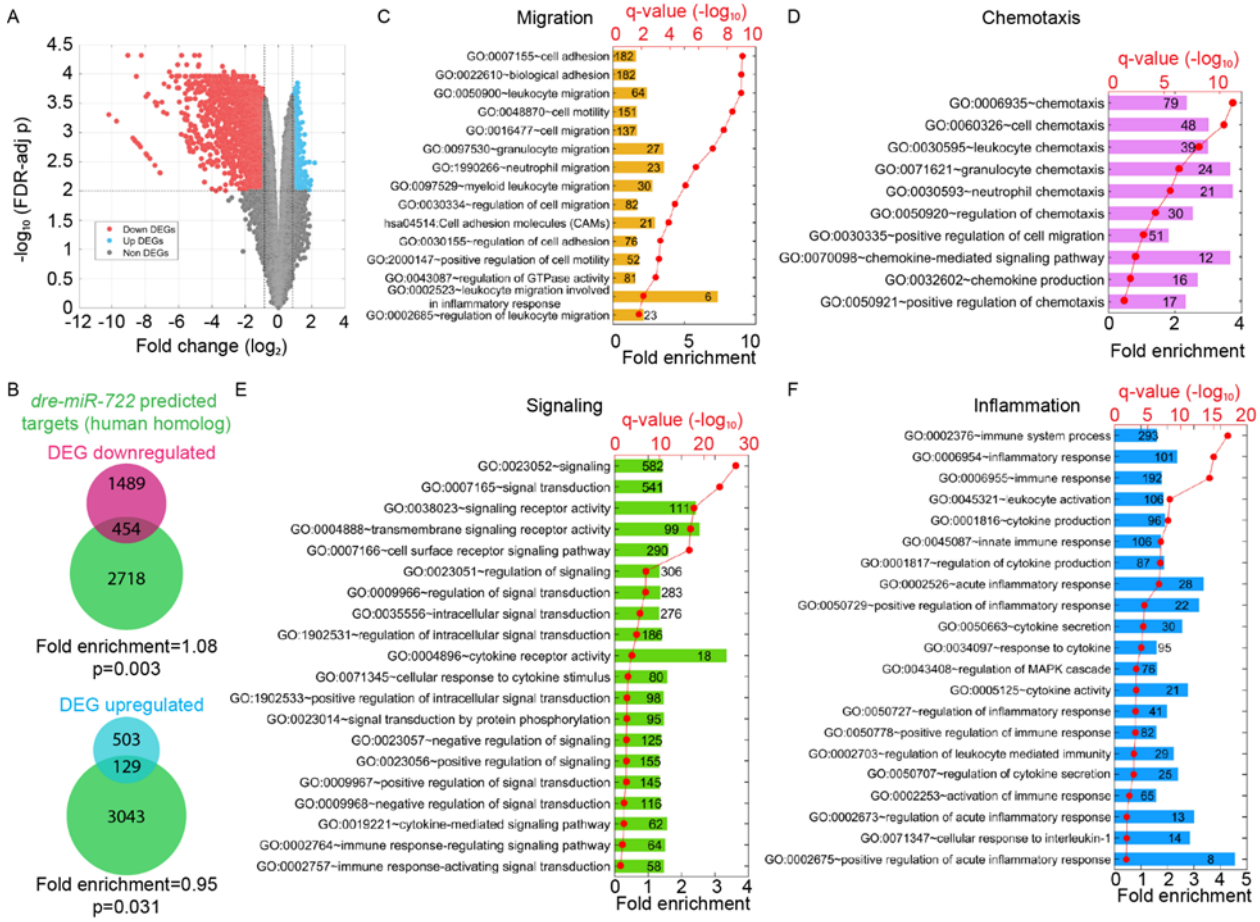


**Figure 4-3 miR-722 overexpression suppresses the expression of cell signaling and migration related genes in dHL-60**

(A) Volcano blot of DEGs with significant changes in expression upon doxycycline induced miR-722 expression. Red: down-regulated differentially expressed genes (DEGs); cyan: up-regulated DEGs. (B) Significant enrichment of human homologues of miR-722 predicted target genes in the down-regulated DEGs. $P < 0.003$, hypergeometric distribution. (C, D, E, F) Clusters of the genes in the pathways significantly altered upon miR-722 overexpression. Number of the genes with significant expression changes in each pathway are labeled in each column. q-values, FDR-adjusted p-values as described in the Methods section.

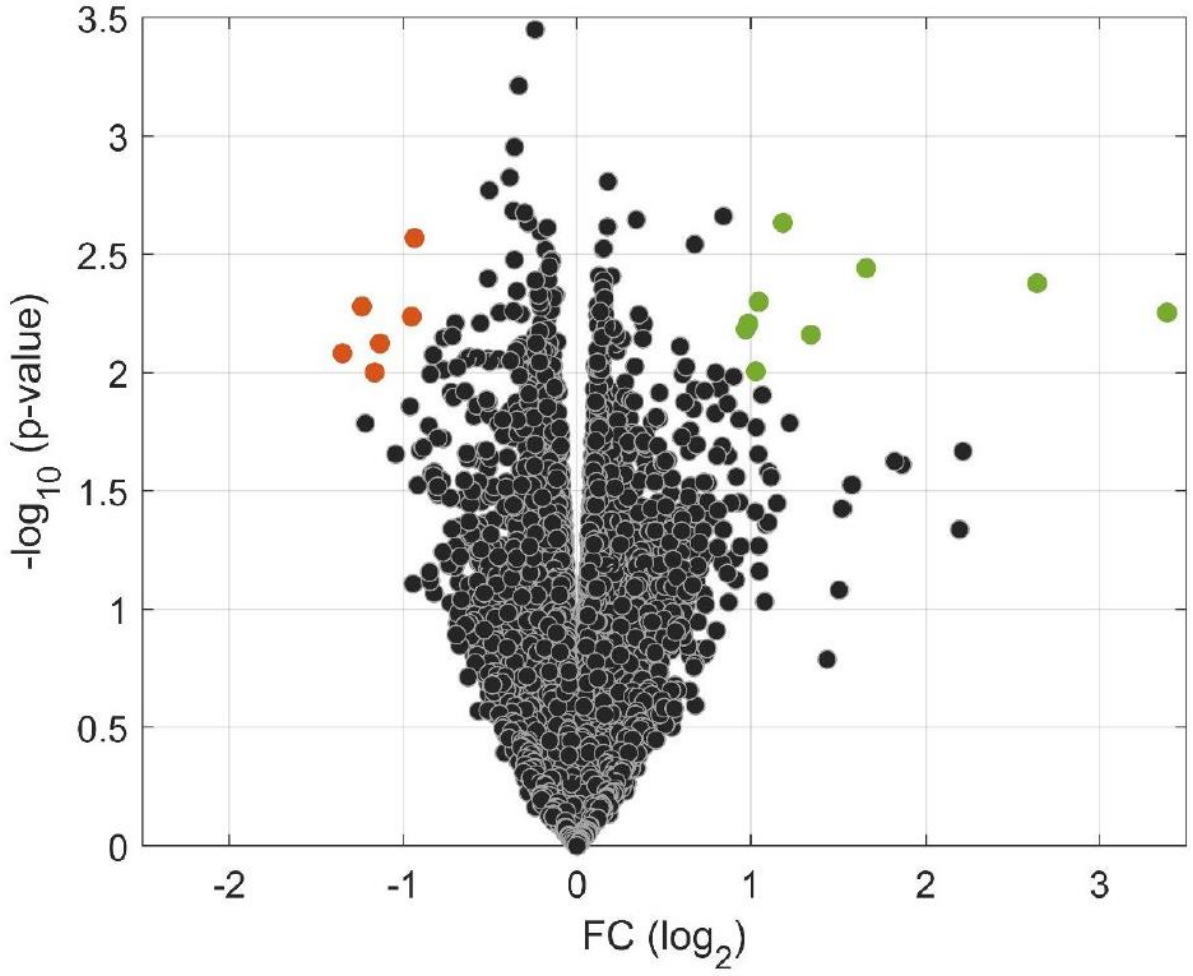


**Figure 4-4 Inducible expression of Dendra2 in dHL-60 has minimal impact on the transcriptome**

Volcano blot of DEGs with significant changes in expression upon doxycycline induced Dendra2 expression. Orange: down regulated DEGs; green: up regulated DEGs.

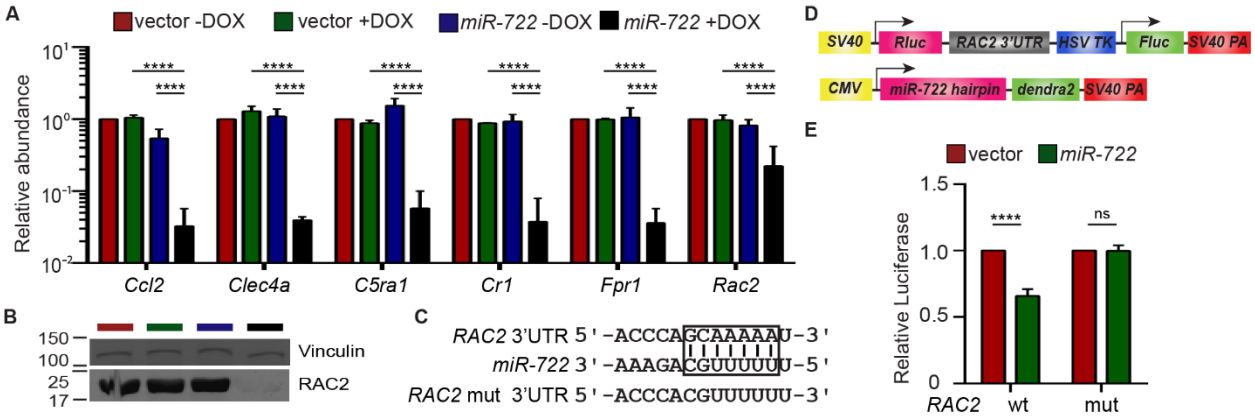


**Figure 4-5 RAC2 is a direct target of miR-722**

(A) Relative abundance of mRNA levels of indicated genes in vector or miR-722 expressing dHL-60 ± DOX. Results are presented as mean ± s.d. from three independent experiments. ****, $p < 0.0001$, Sidak's multiple comparisons test. (B) Immunoblot of RAC2 in vector or miR-722 expressing dHL-60 cells ± DOX. Vinculin is used as a loading control. The blot was cut in half and probed with two different primary antibodies. (C) Alignment of miR-722 seed sequence and the 7mer-m8 seed binding site in the *RAC2* 3´UTR which is then mutated for the reporter assay in (E). (D) Schematics of the constructs used for the luciferase reporter assay. Wild-type or mutated *RAC2* 3´UTR were cloned downstream of a renilla luciferase gene. A firefly luciferase gene on the same plasmid was used as a normalization control. mir-722 or vector hairpin was cloned into a mammalian expression plasmid for expression. (E) Selective suppression of renilla luciferase activity by miR-722 through binding to the seed sequence in *RAC2* 3´UTR. Results are presented as means ± s.d. from three independent experiments. ****, $p < 0.0001$, Mann–Whitney test.

### 4.3.3 miR-722 suppresses chemotaxis and generation of reactive oxygen species in HL-60

RAC2 is essential for actin polymerization and migration in neutrophils (Carstanjen et al., 2005). The chemoattractant N-Formylmethionine-leucyl-phenylalanine (fMLP) induces rapid neutrophil polarization with lamellipodia in the front and a tail in the back (Srinivasan et al., 2003). In dHL-60 cells overexpressing miR-722, the formation of the lamellipodia and the establishment of polarity were significantly inhibited (Figure 4-6A, B). We then measured chemotaxis of the miR-722 line using two independent assays. Cells were allowed to migrate towards fMLP in a chemotaxis slide. miR-722 overexpressing cells displayed a significant defect in velocity but not in directionality, compared with the vector control or the miR-722 expressing line without doxycycline mediated induction (Figure 4-6C-E). Consistently, miR-722 overexpression suppressed cell transwell migration (Figure 4-6F). In addition to the regulation of the cytoskeleton, RAC2 also regulates the activation of the NADPH oxidase and thus the generation of reactive oxygen species (ROS) in human neutrophils (Dusi, Donini, & Rossi, 1996). Upon miR-722 overexpression, the dHL-60 cells secreted significantly reduced amounts of hydrogen peroxide in the culture media when stimulated with phorbol 12-myristate 13-acetate or fMLP (Figure 4-7). The reduced chemotaxis and generation of ROS are consistent with a reduced RAC2 level in the cells, although it is possible that the downregulation of other miR-722 targets also contributes to these phenotype.

**Figure 4-6 MiR-722 overexpression suppresses dHL-60 chemotaxis**

(A, B) Representative fluorescence images (A) and quantification of polarized polymerization of actin (B) of vector or miR-722 expressing dHL-60 ± DOX after fMLP (100 nM) stimulation. Magenta, phalloidin; blue, DAPI; green: dendra2. Scale bar: 10 μm. (B) Results are presented as mean ± s.d. from three independent experiments. ****, $p<0.0001$, Sidak's multiple comparisons test. (C) Representative images and tracks of dHL-60 cells expressing either vector (left) or miR-722 with (right) and without (middle) doxycycline toward fMLP. Scale bar: 200 μm. (D, E) Quantification of velocity (D) and directionality (E) of dHL-60 cells during 2D chemotaxis. Results are representative of three independent experiments. ****, $p < 0.0001$, Sidak's multiple comparisons test. (F) Transwell migration of vector or miR-722 expressing dHL-60 cells towards fMLP. Results are presented as mean ± s.d. from three independent experiments. **, $p < 0.01$; ***, $p<0.001$, Sidak's multiple comparisons test

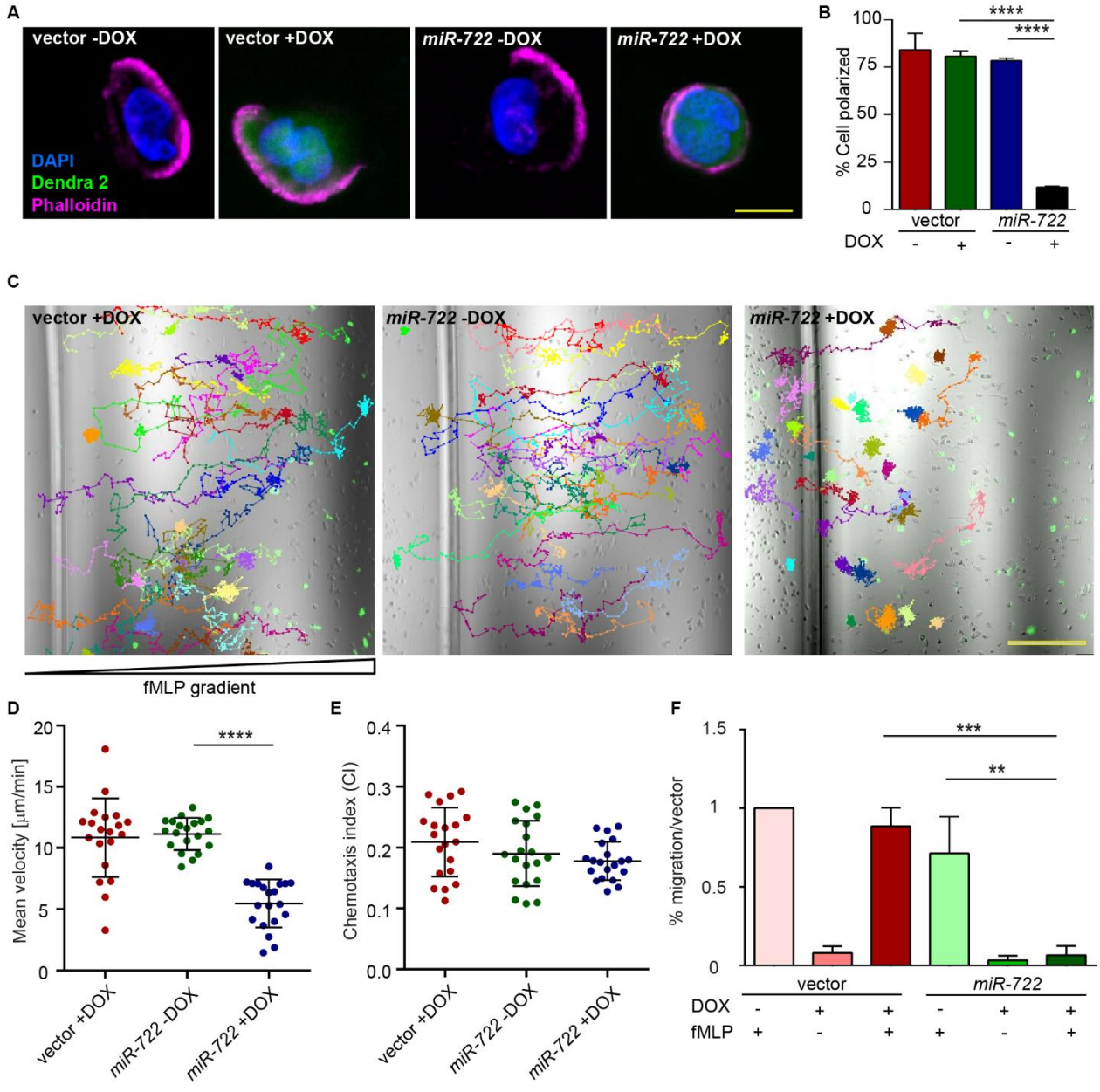
A
vector -DOX
vector +DOX
miR-722 -DOX
miR-722 +DOX
DAPI
Dendra 2
Phalloidin
B
% Cell polarized
100
75
50
25
0
****
****
vector
miR-722
DOX
- + - +
C
vector +DOX
miR-722 -DOX
miR-722 +DOX
fMLP gradient
D
Mean velocity [µm/min]
20
15
10
5
0
****
vector +DOX
miR-722 -DOX
miR-722 +DOX
E
Chemotaxis index (CI)
0.4
0.3
0.2
0.1
0.0
vector +DOX
miR-722 -DOX
miR-722 +DOX
F
% migration/vector
1.5
1
0.5
0
***
**
vector
miR-722
DOX - + + - + +
fMLP + - + + - +

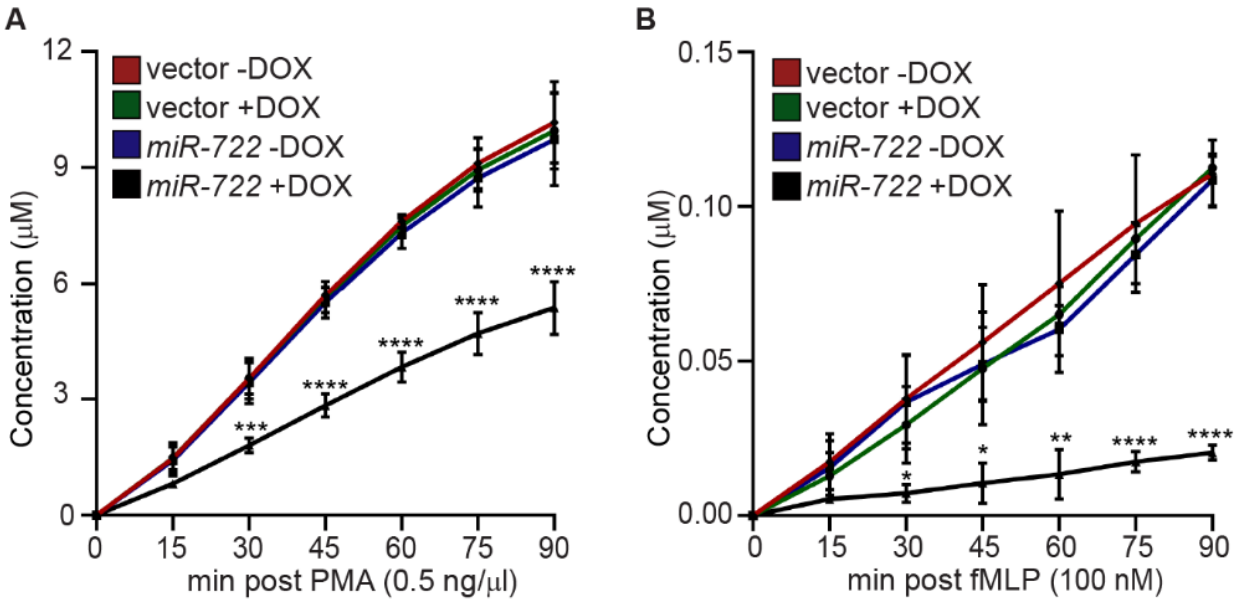


**Figure 4-7 MiR-722 overexpression suppresses ROS production in dHL-60**

(A and B) Secretion of hydrogen peroxide from vector or miR-722 expressing dHL-60 stimulated with PMA (0.5 ng/ml) (A) or fMLP (100 nM) (B). Hydrogen peroxide levels were measured every 15 minutes for 90 minutes. Results are presented as mean ± s.d. of three independent experiments. , *, $p<0.05$, **, $p < 0.01$; ***, $p<0.001$, ****, $p<0.0001$, Sidak's multiple comparisons test.

## 4.4 Discussion

Here we have applied the tet-on system in differentiated HL-60 (dHL-60) cells and uncovered an evolutionally conserved role of miR-722 in suppressing neutrophil migration and signaling.

To our knowledge, it is the first application of the tet-on system in dHL-60 cells. Tet-on and tet-off system is favored in biomedical research because acute depletion or overexpression is more faithfully in reflecting the target gene function. The caveat of chronic depletion or overexpression is the possible compensatory expression of other off-target genes and altered overall cell physiology, which will complicate the result interpretation. An additional challenge with using dHL-60 cell model to study neutrophil function is the required differentiation process. It is essentially impossible to study genes that would affect cell differentiation without an inducible system. The dose of doxycycline dHL-60 could tolerate (1 µg/ml) is significantly lower than that in other cell lines (10 µg/ml). Although doxycycline is a broad spectrum antibiotic that inhibit bacterial protein synthesis, it also inhibits protein synthesis in eukaryotic mitochondria and thus can impair cell metabolism and cause cell death (Chatzispyrou, Held, Mouchiroud, Auwerx, & Houtkooper, 2015; Moullan et al., 2015). The mechanism underlying this increased sensitivity is not clear but could be due to increased uptake and/or decreased efflux of doxycycline in dHL-60. In addition, doxycycline or its degradation products may be highly toxic to dHL-60s. We have optimized our protocol where the cytotoxicity of doxycycline is not observed. Cell proliferation, survival and differentiation were not affected by doxycycline treatment. We expect that our method is equally applicable to the inducible expression of other RNA species such as shRNAs in dHL-60, providing a platform for acute depletion of endogenous proteins to evaluate their biological significance in mature cell function without affecting the differentiation process.

Fundamental biological processes, such as cell proliferation and migration, are conserved through evolution. It is estimated that ~60 % of human protein-coding genes are under selective pressure to maintain miRNA seed binding sites in the 3´UTR which are conserved in vertebrates (Friedman, Farh, Burge, & Bartel, 2009). Data compiled from previous microRNA sequencing experiments suggest that miR-722 is intergenic and predominantly produce a mature 3p strand that harbors binding sequences of specific genes, e.g. *Rac2* (www.miRbase.org). It is not

surprising that both human *RAC2* and zebrafish *Rac2* are direct miR-722 targets. It is intriguing that miR-722 expression in human HL-60 cells resulted in a down-regulation of genes that are significantly enriched for the orthologues of the predicted zebrafish targets. The significantly altered pathways provides explanation of the anti-inflammatory effect of this microRNA in zebrafish as its overexpression protected zebrafish against lethal inflammatory assault (Hsu et al., 2017a).

Rac2 plays a principal role in regulating the actin cytoskeleton, chemotaxis and signaling. Rac2 is required for neutrophil motility and chemotaxis (Yoo et al., 2010), retention in the hematopoietic tissue (Deng et al., 2011b), generation of super oxide ions during infections (Jonzon & Bindslev, 1991) and degranulation of primary granules (Abdel-Latif et al., 2004). The therapeutic potential of Rac2 suppression in controlling inflammation has not been explored. Currently, a Rac2 specific inhibitor is not available and a complete Rac2 inhibition would result in primary immune deficiency and poor wound healing (D. A. Williams et al., 2000). Although the therapeutic potential of miR-722 is not clear without further characterization, our work here has characterized the first microRNA that targets human *RAC2* and established miR-722 as a suppressor for neutrophil migration and signaling.

The miR-722 is not detected in human until now, suggesting that miR-722 itself might not be evolutionarily conserved between zebrafish and human. The miR-129-5p share the same seed sequence (positions 2-8 of the mature miRNA) with miR-722 (with a predominant 3p strand). The miR-129 gene in human however produces both the 5p and 3p strand product. It is likely that miR-129 targets additional sets of genes with two functional microRNA strands. We used bioinformatics to generate the list of predicted human targets of miR-129-5p and human orthologous genes of predicted miR-722 targets in zebrafish. No enrichment of the predicted human miR-129-5p targets was observed in the miR-722 down-regulated genes (Figure 4-3A), suggesting that miR-722 mediated gene suppression is not completely dependent on seed matching. Alternatively, the indirect targets of miR-722 are dominant in the downregulated gene list. Interestingly, the human orthologues of miR-722 targets are significantly enriched in the miR-722 downregulated gene list (Figure 4-3B). In addition, the human orthologues of miR-722

targets are over-represented in the predicted miR-129-5p targets ($p = 0.017$), suggesting an evolutionary conservation of the miR-722 binding sites.

In conclusion, we reported for the first time the method for inducible expression of microRNAs in HL-60 s, which allows studying mature cell function without interfering with cell differentiation. Additionally, we provide evidence that zebrafish miR-722 can suppress human RAC2 gene and cell migration. Nevertheless, further research is still needed to evaluate the therapeutic potential of this microRNA in inflammatory ailments.

# CHAPTER 5. PHENOTYPICAL MICRORNA SCREEN REVEALS A NONCANONICAL ROLE OF CDK2 IN REGULATING NEUTROPHIL MIGRATION

## 5.1 Abstract

Neutrophil migration is essential for inflammatory responses to kill pathogens, however excessive neutrophilic inflammation also lead to tissue injury and adverse effects. To discover novel therapeutic targets that modulate neutrophil migration, we performed a neutrophil-specific microRNA overexpression screen in zebrafish and identified eight microRNAs as potent suppressors of neutrophil migration. Among those, miR-199 decreases neutrophil chemotaxis in zebrafish and human neutrophil-like cells. Intriguingly, in terminally differentiated neutrophils, miR-199 alters the cell cycle-related pathways and directly suppresses cyclin-dependent kinase 2 (cdk2), whose known activity is restricted to cell cycle progression and cell differentiation. Inhibiting CDK2 but not DNA replication, disrupts cell polarity and chemotaxis of zebrafish neutrophils without inducing cell death. Human neutrophil-like cells deficient with CDK2 fail to polarize and display altered signaling downstream of the formyl peptide receptor. Chemotaxis of primary human neutrophils is also reduced upon CDK2 inhibition. Furthermore, miR-199 overexpression or CDK2 inhibition significantly improves the outcome of lethal systemic inflammation challenges in zebrafish. Our results therefore reveal previously unknown functions of miR-199 and CDK2 in regulating neutrophil migration and provide new directions in alleviating systemic inflammation.

## 5.2 Significance Statement

Neutrophil mediated inflammation is often detrimental to the host, thus new methods to mitigate inflammation while preserving immunity are needed. We performed a genetic screen in zebrafish with neutrophil specific overexpression of individual microRNAs and from there, identified miR-199 which can mitigate neutrophil migration and relieve systemic inflammation without generating an overall immunocompromised state. The primary mechanism of action of MiR-199 is through direct suppression of CDK2, a canonical cell cycle regulator, in the context of terminally differentiated neutrophils. In addition, miR-199 overexpression and CDK2 inhibition

dampened human neutrophil migration. Together our work suggests miR-199 and CDK2 as new targets for treating inflammatory ailments and introduces a new avenue of the function for CDK2 outside the cell cycle regulation.

## 5.3 Introduction

Neutrophils are the first cells recruited to an immune stimulus stemming from infection or sterile injuries via a mixture of chemoattractant cues (Sadik, Kim, & Luster, 2011). In addition to eliminating pathogens, neutrophils coordinate inflammation by activating and producing inflammatory signals in the tissue and in some cases cause adverse tissue damage. Over amplified or chronic neutrophil recruitment directly leads to autoimmune diseases including rheumatic arthritis, diabetes, neurodegenerative diseases, and cancer (Nathan, 2006). Dampening neutrophil recruitment is thus, a strategy to intervene in neutrophil-orchestrated chronic inflammation (Soehnlein et al., 2017). Despite intensive research over the past several decades, clinical studies targeting neutrophil migration have been largely unsuccessful, possibly due to the prominent redundancy of adhesion receptors and chemokines (Remick et al., 2001; M. R. Williams, Azcutia, Newton, Alcaide, & Luscinskas, 2011a). Additional challenges also lie in the balance of dampening detrimental inflammation while preserving immunity (Sonego et al., 2016). Furthermore, neutrophil migration is governed by spatially and temporally complex dynamic signaling networks (Mocsai, Walzog, & Lowell, 2015), adding yet another layer of complexity in studying them. Immune cells use both mesenchymal migration (adhesive migration on substrate) and amoeboid migration (actin protrusion driven with weak substrate interaction) to infiltrate tissue using distinct signaling molecules (Lammermann et al., 2008; Yamahashi et al., 2015). Thus, extensive research is required to understand the machinery regulating neutrophil recruitment and the interactions between signals and chemotactic cues, which will lead to the development of exogenous inhibitors for clinical use.

MicroRNAs (miRNAs) are short (20-22 nucleotides) conserved non-coding RNAs that are epigenetic regulators of the transcriptome. By binding primarily to the 3´UTRs of their target transcripts and recruiting the RNA-induced silencing complex, miRNAs down-regulate gene expression (Friedman et al., 2009). miRNAs are generally fine-tuners that suppress gene expression at modest levels, and also master regulators that target the expression of a network of

genes (Gurol et al., 2016). Recently, miRNAs and anti-miRNAs have been used in clinical trials to treat cancer and infection (Rupaimoole & Slack, 2017). In addition, they have been used as screening tools to identify the underlying mechanisms of diseases and cell behavior (Kim, Vinayagam, & Perrimon, 2014; Olarerin-George, Anton, Hwang, Elovitz, & Hogenesch, 2013). In immune cells, an overexpression screen of microRNA was performed to identify microRNAs that regulate B cell tolerance (Gonzalez-Martin et al., 2016). In neutrophils, the functions of the highly expressed microRNAs miR-223 (Johnnidis et al., 2008) and miR-142 (Fan et al., 2014b) have been well characterized. However, other miRNAs and their targets as regulators of neutrophil recruitment remain largely unknown. The absence of this knowledge potentially leads to missed opportunities in harnessing microRNAs and their targets in restraining neutrophilic inflammation.

The zebrafish is a suitable model organism to study neutrophil biology. They have an evolutionarily conserved innate immune system, including the phagocytes and their signaling molecules including miRNAs (Fan et al., 2014b; W. Q. Zhou et al., 2018). The transparent property of zebrafish embryos enables noninvasive imaging of neutrophil behavior under physiological conditions (Lieschke & Currie, 2007; Sullivan & Kim, 2008). Additionally, high fecundity and established genetic tools make zebrafish an ideal platform for genetic screens and drug discovery (Takaki et al., 2012).

We have previously established a system to express individual miRNAs in zebrafish neutrophils to assess their function in vivo (Hsu et al., 2017b). Here we performed a miRNA overexpression screen and identified miR-199 as a novel regulator of neutrophil chemotaxis. Through miR-199 target analysis, we identified the canonical cell cycle related gene cdk2 as a previously unrecognized regulator of neutrophil migration. Overexpression of miR-199 or inhibition of cdk2 in neutrophils improved survival upon infection and sterile inflammatory challenges. Our results were further validated in human neutrophil-like cells and primary human neutrophils, supporting the evolutionary conservation of miR-199 and Cdk2 in vertebrae neutrophil biology. These discoveries expand our current understanding of neutrophil migration and suggests a novel strategy to manage neutrophilic inflammation.

## 5.4 Results

### 5.4.1 Identification and characterization of miRNAs that regulate neutrophil recruitment

As a first step to understand microRNA mediated gene regulation in zebrafish neutrophils, we sequenced microRNAs in zebrafish neutrophils sorted from 3 day old embryos. Consistent with previous reports in humans and mouse, miR-223 and miR-142 were among the microRNAs highly expressed in zebrafish neutrophils (Fig. 5-1A and B). As a control, we sequenced microRNAs in the immotile epical keratinocytes and indeed detected a distinct profile (Fig.5-1C, D). We next performed a functional genetic screen to identify a set of miRNAs when overexpressed, moderate neutrophil migration (Fig. 5-2). Forty-one microRNAs with lower expression levels compared with the whole embryo or keratinocytes were selected. Individual miRNA candidates were cloned and transiently expressed specifically in zebrafish neutrophils, together with a fluorescent reporter gene. The miRNAs whose overexpression resulted in a > 50% reduction in neutrophil recruitment to infection sites were selected for further validation. We generated transgenic zebrafish lines stably expressing each of the nine miRNAs that passed the initial screen. To rule out potential artifacts associated with the transgene integration sites, more than two independent founders were obtained for each line. In eight out of the nine lines, we found a significant decrease in neutrophil recruitment to ear infection sites, regardless of the choice of the founder (Fig. 5-1E). Similarly, neutrophil recruitment was also significantly reduced in all eight lines in a tail fin amputation inflammation model (Fig. 5-1F), demonstrating that the microRNA phenotypic screen was successful in identifying microRNAs that could modulate neutrophil migration. A microRNA characterized in our previous work, miR-722, served as a positive control (Hsu et al., 2017b). Among the eight newly identified miRNAs, miR-146 is a known suppressor of immune cell activation (Taganov, Boldin, Chang, & Baltimore, 2006), whereas the other eight miRNAs have not been characterized for their roles in neutrophil migration. The overexpression of miR-199-3 resulted in the most robust inhibition in both models (Fig. 5-1E-J) and therefore was chosen for further characterization.

**Figure 5-1 Identification of miRNAs that suppress neutrophil recruitment in vivo**

(A) Differentially expressed genes (DEGs) of microRNAs in zebrafish neutrophils compared to whole embryo. (B) Quantification of selected miRs that were differentially expressed in neutrophils. (C) Differentially expressed genes (DEGs) of microRNAs in zebrafish epical keratinocytes compared to whole embryo. (D) Quantification of selected miRs that were differentially expressed in keratinocytes. Assay was done with 3 biological repeats each containing cells sorted from at least 100 larvae/repeat. Result is presented as mean ± SD, Holm-Sidak test. (E) Neutrophil recruitment to the infected ear in transgenic lines with neutrophil specific overexpression of individual microRNAs. Results were normalized to number of neutrophils recruited in the vector expressing control lines in each individual experiment (set as a factor of 1). (F) Neutrophil recruitment to tail fin transection sites in transgenic lines as described in C. (G, H) Representative images (G) and quantification (H) of neutrophils recruited to infected ear in vector or miR-199-3 overexpressing zebrafish line. Scale bar, 100 μm. (I, J) Representative images (I) and quantification (J) of neutrophils recruited to tail fin transection sites in vector or miR-199-3 overexpressing zebrafish line. Scale bar, 200 μm. (G-J) Assays were done with at least 2 individual founders with 3 biological repeats each containing 25 fish per group. Result is presented as mean ± s.d., Kruskal–Wallis test.

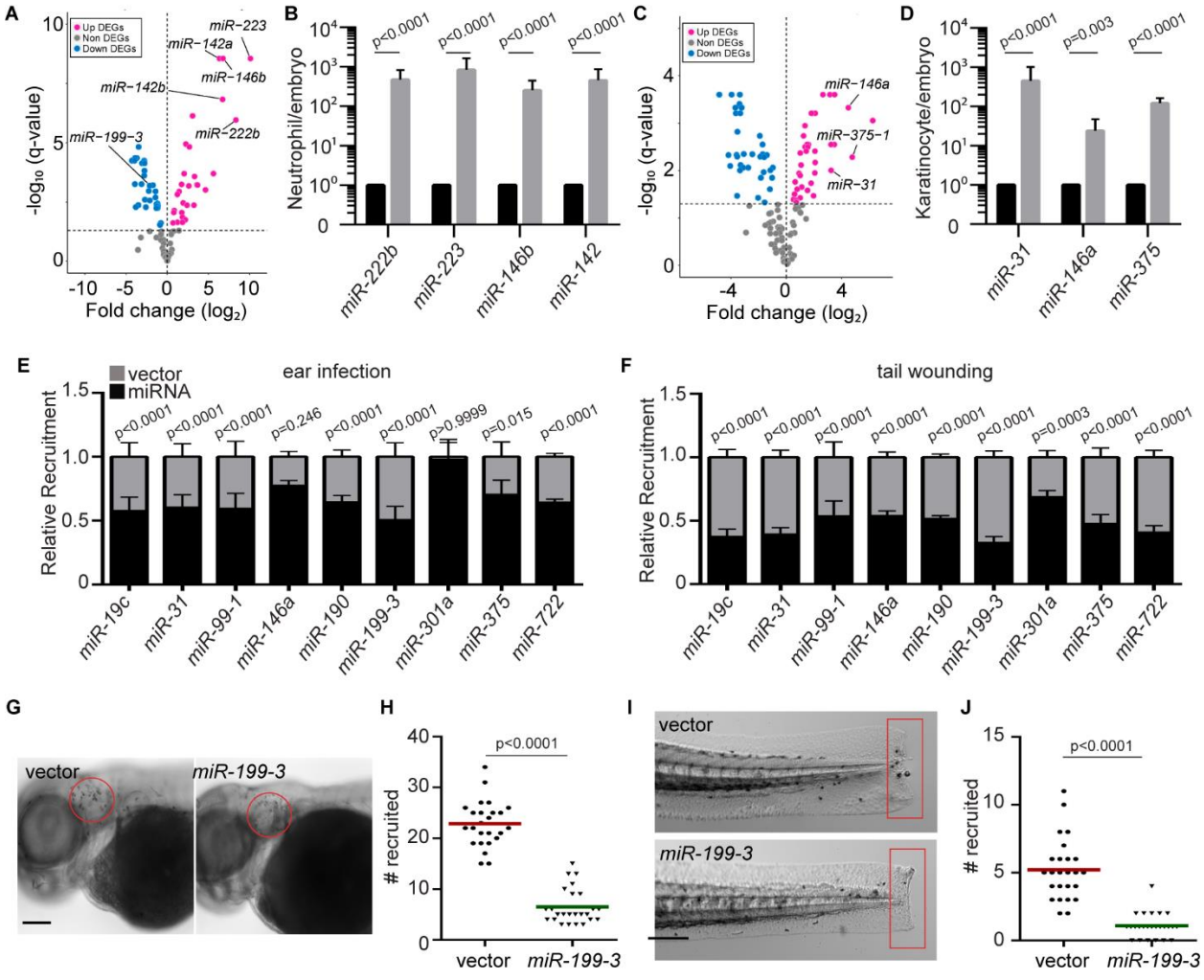
A
Up DEGs
Non DEGs
Down DEGs
miR-223
miR-142a
miR-146b
miR-142b
miR-222b
miR-199-3
-log10 (q-value)
Fold change (log2)
B
Neutrophil/embryo
p<0.0001
miR-222b
miR-223
miR-146b
miR-142
C
Up DEGs
Non DEGs
Down DEGs
miR-146a
miR-375-1
miR-31
-log10 (q-value)
Fold change (log2)
D
Karatinocyte/embryo
p<0.0001
p=0.003
p<0.0001
miR-31
miR-146a
miR-375
E
ear infection
vector
miRNA
Relative Recruitment
p<0.0001
p<0.0001
p<0.0001
p=0.246
p<0.0001
p<0.0001
p>0.9999
p=0.015
p<0.0001
miR-19c
miR-31
miR-99-1
miR-146a
miR-190
miR-199-3
miR-301a
miR-375
miR-722
F
tail wounding
Relative Recruitment
p<0.0001
p<0.0001
p<0.0001
p<0.0001
p<0.0001
p<0.0001
p=0.0003
p<0.0001
p<0.0001
miR-19c
miR-31
miR-99-1
miR-146a
miR-190
miR-199-3
miR-301a
miR-375
miR-722
G
vector
miR-199-3
H
p<0.0001
# recruited
vector
miR-199-3
I
vector
miR-199-3
J
p<0.0001
# recruited
vector
miR-199-3


**Figure 5-2 MicroRNA screen experimental design**

(A) Each of the miR candidate gene is cloned in the intron of a green fluorescence reporter, driven by a neutrophil specific lyzC promoter. The plasmid is injected into 1-cell stage zebrafish embryos to induce expression of miR in a subset of neutrophils. (B) A representative picture of a bacterial infection which induces neutrophil recruitment to the otic vesicle. (C) Decreased neutrophil recruitment due to the overexpression miR-199-3. An inhibition of 50% neutrophil infiltrating into the ear indicates a positive hit.

### 5.4.2 miR-199-3 overexpression inhibits neutrophil motility and chemotaxis

To characterize the zebrafish lines *Tg(lyzC:* miR-199-3-*dendra2)*$^{pu19}$ and *Tg(lyzC:vector-dendra2)*$^{pu7}$, hereby referred as miR-199 and vector lines, we first isolated neutrophils from these lines and performed miRNA RT-qPCR to confirm the mir-199overexpression in the miR-199 line (Fig. 5-3A). The levels of two abundant neutrophil miRNAs, miR-223 and let-7e, were not affected, demonstrating that the overexpression did not disrupt physiological microRNA levels. Total neutrophil numbers in embryos were comparable between the two lines, suggesting that the observed decreased neutrophil recruitment was not an artifact of reduced amount of neutrophils (Fig. 5-3B, C). In addition to the defective recruitment to inflammatory sites, the velocity of neutrophil spontaneous motility in the head mesenchyme was significantly decreased in the mir-199 line (Fig 5-3D and E), whereas their directionality was not affected (Fig. 5-3F). The sequences of the mature zebrafish and human miR-199-5p isoforms are identical (Fig. 5-4D). We therefore sought to determine whether MIR-199 inhibits human neutrophil migration. We used MIR-100, whose overexpression did not result in any phenotype in the initial screen, as a negative control. We expressed human MIR-199a, MIR-100 or the vector alone under the control of a Tet Responsive Element in HL-60 cells, a myeloid leukemia cell line that can be differentiated into neutrophil-like cells as our model (Hsu et al., 2019b; Jacob, Leport, Szilagyi, Allen, Berttand, et al., 2002) (Fig. 5-5A). MIR-100 and MIR-199 were individually induced in the respective lines without affecting cell differentiation, cell death or the expression of two other miRNAs, MIR-223 and LET-7 (Fig. 5-3G and Fig. 5-5B-D). The differentiated (dHL-60) cells were then allowed to migrate towards N-Formylmethionyl-leucyl-phenylalanine (fMLP) in transwells. Only the cells overexpressing MIR-199, but not the vector control or cells overexpressing MIR-100, displayed significant defects in chemotaxis (Fig. 5-3H). Together, our results show that overexpression of MIR-199 inhibits neutrophil migration in both zebrafish and human cell models.

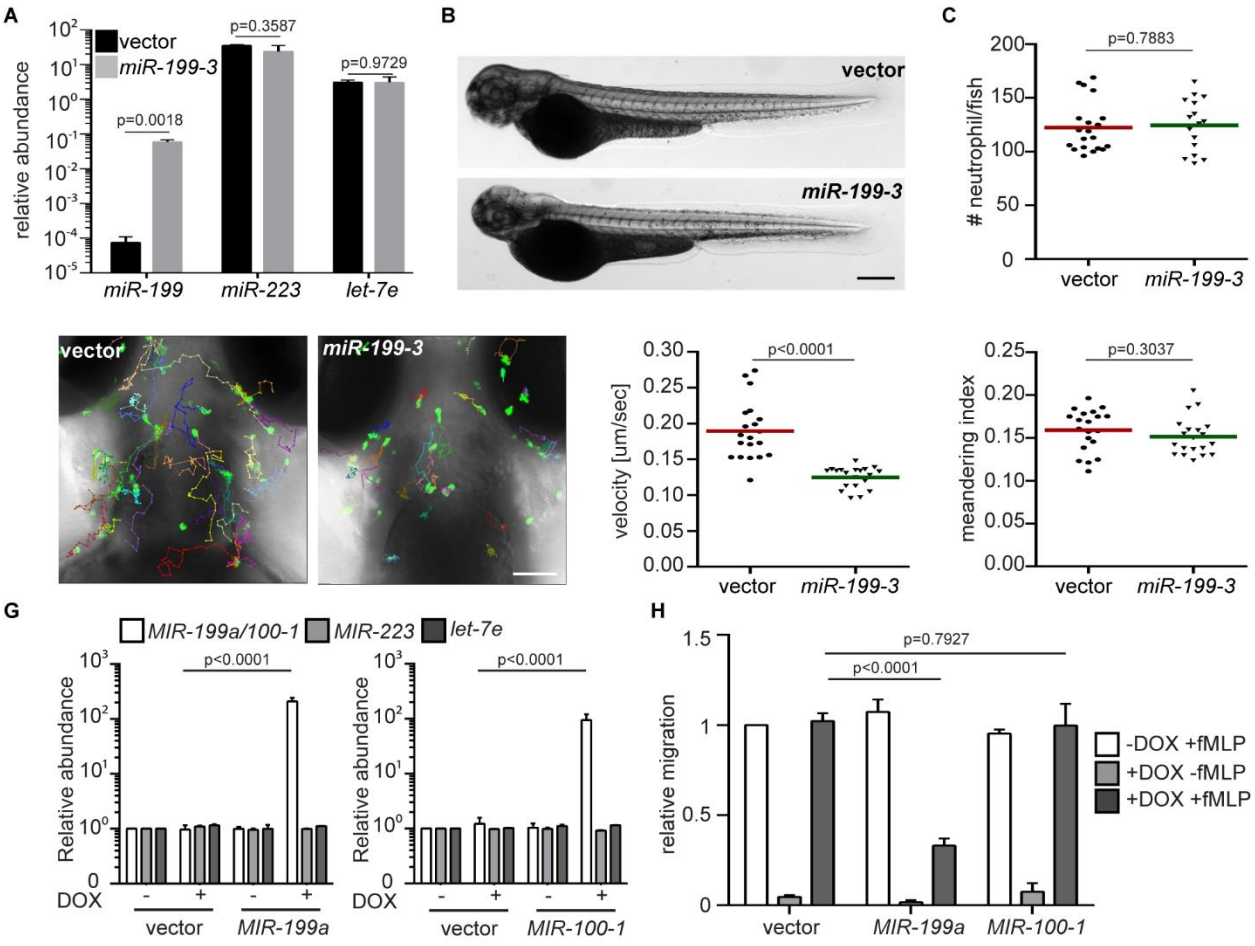


**Figure 5-3 *miR-199-3* overexpression reduces neutrophil migration in zebrafish and human**

(A) Quantification of miR-199, miR-223 and let-7e levels in neutrophils sorted from the vector or miR-199-3 zebrafish lines. Neutrophils were isolated from two adult kidney marrows from two different founders. Result are normalized to u6 expression levels and presented as mean ± s.d., Holm-Sidak test. (B, C) Representative images (B) and quantification (C) of total neutrophils in vector or miR-199-3 zebrafish lines. Scale bar, 500 µm. Assays were done with 3 individual founders with 3 biological repeats each containing 20 fish per group. Result from one representative experiment is shown as mean ± s.d., Mann–Whitney test. (D-F) Representative images (D), velocity (E), and meandering index (F) of neutrophil motility in vector or miR-199-3 zebrafish lines. Scale bar, 100 µm. 3 embryos each from three different founders were imaged and quantification of neutrophils in one representative video is shown. Kruskal–Wallis test. (G) Quantification of MIR-100/199, MIR-233 and LET-7E in dHL-60 cell lines with/without induced expression of the vector control or MIR-100/199. Result from three independent experiments are normalized to U6 expression levels and presented as mean ± s.d., Holm-Sidak test. (H) Transwell migration of dHL-60 cells with/without induced expression of the vector control, MIR-199or MIR-100 toward fMLP. Results are presented as mean ± s.d., from three independent experiments and normalized to vector –DOX +fMLP, Kruskal–Wallis test

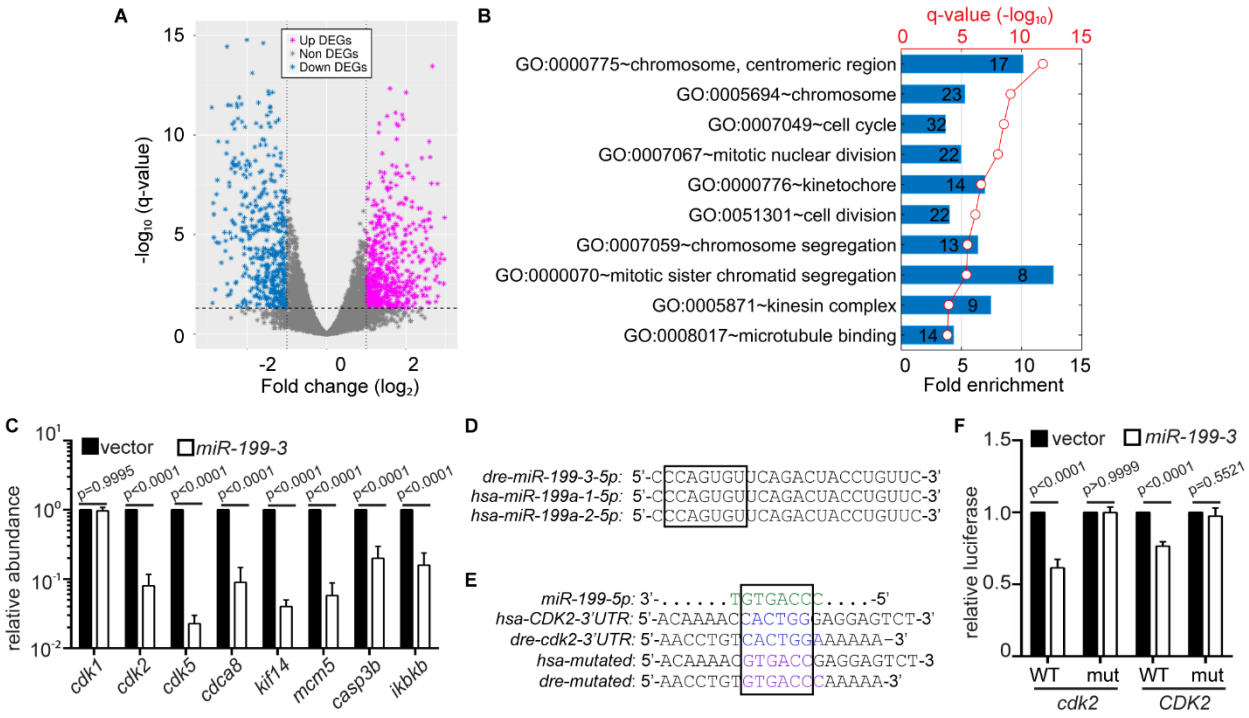


**Figure 5-4 *miR-199-3* overexpression suppresses the expression of *Cdk2* in neutrophils**

(A) Volcano blot of DEGs with significant expression changes in miR-199 expressing neutrophils. Cyan: down-regulated differentially expressed genes (DEGs); Magenta: up-regulated DEGs. (B) Pathway analysis of genes downregulated by miR-199 in neutrophils. (C) Quantification of the transcript levels of downregulated genes in neutrophils sorted from the vector or miR-199-3 zebrafish line (at least 100 embryos per group/repeat). Results from three independent experiments are normalized to *rpl32* and presented as mean ± s.d., Holm-Sidak test. (D) Alignment of mature human and zebrafish miR-199-5p sequences. (E) Alignment of miR-199-5p and predicted miR-199 binding sites in human and zebrafish *CDK2* 3´UTR. (F) Suppression of Renilla luciferase expressing via binding to both zebrafish and human CDK2 3´UTRs by miR-199. Results from three independent experiments are normalized to firefly luciferase and presented as mean ± s.d., Kruskal–Wallis test.

**Figure 5-5 Characterization of dHL-60 cell lines with miR overexpression induced after cell differentiation**

(A) Construct for inducible miRNA expression. The miRNA and a dendra2 reporter (green) is under the control of TRE, Tetracyclin response element (red). The PGK promoter drives constitutive expression of puromycin resistance gene (cyan) and the rtTA, reverse tetracycline-controlled transactivator (red). (B) Cell populations gated for downstream cell profile analysis and transwell quantification. (C) Doxycycline mediated induction in the vector, miR-199, or miR-100 expressing dHL-60 lines. Cells without doxycycline mediated induction were used as a baseline. Percentage of cells with dendra2 level above the baseline are shown. (D) Surface CD11b levels in vector, miR-199, or miR-100 expressing dHL-60 cells. Undifferentiated cells or differentiated cells stained with an isotype control were used as a baseline. Percentage of cells with CD11b levels above the baseline with or without doxycycline mediated induction are shown. (E) Annexin V staining in the total cell population (excluding debris) of vector, miR-199, or miR-100 expressing dHL-60 cells. An unstained live sample is used to determine the baseline. Percentage of cells with AnnexinV levels above the baseline with or without doxycycline mediated induction are shown. (B-E) One representative experiment of three independent trials is shown.

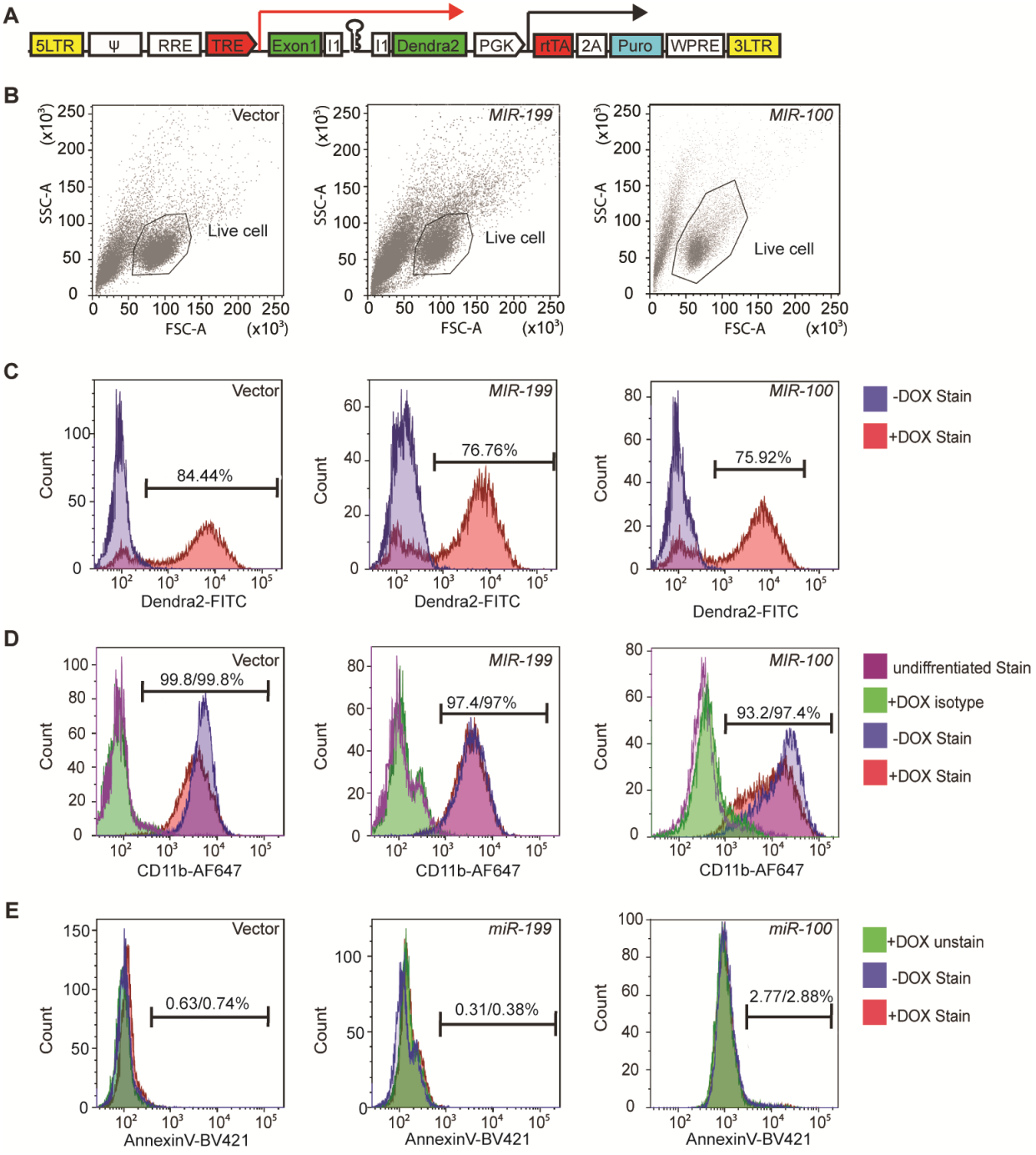
A
5LTR
Ψ
RRE
TRE
Exon1
I1
I1
Dendra2
PGK
rtTA
2A
Puro
WPRE
3LTR
B
Vector
MIR-199
MIR-100
SSC-A (x10³)
FSC-A (x10³)
Live cell
C
Count
Dendra2-FITC
84.44%
76.76%
75.92%
-DOX Stain
+DOX Stain
D
CD11b-AF647
99.8/99.8%
97.4/97%
93.2/97.4%
undiffrentiated Stain
+DOX isotype
-DOX Stain
+DOX Stain
E
AnnexinV-BV421
0.63/0.74%
0.31/0.38%
2.77/2.88%
miR-199
miR-100
+DOX unstain
-DOX Stain
+DOX Stain

### 5.4.3 miR-199 suppresses the expression of cell cycle-related genes including cdk2

To understand the underlying molecular mechanism of how miR-199 regulates neutrophil migration, neutrophils from the miR-199 or vector lines were isolated and their transcripts subjected to RNAseq. Since microRNAs generally suppress the expression of target transcripts (He & Hannon, 2004), we focused on the 512 genes significantly repressed by miR-199. The top 10 pathways associated with the downregulated transcripts were related to cell cycle processes (Fig. 5-4A and B). This result was surprising because neutrophils are known to be terminally differentiated, non-proliferative, and have exited the cell cycle (Lahoz-Beneytez et al., 2016). To validate the RNAseq results, we selected five genes, *cdk2, cdk5, cdca8, kif14,* and *mcm5,* and confirmed their reduced transcript levels in the miR-199-overexpressing neutrophils using RT-qPCR (Fig. 5-4C). The zebrafish orthologue of IKBKB, a known target of human MIR-199 (R. Chen et al., 2008) and a critical component in the NF-κB pathway, was also downregulated, supporting the conservation of microRNA-target interactions in zebrafish. The level of cyclin dependent kinase 1 (*cdk1*) mRNA was not altered. Among the down regulated cell cycle genes, the 3´UTRs of both human and zebrafish CDK2 contain predicted binding sites for miR-199-5p while the protein sequence of CDK2 is more than 90% identical between the two species, showing a high degree of conservation (Fig. 5-4D). In addition, among the 69 downregulated genes in the top 10 pathways (Fig. 5-4B), 36 of which (52.1%) have interactions with *cdk2*, presenting a significant enrichment ($p = 2.87\times10^{-32}$) over the background of 4.1% (326 *Cdk2* interacting genes out of 7927 genes expressed in zebrafish neutrophils) (string-db.org). On the contrary, *cdk5*, despite its downregulation upon miR-199 overexpression, is not a classical cell cycle related gene, and does not have significant interactions with other downregulated genes. To demonstrate the direct targeting of *cdk2* mRNAs by miR-199-5p, we performed dual-luciferase reporter assays. miR-199 significantly reduced the relative luciferase activity controlled by both the human and zebrafish *cdk2* 3´UTRs but did not show the repression of luciferase activity when the predicted binding sites were mutated (Fig. 5-4E, F). These results indicate that miR-199 suppresses classical cell cycle pathways in neutrophils and could directly target *cdk2* in both zebrafish and humans.

### 5.4.4 Pharmacological inhibition of Cdk2 decreases neutrophil motility and chemotaxis

CDK2 is expressed and active in human neutrophils (Rossi et al., 2006b), but its function in neutrophils was previously unknown as CDK2 is traditionally thought to be involved in regulating G1/S phase in the cell cycle (Malumbres & Barbacid, 2009), where neutrophils have exited the cell cycle and are terminally differentiated. To test whether *cdk2* regulates neutrophil migration, we used NU6140 (Pennati et al., 2005), a selective CDK2 inhibitor, with at least 10 fold selectivity over other CDKs. At a concentration of 100 μM, NU6140 did not affect zebrafish survival or neutrophil numbers (Fig. 5-6). As a control for inhibiting cell cycle progression and DNA replication, we used a mixture of Aphidicolin and hydoxyurea (ApH), as previously reported (Fukuhara et al., 2014; L. X. Zhang, Kendrick, Julich, & Holley, 2008) to uncouple the role of Cdk2 from DNA replication. Neutrophil recruitment to the infected ear (Fig. 5-7A, B) or tailfin amputation sites (Fig. 5-7C, D) as well as neutrophil motility (Fig. 5-7G-I) were significantly reduced only by the Cdk2 inhibition, recapitulating the phenotypes caused by miR-199 overexpression. As a control, Cdk2 inhibition did not affect total neutrophil numbers in the fish (Fig. 5-7E, F). To increase our confidence of the results obtained with pharmacological Cdk2 inhibition, two additional Cdk2 inhibitors (Bhattacharjee, Banks, Trotter, Lee, & Archer, 2001) were used. A CDK2 selective inhibitor CTV313 and a pan-CDK inhibitor roscovitine also blocked neutrophil motility and recruitment in inflammation models (Fig. 5-8). A previous report showed that high doses and prolonged treatment of roscovitine could lead to neutrophil apoptosis (Rossi et al., 2006a). To rule out the possibility that the reduced migration resulted from the acute inhibition of CDK2 was due to cell apoptosis, we washed out the reversible inhibitors CTV313 and roscovitine after neutrophil motility was reduced. Neutrophil motility recovered after the removal of the inhibitors (Fig. 5-9), indicating that CDK2 inhibitor treatments do not result in terminal apoptosis. We then tested whether the neutrophils under investigation had indeed exited the cell cycle. No cell division was observed during wounding or infection (Fig. 5-10A and B), suggesting that neutrophil division is a rare event. Additionally, less than 3% of the neutrophils in adult kidney marrow were in the S or G2 phase of the cell cycle (Fig. 5-10C-E). Because *cdk2* has not been previously implicated in regulating neutrophil migration, we thus determined if our findings could apply to humans. Primary human neutrophils were isolated and treated with NU6140. Inhibition of CDK2 significantly reduced chemotaxis toward Interleukin-

8, with a decreased velocity and chemotaxis index (Fig. 5-7J-L). In summary, we report a previously unknown role for CDK2 in regulating neutrophil chemotaxis in a way separable from its function in DNA replication.

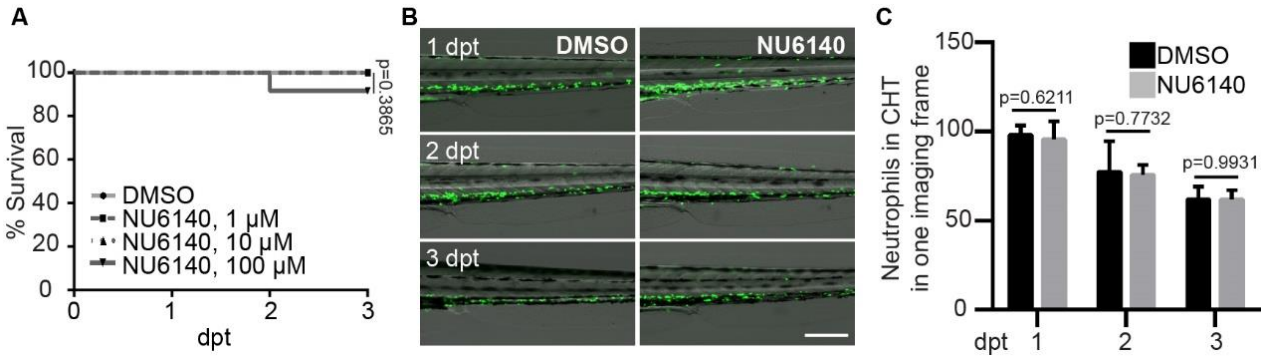


**Figure 5-6 Cytotoxicity of CDK2 inhibitor NU6140**

(A) Survival of 3 dpf zebrafish embryos treated with indicated doses of NU6140. Survival rates were tallied daily. One representative experiment of three independent experiments (n =20 each group) is shown, Gehan–Breslow–Wilcoxon test. (B, C) Representative images (B) and quantification (C) of neutrophils in the caudal hematopoietic tissue of the 3 dpf embryos from Tg(lyzC:gfp) treated with 100 µM of NU6140 for 3 days. Scale bar: 500 µm. Results are presented as mean ± s.d. of three individual trials, Kruskal–Wallis test.

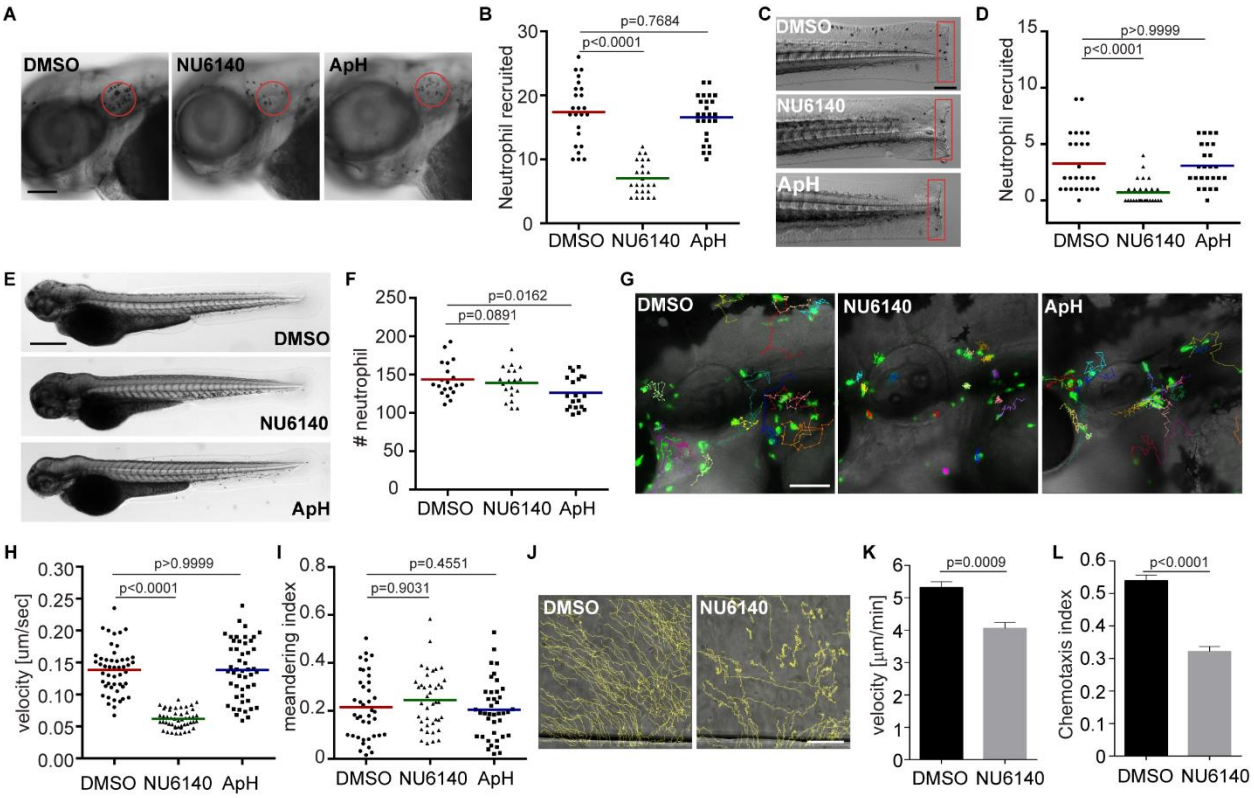


**Figure 5-7 Inhibition of CDK2 reduces neutrophil motility and chemotaxis in zebrafish and humans**

(A, B) Representative images (A) and quantification (B) of neutrophils recruited to infected ear in zebrafish larva treated with cdk2 inhibitor (NU6140) or DNA replication inhibitor Aphidicolin +hydoxyurea (ApH). Scale bar, 100 µm. (C, D) Representative images (C) and quantification (D) of neutrophils recruited to tail fin transection sites in zebrafish larva treated with NU6140 or ApH. Scale bar, 200 µm. (E, F) Representative images (E) and quantification (F) of total neutrophil number zebrafish larva treated with NU6140 or ApH. Scale bar: 500 µm. (A-F) Assays were done with 3 individual founders with 3 biological repeats each containing 20 (for motility) or 25 (for neutrophil recruitment) fish per group. Result from one representative experiment is shown as mean ± s.d., Mann–Whitney test. (G-I) Representative images (G), velocity (H), and meandering index (I) of neutrophil motility in zebrafish larvae treated with NU6140 or ApH. Scale bar, 100 µm. 3 embryos each from three different founders were imaged and quantification of neutrophils in one representative video is shown, Kruskal–Wallis test. (J-L) Representative tracks (J), mean velocity (K), and chemotaxis index (L) of primary human neutrophils treated with DMSO or NU6140 (50 µM) migrating towards IL-8. Scale bar, 100 µm. Results representative for 3 separate trials are shown. Result is presented as mean ± s.e.m., Two-way paired Welch's t-test.

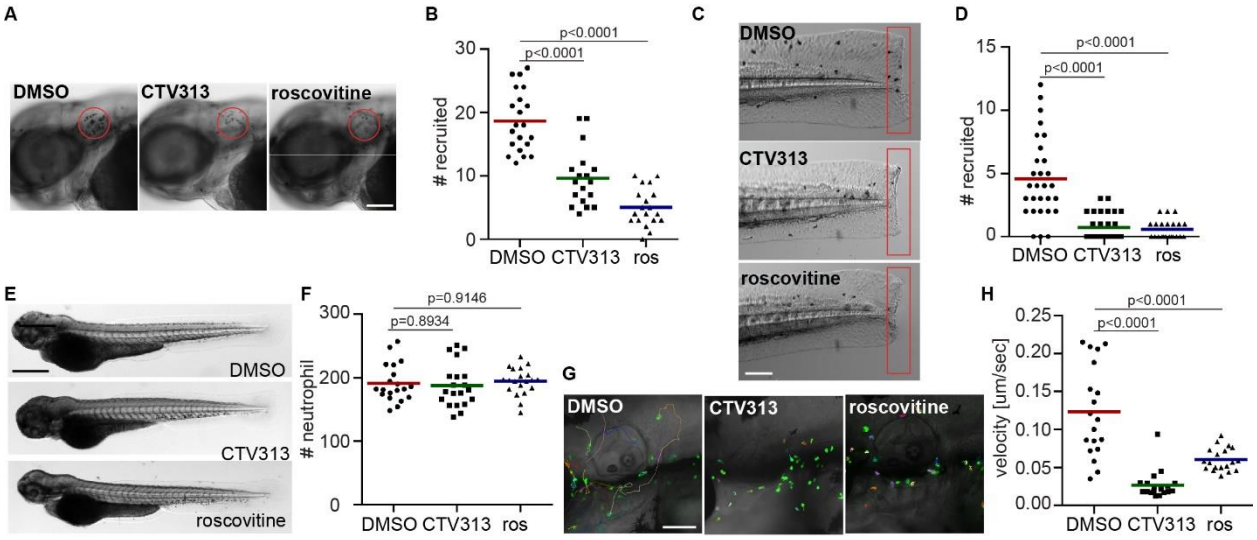


**Figure 5-8 The CDK2 inhibitor CTV313 or a pan cdk inhibitor roscovitine reduces neutrophil migration**

(A, B) Representative images (A) and quantification (B) of neutrophils recruited to infected ear in zebrafish larva treated with a cdk2 inhibitor (CTV313) or a pan-CDK inhibitor (roscovitine). Scale bar: 100 µm. (C, D) Representative images (C) and quantification (D) of neutrophils recruited to tail fin transection sites in zebrafish larva treated with CTV313 or roscovitine. Scale bar: 200 µm. (E, F) Representative images (E) and quantification (F) of total neutrophil number in zebrafish larva treated with CTV313 or roscovitine. Scale bar: 500 µm. (A-F) Assays were done with at least 3 individual founders with 3 biological repeats each containing 20 (for motility) or 25 (for neutrophil recruitment) fish per group. Result is presented as mean ± s.d., Mann–Whitney test. (G, H) Representative images (G), and quantification of velocity (H) of neutrophils in zebrafish larvae treated with CTV313 or Roscovitine. Scale bar: 100 µm. 3 embryos each from three different founders were imaged and quantification of neutrophils is shown, Kruskal–Wallis test.

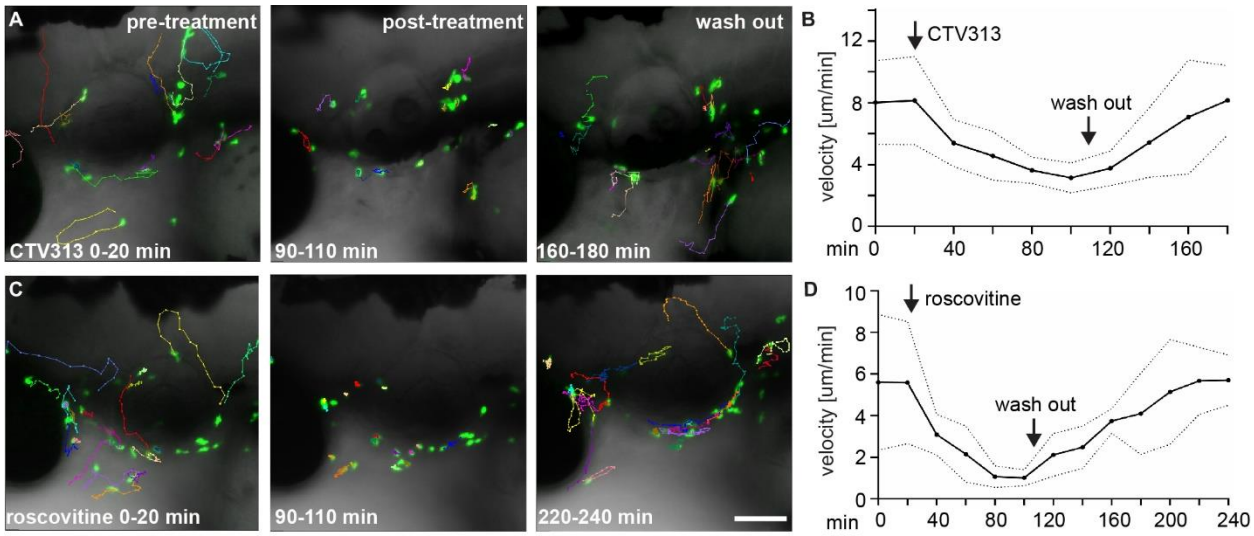


**Figure 5-9 Dynamic changes of neutrophil motility after the addition and washout of CTV313 or roscovitine**

(A, B) Representative tracks (A) and quantification of velocity (B) of neutrophils in zebrafish larvae treated with CTV313. (C, D) Representative tracks (C) and quantification of velocity (D) of neutrophils in zebrafish larvae treated with roscovitine. Arrows indicate time of drug introduction and washout. Scale bar: 100 µm. Results are presented as mean (solid lines) ± s.d. (dashed lines).

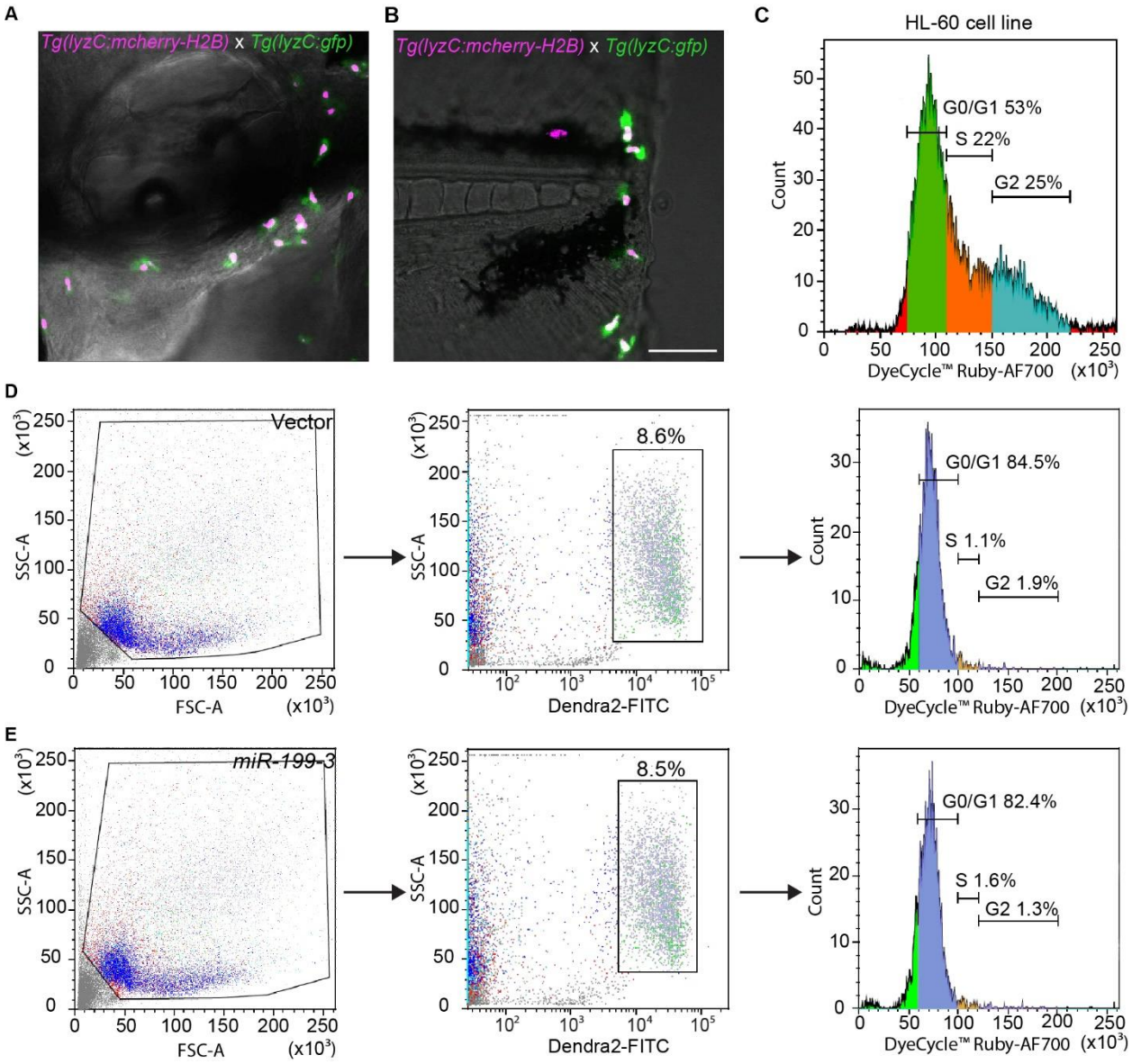


**Figure 5-10 Cell cycle profiling of zebrafish neutrophils**

(A) A representative image of 3 dpf embryos from Tg(lyzC:mcherry-H2B) (nucleus magenta label) crossed with Tg(lyzC:gfp) (cytosol green label) at 30 min post ear infection. One representative image of three independent experiments are shown. (B) A representative image of 3 dpf embryos from Tg(lyzC:mcherry-H2B) (nucleus red label) crossed with Tg(lyzC:gfp) (cytosol green label) at 30 min post tail wounding as described in (A). (C) Cell cycle profile of dHL-60 cell line. Cells were separated into G1, S and G2 phased based on the fluorescence intensity of the cell cycle dye. (D) Cell cycle profile (right panel) of neutrophils in adult kidney marrow from the vector control line. Live cells were gated (left panel) and dendra2+ cells were selected for analysis (middle panel). One representative experiment of three biological repeats are shown. (E) Cell cycle profile of neutrophils in adult kidney marrow from the miR-199 line as described in (D).

### 5.4.5 Catalytic activity of Cdk2 is required for neutrophil motility

To further test our hypothesis that the kinase activity of Cdk2 is essential for neutrophil motility, we cloned the zebrafish *cdk2* gene and tagged it with mCherry at the N-terminus using a self-cleavable 2a peptide (Fig. 5-11A). Mutations at D145, a residue that chelates $Mg^{2+}$ and facilitates ATP binding to the catalytic cleft, would result in a catalytic-dead and dominant-negative form of Cdk2 (van den Heuvel & Harlow, 1993). We constructed zebrafish lines overexpressing *cdk2* (D145N) in neutrophils, *Tg(lyzC:mcherry-2a-cdk2-d145n)*$^{pu19}$, together with a control line *Tg(lyzC:mcherry-2a-cdk2)*$^{pu20}$, hereby referred to as cdk2 D145N or the WT lines, respectively. We observed a significant reduction of neutrophil motility (Fig. 5-11B-D) and recruitment to the tail amputation site (Fig. 5-11E, F) in the D145N line, coinciding with our results from miR-199 overexpression and CDK2 pharmacological inhibition. To characterize neutrophil chemotaxis to a single chemoattractant, we bathed embryos in Leukotriene B4 and quantified neutrophil emigration from the caudal hematopoietic tissue (CHT) to the caudal fin. The percentage of neutrophils migrating outside the CHT and the distance neutrophils traveled in the caudal fin were significantly reduced in the D145N line (Fig. 5-11G, H and Fig. 5-12A, B). In addition, neutrophil motility in the CHT was reduced (Fig. 5-12C, D). To visualize neutrophil polarization, the cdk2 D145N or the WT lines were crossed with *Tg(mpx:GFP-UtrCH*) which labels stable actin in the trailing edge of migrating neutrophils (Deng, Yoo, Cavnar, Green, & Huttenlocher, 2011a). In Cdk2 D145N expressing neutrophils, stable actin is enriched in transient cell protrusions that quickly retract, displaying disrupted cell polarity and actin dynamics (Fig.5-11I). Hence, our results indicate that the catalytic activity of Cdk2 is required for neutrophil polarization and efficient chemotaxis.

To test whether *cdk2* is the primary target of miR-199 that regulates cell migration, we restored the Cdk2 expression in the miR-199-overexpressing zebrafish neutrophils. Cdk2 expression alone could partially rescue the migration defects of the neutrophils carrying miR-199, but not to the vector control level (Fig. 5-13), suggesting that other miR-199 targets possibly also regulate neutrophil migration. To further confirm the specific requirement of CDK2 activity in neutrophil migration, we incubated dHL-60 cells with increasing doses of inhibitors of CDK1, CDK1/5, CDK2 or CDK4/6. Indeed, only the CDK2 inhibitor reduced transwell migration in a dose-

dependent manner (Fig. 5-14). In addition, transient expression of dominant-negative Cdk2, but not dominant-negative Cdk5 reduced neutrophil migration in zebrafish (Fig. 5-15). Along the same line, knocking down CDK5 in dHL-60 cells did not affect transwell migration (Fig. 5-16C-H). These results suggest a specific requirement of CDK2 in regulating neutrophil migration.

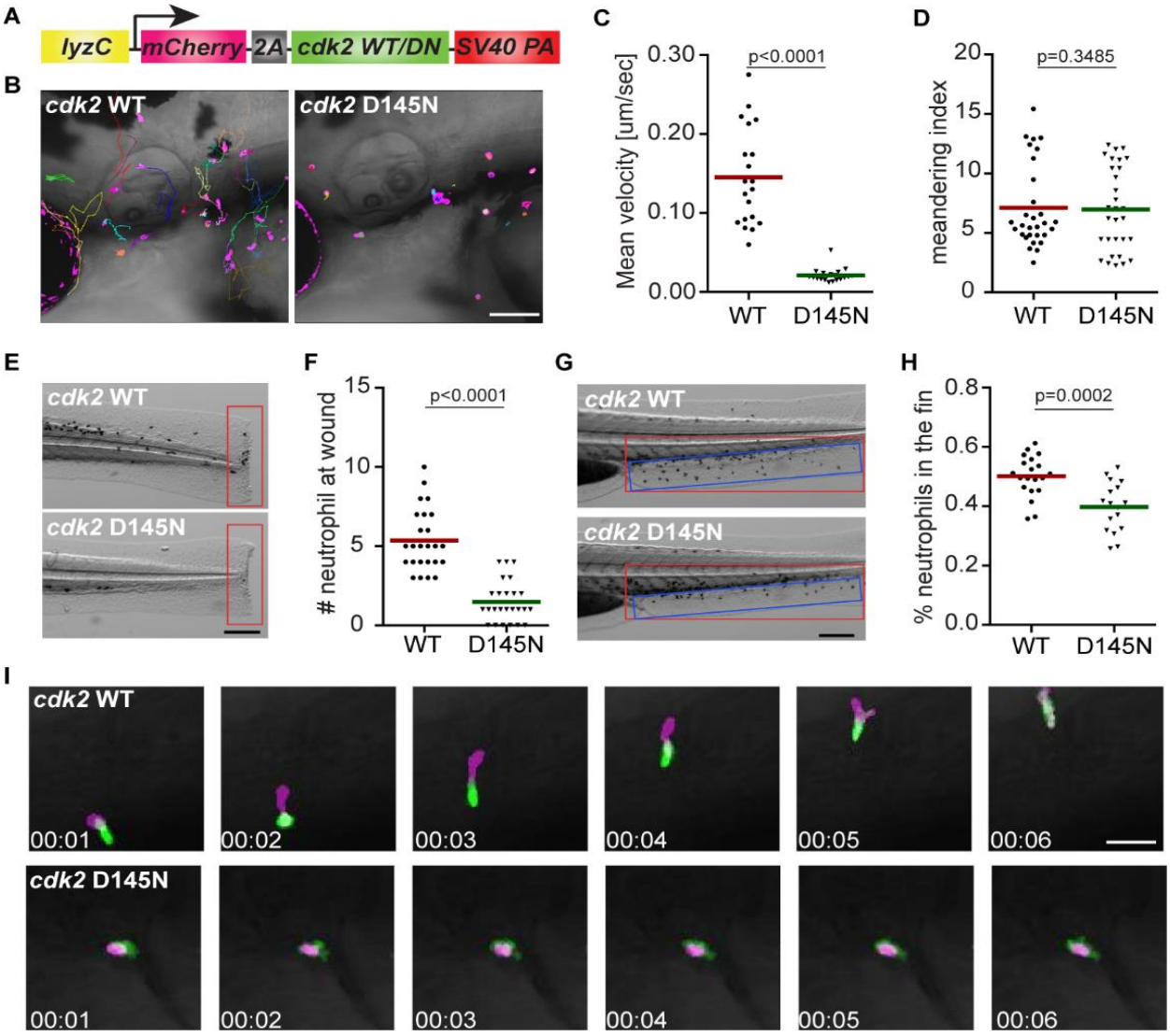


**Figure 5-11 Dominant-negative CDK2 suppresses neutrophil motility and chemotaxis**

(A) Schematic of the construct for neutrophil specific expression of CDK2 wild-type (WT) or D145N. (B-D) Representative images (B), velocity (C), and meandering index (D) of neutrophil motility in CDK2 WT or D145N zebrafish line. Scale bar, 100 μm. 3 embryos each from three different founders were imaged and quantification of neutrophils in one representative video is shown, Kruskal–Wallis test. (E, F) Representative images (E) and quantification (F) of neutrophil recruitment to the tailfin transection sites in CDK2 WT or D145N zebrafish line. Scale bar, 200 μm. (G, H) Representative images (G) and quantification (H) of neutrophils migrated to the caudal fin (blue box) normalized to total neutrophils in the trunk (red box) in CDK2 WT or D145N zebrafish line. Scale bar, 200 μm. (I) Simultaneous imaging of utrophin-GFP distribution in neutrophils expressing either WT or D145N Cdk2. Data are representative of more than three separate time-lapse videos. Scale Bar, 50μm. (E-H) Assays were done with 3 individual founders with 3 biological repeats each containing 20 (for motility) or 25 (for neutrophil recruitment) fish per group. Result is presented as mean ± s.d., Mann–Whitney test.

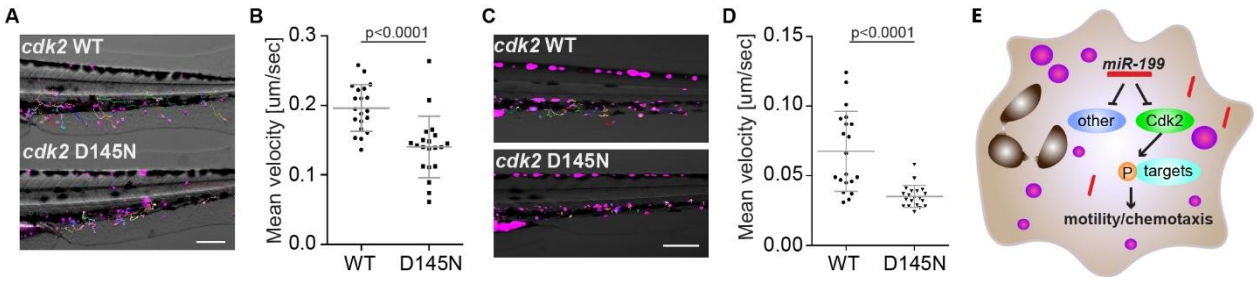


**Figure 5-12 Cdk2 D145N inhibits neutrophil motility and chemotaxis and the working model**

(A) Representative images and (B) quantification of velocity of neutrophils in 3 dpf zebrafish embryos from the WT or D145N line in a LTB4 bath. Scale bar: 200 µm. (C) Representative images and (D) quantification of velocity of neutrophil motility in 3 dpf zebrafish embryos from the WT or D145N line in the caudal hematopoietic tissue. Scale bar: 200 µm. Assays were performed with at least 3 individual founders with 3 biological repeats each containing at least 3 fish per group. Result is presented as mean ± s.d., Mann–Whitney test. (E) Working model of how miR-199 inhibits neutrophil migration.

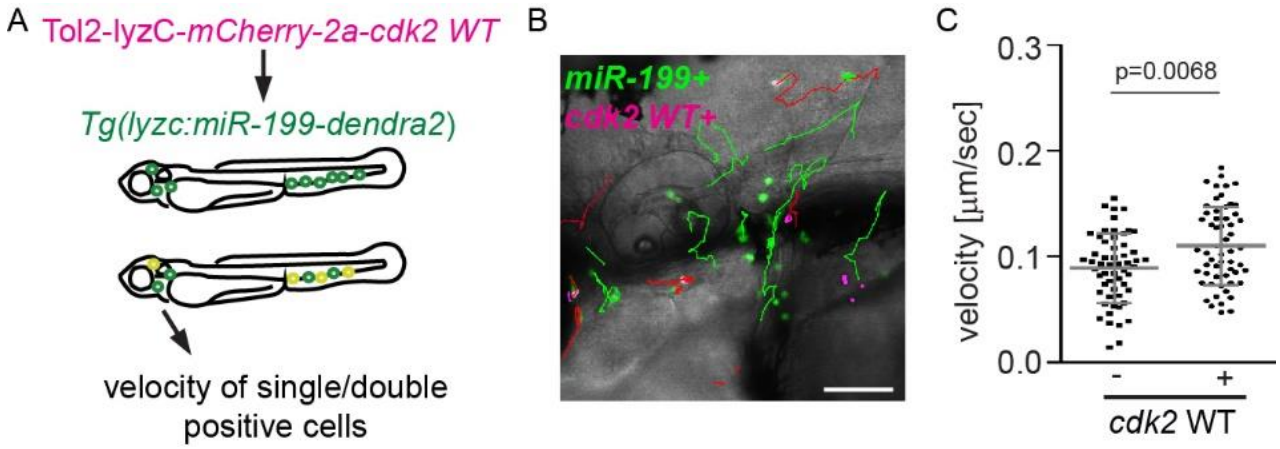


**Figure 5-13 WT Cdk2 partially rescues neutrophil motility defects resulted from miR-199 overexpression**

(A) Schematics of experimental design. Embryos from Tg(lyzC:miR-199-Dendra2)pu19 were injected with a plasmid driving miR-199-resistant cdk2 expression in neutrophils, Tol2-lyzC-mCherry-2a-Cdk2 WT . Single (GFP+, miR-199 only) and double positive cells (GFP+mCherry+, miR-199+cdk2+) from the same embryos were tracked. (B, C) Representative images and tracks (B), and quantification of velocity (C) single and double positive cells. Scale bar: 100 µm. Green tracks: miR-199 expression only; Red tracks: miR-199 and cdk2 WT expression. 3 embryos each from three different founders were individual injected, imaged and quantified. Results are presented as mean ± s.d., Mann–Whitney test.

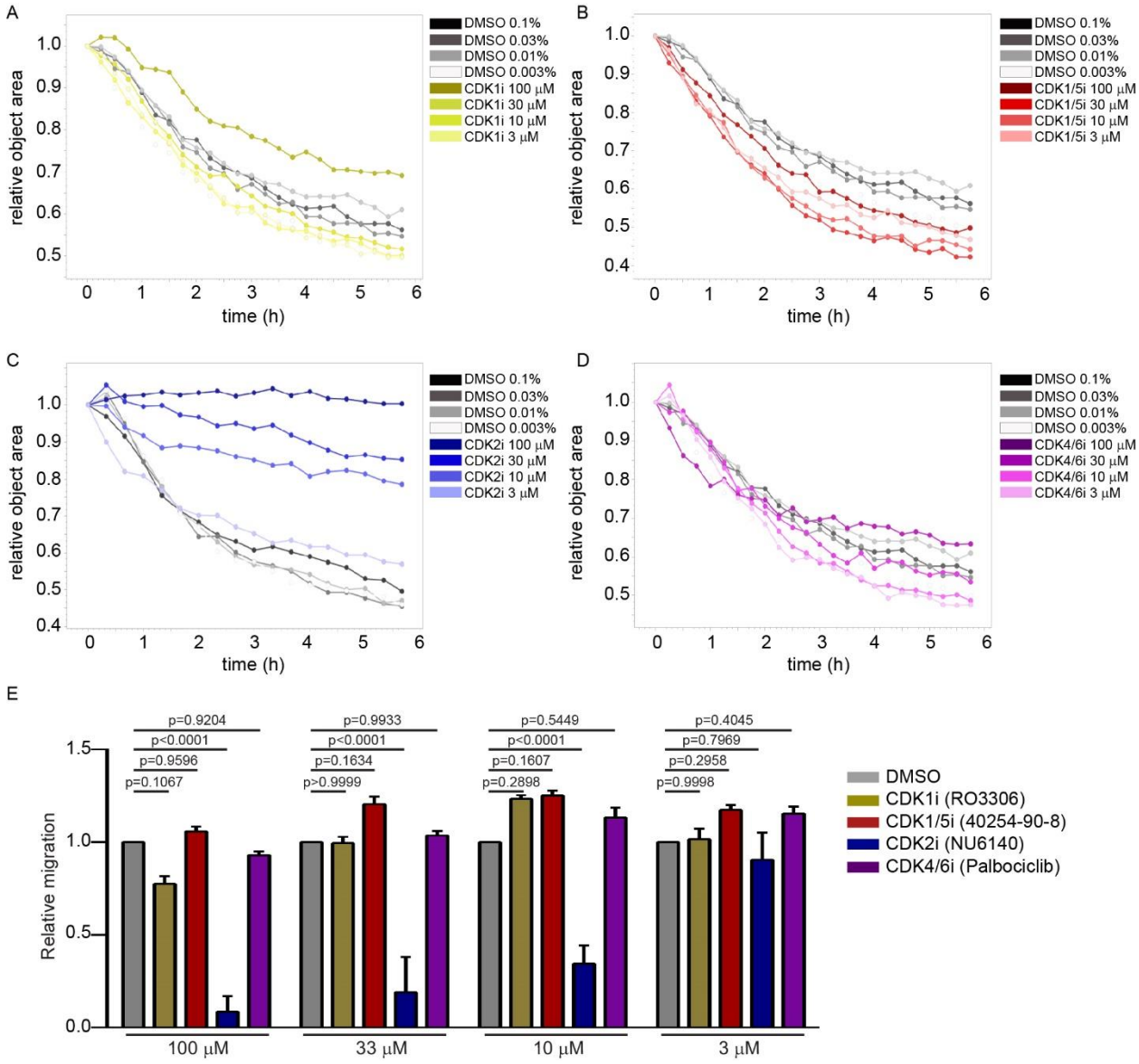


**Figure 5-14 Selective inhibition of dHL-60 transwell migration by the CDK2 inhibitor**

(A-D) Dynamic transwell migration of dHL-60 cells in the presence of increasing doses of the DMSO vehicle control or CDK1 inhibitor RO3306 (A), CDK1/5 inhibitor 40254-90-8 (B), CDK2 inhibitor NU6140 (C) and CDK4/6 inhibitor Palbocicib (D). Object area above the transwell inserts, normalized to time 0, was used to reflect the % cells not yet migrated. Results from one representative experiment of three individual experiments are shown. (E) Quantification of transwell migration (1-relative object area) at 2h. Results are normalized to respective DMSO controls and presented as mean ± s.d. from three independent experiments. Kruskal–Wallis test.

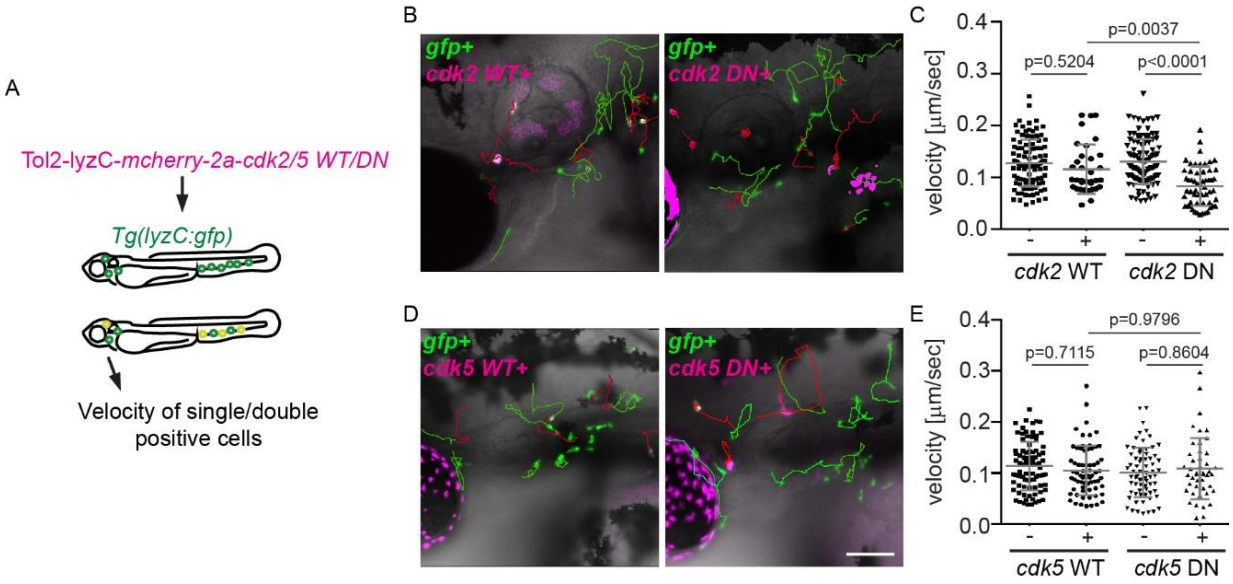


**Figure 5-15 Cdk2, but not Cdk5 DN hinders neutrophil motility in zebrafish**

(A) Schematic of experimental design. Embryos from Tg(lyzC:GFP) were injected with a plasmid driving neutrophil specific expression of cdk2 or cdk5 WT/DN. Single (GFP+) and double positive cells (GFP+mCherry+, gfp+cdk2/5 WT/DN+)from the same embryos were tracked. (B, C) Representative images and tracks (B) and quantification of velocity (C) for cdk2 WT/DN expressing neutrophils. (D, E) Representative images and tracks (D) and quantification of velocity (E) for cdk5 WT/DN expressing neutrophils. Scale bar: 100 µm. Quantification was done with at least 3 embryos from three independent injections. Green tracks: gfp only; Red tracks: gfp and cdk double positive. Results are presented as mean ± s.d.. Mann–Whitney test.

**Figure 5-16 Construction and characterization of CDK2 and CDK5 knockdown dHL-60 cells**

(A, B) Representative blots (A) and quantification (B) of CDK1/2/5 and β-Tubulin levels in control (open) or CDK2 knockdown (sh1, solid and sh2, dashed) dHL-60 cell lines. (C, D) Representative blots (C) and quantification (D) of CDK1/2/5 and Tubulin levels in control (open) or CDK5 knockdown (sh1, solid and sh2, dashed) dHL-60 cell lines. Protein levels were quantified by normalizing respective bands to the Tubulin loading control. Results are presented as mean ± s.d. from three independent experiments. Kruskal–Wallis test. (E) Cell populations gated for cell profile analysis and transwell quantification. (F) Surface CD11b levels of indicated dHL-60 cells. Respective samples stained with an isotype control were used to determine the baseline. Percentage of cells with CD11b levels above the baseline is shown. (G) Annexin V staining in the total cell population (excluding debris) of indicated dHL-60 cells. Respective unstained live samples were used to determine the baseline. Percentage of cells with AnnexinV levels above the baseline is shown. (E-G) One representative experiment of three independent trials is shown. (H) Transwell migration of the indicated dHL-60 cells ±fMLP. Results are presented as mean ± s.d. from three independent experiments and normalized to control –fMLP. Kruskal–Wallis test.

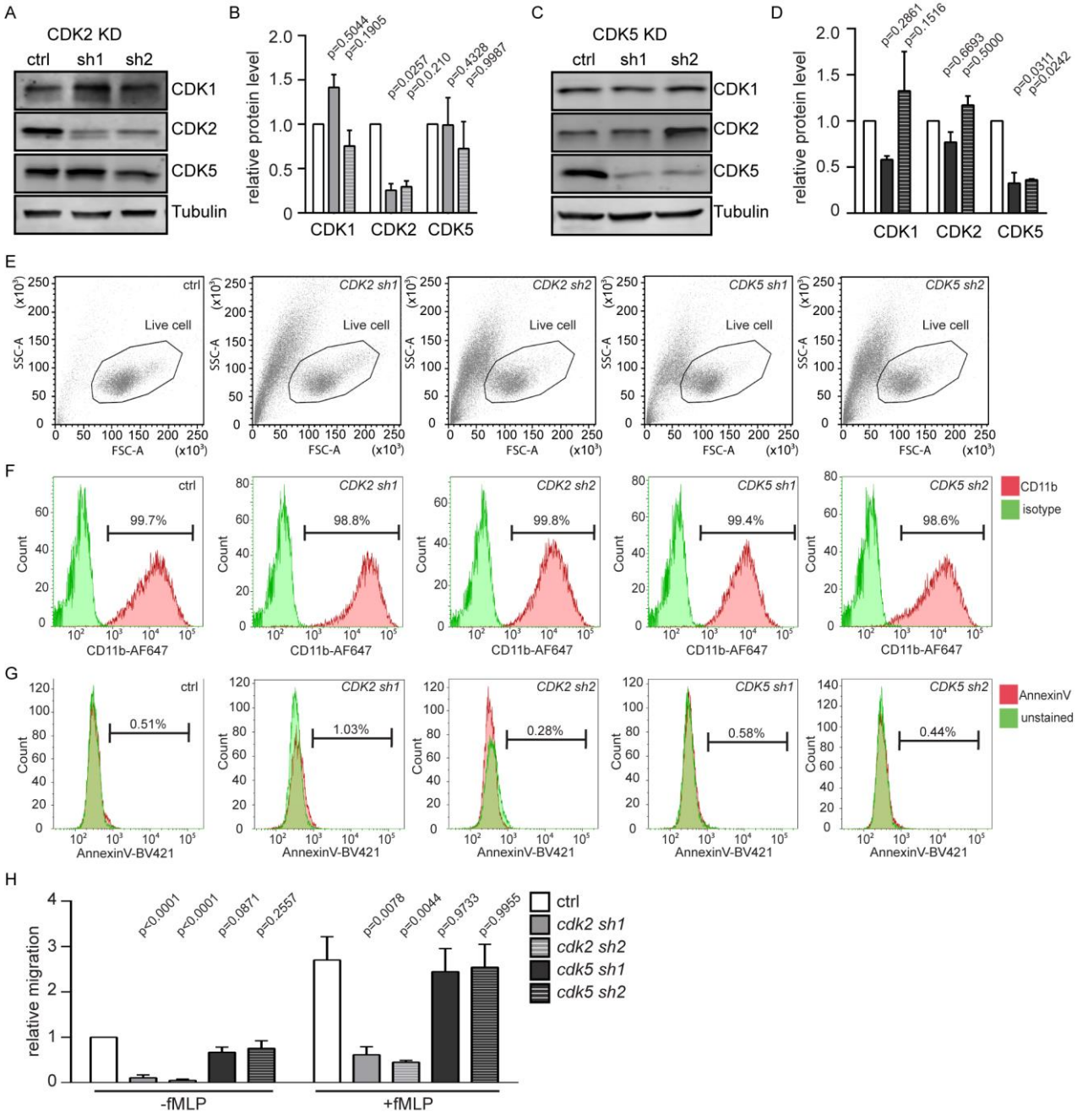
A
CDK2 KD
ctrl
sh1
sh2
CDK1
CDK2
CDK5
Tubulin
B
relative protein level
p=0.5044
p=0.1905
p=0.0257
p=0.0.210
p=0.4328
p=0.9987
CDK1
CDK2
CDK5
C
CDK5 KD
D
p=0.2861
p=0.1516
p=0.6693
p=0.5000
p=0.0311
p=0.0242
E
ctrl
CDK2 sh1
CDK2 sh2
CDK5 sh1
CDK5 sh2
Live cell
SSC-A
FSC-A
F
99.7%
98.8%
99.8%
99.4%
98.6%
Count
CD11b-AF647
CD11b
isotype
G
0.51%
1.03%
0.28%
0.58%
0.44%
AnnexinV-BV421
AnnexinV
unstained
H
relative migration
p<0.0001
p<0.0001
p=0.0871
p=0.2557
p=0.0078
p=0.0044
p=0.9733
p=0.9955
ctrl
cdk2 sh1
cdk2 sh2
cdk5 sh1
cdk5 sh2
-fMLP
+fMLP

### 5.4.6 CDK2 regulates polarization and signaling in dHL-60 cells

To gain more insights into how CDK2 regulates neutrophil migration, two CDK2 knockdown dHL-60 cell lines were generated using two different shRNAs. The CDK2 protein levels in these two lines were significantly reduced whereas the level of CDK1 or CDK5 remained relatively constant (Fig. 5-16A, B). Cells deficient with CDK2 were viable with comparable surface levels of CD11b, indicating that CDK2 knockdown did not affect cell differentiation (Fig. 5-16E-G). CDK2 knockdown cells exhibited hindered transwell migration toward fMLP (Fig. 5-16H) and could not establish prominent actin rich lamilipodia when stimulated with a uniform field of fMLP (Fig. 5-17A, B). Phospho-Myosin light chain 2, which labels the rear of the cell and drives tail retraction (J. Xu et al., 2003), was also mislocalized (Fig. 5-17A, C). After fMLP stimulation, the activation of Rac (indicated by the level of p-PAK) or the level of phosphatidylinositol (3,4,5)-trisphosphate (indicated by the level of p-AKT) (Graziano et al., 2017) was also reduced in the CDK2 knockdown cells, whereas the p-ERK level (E. R. Zhang, Liu, Wu, Altschuler, & Cobb, 2016) was not affected (Fig. 5-17D-F), indicating a specific requirement for CDK2 in activating the PI3K-Rac axis. In addition, unlike CDK4 (Amulic et al., 2017), CDK2 does not regulate NET formation (Fig. 5-18), reiterating that different CDKs have unique functions in neutrophils.

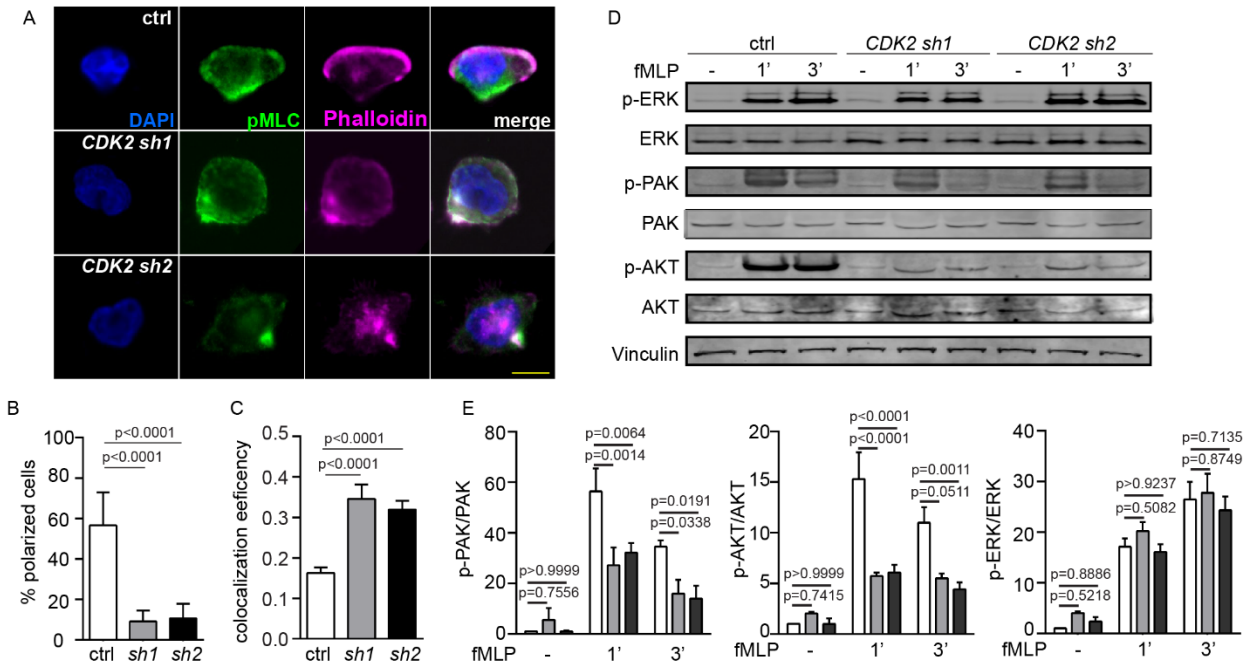


**Figure 5-17 CDK2 knock down dysregulates polarization, phospho-myosin localization, and signaling in dHL-60 cells**

(A-C) Representative immunofluorescence images (A), quantification of cells with polarized F-actin (B) and colocalization of phospho-myosin light chain II (pMLC) with F-actin (C) in control or CDK2 knockdown dHL-60s after fMLP stimulation. Magenta, phalloidin; green: phospho-myosin light chain II; blue, DAPI. Scale bar: 10 μm. (B, C) Results are presented as mean ± s.d. from three independent experiments. n=2345 (ctrl), n= 1410 (CDK2 sh1), and n=1346 (CDK2 sh2) cells from three independent experiments were quantified. Kruskal–Wallis test. (D-E) Immunoblots (D) and quantification of phospho-PAK, phospho-AKT, and phospho-ERK (E) in control or CDK2 knockdown dHL-60s without fMLP (-), or at indicated time points post fMLP stimulation. Vinculin was used as a loading control. Results are presented as mean ± s.d. from three independent experiments. Kruskal–Wallis test.

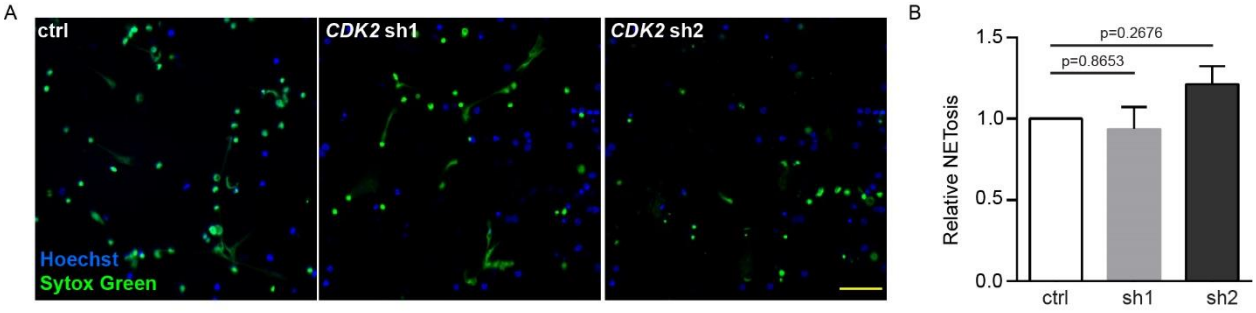


**Figure 5-18 NETosis is not affected by CDK2 knock down in dHL-60 cells**

(A, B) Representative images (A) and quantification (B) of NET formation in CDK2 knockdown dHL-60 or control cell expressing a non-targeting shRNA. NET was induced with 50 nM PMA for 4h. Scale bar: 100 µm. Cells were stained with Hoechst and Sytox Green to label total and extracellular DNA. Results are presented as mean ± s.d. from three independent experiments. Kruskal–Wallis test.

### 5.4.7 miR-199 overexpression or Cdk2 inhibition ameliorates systemic inflammation

With the findings that miR-199 overexpression or *cdk2* abrogation hinders neutrophil chemotaxis, we sought to determine whether these manipulations could alleviate acute systemic inflammation caused by a lethal dose of *P. aeruginosa* in the circulation (Brannon et al., 2009). Survival of the zebrafish embryos was significantly improved in the miR-199 line and the *cdk2* D145N line compared to their respective controls (Fig. 5-19A, B). Consistently, NU6140 treatment improved the infection outcome whereas DNA replication inhibitors were detrimental to the infected host (Fig. 5-19C). Roscovitine, the pan-CDK inhibitor (Bach et al., 2005) currently in phase-II trial, also displayed a protective effect at 15 µM but was detrimental at 30 µM, possibly due to the inhibitory effect on cell proliferation and tissue repair as previously reported in cell culture and *ex vivo* bone marrow isolations (Cui, Wang, Wang, Zhao, & Peng, 2013) (Fig. 5-19D). To further assess their protective effect in another model, we utilized a previously described sterile inflammation model of endotoxemia (Hsu et al., 2018). Neutrophil-specific miR-199 overexpression or roscovitine treatment again reduced host mortality (Fig. 5-19E, F). These results indicate that miR-199 overexpression or Cdk2 inhibition can have a protective effect during acute systemic inflammation and infection, without generating an immune suppression status with defects in pathogen clearance.

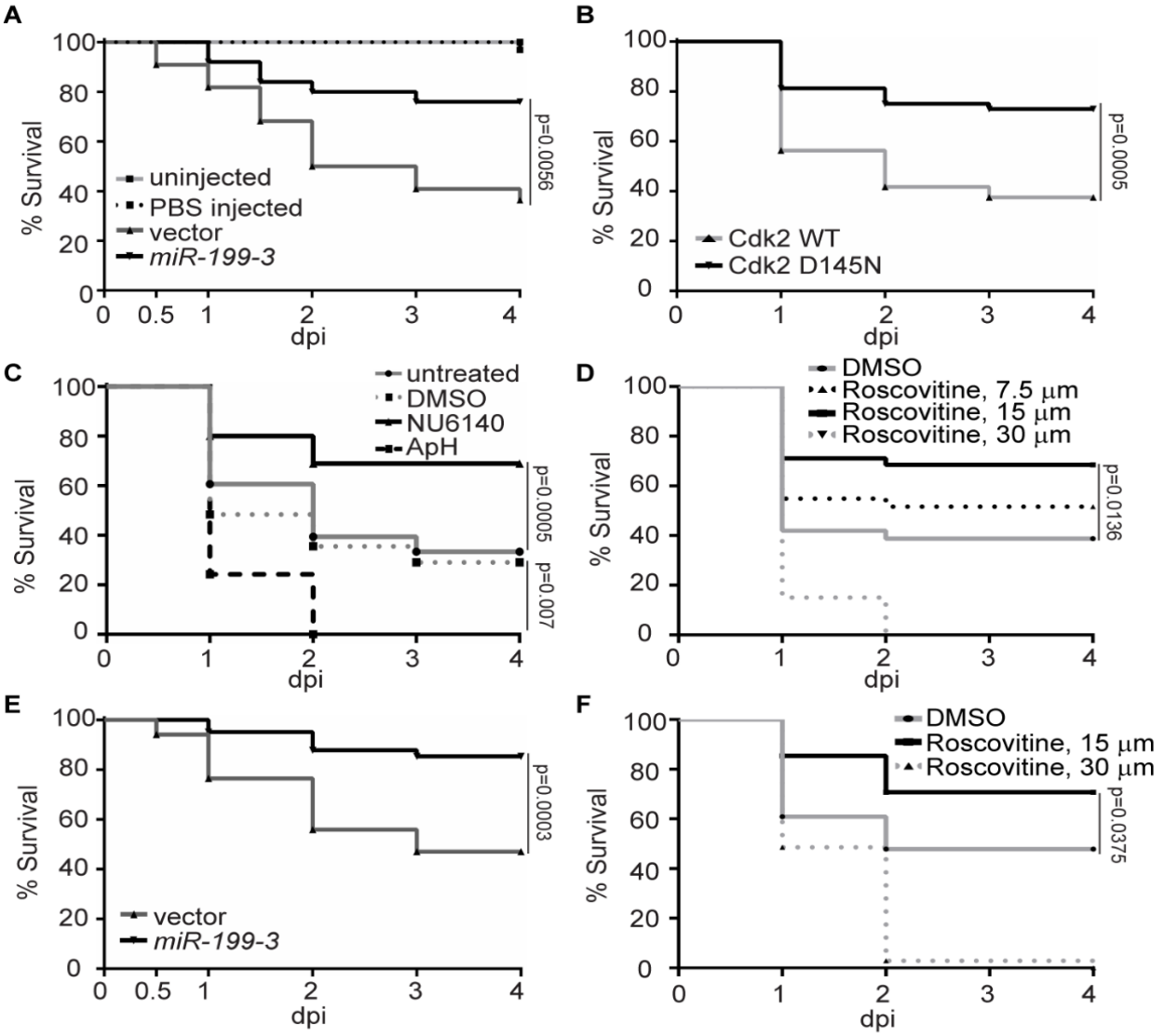


**Figure 5-19 Cdk2 inhibition and miR-199 overexpression improves zebrafish survival during systemic bacterial infection or sterile inflammation**

(A) Survival of zebrafish larvae after infection of 1000 CFU of *P. aeruginosa* i.v in the vector or miR-199 zebrafish line. Vector lines were left uninfected or injected with PBS as a control. (B) Survival of zebrafish larvae after infection of 1000 CFU of *P. aeruginosa* i.v in the CDK2 WT or D145N zebrafish line. (C) Survival of zebrafish larvae treated with vehicle, NU6140 (100 μM), ApH (150 μM/20 mM) or left untreated after infection of 1000 CFU of *P. aeruginosa* i.v. (D) Survival of zebrafish larvae treated with indicated dilutions of roscovitine infected with 1000 CFU of *P. aeruginosa* i.v.. (E) Survival of zebrafish larvae after injection of 25 ng LPS i.v. in the vector or miR-199 zebrafish line. (F) Survival of zebrafish larvae treated with indicated dilutions of roscovitine injected with 25ng LPS i.v. (A-F) One representative experiment of three independent experiments (n >=20 each group) is shown, Gehan–Breslow–Wilcoxon test.

## 5.5 Discussion

microRNAs play a pivotal role in diseases driven by neutrophilic inflammation (Arroyo et al., 2018; Cao, Shikama, Anzai, & Kimura, 2015; Surmiak, Hubalewska-Mazgaj, Wawrzycka-Adamczyk, Musia, & Sanak, 2015) where both protective and detrimental effects are observed. Currently, there is no systemic screen to identify miRNAs that regulate neutrophil migration, possibly because neutrophils are terminally differentiated and not genetically tractable in cell culture. In the present study, we performed an in vivo functional screen in zebrafish and identified miR-199 as a critical regulator of neutrophil migration and chemotaxis. miR-199 hinders neutrophil motility by downregulating genes in the canonical cell cycle pathways, and directly targets Cdk2. We further demonstrate that the catalytic activity of CDK2 is critical for neutrophil migration and chemotaxis, whereas DNA replication and an active cell cycle are not essential (Fig. 5-12E).

Although no prior studies have investigated the role of miR-199 in neutrophils, its role in suppressing inflammation and cell migration has been reported in cancer cells. In ovarian cancer cells, miR-199 inhibits canonical NF-κB signaling by targeting *ikbkb*, thus preventing the production of pro-inflammatory cytokines (R. Chen et al., 2008). In our current work, the miR-199-*ikbkb* axis was also validated in neutrophils, further supporting the evolutionary conservation of miRNA-target interaction in vertebrates. Suppression of *ikbkb* may also contribute to the survival of zebrafish during systemic inflammatory challenge due to its central role in inflammation. From the perspective of cell migration and recruitment, miR-199 hinders cancer cell migration and invasion by downregulating β1 integrin levels (W. T. Li et al., 2016), decreasing CD44 expression and hence interaction with Ezrin (S. H. Wang et al., 2014), or by directly targeting α3 integrin (Koshizuka et al., 2017) in various cancer cells. Introduction of miR-199 alleviated invasiveness *in vitro* through targeting the Wnt or HIF-1α/VEGF pathways (Song et al., 2014; Ye et al., 2015). Here we provide evidence that miR-199 is a suppressor of cell migration in leukocytes, expanding its role beyond cancer biology. miR-199a-5p levels were increased in the plasma of patients with neutrophilic asthma (Y. Huang et al., 2018) and inflammatory bowel disease *(X. M. Xu & Zhang, 2016)*, suggesting that miR-199 possibly plays physiological functions in inflammation. In addition, miR-199b suppresses myeloid

differentiation (Favreau, McGlauflin, Duarte, & Sathyanarayana, 2016), which can also contribute to its role in suppressing the innate immunity.

The most surprising finding of our study is that miR-199 predominantly regulates the cell cycle-dependent kinase *CDK2* in terminally differentiated neutrophils. A significant inverse relationship of MIR-199 and *CDK2* was observed in samples of patients with breast cancer or head and neck cancer, indicating that MIR-199 possibly regulates *CDK2* in human pathological conditions (Fig. 5-20). CDK2 is a cell cycle-dependent kinase whose cofactors, cyclin E and A, are expressed during mitosis, activating its kinase activity and cell cycle progression (Malumbres & Barbacid, 2009). CDK2 phosphorylates transcriptional factors to drive cell cycle progression and cell differentiation, and to alter cell metabolism and DNA double-strand break repair (reviewed in (Hydbring, Malumbres, & Sicinski, 2016)). Although the literature on CDK2 in the context of innate immunity and inflammation is scarce, as reviewed in (Laphanuwat & Jirawatnotai, 2019), CDK2 possibly regulates the secretion of inflammatory cytokines in macrophages. In addition, a single nucleotide polymorphism of CDK2 is significantly enriched in asthma patients (Hirota et al., 2011), supporting the possible function of CDK2 in regulating inflammation.

Here we provide evidence that the kinase activity of CDK2 is required for neutrophil migration. Although the cytosolic CDK inhibitors have been implicated in regulating cell migration (Gui et al., 2014), there are no previous reports showing that CDK2 directly regulates cell migration. However, there is a limitation in our work that the substrates directly phosphorylated by CDK2 in neutrophils are not yet identified. CDK2 is a serine/threonine protein kinase, which uses the KLAD*FGLA kinase consensus domain to phosphorylate the "Ser/Thr-Pro-X-H/K/R" motif of target proteins, with additional prevalent noncanonical target motifs (Higashi et al., 1995). Over a hundred proteins are likely phosphorylated by CDK2-cyclinA in HEK cells (Chi et al., 2008) and the CDK2-cyclinE substrates are not well characterized. Extensive work will be required to characterize how CDK2 contributes to the signaling network required for neutrophil chemotaxis. CDK2 is possibly present in the neutrophil cytosol and its expression is upregulated upon LPS stimulation (Leitch et al., 2012), supporting the possibility that CDK2 ties in the signaling pathways downstream of the chemokine receptors. As a step closer to the potential mechanism,

we have observed defective cell polarization in both zebrafish neutrophils and dHL-60 cells upon CDK2 abrogation. In addition, a specific defect in activating the Rac2-PI3K axis is observed in CDK2 deficient dHL-60 cells, providing a direction for our future research.

Acute neutrophilic over-inflammation is a pressing concern in many disease pathologies (Sadik et al., 2011) and methods that simultaneously hinder neutrophil migration and inflammation while preserving immune integrity are highly desired. Our study presents an acute method to dampen neutrophil recruitment by inhibiting CDK2, which reduces the lethality caused by acute systemic inflammation. Although reduced migration alone can contribute to reduced inflammation, alterations in other neutrophil functions such as NETosis, phagocytosis, oxidative burst, degranulation, cytokine release, may also contribute to increased survival. Previous studies have demonstrated roles for CDK4/6 in the formation of neutrophil extracellular traps (Amulic et al., 2017), CDK7/9 in neutrophil apoptosis (Leitch et al., 2012), and CDK5 in the secretion of neutrophil-specific granules (J. L. Rosales, Ernst, Hallows, & Lee, 2004). It remains to be determined whether other neutrophil functions in addition to migration are also regulated by CDK2. The pan-CDK inhibitor roscovitine competes with ATP for the occupation of the kinase active site (Otyepka, Bartova, Kriz, & Koca, 2006) and is currently in multiple phase II clinical trials to inhibit cystic fibrosis and multiple types of tumors (clinicaltrials.gov). Previous studies in mouse have shown that treatment of roscovitine at 10-100 mg/kg for 3-7 days after inflammation induction resulted in decreased neutrophil infiltration into the inflamed tissue and better clinical outcome (Rossi et al., 2006c). This reduced neutrophil recruitment was attributed to CDK9 inhibition and neutrophil apoptosis (Hoodless et al., 2016) whereas a direct link to CDK2 was not shown. Our data adds to the list of non-cell cycle related functions of CDKs where acute inhibition of CDK2 suppresses neutrophil migration without affecting their viability. In *Cdk2* knockout mouse, normal myeloid cell numbers during resting and stressed conditions were observed (Jayapal et al., 2015) and no developmental defects other than a smaller body size and sterility were noted (Berthet, Aleem, Coppola, Tessarollo, & Kaldis, 2003). Thus CDK2 inhibition is not expected to cause adverse side effect and is thus presents an attractive strategy for short-term and long-term control of inflammation, which may be better tolerated than a pan-CDK inhibitor such as roscovitine.

In summary, our present study demonstrates previously unappreciated roles of miR-199 and CDK2 in regulating neutrophil migration and points to new directions in managing neutrophilic inflammation.

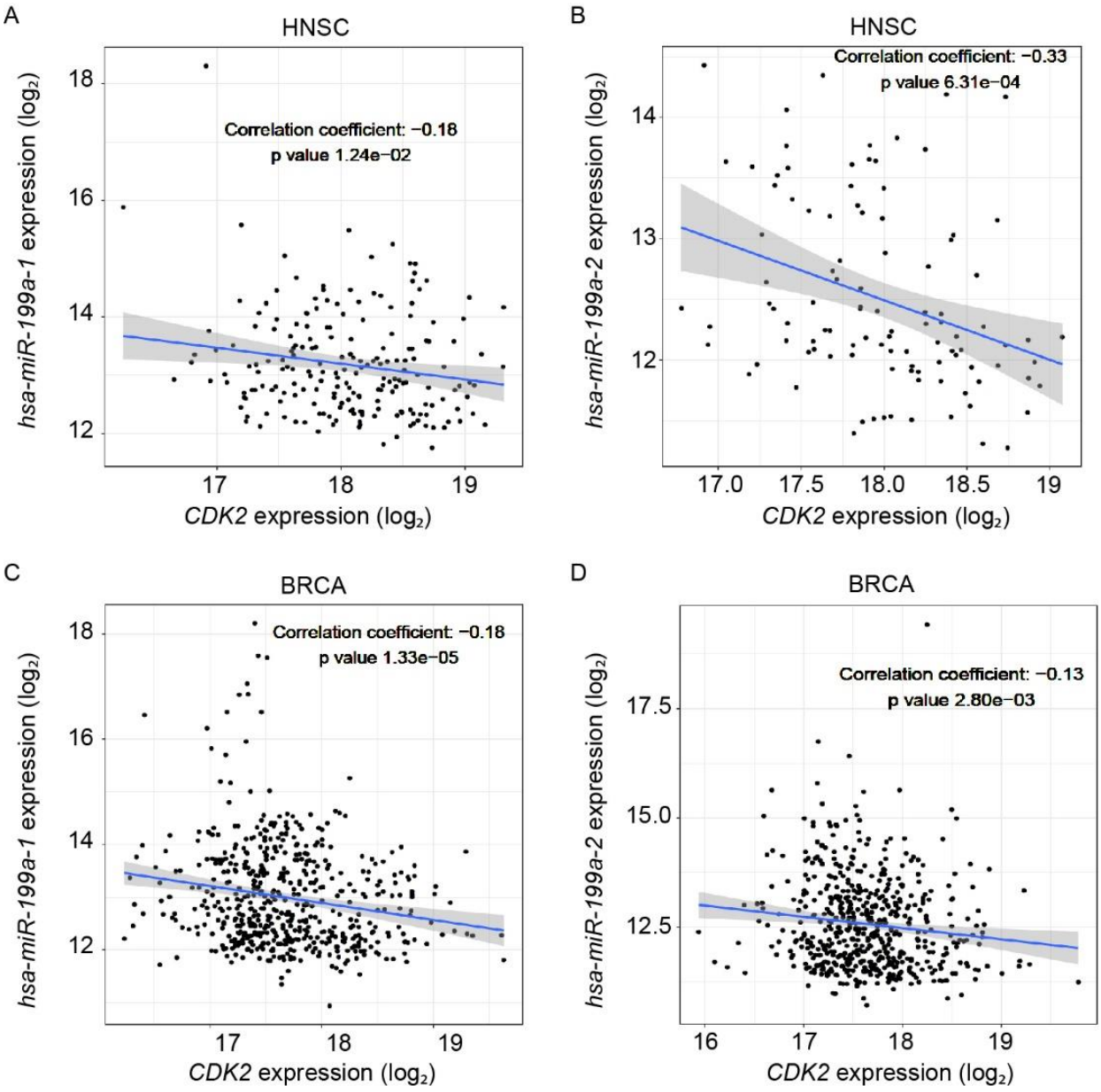


**Figure 5-20 Negative correlation of gene expression between CDK2 and hsa-miR-199a**

(A-D) Negative correlation of gene expression between CDK2 and hsa-miR-199a-1/199a-2 in head-neck squamous cell carcinoma (HNSC) (A, B) and breast cancer (BRCA) (C, D), respectively. Gene expression levels in cancer patients were retrieved from the TCGA database.

# CHAPTER 6. MATERIALS AND METHODS

## 6.1 Development and characterization of an endotoxemia model in zebrafish

### 6.1.1 Fish husbandry

This study was carried out in accordance with the recommendations of "Use of Zebrafish in the NIH Intramural Research Program". The Animal Care and Use Protocol was approved by The Purdue Animal Care and Use Committee (PACUC) (Protocol number: 1401001018). The transgenic lines *Tg(NFkB:GFP)*, (van Ham, Mapes, Kokel, & Peterson, 2010), *Tg(mpx:mcherry)* (Yoo et al., 2011), and *Tg(mpeg:EGFP-H2B)* (J. M. Davis, Huang, Botts, Hull, & Huttenlocher, 2016), were previously described. SecAV-YFP was PCR amplified using the forward: 5'-TATAGGGCGAATTGGGTACCGCCACCATGCATAAGGTTT-3', reverse: 5'-ACCGCGGTGGCGGCCGCTTACTTGTACAGCTCGTCC-3' from pBH-UAS-secA5-FP (Addgene plasmid #32359) and inserted into the KpnI/NotI cloning site of pMe Gateway plasmid (Invitrogen). Three way LR reaction with p5e- βactin, pMe-SecAV-YFP, and p3e-SV40polyA was performed in pDestR4R3 backbone to obtain pTol2-βactin:SecAV-YFP. The plasmids will be deposited to Addgene before acceptance of the paper. More than 3 founders (F0) for *Tg(βactin:SecAV-YFP)*$^{pu17}$ were obtained as described (Deng et al., 2011b). All experiments were performed with embryos at 3 day post fertilization (dpf) unless noted otherwise.

### 6.1.2 Injection plate Design

A 3D printer (Model Ultimaker 2+) was used to print the mold from an autoCAD schematic drawing with solid filling at 150 µM resolution. The mold is a negative of a 10cm petri dish with the upper portion resting on the walls of the dish. 3% Agar/E3 media was heated and poured directly into the petri dish and the mold was directly layered on the top. The mold was then removed from the petri dish and the injection plate was ready to use.

### 6.1.3 Microinjection

All injections were performed by microinjection. Embryos were collected before the first cell division and injected directly into the cell. Injection needles (Warner instruments 6100TF-3) were pulled with P-1000 micropipette puller (Sutter instruments) using program #37 with ramp=540. Embryos were placed under a Leica M125 dissection microscope. Microinjections were performed with a picospritzer II (Parker Hannifin) with an output pressure of 30 psi and a pressure duration between 20-30 msec. Injection volume was calibrated using volume=$4/3\pi r^3$, where a radius (r) of 5µm gives an volume of 1nl. To perform blood injection, staged larvae were placed in the injection mold under an Olympus SZ61 dissection microscope. Injection needles (Sutter instruments BF100-5810) were pulled with P-1000 micropipette puller (Sutter instruments) using program #34 with ramp=570. Injection was performed with a picospritzer III (Parker Hannifin) with a output pressure at 40 psi and pressure duration between 30-50 msec. Injection volume was calibrated and set to 1nl as described above.

### 6.1.4 Survival assay

Larvae were injected with 1nl of 25ng/nl LPS (Sigma, L9143) into the tail vein and incubated individually in 96 well plates. Survival was tracked for 5 days or when one group reached 100% mortality. Representative experiments of at least three independent repeats (n=20 larvae in each experiment) were shown.

### 6.1.5 Proteomic analysis

For global proteomic analysis, 40 larvae at 3 dpf were injected with PBS or LPS intravenously, with 40 uninjected larvae as control. At 8 and 24 hours post injection (hpi) , 20 larvae each were deyolked and frozen at -80 $^{o}$C and sent for proteomic analysis. Samples from three individual repeats were collected, and the global proteomics profiling and downstream statistical analysis were performed by the Purdue Proteomics Facility. The result from the mass spectrometer were processed using the MaxQuant computational proteomics platform version 1.5.8.3 (Cox & Mann, 2008). The peak list generated was searched against the *Danio rerio* sequences from UNIPROT retrieved on 04/27/2017 and a common contaminants database. The following settings were used for MaxQuant: default Orbitrap parameters, minimum peptides length of

seven amino-acid, data was analyzed with 'Label-free quantification' (LFQ) checked and the 'Match between runs' interval set to 1 min, protein FDR was set to 1%, enzyme trypsin and LysC allowing for two missed cleavage and three modifications per peptide, fixed modifications were carbamidomethyl (C), variable modifications were set to Acetyl (Protein N-term) and Oxidation (M). An in-house script was used to perform the following steps on the MaxQuant results: removal of all the common contaminant proteins, log transformed [$\log_2(x)$] the LFQ intensity values, input the missing values using the average values of the other two samples when just one sample was missing and use half of the lowest intensity when all three samples were missing in one group and presented in all three samples in the other group. The heatmaps and statistical analyses were performed in the R environment (www.cran.r-project.org). A t-test was performed on the LFQ intensities and only proteins with *p-value* < 0.05 and fold change greater than 1.5 or less than -1.5 were used for the heatmap and Pathway analyses. The pathway analysis was conducted with MetaCore™ version 6.30 build 68780 and the selected genes were mapped to the *Homo sapiens* pathways. Proteomic data was deposited to Mass Spectrometry Interactive Virtual Environment (MassIVE) at UCSD. MassIVE ID: MSV000081612 (ftp://MSV000081612@massive.ucsd.edu provisory Username: MSV000081612 Password: hsualan2017; these data will be free available after publication)

### 6.1.6 TUNEL and AO staining

Terminal deoxynucleotidyl transferase-mediated dUTP-biotin Nick End Labeling (TUNEL) staining was performed as described (Deng et al., 2011b). Briefly, embryos were fixed in 4% paraformaldehyde in phosphate-buffered saline for 2h and stored in 100% methanol overnight before rehydration and staining with TUNEL label and enzyme Mix (Roche). Acridine Orange (AO) staining was performed by incubating larvae in the dark for 30 minutes with 5 µg/ml Acridine Orange (Sigma A6014), followed by washing with fresh E3 for at least 5 times andvisualization with the GFP channel.

### 6.1.7 Live imaging and image quantification

Larvae at 3 dpf were placed on a glass-bottom dish in E3 media containing 0.02% tricaine (Sigma). Representative images were taken with AXIO Zoom V16 microscope (Zeiss) at 70%

magnification (zoom 7) at the trunk region in AO and SecAV-YFP imaging, 100% (zoom 10) magnification for TUNEL imaging, and 25% (zoom 2.7) for whole body imaging. All images were taken with the same exposure to avoid saturation of the CCD detector. Images were processed with Image J by background subtraction with the rolling ball radius as 50 then quantified for signal intensity in the region of interest. For quantification of fluorescence labeled neutrophils and macrophages, cells were counted blindly in the indicated caudal hematopoietic tissue (CHT) regions at the designated time points. Each experiment included at least 20 zebrafish larvae and was independently repeated 3 times. Graphs were generated using PRISM 6 (GraphPad).

### 6.1.8 Reverse Transcription-quantitative PCR (RT-qPCR)

Total RNA was extracted using RNeasy RNA purification kit (Qiagen). Messenger RNAs were reverse transcribed with Transcriptor First Strand cDNA Synthesis Kit (Roche). qPCR were performed with the FastStart Essential DNA Green Master (Roche). All primers amplified a single product according to the melt-curve analysis. The relative fold change is calculated following instructions provided by Real-time PCR Minor with correction of the primer efficiencies (http://ewindup.info/miner/data_submit.htm). At least 20 larvae were used in each biological replicate to generate an average value that was used to calculate the final mean ± s.d. from three independent experiments.

### 6.1.9 Knock out with CRISPR/Cas9

*Myd88* knockout was performed as previously described (W. Zhou, A. Pal, et al., 2018). Breifly, sgRNAs against MyD88 and RFP without off targeting were selected using CRISPRScan (Moreno-Mateos et al., 2015). Two individual sgRNAs were synthesized for *myd88* and *rfp*. 1 nl of solution containing 400 ng/µl sgRNAs and 400 ng/µl Cas9 protein (PNA, CP01) was injected into the one-cell stage of fertilized embryos. No development abnormality was observed at 3 dpf (W. Zhou, A. Pal, et al., 2018). Primers used to synthesize templates of sgRNAs are listed below from 5' to 3': MyD88 sgRNA1 forward: TAATACGACTCACTATAGGCGGCAGACTGGAGGACAGGTTTTAGAGCTAGAAATAG CAAG; MyD88 sgRNA2 forward:

TAATACGACTCACTATAGGAAAAGGTCTTGACGGACTGTTTTAGAGCTAGAAATAGC
AAG; RFP sgRNA1 forward:
TAATACGACTCACTATAGGAGGGCTTGCCTTCGCCCTGTTTTAGAGCTAGAAATAGC
AAG; RFP sgRNA2 forward:
TAATACGACTCACTATAGGTCGGGGATGCCCTGGGTGGTTTTAGAGCTAGAAATAGC
AAG. The reverse primer for all sgRNA templates is 5'-
AAAAGCACCGACTCGGTGCCACTTTTTCAAGTTGATAACGGACTAGCCTTATTTTAA
CTTGCTATTTCTAGCTCTAAAAC-3'.

### 6.1.10 Anti-inflammatory chemical and drug treatment

Larvae at 3 dpf were incubated in dexamethasone (sigma) and hydrocortisone (sigma) at a final concentration at 100 μM, in 1% DMSO in E3 as previously reported (d'Alencon et al., 2010), or with 0.6 μM (3ki) Shp2 inhibitor 11a-1 (Zeng et al. 2014). At the specified concentrations no development abnormality was observed.

### 6.1.11 Statistical Analysis

Statistical analysis was carried out using PRISM 6 (GraphPad) and Mann–Whitney test (comparing two groups), Kruskal-Wallis test (when comparing to a single group). For qPCR, each gene was normalized to the reference gene *ef1α* and compared with Sidak's multiple comparisons test for gene panels and Mann–Whitney test for single comparisons. For survival assays, Gehan-Breslow-Wilcoxon test was performed with a log-rank test and confirmed with Kaplan-Meier curve to ensure compatibility.

## 6.2 Overexpression of microrna-722 fine-tunes neutrophilic inflammation through inhibiting rac2 in zebrafish

### 6.2.1 Generation of transgenic zebrafish lines

The zebrafish experiment was conducted in accordance to the internationally accepted standards. The Animal Care and Use Protocol was approved by The Purdue Animal Care and Use Committee (PACUC), adhering to the Guidelines for Use of Zebrafish in the NIH Intramural

Research Program (Protocol number: 1401001018). A 206 bp genomic DNA sequence flanking microRNA-722 (MI0004765) was PCR amplified using forward: 5'-AATCAGGACTGTGTTGCTGTCT-3', reverse: 5'-CCTCTTCGTCTTCCTCTCGGC-3' and inserted into the BbsI site in the intron of the vector modified from (De Rienzo, Gutzman, & Sive, 2012). GFP was replaced with Dendra2 and then cloned into the Tol2 backbone containing the lyzC promoter and SV40 polyA. The plasmids were deposited to Addgene. More than 3 founders (F0) for both *Tg(lyzC:miR-722/Dendra2)*$^{pu6}$ and *Tg(LyzC:Dendra2)*$^{pu7}$ were obtained as described in the AB background (Deng et al., 2011b). Experiments were performed with F2 larvae produced by F1 fish.

### 6.2.2 Zebrafish neutrophil recruitment assay

Zebrafish wounding and infection were performed as described (Deng et al., 2011b). Hindbrain injection was done as described in (Gutzman & Sive, 2009). Briefly, 2 or 3 dpf larvae were amputated posterior to the notochord, inoculated with *P. aeruginosa* (PAK) into the left otic vesicle or into the ventricle region of the brain at 1000 CFU/embryo respectively. The larvae were fixed in 4% paraformaldehyde at 1 hour post wounding or infection. Neutrophils were stained with Sudan black and the number at the indicated regions were quantified.

### 6.2.3 Dual luciferase reporter assay

Zebrafish *rac2* 3'UTR was amplified with One Step Ahead RT-PCR kit (Qiagen) from zebrafish mRNA using the following primers and inserted into pCS2+GFP using EcoRI/NotI sites: z*Rac2*+: 5'-GTACAAGTGAGAATTCAGATACACGATTCGTCACTG-3'; z*Rac2*-: 5'-ATTGGCGCCGCGGCCGCCAGTTGTACAGTTTATTTTTGC-3'; *Rac2* mutant 3'UTR constructs were generated using Infusion HD cloning kit (Clontech) with the following primers: z*Rac2* mut+: 5'-TTTTGGCAGAAAATGCGTTTTTTAAACTGTACAACTGGCGGCC-3'; z*Rac2* mut-: 5'- CATTTTCTGCCAAAAATAATTCCATAC-3'. The mutations were confirmed by sequencing.

The suppression of the reporter expression was measured. Reporter assay constructs were then cloned into psiCHECK2 (Promega) at XhoI and NotI cloning sites using the following primers to

amplify both wild-type and mutation 3'UTRs from pCS2+ constructs. Psi-z*Rac2*+: 5'-TAGGCGATCGCTCGAGAGATACACGATTCGTCACTGT-3'; Psi-z*Rac2*-: 5'-TTGCGGCCAGCGGCCGCCAGTTGTACAGTTTATTTTTGCCA-3'; Psi-z*Rac2* Mut-: 5'-TTGCGGCCAGCGGCCGCCAGTTGTACAGTTTAAAAAACGCA-3'. MiR-722 expression vector was cloned by amplifying the 722 hairpin from the lyzC:miR-722 vector used to create the transgenic line and inserted into pcDNA3.1 at the HindIII/XbaI cloning sites using the following primers: pcDNA-722+: 5'-GTTTAAACTTAAGCTTGCCACCATGGATGAGGAAATCGC-3'; pcDNA-722-: 5' – AAACGGGCCCTCTAGAGACCGGTACCCCCGGGCTGC-3';
Plasmids were co-transfected into HEK293 cells with Lipofectamine 3000 (Invitrogen). Cells were harvested after 48h. Renilla luciferase activity was normalized with photynus luciferase activity, which were sequentially determined using a dual luciferase reporter assay (Promega) and a plate reader (BioTek). Three independent biological repeats were performed for each 3'UTR.

### 6.2.4 Confocal Imaging

Larvae at 3 dpf were settled on a glass-bottom dish. Time-lapse fluorescence images were acquired with a laser-scanning confocal microscope (LSM710; Zeiss) with a Plan-Apochromat 20x/0.8 M27 objective. The green and red channels were acquired sequentially with 0.1% power of the 488nm laser and 0.4% of 561 nm laser respectively with a 200 μm pinhole at a speed of 1.27 μs/pixel and averaged (line 2). The fluorescent stacks were flattened using the maximum intensity projection and overlayed with a single slice of the bright field image. Neutrophil speed was quantified using ImageJ plug-in MTrackJ (Meijering, Dzyubachyk, & Smal, 2012).

### 6.2.5 RT-qPCR

Total RNA was purified using MiRVANA miRNA purification kit (ThermoFisher). MicroRNAs were reverse transcribed with Universal cDNA Synthesis Kit II (Exiqon). MicroRNA RT-qPCR was performed with ExiLENT SYBR® Green master mix (Exiqon) using LightCycler ® 96 Real-Time PCR System (Roche Life Science). Primers used in this study are: miR-223-3p (205986), dre-let-7e-5p (2106780), dre-miR-722 (2107521) and dre U6 (206999). Messenger

RNAs were reverse transcribed with Transcriptor First Strand cDNA Synthesis Kit (Roche). RT-qPCR were performed with FastStart Essential DNA Green Master (Roche). All primers amplified a single product according to the melt-curve analysis. The relative fold change is calculated following instructions provided by Real-time PCR Minor with correction of the primer efficiencies (http://ewindup.info/miner/data_submit.htm). 10-20 larvae were used in each repeat to generate an average value that was used to calculate the final mean ± s.d. from three independent experiments.

### 6.2.6 FACS of dissociated embryo neutrophils and one-step qRT

Larvae at 3 dpf from Tg(lyzC:miR-722/Dendra2)pu6 and Tg(LyzC:Dendra2)pu7 were injected with 1000 CFU P. aeruginosa (PAK) into the tail vein and incubated to 8hpi. Neutrophils were sorted out by FACSARIA II with the 488 laser as described (Deng et al., 2011b). Neutrophil RNA was extracted as described above and one-step qRT was performed with SuperScript® III Platinum® SYBR® Green One-Step qRT-PCR Kit (Invitogen), using LightCycler ® 96 Real-Time PCR System (Roche Life Science).

### 6.2.7 Survival assay

Larvae at 3 dpf were injected with 1nl of 25ng/nl LPS or 1000 CFU *P. aeruginosa* (PAK) into the tail vein and incubated individually in 96 well plates. Survival was tracked for 7 days or when one group reached 100% mortality. Representative experiments of at least three independent repeats (n>=20 larvae in each experiment) were shown.

### 6.2.8 MicroRNA mimic and inhibitor delivery

All mimics and the miR-722 inhibitor were synthesized by ThermoFisherScientific. Embryos at the one-cell stage were injected with 1nl of 15 µM dre-miR-722 mimic (#4464066), dre-miR-722 inhibitor (#4464084), hsa-miR-129-5p mimic (#4464084), 1 µM dre-miR-223 mimic (#4464066) or buffer as a control. Tail wounding and survival assays were carried out as described above but at 2 dpf.

### 6.2.9 Statistical Analysis

Statistical analysis was carried out by PRISM 6 (GraphPad). Unpaired Student's t-test (comparing two groups), one-way ANOVA (when comparing to single group), or two-way ANOVA (for multiple comparisons) were utilized in neutrophil recruitment assays and the reporter assays. For RT-qPCR, each gene was normalized to the reference gene and compared with paired Student's t-test. For survival assays, Gehan-Breslow-Wilcoxon test was performed with a log-rank test and confirmed with Kaplan-Meier curve to ensure compatibility.

## 6.3 Inducible overexpression of zebrafish microrna-722 suppresses chemotaxis of human neutrophil like cells

### 6.3.1 Generation of stable HL-60 cell lines

HEK-293 cells were cultured in DMEM supplemented with 10% FBS, 4.5 g/glucose and sodium bicarbonate. HL-60 cells were obtained from ATCC (CCL-240) and cultured using RPMI-1640 with HEPEs supplemented with 10% FBS with sodium bicarbonate. The lentiviral backbone pLIX_403 was a gift from David Root (Addgene plasmid # 41395). DNA sequence encoding microRNA-722 tagged with Dendra2 were amplified from (Addgene plasmid # 97163) with the following primers: pLIX-mir+: 5'-TGGAGAATTGGCTAGCGCCACCATGGATGAGGAAA TCGC-3', pLIX-mir-: 5'-CATACGGATAACCGGTTACCACACCTGGCTGGGC-3'and cloned into pLIX_403 vector using the NheI/AgeI sites. Stable HL-60 cell lines were generated as described (Cavnar, Berthier, Beebe, & Huttenlocher, 2011). Briefly, HEK-293 cells were transfected with pLIX_403, VSV-G and CMV8.2 using lipofectamine 3000 (ThermoFisher). The viral supernatant was harvested on day three and concentrated with Lenti-X concentrator (Clontech). HL-60 Cells were spin infected at 2000 g for two hours at 32 ºC and then selected and maintained in medium supplemented with 1 µg/ml puromycin. Live cells that excluded trypan blue stained cells were counted using a hemocytometer.

### 6.3.2 Epifluorescence microscope imaging

Induction of the Dendra2 reporter expression was verified by imaging the green fluorescence using AXIO Zoom V16 microscope (Zeiss) at 110 % magnification. All images were acquired under the same condition within the linear range of the CCD detector. Dendra2+ Cell

quantification was done by image J by measuring the mean fluorescence intensity of the dendra2 channel and divided by DAPI based cell count.

### 6.3.3 RT-qPCR

Total RNA was purified using MiRVANA miRNA purification kit (ThermoFisher). MicroRNAs were reverse transcribed with Universal cDNA Synthesis Kit II (Exiqon). MicroRNA RT-qPCR was performed with ExiLENT SYBR® Green master mix (Exiqon) using LightCycler ® 96 Real-Time PCR System (Roche Life Science). Primers used in this study are: miR-223-3p (205986), dre-miR-722 (2107521), hsa-let-7e-5p (205711) and human U6 (203907). Messenger RNAs were reverse transcribed with Transcriptor First Strand cDNA Synthesis Kit (Roche). RT-qPCR were performed with FastStart Essential DNA Green Master (Roche). Primers used are: *Pre722+: 5'-cggagtggaatttgaaacgttttggc-3'; Pre722-:5'-cggagcgaaatctgaaacgtttctgc-3'; Ccl2+: 5'-agtctctgccgcccttct-3'; CCL2-: 5'-gtgactggggcattgattg-3'; CLEC4A+: 5'-cccctcttgaggatatgtgc-3'; CLEC4A-: 5'-aggaaccaaacatggtggtaa-3'; C5AR1+: 5'-aagtaatgatacagagggatcttgtg-3'; C5AR1-: 5'-ttgcaagatgttgccattg-3'; CR1+: 5'-ctccccctcggtgtatttct-3'; CR1-: 5'-cctgtttcctggtactctaattgc-3'; FPR1+: 5'-tctctgctggtccccatatc-3'; FPR1-: 5'-ttgcaataactcacggattctg-3'; RAC2+: 5'-gatgcaggccatcaagtgt-3'; RAC2-: 5'-ctgatgagaaggcaggtcttg-3'; GAPDH+: 5'-ccccggtttctataaattgagc-3'; GAPDH-: 5'-cttccccatggtgtctgag-3'*. The specificity of the primers were verified with a single peak in the melt-curve. The relative fold change with correction of the primer efficiencies was calculated following instructions provided by Real-time PCR Minor (http://ewindup.info/miner/data_submit.htm) and normalized to *U6* (miRNA) and *GAPDH* (mRNA) respectively.

### 6.3.4 Flow Cytometry

Cells were stained with Alexa Fluor 647 conjugated CD11b (neutrophil differentiation marker, Biolegend, 301319, clone IV-M047) or the isotype control antibody (Biolegend, 400130, clone MOPC-21) and RUO AnnexinV (apoptosis marker, BD, 563973). Cells were stained in staining buffer (1%BSA 0.1% $NaN_3$) and incubated on ice for 1 hour, washed three times with staining buffer and resuspended to suitable volume. Dendra 2 reporter expression levels were collected

with the 488nM excitation filter and 530/30 PMT. Fluorescence intensity and collected using BD LSR Fortessa. Results were analyzed with Beckman Kaluza 2.1 software.

### 6.3.5 RNAseq

HL-60 cells were differentiated for 4 days in 1.3% DMSO (Jacob, Leport, Szilagyi, Allen, Bertrand, et al., 2002), induced with 1µg/ml doxycycline or left un-induced for 2 additional days, and then pelleted into microtubes each containing 107 cells. Total mRNA was extracted using RNeasy Plus Mini Kit (Qiagen #74104). RNAseq was performed at The Center for Medical Genomics at Indiana University School of Medicine. Samples were polyA enriched and sequenced with Illumina HiSeq 4000 with reads range from 37M to 44M. The RNA-seq raw data and processed data are in the process of being submitted to the Gene Expression Omnibus (GEO) and will be publicly available upon the acceptance of the manuscript.

### 6.3.6 Bioinformatics analysis on RNA-seq data:

The sequencing reads was mapped to the human genome using STAR v2.5 RNA-seq aligner (Dobin et al., 2013) with the following parameter: "--outSAMmapqUnique 60". Uniquely mapped sequencing reads were assigned to hg38 genes using featureCounts v1.6.2 (Liao, Smyth, & Shi, 2014) with the following parameters: "-s 2 –p –Q 10". The genes were filtered if their count per million of reads were less than 0.5 in more than 4 of the samples. The trimmed mean of M values method was used for normalization on gene expression profile across all samples, followed by the differential expression analysis using edgeR v3.20.8 (McCarthy, Chen, & Smyth, 2012; Robinson, McCarthy, & Smyth, 2010). The gene was determined as differentially expressed gene if its p-value after FDR-adjusted multiple-test correction was less than 0.01 and its amplitude of fold change was larger than 1.8. We identified 1943 down-regulated DEGs and 632 up-regulated DEGs by comparing miR-722 ± Dox. However, no DEG was recognized for the control line based on the same cutoffs. The software package, DAVID Bioinformatics Resources 6.8 (Huang da, Sherman, & Lempicki, 2009a, 2009b) was adopted for Gene Ontology and KEGG pathway enrichment analysis. The significant enriched GO terms or KEGG pathways were selected if their FDR-adjusted p-values (q-values) were less than 0.05 after multiple test

correction, when we compared DEGs down-regulated by miR-722 +Dox with all expressed genes tested by RNA-seq.

### 6.3.7 Immunoblotting

HL-60 cells were differentiated for 4 days in 1.3% DMSO (Jacob, Leport, Szilagyi, Allen, Bertrand, et al., 2002), induced with 1ug/ml Doxycycline or left un-induced for 2 additional days, and then pelleted into microtubes each containing $10^6$ cells. Cells were lysed with RIPA buffer (Thermo #89900) supplemented with proteinase inhibitor cocktail (Roche # 4693132001). Protein content in the supernatant was determined with BCA assay (Thermo #23225) and 25~50 µg of protein were subjected to SDS-PAGE and transferred to nitrocellulose membrane. Immunoblotting was performed with a mouse anti-RAC2 antibody (Millipore 07-604-I), a rabbit anti-Vinculin antibody (Sigma V9131) and goat anti-mouse (Invitrogen 35518) or anti-rabbit (Thermo SA5-35571) secondary antibodies. The fluorescence intensity was measured using an Odyssey imaging system (LI-COR).

### 6.3.8 Reporter assay

miR-722 or vector control constructs were cloned into PCDNA3.1 as described (Hsu et al., 2017a). Human *RAC2* 3'UTR was amplified with One Step Ahead RT-PCR kit (Qiagen) from human mRNA using the following primers *RAC2* 3'UTR+: 5'-TAGGCGATCGCTCGAGGGGTTGCACCCCAGCGCT-3', *RAC2* 3'UTR- : 5'-TTGCGGCCAGCGGCCGCTCTCCAAACTTGAATCAATAAATTT-3' and inserted into a dual luciferase psiCHECK2 backbone (Promega). *RAC2* mutant 3'UTR constructs were generated using Infusion HD cloning kit (Clontech) with the following primers: *RAC2* mut+: 5'-GAGTTCCTCTACCCACGTTTTTTGAGTGTCTCAGAAGTGTGC-3', *RAC2* mut–: 5'-TGGGTAGAGGAACTCTCTGG-3. Mutation was confirmed with Sanger sequencing. HEK-293T cells seeded at $2x10^5$/well in 12 well plates and transfected with the indicated miR-722 overexpression and the *RAC2* 3'UTR reporter plasmids with Lipofectamine 3000 (Invitrogen). Cells were harvested and lysed at 48 h post transfection and luciferase activity was measured with Dual Glo-Luciferase reagent (Promega, PF-E2920) in a Synergy 2 (Biotek) plate reader.

The renilla luciferase activity was normalized to the firefly luciferase, which was then normalized to the vector control.

### 6.3.9 Transwell migration assay

HL-60 transwell assays were performed as described (Cavnar et al., 2011). Briefly, differentiated cells were resuspended in HBSS buffer and allowed to migration for 2 h towards fMLP (100 nM). Cells that migrated to the lower chamber were released with 0.5M EDTA and counted using a BD LSRFortessa flow cytometer with an acquisition time of 30 sec. The counts were normalized with the total numbers of cells added to each well the data was then gated for live cells and analyzed with Beckman Kaluza 2.1 software.

### 6.3.10 2D Chemotaxis assay

Differentiated HL-60 cells were resuspended in HBSS with 20mM HEPES and 0.5% FBS and loaded in collagen-coated IBIDI chemotaxis µ-slides (ibidi # 80326) and incubated at 37ºC for 30 minutes to allow cells to adhere. 15 ul of 1000 nM fMLP was loaded into the right reservoir yielding a final fMLP concentration of 187 nM. Cell migration was recorded every 60 sec for 120 minutes using LSM 710 (with Ziess EC Plan-NEOFLUAR 10X/0.3 objective) at 37ºC. Cells expressing Dendra2 with initial position on the left half of the channel were tracked with ImageJ plug-in MTrackJ as previously described (Meijering et al., 2012). Velocity and chemotaxis index were quantified using the ibidi cell migration tool.

### 6.3.11 Fluorescence microscopy

dHL-60 cells were resuspended in HBSS with 20 mM HEPES and 0.5% FBS and attached to fibrinogen-coated slides for 30 min at 37ºC. Cells were then stimulated with 100 nM fMLP for 3 min at 37ºC and fixed with 4% paraformaldehyde in PBS for 15 min at 37ºC. The staining of fixed cells were performed as previously described (Fayngerts et al., 2017). Cells were permeabilized with 0.1% Triton X-100 and 3% BSA in PBS for 1 h at room temperature and blocked with 3% BSA in PBS for 1 h at room temperature. dHL-60 cells were incubated with phalloidin -AlexaFluor 568 (Invitrogen A12380) diluted 1:100 in 3% BSA overnight at 4ºC. The cells were then stained with 1µg/ml DAPI (Invitrogen D3571) in 3% BSA for 1 h at room

temperature. Images were acquired using a laser scanning confocal microscope LSM 710 (Zeiss) with a Plan-Apochromat 63x/1.4 Oil M27 or Plan-NEOFLUAR 10X/0.3 objective and processed with ImageJ.

### 6.3.12 ROS measurement

dHL-60s were treated with PMA 0.5 ng/µl or 100 nM fMLP and hydrogen peroxide levels in the culture media were measured using the Amplex® Red Hydrogen Peroxide/Peroxidase Assay Kit (Invitrogen A22188). Results were obtained using a Flexstation Multi-Mode Microplate Reader (Molecular Devices) with 544nM monochrome excitation and 590 emission bandpass filter. Background was normalized by subtracting the reading from samples treated with the vehicle control (DMSO for fMLP and ethanol for PMA respectively). Concentrations were calculated using a hydrogen peroxide standard curve.

### 6.3.13 Statistical Analysis

Statistical analysis was carried out using PRISM 6 (GraphPad). Mann–Whitney test (comparing two groups) and Kruskal–Wallis test (when comparing to single group) were used in this study as indicated in the figure legends. A representative experiment of at least three independent repeats were shown. For qPCR, each gene was normalized to the reference gene and compared with Mann–Whitney tests. The statistical significance of overlap between miR-722 down-/up-regulated genes and miR-722 target genes was calculated using hypergeometric distribution.

## 6.4 Phenotypical microRNA screen reveals a noncanonical role of CDK2 in regulating neutrophil migration

### 6.4.1 microRNA seq

Neutrophil and apical epithelial cells were sorted from transgenic zebrafish lines *Tg(lyzC:GFP)* and *Tg(Krt4:GFP*) at 3 day post fertilization (dpf) using fluorescence-activated cell sorting. Total RNA was exacted using Ambion mirVana kit (without enrichment for small RNA). Library was prepared using TruSeq Small RNA Preparation (illumina). DNA of 145-160 bp were excited from Invitrogen 6% Novex TBE Gel and sequenced using Illumina HiSeq2000 with paired-end

reads of 50 bp with a total of 2-3M/sample. MicroRNA sequence is performed at University of Wisconsin Collaborative Genomics Core. For analysis, sequencing reads were mapped to the zebrafish genome (GRCz11) using RNA-seq aligner from STAR (v2.5) (Dobin et al., 2013) using previously descried parameters (Simopoulos, 1966) to evaluate expression levels of zebrafish mature microRNAs based on uniquely mapped reads with the parameters: "-s 1 –Q 10". Before TMM normalization and DE analysis by edgeR (v3.20.8) (Robinson et al., 2010), microRNAs whose CPM was less than 10 were removed from all samples. Differentially expressed microRNAs were selected if their FDR-adjusted p-values were less than 0.05.

### 6.4.2 RNA seq

Kidney marrow was dissected from 2 adults from *Tg(lyzC:* miR-199-3-*dendra2)*$^{pu19}$ or *Tg(lyzC: vector-dendra2)*$^{pu7}$ and neutrophils were sorted using FACS. Total RNA was extracted using RNeasy Plus Mini Kit (Qiagen #74104). RNAseq was performed at The Center for Medical Genomics at Indiana University School of Medicine. Samples were polyA enriched and sequenced with Illumina HiSeq 4000 ultra-low with reads range from 37M to 44M. The RNA-seq aligner from the STAR (v2.5) (Dobin et al., 2013) were employed to map RNA-seq reads to the reference genome, zebrafish (GRCz11), with previously the following parameter: "--outSAMmapqUnique 60". Uniquely mapped sequencing reads were assigned to genes using featureCounts (from subread v1.5.1) (Liao et al., 2014) with the following parameters: "-p -Q 10". The genes were filtered for further analysis if their count per million (CPM) of reads was less than 0.5 in more than 3 samples. The method of trimmed mean of M values (TMM) was adopted for gene expression normalization cross all samples, followed by differential expression analysis between different conditions using edgeR (v3.20.8). Differentially expressed gene was determined for the comparison if its false discovery rate (FDR) adjusted p-value was less than 0.05 and the amplitude of fold change (FC) was larger than linear 2-fold. The functional analysis was performed on DEGs of our interest with a cutoff of FDR < 0.05 to identify significantly over-represented Gene Ontology (GO) and/or KEGG pathways by using the DAVID (Huang da et al., 2009b).

### 6.4.3 Protein-Protein interactions (PPIs)

Genes/proteins interacting with *cdk2* or *cdk5* in *Danio rerio* were retrieved from the PPI database, STRING v11 (https://string-db.org/). The pairs were filtered if their confidence scores are less than 0.4. The significance value of enrichment was calculated based on hypergeometric model.

### 6.4.4 Quantitative RT-PCR

Total RNA was purified using MiRVANA miRNA purification kit (ThermoFisher) for miRNA or RNeasy Plus Mini Kit (Qiagen #74104) for mRNA. MicroRNAs were reverse transcribed with Universal cDNA Synthesis Kit II (Exiqon). MicroRNA RT-qPCR was performed with ExiLENT SYBR® Green master mix (Exiqon) and mRNA with one-step RT-qPCR was performed with SuperScript® III Platinum® SYBR® Green kit (Invitrogen) using LightCycler ® 96 Real-Time PCR System (Roche Life Science). The specificity of the primers were verified with a single peak in the melt-curve. The relative fold change with correction of the primer efficiencies was calculated following instructions provided by Real-time PCR Miner (http://ewindup.info/miner/data_submit.htm) and normalized to *U6*. miRNA Primers used in this study were purchased from Exiqon. The relative fold change with correction of the primer efficiencies was calculated following instructions provided by Real-time PCR Miner and normalized to *rpl32*. Primers: dre-cdk1+: 5'-ttggggtcccagtaagagtcta-3'; dre-cdk1-: 5'-ggtgtggaatagcgtgaagc-3'; dre-cdk2+: 5'-agatggcagagaccttctcg-3'; dre-cdk2-: 5'-cggaaaaaccgatgaacaag-3' ; dre-cdk5+: 5'-tgggaacgccaacagaag-3'; dre-cdk5-: 5'-agctggatacatcgggtacg-3' ; dre-cdca8+: 5'-atggcaccgctgaagtctac-3'; dre-cdca8-: 5'-cgttgaaggagctttctttga-3' ; dre-kif14+: 5'-aggaggctcgcttgaagg-3'; dre-kif14-: 5'-ctctttagccacctgaatgc-3' ; dre-mcm5+: 5'-aagctattgcctgcctgct-3'; dre-mcm5-: 5'-ccctcttcgtgtcagaccat-3' ; dre-casp3b+: 5'- caggatattacgcatggagga-3'; dre-casp3b-: 5'-tcgcacagcgaggagataa-3' ; dre-ikbkb+: 5'-gaggagcgagaaacaactgc-3'; dre-ikbkb-: 5'-tggactgcgaactttactgc-3' ; dre-rpl32+: 5'- tcagtctgaccgctatgtcaa-3'; dre-rpl32-: 5'-tgcgcactctgttgtcaatac-3'.

### 6.4.5 Generation of transgenic zebrafish lines

300-600bp genomic DNA fragments flanking the respective miRNA were PCR amplified from zebrafish genomic DNA using specific primers and inserted into the *Bbs*I site in the vector backbone as described (Hsu et al., 2017b) Briefly, the miRNA along with the flanking sequences was inserted into an intron cassette in a Tol2 backbone containing the *lyzC* promoter and SV40 polyA for neutrophil specific expression. Zebrafish *cdk2* gene was cloned from zebrafish mRNA using SuperScript III RT-kit (Invitrogen #18080044) and amplified with the following primers. zCdk2+: 5′- gaaaaccccggtcctatggagtcttttcagaaagtggag-3′; zCdk2-: 5′- catggctgattatgattataggcgtaaaggaggcactgg-3 and inserted into a Tol2-lyzC-mcherry-2A backbone. Point mutation was generated using infusion (Takara #638920) site directed mutagenesis with zCdk2 DN+: 5′- actggctaactttggtttggccagagcgttc -3′; zCdk2 DN -: 5′- ccaaagttagccagtttgatctcgccctg -3' Microinjections of fish embryos were performed by injecting 1nl of mixture containing 25 ng/µl plasmid and 35 ng/µl tol2 transposase mRNA in a isotonic solution into the cytoplasm of embryos at one-cell stage. The plasmids were injected into zebrafish embryo at 1-cell stage and the stable line were generated as previously described (Deng et al., 2011a). At least two founders (F0) for each *line* were obtained. Experiments were performed using F2 larvae produced by F1 fish derived from multiple founder to minimize the artifacts associated with random insertion sites.

### 6.4.6 Dual luciferase reporter assay

Both zebrafish and human *CDK2* 3′UTR were amplified from zebrafish or HL-60 cell genomic DNA with SuperScript III RT-kit (Invitrogen #18080044) and cloned into psiCHECK2 (Promega) at *Xho*I and *Not*I cloning sites with the following primers: zCDK2+:5'- taggcgatcgctcgagaacgagatcaactttggcaag-3'; zCdk2-: 5'- ttgcggccagcggccgctgtaacaacataaaccaaatgtt-3';,hCDK2+: 5'- taggcgatcgctcgagagccttcttgaagccccca-3'; hCdk2-: 5'- ttgcggccagcggccgctataaaactaggcacatttttttaa-3'. Mutated 3´UTR constructs were generated using Infusion HD cloning kit (Clontech) with the following primers: zCdk2 mut+: 5'- cctgtgtgacccaaaaaaacagctgtgctaatagt-3'; zCdk2 mut-: 5'- tttgggtcacacaggttgcaatggataatcttca-3', hCdk2 mut+: 5'- aaaacgtgaccgaggagtctattttaaagaattcgg-3'. DNA encoding miR-199 or vector were amplified from the construct used for expression in zebrafish and inserted into pcDNA3.1

at the *Hin*dIII/*Xba*I cloning sites using the following primers: pcDNA-199+: 5;-gtttaaacttaagcttgccaccatggatgaggaaatcgc-3'; pcDNA-199-: 5'-aaacgggccctctagagaccggtacccccgggctgc-3'.

### 6.4.7 Live imaging

Larvae at 3 dpf were settled on a glass-bottom dish and imaging was performed at 28 ºC. Time-lapse fluorescence images in the head mesenchyme were acquired with a laser-scanning confocal microscope (LSM710, Zeiss) with a Plan-Apochromat 20×/0.8 M27 objective. Neutrophil motility at the caudal hematopoietic tissue was imaged using Zeiss EC Plan-NEOFLUAR 10X/0.3 objective. For neutrophil nucleus and cytosol reporter line imaging, a LD C-Apochromat 40x/1.1 W Korr M27 was used. The green and red channels were acquired sequentially with 0.1~0.3% power of the 488 nm laser and 0.5%~2% of 561 nm laser, respectively, with a 200 µm pinhole at a speed of 1.27 µs/pixel and averaged (line 2). The fluorescent stacks were flattened using the maximum intensity projection and overlaid with a single slice of the bright-field image. Neutrophil chemotaxis upon LTB4 treatment was captured with a Zeiss ZV16 dissection microscope at 2x magnification every 15s for 30min.

### 6.4.8 Inflammation assays in zebrafish

Zebrafish wounding and infection were performed as described (Hsu et al., 2017b). Briefly, 3 dpf larvae were amputated posterior to the notochord, or inoculated with *P. aeruginosa* (PAK) into the left otic vesicle or into the vasculature at 1000 CFU/embryo. The larvae were fixed in 4% paraformaldehyde at 1h post-wounding or -infection. Neutrophils were stained with Sudan black and the number at the indicated regions were quantified. For LTB4 recruitment assays, 3 dpf zebrafish larvae were treated with 30 nM LTB4 for 15 min and fixed. Neutrophils were stained with Sudan Black and the number at the indicated regions were quantified.

### 6.4.9 Generation of stable HL-60 cell lines

HL-60 cells were obtained from ATCC (CCL-240) and cultured using RPMI-1640 with HEPES supplemented with 10% FBS and sodium bicarbonate. The lentiviral backbone pLIX_403 was a gift from David Root (Addgene plasmid # 41395). The DNA sequence flanking MIR-199 was

cloned from HL-60 cell genomic DNA and cloned into a backbone containing *dendra2*. The miRNA and *dendra2* reporter were then cloned into pLIX_403 vector using the NheI/AgeI sites with primer set: pLIX-mir+: 5' tggagaattggctagcgccaccatggatgaggaaatcgc-3', pLIX-mir-: 5'-catacggataaccggttaccacacctggctgggc-3'. Stable HL-60 cell lines were generated as described (Cavnar et al., 2011; Hsu et al., 2019b). Briefly, HEK-293 cells were transfected with pLIX_403 or pLKO.1, together with VSV-G and CMV8.2 using lipofectamine 3000 (ThermoFisher). The viral supernatant was harvested on day three and concentrated with Lenti-X concentrator (Clontech 631232). HL-60 cells were infected with concentrated lentivirus in complete RPMI medium supplemented with 4 µg/ml polybrene (Sigma TR-1003-G) at 2500g for 1.5h at 32 ºC and then selected with 1 µg/ml puromycin (Gibco A1113803) to generate stable lines.

### 6.4.10 Inhibitor treatment for zebrafish larvae

CDK2 inhibitors NU6140 (Enzo # ALX-270-441), CTV313 (Sigma #238803) and roscovitine (Selleckchem #S1153) were dissolved in DMSO to make a 100 mM stock, then further diluted in E3 to working concentrations (100 µM for recruitment and motility assays, and indicated concentration for survival assays). For inhibiting DNA replication, 150 µM aphidicolin and 20 mM hydroxyurea (Sigma #A0781) in 1% DMSO was used as previously described (L. X. Zhang et al., 2008). For neutrophil recruitment and random motility assays, larval were pretreated with the inhibitor for 1h before experimental procedures. For survival assays, larval were pretreated and kept in the inhibitors from 1 hour post infection.

### 6.4.11 Transwell migration assay

dHL-60 transwell assays were performed as described (Cavnar et al., 2011). Briefly, $2x10^6$ cells/ml differentiated cells were resuspended in HBSS with 0.5%FBS and 20 mM HEPES. 100 µl were placed into a 6.5 mm diameter 3 µm pore size transwell inset (Corning#3415) and allowed to migrate for 2h at 37°C towards 100 nM fMLP in 500 µl of HBSS in a 24-well plate. Loading controls were done by directly adding 100 µl of cells to 400 µl of HBSS. Cells that migrated to the lower chamber were released with 0.5M EDTA and counted using a BD LSRFortessa flow cytometer with an acquisition time of 30s. The counts were normalized with

the total numbers of cells added to each well the data was then gated for live cells and analyzed with Beckman Kaluza 2.1 software.

### 6.4.12 Primary neutrophil isolation and chemotaxis assay

Primary human neutrophils were isolated with Milteny MACSxpress Neutrophil Isolation Kit. Cells were stain for 10 min with Calcein AM and washed with PBS. $10^7$ cells/ml were incubated in RPMI+0.1% HSA containing 50 μM NU6104 or DMSO at 37ºC/5% $CO_2$ for 45min. Microfluidic devices were fabricated as previously described (Berthier et al., 2013). Microfluidic chambers were coated with 10 μg/ml fibrinogen for 1h at 37 °C in PBS. 3 μl of neutrophil suspension ($4 \times 10^6$ cells/ml) was added to the device, and 5 μM IL-8 was added to the source port. The gradient was allowed to set up and equilibrate in a 37 ℃ humidified chamber for 15min before imaging. Time-lapse imaging was performed using a 10×, NA of 0.45, or 60×, NA of 1.4 objective and motorized stage (Ludl Electronic Products) on an inverted microscope (Eclipse TE300) using a charge-coupled device camera (CoolSNAP ES2) and captured into MetaVue imaging software v6.2. Images were taken every 30s for 30–45min with up to eight devices being imaged simultaneously. Tracking and velocity quantification were performed as described (Yamahashi et al., 2015).

### 6.4.13 Survival assay

Larvae at 3 dpf were injected with 1 nl of 25 ng/nl LPS or 1000 CFU *P. aeruginosa* (PAK) into the tail vein and incubated individually in 96-well plates. Survival was tracked for 4 days or when one group reached 100% mortality. Representative results of at least three independent experiments ($n \geq 20$ larvae in each experiment) were shown.

### 6.4.14 Statistical analysis

Statistical analysis was carried out using PRISM 6 (GraphPad). Mann–Whitney test (comparing two groups), Kruskal–Wallis test (when comparing to single group), and Gehan–Breslow–Wilcoxon test (for survival curve comparison) were used in this study as indicated in the figure legends. Individual p values are indicated in the figure with no data points excluded from statistical analysis. One representative experiment of at least three independent repeats are

shown. For qPCR, each gene was normalized to a reference gene and compared with Holm-Sidak test (individual comparison with paired value) where each p value and DF was adjusted for respective multiple comparisons.

### 6.4.15 Study Design

The objective of this research is to identify new molecules that regulate neutrophil migration. The zebrafish experiment was conducted in accordance with internationally accepted standards. The Animal Care and Use Protocol was approved by The Purdue Animal Care and Use Committee (PACUC), adhering to the Guidelines for Use of Zebrafish in the NIH Intramural Research Program (protocol number: 1401001018). We used MATLAB and the samplesizepwr function to calculate the sample sizes required for each experiment based on conservative estimates for the variability in the controls for each type of experiments. With a power of 0.9 (significance level of 0.05) in two sample t test, we need a sample size of 15 neutrophils to detect a change of 20% in the motility assay; 11 embryos to detect a change of 20% in LTB4 fin recruitment assay; 11 embryos to detect a change of 20% in total neutrophil numbers; 22 and 25 embryos to detect a 50% change of neutrophil numbers recruited to the wound and ear infection sites respectively. Results were derived from multiple founders for each transgenic line. All data were included in final analysis and quantified blindly. All experiments were repeated at least three times.

### 6.4.16 Generation of stable CDK2 and CDK5 knockdown HL-60 cell lines

To generate knock down lines of CDK2 and CDK5 in HL-60 cells, pLKO.1 lentiviral constructs with shRNA were obtained from Sigma-Aldrich. CDK2-sh1: TRCN0000010470; CDK2-sh2: TRCN0000010471; CDK5-sh1: TRCN0000021465; CDK5-sh2: TRCN0000021466; non-targeting control: SHC016.

Stable HL-60 cell lines were generated as described(1, 2) Briefly, HEK-293 cells were transfected with pLIX_403 or pLKO.1, together with VSV-G and CMV8.2 using lipofectamine 3000 (ThermoFisher). The viral supernatant was harvested on day three and concentrated with Lenti-X concentrator (Clontech 631232). HL-60 cells were infected with concentrated lentivirus

in complete RPMI medium supplemented with 4 µg/ml polybrene (Sigma TR-1003-G) at 2500g for 1.5h at 32 ºC and then selected with 1 µg/ml puromycin (Gibco A1113803) to generate stable lines.

### 6.4.17 Transient expression of Cdk2 and Cdk5 in zebrafish

Zebrafish cdk2 and cdk5 genes was cloned from zebrafish mRNA using SuperScript III RT-kit (Invitrogen #18080044) and amplified with the following primers. zCdk2+: 5'-gaaaaccccggtcctatggagtcttttcagaaagtggag-3'; zCdk2-: 5'-catggctgattatgattataggcgtaaaggaggcactgg-3' , zCdk5+: 5'-gaaaaccccggtcctatgcaaaagtatgagaagctgg-3'; zCdk5-: 5'- catggctgattatgattatggtgggcagaaatcagc-3' and inserted into a Tol2-lyzC-mcherry-2A backbone. Point mutation was generated using infusion (Takara #638920) site directed mutagenesis with zCdk2 DN+: 5'-actggctaactttggtttggccagagcgttc -3'; zCdk2 DN -: 5'- ccaaagttagccagtttgatctcgccctg -3', zCdk5 DN+: 5'- gttggctaatttcggcttggccagagcg -3'; zCdk5 DN -: 5'- ccgaaattagccaacttcagttccccg -3'. Microinjections of fish embryos were performed by injecting 1nl of mixture containing 25 ng/µl plasmid and 35 ng/µl tol2 transposase mRNA in a isotonic solution into the cytoplasm of embryos at one-cell stage of Tg(lyzC:GFP) lines.

### 6.4.18 Fluorescence microscopy

dHL-60 cells were resuspended in HBSS with 20 mM HEPES and 0.5% FBS and allowed to attach to fibrinogen-coated slides for 30min at 37 ºC. Cells were then stimulated with 100 nM fMLP for 3min at 37 ºC and fixed with 4% paraformaldehyde in PBS for 15min at 37 ºC. Immuno- staining was performed as previously described (3). Briefly, cells were permeabilized with 0.5% Triton X-100 and 3% BSA in PBS for 1h at RT and blocked with 3% BSA in PBS for 1h. dHL-60 cells were incubated with phalloidin -AlexaFluor 568 (Invitrogen A12380) and anti-phosho-myosin light chain II (Cell signaling #3671S) (diluted 1:100 in 3% BSA) overnight at 4ºC. The cells were then stained with 1 µg/ml DAPI (Invitrogen D3571) and goat anti rabbit AlexaFluor488 (Invitrogen A27034) (1:500 in 3% BSA) for 1h at RT. Images were acquired using a laser scanning confocal microscope LSM 710 (Zeiss) with a Plan-Apochromat 63x/1.4 Oil M27 or Plan-NEOFLUAR 10X/0.3 objective and processed with ImageJ. Colocalization

efficiency was quantified with the ImageJ plugin coloc2 with background subtraction and ROI selection. Results are presented as normalized Pearson's correlation.

### 6.4.19 Flow cytometry

Cells were stained with Alexa Fluor 647 conjugated CD11b (neutrophil differentiation marker, Biolegend, 301319, clone IV-M047, 2ul to 1X106 cells) or the isotype control antibody (Biolegend, 400130, clone MOPC-21, 2ul to 1X106 cells) and RUO AnnexinV (apoptosis marker, BD, 563973, 5ul to 1X106 cells). Cells were stained in staining buffer (1% BSA, 0.1% NaN3) and incubated on ice for 1 hour, washed three times with staining buffer and resuspended in suitable volumes. Cell cycle profiling was obtained using Vybrant™ DyeCycle™ Ruby Stain (Thermo #V10309) following the manufacture's protocol. Fluorescence intensity were collected using BD LSR Fortessa. Results were analyzed with Beckman Kaluza 2.1 software.

### 6.4.20 Immunoblotting

dHL-60 cells were differentiated for 6 days in 1.3% DMSO (Jacob et al., 2002) and 106 cells were pelleted in microcentrifuge tubes. Cells were lysed with RIPA buffer (Thermo #89900) supplemented with proteinase inhibitor cocktail (Roche # 4693132001). Protein contents in the supernatant were determined with BCA assay (Thermo #23225) and 25~50 µg of proteins were subjected to SDS-PAGE and transferred to PVDF membranes. Immunoblotting was performed with anti-CDK1 (Santa Cruz #sc-54), anti-CDK2 (abcam #ab32147), anti-CDK5 (Santa Cruz #sc-249), anti-Vinculin antibody (Sigma V9131), or anti-beta-Tubulin (DSHB, E7). Phosho-protein probing was performed as described (4). Briefly, 1.5x106 cells/ml dHL-60s were starved in serum free media for 1h at 37°C/5% CO2. Cells were then stimulated with 10 nM fMLP for 1 or 3min at RT and immediately put on ice with addition of ice cold lysis solution in a 1:1 ratio (20% TCA, 40 mM NaF, and 20 mM β-glycerophosphate, (Sigma #T6399, #G9422, #s6776)). Cells were incubated on ice for 1h and proteins were pelleted down and washed once with 0.75 ml of ice-cold 0.5% TCA and resuspended in 2× Laemmli sample buffer (Bio-Rad Laboratories). Western blot was performed as described with anti-phospho-PAK (Cell signaling #2605S), anti-PAK (Cell signaling #2604), anti-phospho-Akt (Cell signaling #4060S), anti-Akt (Cell signaling #2920S), anti-phospho-Erk1/2 (Cell signaling #4370S), anti-Erk1/2 (Cell signaling #4696S),

along with Vinculin as a loading control. Membranes were incubated with primary antibodies O/N at 4ºC, then with goat anti-mouse (Invitrogen 35518) or anti-rabbit (Thermo SA5-35571) secondary antibodies. The fluorescence intensity was measured using an Odyssey imaging system (LI-COR). Band intensity was quantified using image studio (LI-COR) and normalized with respective loading controls.

### 6.4.21 Real time transwell assay

dHL-60 real time transwell assays were performed following the manufacture instruction "chemotaxis migration module for non-adherent cells" using the transwell module on the IncuCyte S3 live cell analysis system (Sartorius). 60 µl of 2x105 cells/ml dHL-60 cells were incubated with indicated inhibitors for 45min in 0.5% HSA RPMI and placed in a transwell insets precoated with 10 µg/ml fibrinogen. The insets were equilibrated in HBSS reservoir plates for 1h at 37℃ and transferred to reservoirs containing 100 nM fMLP in HBSS. Images on the top of the inserts were taken every 20min for 6h at 37℃ with 5% CO2. Incucyte analysis software (Essen Biosciences) was used to mask and quantify the area of cells remaining on the top of the transwell membrane at each time point, normalizing to the area at time 0. Statistical analysis was done with percent cells migrated (1-%remaining area) at 2h post fMLP stimulation. Inhibitors used in this assay: RO-3306 (Millipore #217699), 40254-90-8 (Millipore #217720), NU6140 (Tocris #3301), Palbociclib (Selleckchem #S1116).

### 6.4.22 NETosis assay

dHL-60 cells were resuspended in HBSS in 20 mM HEPES with 0.5% FBS and allowed to attach to fibrinogen-coated slides for 30min at 37 ºC. Neutrophil extracellular traps (NETs) were induced with 50 nM PMA (sigma #P1585) in HBSS for 4h at 37 ºC. NETs were enumerated using cell permeable Hoechst 33258 (Thermo #62249) at 1 µg/ml and cell impermeable Sytox green (Thermo #37020) at 1 µg/ml. Images were acquired using a laser scanning confocal microscope LSM 710 (Zeiss) with a Plan-Apochromat 63x/1.4 Oil M27 or Plan-NEOFLUAR 10X/0.3 objective and processed with ImageJ. Percentage of cells forming NET was calculated dividing the number of Sytox green positive cells with Hoechst positive cells.

### 6.4.23 TCGA data mining

Normalized RNA-seq data for genes MIR-199 and CDK2 were retrieved from HTSeq FPKM-UQ (Fragments Per Kilobase of transcript per Million mapped reads Upper Quartile) from The Cancer Genome Atlas (TCGA) RNA-seq data from NCI's Genomic Data Commons (GDC) (5). Pearson correlation coefficiency and p-value between MIR-199 and CDK2 in each cancer type were calculated using log2 transformed FPKM-UQ data.

# CHAPTER 7. DATA AVAILABILITY STATEMENT

## 7.1 Inducible overexpression of zebrafish *microRNA-722* suppresses chemotaxis of human neutrophil like cells

The RNA-seq raw data and processed data deposited to Gene Expression Omnibus (GEO) GSE126527 (https://www.ncbi.nlm.nih.gov/geo/query/acc.cgi?acc=GSE126527). Plasmids are available on Addgene: pCDNA miR-722-Dendra (#97163), pcDNA3.1 Dendra2 (#103967), pSi-check2-h*Rac2* 3'UTR (#97160), pSi-check2-h*Rac2* - mut 3'UTR (#97161), plix4.03-miR-722 (#97140), plix4.03-vector (#97141).

## 7.2 Phenotypical microRNA screen reveals a noncanonical role of CDK2 in regulating neutrophil migration

Data and materials availability: The microRNA-seq and RNA-seq raw and processed data are submitted to the Gene Expression Omnibus (GSE127174). Plasmids are available on Addgene.

# REFERENCES


Abdallah, D. S. A., Egan, C. E., Butcher, B. A., & Denkers, E. Y. (2011). Mouse neutrophils are professional antigen-presenting cells programmed to instruct T(h)1 and T(h)17 T-cell differentiation. *International Immunology, 23*(5), 317-326. doi:10.1093/intimm/dxr007

Abdel-Latif, D., Steward, M., Macdonald, D. L., Francis, G. A., Dinauer, M. C., & Lacy, P. (2004). Rac2 is critical for neutrophil primary granule exocytosis. *Blood, 104*(3), 832-839. doi:10.1182/blood-2003-07-2624

Abi Abdallah, D. S., Egan, C. E., Butcher, B. A., & Denkers, E. Y. (2011). Mouse neutrophils are professional antigen-presenting cells programmed to instruct Th1 and Th17 T-cell differentiation. *Int Immunol, 23*(5), 317-326. doi:10.1093/intimm/dxr007

Abraham, E. (2003). Nuclear factor-kappaB and its role in sepsis-associated organ failure. *J Infect Dis, 187 Suppl 2*, S364-369. doi:10.1086/374750

Afonso, P. V., Janka-Junttila, M., Lee, Y. J., McCann, C. P., Oliver, C. M., Aamer, K. A., . . . Parent, C. A. (2012). LTB4 Is a Signal-Relay Molecule during Neutrophil Chemotaxis. *Dev Cell, 22*(5), 1079-1091. doi:10.1016/j.devcel.2012.02.003

Allingham, M. J., van Buul, J. D., & Burridge, K. (2007). ICAM-1-mediated, Src- and Pyk2-dependent vascular endothelial cadherin tyrosine phosphorylation is required for leukocyte transendothelial migration. *J Immunol, 179*(6), 4053-4064. Retrieved from https://www.ncbi.nlm.nih.gov/pubmed/17785844

Amulic, B., Cazalet, C., Hayes, G. L., Metzler, K. D., & Zychlinsky, A. (2012). Neutrophil function: from mechanisms to disease. *Annu Rev Immunol, 30*, 459-489. doi:10.1146/annurev-immunol-020711-074942

Amulic, B., Knackstedt, S. L., Abu Abed, U., Deigendesch, N., Harbort, C. J., Caffrey, B. E., . . . Zychlinsky, A. (2017). Cell-Cycle Proteins Control Production of Neutrophil Extracellular Traps. *Dev Cell, 43*(4), 449-462 e445. doi:10.1016/j.devcel.2017.10.013

Andreasen, A. S., Krabbe, K. S., Krogh-Madsen, R., Taudorf, S., Pedersen, B. K., & Moller, K. (2008). Human endotoxemia as a model of systemic inflammation. *Curr Med Chem, 15*(17), 1697-1705. Retrieved from http://www.ncbi.nlm.nih.gov/pubmed/18673219

Anel, R., & Kumar, A. (2005). Human endotoxemia and human sepsis: limits to the model. *Crit Care, 9*(2), 151-152. doi:10.1186/cc3501

Arroyo, A. B., de los Reyes-Garcia, A. M., Rivera-Caravaca, J. M., Valledor, P., Garcia-Barbera, N., Roldan, V., . . . Gonzalez-Conejero, R. (2018). MiR-146a Regulates Neutrophil Extracellular Trap Formation That Predicts Adverse Cardiovascular Events in Patients With Atrial Fibrillation. *Arteriosclerosis Thrombosis and Vascular Biology, 38*(4), 892-902. doi:10.1161/Atvbaha.117.310597

Bach, S., Knockaert, M., Reinhardt, J., Lozach, O., Schmitt, S., Baratte, B., . . . Meijer, L. (2005). Roscovitine targets, protein kinases and pyridoxal kinase. *J Biol Chem, 280*(35), 31208-31219. doi:10.1074/jbc.M500806200

Benard, E. L., van der Sar, A. M., Ellett, F., Lieschke, G. J., Spaink, H. P., & Meijer, A. H. (2012). Infection of zebrafish embryos with intracellular bacterial pathogens. *J Vis Exp*(61). doi:10.3791/3781

Bernhagen, J., Calandra, T., Mitchell, R. A., Martin, S. B., Tracey, K. J., Voelter, W., . . . Bucala, R. (1995). Mif Is a Pituitary-Derived Cytokine That Potentiates Lethal Endotoxaennia (Vol 365, Pg 756, 1995). *Nature, 378*(6555), 419-419. Retrieved from <Go to ISI>://WOS:A1995TF89300068

Berthet, C., Aleem, E., Coppola, V., Tessarollo, L., & Kaldis, P. (2003). Cdk2 knockout mice are viable. *Current Biology, 13*(20), 1775-1785. doi:DOI 10.1016/j.cub.2003.09.024

Berthier, E., Lim, F. Y., Deng, Q., Guo, C. J., Kontoyiannis, D. P., Wang, C. C. C., . . . Keller, N. P. (2013). Low-Volume Toolbox for the Discovery of Immunosuppressive Fungal Secondary Metabolites. *PLoS Pathog, 9*(4). doi:ARTN e100328910.1371/journal.ppat.1003289

Bhattacharjee, R. N., Banks, G. C., Trotter, K. W., Lee, H. L., & Archer, T. K. (2001). Histone H1 phosphorylation by cdk2 selectively modulates mouse mammary tumor virus transcription through chromatin remodeling. *Mol Cell Biol, 21*(16), 5417-5425. doi:Doi 10.1128/Mcb.21.16.5417-5425.2001

Bollu, L. R., Mazumdar, A., Savage, M. I., & Brown, P. H. (2017). Molecular Pathways: Targeting Protein Tyrosine Phosphatases in Cancer. *Clinical Cancer Research, 23*(9), 2136-2142. doi:10.1158/1078-0432.CCR-16-0934

Bordon, J., Aliberti, S., Fernandez-Botran, R., Uriarte, S. M., Rane, M. J., Duvvuri, P., . . . Ramirez, J. A. (2013). Understanding the roles of cytokines and neutrophil activity and neutrophil apoptosis in the protective versus deleterious inflammatory response in pneumonia. *International Journal of Infectious Diseases, 17*(2), E76-E83. doi:10.1016/j.ijid.2012.06.006

Borregaard, N. (2010). Neutrophils, from marrow to microbes. *Immunity, 33*(5), 657-670. doi:10.1016/j.immuni.2010.11.011

Bousquet, M., Quelen, C., Rosati, R., Mansat-De Mas, V., La Starza, R., Bastard, C., . . . Brousset, P. (2008). Myeloid cell differentiation arrest by miR-125b-1 in myelodysplastic syndrome and acute myeloid leukemia with the t(2;11)(p21;q23) translocation. *J Exp Med, 205*(11), 2499-2506. doi:10.1084/jem.20080285

Brannon, M. K., Davis, J. M., Mathias, J. R., Hall, C. J., Emerson, J. C., Crosier, P. S., . . . Moskowitz, S. M. (2009). Pseudomonas aeruginosa Type III secretion system interacts with phagocytes to modulate systemic infection of zebrafish embryos. *Cell Microbiol, 11*(5), 755-768. doi:10.1111/j.1462-5822.2009.01288.x

Broderick, J. A., & Zamore, P. D. (2011). MicroRNA therapeutics. *Gene Ther, 18*(12), 1104-1110. doi:10.1038/gt.2011.50

Bruehl, R. E., Moore, K. L., Lorant, D. E., Borregaard, N., Zimmerman, G. A., McEver, R. P., & Bainton, D. F. (1997). Leukocyte activation induces surface redistribution of P-selectin glycoprotein ligand-1. *J Leukoc Biol, 61*(4), 489-499. Retrieved from https://www.ncbi.nlm.nih.gov/pubmed/9103236

Buchman, A. L. (2001). Side effects of corticosteroid therapy. *J Clin Gastroenterol, 33*(4), 289-294. Retrieved from http://www.ncbi.nlm.nih.gov/pubmed/11588541

Bunting, M., Harris, E. S., McIntyre, T. M., Prescott, S. M., & Zimmerman, G. A. (2002). Leukocyte adhesion deficiency syndromes: adhesion and tethering defects involving beta 2 integrins and selectin ligands. *Curr Opin Hematol, 9*(1), 30-35. Retrieved from https://www.ncbi.nlm.nih.gov/pubmed/11753075

Cai, Y. X., Shen, Y. B., Gao, L. L., Chen, M. M., Xiao, M., Huang, Z. W., & Zhang, D. M. (2016). Karyopherin Alpha 2 Promotes the Inflammatory Response in Rat Pancreatic Acinar Cells Via Facilitating NF-kappa B Activation. *Dig Dis Sci, 61*(3), 747-757. doi:10.1007/s10620-015-3948-6

Cao, M. W., Shikama, Y., Anzai, M., & Kimura, J. (2015). Impaired Neutrophil Migration Resulting from Mir-34a and Mir-155 Overexpressed in Neutrophils from Myelodysplastic Syndrome Patients. *Blood, 126*(23). Retrieved from <Go to ISI>://WOS:000368019003123

Cao, M. W., Shikama, Y., Kimura, H., Noji, H., Ikeda, K., Ono, T., . . . Kimura, J. (2017). Mechanisms of Impaired Neutrophil Migration by MicroRNAs in Myelodysplastic Syndromes. *J Immunol, 198*(5), 1887-1899. doi:10.4049/jimmunol.1600622

Carstanjen, D., Yamauchi, A., Koornneef, A., Zang, H., Filippi, M. D., Harris, C., . . . Williams, D. A. (2005). Rac2 regulates neutrophil chemotaxis, superoxide production, and myeloid colony formation through multiple distinct effector pathways. *J Immunol, 174*(8), 4613-4620. doi:DOI 10.4049/jimmunol.174.8.4613

Cavnar, P. J., Berthier, E., Beebe, D. J., & Huttenlocher, A. (2011). Hax1 regulates neutrophil adhesion and motility through RhoA. *J Cell Biol, 193*(3), 465-473. doi:10.1083/jcb.201010143

Chatzispyrou, I. A., Held, N. M., Mouchiroud, L., Auwerx, J., & Houtkooper, R. H. (2015). Tetracycline Antibiotics Impair Mitochondrial Function and Its Experimental Use Confounds Research. *Cancer Res, 75*(21), 4446-4449. doi:10.1158/0008-5472.CAN-15-1626

Chen, H., Chen, Q., Fang, M., & Mi, Y. (2010). microRNA-181b targets MLK2 in HL-60 cells. *Science China-Life Sciences, 53*(1), 101-106. doi:10.1007/s11427-010-0002-y

Chen, R., Alvero, A. B., Silasi, D. A., Kelly, M. G., Fest, S., Visintin, I., . . . Mor, G. (2008). Regulation of IKK beta by miR-199a affects NF-kappa B activity in ovarian cancer cells. *Oncogene, 27*(34), 4712-4723. doi:10.1038/onc.2008.112

Cheretakis, C., Leung, R., Sun, C. X., Dror, Y., & Glogauer, M. (2006). Timing of neutrophil tissue repopulation predicts restoration of innate immune protection in a murine bone marrow transplantation model. *Blood, 108*(8), 2821-2826. doi:10.1182/blood-2006-04-018184

Chi, Y., Welcker, M., Hizli, A. A., Posakony, J. J., Aebersold, R., & Clurman, B. E. (2008). Identification of CDK2 substrates in human cell lysates. *Genome Biol, 9*(10), R149. doi:10.1186/gb-2008-9-10-r149

Christoffersson, G., & Phillipson, M. (2018). The neutrophil: one cell on many missions or many cells with different agendas? *Cell Tissue Res, 371*(3), 415-423. doi:10.1007/s00441-017-2780-z

Christopher, A. F., Kaur, R. P., Kaur, G., Kaur, A., Gupta, V., & Bansal, P. (2016). MicroRNA therapeutics: Discovering novel targets and developing specific therapy. *Perspect Clin Res, 7*(2), 68-74. doi:10.4103/2229-3485.179431

Clatworthy, A. E., Lee, J. S., Leibman, M., Kostun, Z., Davidson, A. J., & Hung, D. T. (2009). Pseudomonas aeruginosa infection of zebrafish involves both host and pathogen determinants. *Infect Immun, 77*(4), 1293-1303. doi:10.1128/IAI.01181-08

Cocco, G., Chu, D. C., & Pandolfi, S. (2010). Colchicine in clinical medicine. A guide for internists. *Eur J Intern Med, 21*(6), 503-508. doi:10.1016/j.ejim.2010.09.010

Copeland, S., Warren, H. S., Lowry, S. F., Calvano, S. E., Remick, D., Inflammation, & the Host Response to Injury, I. (2005). Acute inflammatory response to endotoxin in mice and humans. *Clin Diagn Lab Immunol, 12*(1), 60-67. doi:10.1128/CDLI.12.1.60-67.2005

Coutinho, A. E., & Chapman, K. E. (2011). The anti-inflammatory and immunosuppressive effects of glucocorticoids, recent developments and mechanistic insights. *Mol Cell Endocrinol, 335*(1), 2-13. doi:10.1016/j.mce.2010.04.005

Cox, J., & Mann, M. (2008). MaxQuant enables high peptide identification rates, individualized p.p.b.-range mass accuracies and proteome-wide protein quantification. *Nat Biotechnol, 26*(12), 1367-1372. doi:10.1038/nbt.1511

Cui, C. Y., Wang, Y. N., Wang, Y. J., Zhao, M., & Peng, S. Q. (2013). Exploring the Relationship between the Inhibition Selectivity and the Apoptosis of Roscovitine-Treated Cancer Cells. *Journal of Analytical Methods in Chemistry*. doi:Artn 38939010.1155/2013/389390

d'Alencon, C. A., Pena, O. A., Wittmann, C., Gallardo, V. E., Jones, R. A., Loosli, F., . . . Allende, M. L. (2010). A high-throughput chemically induced inflammation assay in zebrafish. *BMC Biol, 8*, 151. doi:10.1186/1741-7007-8-151

Dancey, J. T., Deubelbeiss, K. A., Harker, L. A., & Finch, C. A. (1976). Neutrophil kinetics in man. *J Clin Invest, 58*(3), 705-715. doi:10.1172/JCI108517

Davis, J. M., Huang, M. W., Botts, M. R., Hull, C. M., & Huttenlocher, A. (2016). A Zebrafish Model of Cryptococcal Infection Reveals Roles for Macrophages, Endothelial Cells, and Neutrophils in the Establishment and Control of Sustained Fungemia. *Infect Immun, 84*(10), 3047-3062. doi:10.1128/Iai.00506-16

Davis, R. E., Sharma, S., Chen, Y., Sundar, S., & Wilson, M. E. (2017). Inhibitory Ligand Pd-L1 on Mhc Class Ii-Expressing Neutrophils and Murine Leishmaniasis in Human. *American Journal of Tropical Medicine and Hygiene, 97*(5), 241-241. Retrieved from <Go to ISI>://WOS:000423215203140

de Buhr, N., & von Kockritz-Blickwede, M. (2016). How Neutrophil Extracellular Traps Become Visible. *J Immunol Res*. doi:Artn 4604713 10.1155/2016/4604713

De Rienzo, G., Gutzman, J. H., & Sive, H. (2012). Efficient shRNA-mediated inhibition of gene expression in zebrafish. *Zebrafish, 9*(3), 97-107. doi:10.1089/zeb.2012.0770

Deguine, J., & Barton, G. M. (2014). MyD88: a central player in innate immune signaling. *F1000Prime Rep, 6*, 97. doi:10.12703/P6-97

Deichmann, A., Hacein-Bey-Abina, S., Schmidt, M., Garrigue, A., Brugman, M. H., Hu, J., . . . Cavazzana-Calvo, M. (2007). Vector integration is nonrandom and clustered and influences the fate of lymphopoiesis in SCID-X1 gene therapy. *Journal of Clinical Investigation, 117*(8), 2225-2232. doi:10.1172/JCI31659

Deng, Q., & Huttenlocher, A. (2012). Leukocyte migration from a fish eye's view. *J Cell Sci, 125*(Pt 17), 3949-3956. doi:10.1242/jcs.093633

Deng, Q., Yoo, S. K., Cavnar, P. J., Green, J. M., & Huttenlocher, A. (2011a). Dual Roles for Rac2 in Neutrophil Motility and Active Retention in Zebrafish Hematopoietic Tissue. *Dev Cell, 21*(4), 735-745. doi:10.1016/j.devcel.2011.07.013

Deng, Q., Yoo, S. K., Cavnar, P. J., Green, J. M., & Huttenlocher, A. (2011b). Dual roles for Rac2 in neutrophil motility and active retention in zebrafish hematopoietic tissue. *Dev Cell, 21*(4), 735-745. doi:10.1016/j.devcel.2011.07.013

Denlinger, L. C., Garis, K. A., Sommer, J. A., Guadarrama, A. G., Proctor, R. A., & Bertics, P. J. (1998). Nuclear translocation of NF-kappaB in lipopolysaccharide-treated macrophages fails to correspond to endotoxicity: evidence suggesting a requirement for a gamma interferon-like signal. *Infect Immun, 66*(4), 1638-1647. Retrieved from http://www.ncbi.nlm.nih.gov/pubmed/9529092

Diaz-Pascual, F., Ortiz-Severin, J., Varas, M. A., Allende, M. L., & Chavez, F. P. (2017). In vivo Host-Pathogen Interaction as Revealed by Global Proteomic Profiling of Zebrafish Larvae. *Frontiers in Cellular and Infection Microbiology, 7*. doi:Artn 33410.3389/Fcimb.2017.00334

Dillingh, M. R., van Poelgeest, E. P., Malone, K. E., Kemper, E. M., Stroes, E. S. G., Moerland, M., & Burggraaf, J. (2014). Characterization of inflammation and immune cell modulation induced by low-dose LPS administration to healthy volunteers. *Journal of Inflammation-London, 11*. doi:ARTN 28 10.1186/s12950-014-0028-1

Dobin, A., Davis, C. A., Schlesinger, F., Drenkow, J., Zaleski, C., Jha, S., . . . Gingeras, T. R. (2013). STAR: ultrafast universal RNA-seq aligner. *Bioinformatics, 29*(1), 15-21. doi:10.1093/bioinformatics/bts635

Du, D., Xu, F., Yu, L., Zhang, C., Lu, X., Yuan, H., . . . Chen, Z. (2010). The tight junction protein, occludin, regulates the directional migration of epithelial cells. *Dev Cell, 18*(1), 52-63. doi:10.1016/j.devcel.2009.12.008

Dugo, L., Collin, M., Allen, D. A., Patel, N. S., Bauer, I., Mervaala, E., . . . Thiemermann, C. (2007). Inhibiting glycogen synthase kinase 3beta in sepsis. *Novartis Found Symp, 280*, 128-142; discussion 142-126, 160-124. Retrieved from http://www.ncbi.nlm.nih.gov/pubmed/17380792

Duquette, P. M., & Lamarche-Vane, N. (2014). Rho GTPases in embryonic development. *Small GTPases, 5*(2), 8. doi:10.4161/sgtp.29716

Dusi, S., Donini, M., & Rossi, F. (1996). Mechanisms of NADPH oxidase activation: translocation of p40phox, Rac1 and Rac2 from the cytosol to the membranes in human neutrophils lacking p47phox or p67phox. *Biochem J, 314 ( Pt 2)*, 409-412. doi:10.1042/bj3140409

Eash, K. J., Greenbaum, A. M., Gopalan, P. K., & Link, D. C. (2010). CXCR2 and CXCR4 antagonistically regulate neutrophil trafficking from murine bone marrow. *J Clin Invest, 120*(7), 2423-2431. doi:10.1172/JCI41649

Ergin, K., Bozkurt, G., Cubuk, C., & Aktas, S. (2015). Effect of Resveratrol on microRNA Profile and Apoptosis in HL-60 Leukemia and Raji Lymphoma Cells. *Meandros Medical and Dental Journal, 16*(3), 83-90. doi:10.4274/meandros.2369

Ertel, W., Keel, M., Steckholzer, U., Ungethum, U., & Trentz, O. (1996). Interleukin-10 attenuates the release of proinflammatory cytokines but depresses splenocyte functions in murine endotoxemia. *Arch Surg, 131*(1), 51-56. Retrieved from http://www.ncbi.nlm.nih.gov/pubmed/8546577

Fabian, M. R., & Sonenberg, N. (2012). The mechanics of miRNA-mediated gene silencing: a look under the hood of miRISC. *Nat Struct Mol Biol, 19*(6), 586-593. doi:10.1038/nsmb.2296

Faix, J. D. (2013). Biomarkers of sepsis. *Crit Rev Clin Lab Sci, 50*(1), 23-36. doi:10.3109/10408363.2013.764490

Fan, H. B., Liu, Y. J., Wang, L., Du, T. T., Dong, M., Gao, L., . . . Zhou, Y. (2014a). miR-142-3p acts as an essential modulator of neutrophil development in zebrafish. *Blood, 124*(8), 1320-1330. doi:DOI 10.1182/blood-2013-12-545012

Fan, H. B., Liu, Y. J., Wang, L., Du, T. T., Dong, M., Gao, L., . . . Zhou, Y. (2014b). miR-142-3p acts as an essential modulator of neutrophil development in zebrafish. *Blood, 124*(8), 1320-1330. doi:10.1182/blood-2013-12-545012

Faurschou, M., & Borregaard, N. (2003). Neutrophil granules and secretory vesicles in inflammation. *Microbes Infect, 5*(14), 1317-1327. Retrieved from https://www.ncbi.nlm.nih.gov/pubmed/14613775

Favreau, A. J., McGlauflin, R. E., Duarte, C. W., & Sathyanarayana, P. (2016). miR-199b, a novel tumor suppressor miRNA in acute myeloid leukemia with prognostic implications. *Experimental Hematolgy & Oncology, 5*. doi:Artn 410.1186/S40164-016-0033-6

Fayngerts, S. A., Wang, Z., Zamani, A., Sun, H., Boggs, A. E., Porturas, T. P., . . . Chen, Y. H. (2017). Direction of leukocyte polarization and migration by the phosphoinositide-transfer protein TIPE2. *Nature Immunology, 18*(12), 1353-1360. doi:10.1038/ni.3866

Felice, B., Cattoglio, C., Cittaro, D., Testa, A., Miccio, A., Ferrari, G., . . . Mavilio, F. (2009). Transcription factor binding sites are genetic determinants of retroviral integration in the human genome. *PLoS One, 4*(2), e4571. doi:10.1371/journal.pone.0004571

Fine, D. P. (1974). Activation of the classic and alternate complement pathways by endotoxin. *J Immunol, 112*(2), 763-769. Retrieved from http://www.ncbi.nlm.nih.gov/pubmed/4205207

Fink, M. P. (2014). Animal models of sepsis. *Virulence, 5*(1), 143-153. doi:10.4161/viru.26083

Finley, R. J., Holliday, R. L., Lefcoe, M., & Duff, J. H. (1975). Pulmonary edema in patients with sepsis. *Surg Gynecol Obstet, 140*(6), 851-857. Retrieved from http://www.ncbi.nlm.nih.gov/pubmed/1129675

Fisher, B. J., Kraskauskas, D., Martin, E. J., Farkas, D., Wegelin, J. A., Brophy, D., . . . Natarajan, R. (2012). Mechanisms of attenuation of abdominal sepsis induced acute lung injury by ascorbic acid. *Am J Physiol Lung Cell Mol Physiol, 303*(1), L20-32. doi:10.1152/ajplung.00300.2011

Forn-Cuni, G., Varela, M., Pereiro, P., Novoa, B., & Figueras, A. (2017). Conserved gene regulation during acute inflammation between zebrafish and mammals. *Sci Rep, 7*, 41905. doi:10.1038/srep41905

Friedman, R. C., Farh, K. K. H., Burge, C. B., & Bartel, D. P. (2009). Most mammalian mRNAs are conserved targets of microRNAs. *Genome Res, 19*(1), 92-105. doi:10.1101/gr.082701.108

Fuchs, T. A., Abed, U., Goosmann, C., Hurwitz, R., Schulze, I., Wahn, V., . . . Zychlinsky, A. (2007). Novel cell death program leads to neutrophil extracellular traps. *J Cell Biol, 176*(2), 231-241. doi:10.1083/jcb.200606027

Fukuhara, S., Zhang, J. H., Yuge, S., Ando, K., Wakayama, Y., Sakaue-Sawano, A., . . . Mochizuki, N. (2014). Visualizing the cell-cycle progression of endothelial cells in zebrafish. *Dev Biol, 393*(1), 10-23. doi:10.1016/j.ydbio.2014.06.015

Gaestel, M., Kotlyarov, A., & Kracht, M. (2009). Targeting innate immunity protein kinase signalling in inflammation. *Nat Rev Drug Discov, 8*(6), 480-499. doi:10.1038/nrd2829

Galindo-Villegas, J., Garcia-Moreno, D., de Oliveira, S., Meseguer, J., & Mulero, V. (2012). Regulation of immunity and disease resistance by commensal microbes and chromatin modifications during zebrafish development. *Proc Natl Acad Sci U S A, 109*(39), E2605-2614. doi:10.1073/pnas.1209920109

Gantier, M. P. (2013). The not-so-neutral role of microRNAs in neutrophil biology. *J Leukoc Biol, 94*(4), 575-583. doi:10.1189/jlb.1012539

Gonzalez-Martin, A., Adams, B. D., Lai, M., Shepherd, J., Salvador-Bernaldez, M., Salvador, J. M., . . . Xiao, C. (2016). The microRNA miR-148a functions as a critical regulator of B cell tolerance and autoimmunity. *Nat Immunol, 17*(4), 433-440. doi:10.1038/ni.3385

Gotts, J. E., & Matthay, M. A. (2016). Sepsis: pathophysiology and clinical management. *BMJ, 353*, i1585. doi:10.1136/bmj.i1585

Graziano, B. R., Gong, D., Anderson, K. E., Pipathsouk, A., Goldberg, A. R., & Weiner, O. D. (2017). A module for Rac temporal signal integration revealed with optogenetics. *J Cell Biol, 216*(8), 2515-2531. doi:10.1083/jcb.201604113

Greenbaum, A. M., & Link, D. C. (2011). Mechanisms of G-CSF-mediated hematopoietic stem and progenitor mobilization. *Leukemia, 25*(2), 211-217. doi:10.1038/leu.2010.248

Grossmann, K. S., Rosario, M., Birchmeier, C., & Birchmeier, W. (2010). The tyrosine phosphatase Shp2 in development and cancer. *Adv Cancer Res, 106*, 53-89. doi:10.1016/S0065-230X(10)06002-1

Grossmann, K. S., Wende, H., Paul, F. E., Cheret, C., Garratt, A. N., Zurborg, S., . . . Birchmeier, C. (2009). The tyrosine phosphatase Shp2 (PTPN11) directs Neuregulin-1/ErbB signaling throughout Schwann cell development. *Proc Natl Acad Sci U S A, 106*(39), 16704-16709. doi:10.1073/pnas.0904336106

Gui, P., Labrousse, A., Van Goethem, E., Besson, A., Maridonneau-Parini, I., & Le Cabec, V. (2014). Rho/ROCK pathway inhibition by the CDK inhibitor p27(kip1) participates in the onset of macrophage 3D-mesenchymal migration. *J Cell Sci, 127*(Pt 18), 4009-4023. doi:10.1242/jcs.150987

Gupta, S., & Kaplan, M. J. (2016). The role of neutrophils and NETosis in autoimmune and renal diseases. *Nat Rev Nephrol, 12*(7), 402-413. doi:10.1038/nrneph.2016.71

Gurol, T., Zhou, W., & Deng, Q. (2016). MicroRNAs in neutrophils: potential next generation therapeutics for inflammatory ailments. *Immunol Rev, 273*(1), 29-47. doi:10.1111/imr.12450

Gutzman, J. H., & Sive, H. (2009). Zebrafish brain ventricle injection. *J Vis Exp*(26). doi:10.3791/1218

Ha, M., & Kim, V. N. (2014). Regulation of microRNA biogenesis. *Nat Rev Mol Cell Biol, 15*(8), 509-524. doi:10.1038/nrm3838

Hall, C., Flores, M. V., Storm, T., Crosier, K., & Crosier, P. (2007). The zebrafish lysozyme C promoter drives myeloid-specific expression in transgenic fish. *BMC Dev Biol, 7*, 42. doi:10.1186/1471-213X-7-42

Hall, C. J., Boyle, R. H., Sun, X., Wicker, S. M., Misa, J. P., Krissansen, G. W., . . . Crosier, P. S. (2014). Epidermal cells help coordinate leukocyte migration during inflammation through fatty acid-fuelled matrix metalloproteinase production. *Nat Commun, 5*, 3880. doi:10.1038/ncomms4880

Hall, C. J., Flores, M. V., Oehlers, S. H., Sanderson, L. E., Lam, E. Y., Crosier, K. E., & Crosier, P. S. (2012). Infection-responsive expansion of the hematopoietic stem and progenitor cell compartment in zebrafish is dependent upon inducible nitric oxide. *Cell Stem Cell, 10*(2), 198-209. doi:10.1016/j.stem.2012.01.007

Hammerschmidt, M., Pelegri, F., Mullins, M. C., Kane, D. A., van Eeden, F. J., Granato, M., . . . Nusslein-Volhard, C. (1996). dino and mercedes, two genes regulating dorsal development in the zebrafish embryo. *Development, 123*, 95-102. Retrieved from http://www.ncbi.nlm.nih.gov/pubmed/9007232

Harvie, E. A., Green, J. M., Neely, M. N., & Huttenlocher, A. (2013). Innate immune response to Streptococcus iniae infection in zebrafish larvae. *Infection and Immunity, 81*(1), 110-121. doi:10.1128/IAI.00642-12

Harvie, E. A., & Huttenlocher, A. (2015). Neutrophils in host defense: new insights from zebrafish. *J Leukoc Biol, 98*(4), 523-537. doi:10.1189/jlb.4MR1114-524R

Hayes, J., Peruzzi, P. P., & Lawler, S. (2014). MicroRNAs in cancer: biomarkers, functions and therapy. *Trends Mol Med, 20*(8), 460-469. doi:10.1016/j.molmed.2014.06.005

He, L., & Hannon, G. J. (2004). Micrornas: Small RNAs with a big role in gene regulation. *Nature Reviews Genetics, 5*(7), 522-531. doi:10.1038/nrg1379

Helwak, A., Kudla, G., Dudnakova, T., & Tollervey, D. (2013). Mapping the human miRNA interactome by CLASH reveals frequent noncanonical binding. *Cell, 153*(3), 654-665. doi:10.1016/j.cell.2013.03.043

Henry, K. M., Loynes, C. A., Whyte, M. K., & Renshaw, S. A. (2013). Zebrafish as a model for the study of neutrophil biology. *J Leukoc Biol, 94*(4), 633-642. doi:10.1189/jlb.1112594

Higashi, H., Suzuki-Takahashi, I., Taya, Y., Segawa, K., Nishimura, S., & Kitagawa, M. (1995). Differences in substrate specificity between Cdk2-cyclin A and Cdk2-cyclin E in vitro. *Biochem Biophys Res Commun, 216*(2), 520-525. Retrieved from http://www.ncbi.nlm.nih.gov/pubmed/7488142

Hirota, T., Takahashi, A., Kubo, M., Tsunoda, T., Tomita, K., Doi, S., . . . Tamari, M. (2011). Genome-wide association study identifies three new susceptibility loci for adult asthma in the Japanese population. *Nature Genetics, 43*(9), 893-896. doi:10.1038/ng.887

Hong, C., Kidani, Y., N, A. G., Phung, T., Ito, A., Rong, X., . . . Bensinger, S. J. (2012). Coordinate regulation of neutrophil homeostasis by liver X receptors in mice. *J Clin Invest, 122*(1), 337-347. doi:10.1172/JCI58393

Hoodless, L. J., Lucas, C. D., Duffin, R., Denvir, M. A., Haslett, C., Tucker, C. S., & Rossi, A. G. (2016). Genetic and pharmacological inhibition of CDK9 drives neutrophil apoptosis to resolve inflammation in zebrafish in vivo. *Sci Rep, 5*, 36980. doi:10.1038/srep36980

Howard, M., Muchamuel, T., Andrade, S., & Menon, S. (1993). Interleukin 10 protects mice from lethal endotoxemia. *J Exp Med, 177*(4), 1205-1208. Retrieved from http://www.ncbi.nlm.nih.gov/pubmed/8459215

Howe, K., Clark, M. D., Torroja, C. F., Torrance, J., Berthelot, C., Muffato, M., . . . Stemple, D. L. (2013). The zebrafish reference genome sequence and its relationship to the human genome. *Nature, 496*(7446), 498-503. doi:10.1038/nature12111

Hsu, A. Y., Gurol, T., Sobreira, T. J. P., Zhang, S., Moore, N., Cai, C. F., . . . Deng, Q. (2018). Development and Characterization of an Endotoxemia Model in Zebra Fish. *Front Immunol, 9*. doi:Artn 60710.3389/Fimmu.2018.00607

Hsu, A. Y., Liu, S., Syahirah, R., Brasseale, K. A., Wan, J., & Deng, Q. (2019a). Inducible overexpression of zebrafish microRNA-722 suppresses chemotaxis of human neutrophil like cells. *Molecular Immunology, 112*, 206-214. doi:10.1016/j.molimm.2019.06.001

Hsu, A. Y., Liu, S., Syahirah, R., Brasseale, K. A., Wan, J., & Deng, Q. (2019b). Inducible overexpression of zebrafish microRNA-722 suppresses chemotaxis of human neutrophil like cells. *Mol Immunol, 112*, 206-214. doi:10.1016/j.molimm.2019.06.001

Hsu, A. Y., Wang, D., Gurol, T., Zhou, W., Zhu, X., Lu, H. Y., & Deng, Q. (2017a). Overexpression of microRNA-722 fine-tunes neutrophilic inflammation by inhibiting Rac2 in zebrafish. *Dis Model Mech, 10*(11), 1323-1332. doi:10.1242/dmm.030791

Hsu, A. Y., Wang, D. C., Gurol, T., Zhou, W. Q., Zhu, X. G., Lu, H. Y., & Deng, Q. (2017b). Overexpression of microRNA-722 fine-tunes neutrophilic inflammation by inhibiting Rac2 in zebrafish. *Dis Model Mech, 10*(11), 1323-1332. doi:10.1242/dmm.030791

Huang da, W., Sherman, B. T., & Lempicki, R. A. (2009a). Bioinformatics enrichment tools: paths toward the comprehensive functional analysis of large gene lists. *Nucleic Acids Res, 37*(1), 1-13. doi:10.1093/nar/gkn923

Huang da, W., Sherman, B. T., & Lempicki, R. A. (2009b). Systematic and integrative analysis of large gene lists using DAVID bioinformatics resources. *Nature Protocols, 4*(1), 44-57. doi:10.1038/nprot.2008.211

Huang, H. M., Li, H. D., Chen, X., Yang, Y., Li, X. F., Li, W. X., . . . Li, J. (2017). HMGA2, a driver of inflammation, is associated with hypermethylation in acute liver injury. *Toxicology and Applied Pharmacology, 328*, 34-45. doi:10.1016/j.taap.2017.05.005

Huang, K., Dong, B., Wang, Y., Tian, T., & Zhang, B. (2015). MicroRNA-519 enhances HL60 human acute myeloid leukemia cell line proliferation by reducing the expression level of RNA-binding protein human antigen R. *Mol Med Rep, 12*(6), 7830-7836. doi:10.3892/mmr.2015.4455

Huang, Y., Zhang, S., Fang, X., Qin, L., Fan, Y., Ding, D., . . . Xie, M. (2018). Plasma miR-199a-5p is increased in neutrophilic phenotype asthma patients and negatively correlated with pulmonary function. *PLoS One, 13*(3), e0193502. doi:10.1371/journal.pone.0193502

Hydbring, P., Malumbres, M., & Sicinski, P. (2016). Non-canonical functions of cell cycle cyclins and cyclin-dependent kinases. *Nat Rev Mol Cell Biol, 17*(5), 280-292. doi:10.1038/nrm.2016.27

Jacob, C., Leport, M., Szilagyi, C., Allen, J. M., Bertrand, C., & Lagente, V. (2002). DMSO-treated HL60 cells: a model of neutrophil-like cells mainly expressing PDE4B subtype. *Int Immunopharmacol, 2*(12), 1647-1656. Retrieved from http://www.ncbi.nlm.nih.gov/pubmed/12469939

Jacob, C., Leport, M., Szilagyi, C., Allen, J. M., Berttand, C., & Lagente, V. (2002). DMSO-treated HL60 cells: a model of neutrophil-like cells mainly expressing PDE4B subtype. *Int Immunopharmacol, 2*(12), 1647-1656. doi:Pii S1567-5769(02)00141-8 Doi 10.1016/S1567-5769(02)00141-8

Jayapal, S. R., Wang, C. Q., Bisteau, X., Caldez, M. J., Lim, S., Tergaonkar, V., . . . Kaldis, P. (2015). Hematopoiesis specific loss of Cdk2 and Cdk4 results in increased erythrocyte size and delayed platelet recovery following stress. *Haematologica, 100*(4), 434-441. doi:10.3324/haematol.2014.106468

Jian, P., Li, Z. W., Fang, T. Y., Jian, W., Zhuan, Z., Mei, L. X., . . . Jian, N. (2011). Retinoic acid induces HL-60 cell differentiation via the upregulation of miR-663. *J Hematol Oncol, 4*, 20. doi:10.1186/1756-8722-4-20

Johnnidis, J. B., Harris, M. H., Wheeler, R. T., Stehling-Sun, S., Lam, M. H., Kirak, O., . . . Camargo, F. D. (2008). Regulation of progenitor cell proliferation and granulocyte function by microRNA-223. *Nature, 451*(7182), 1125-1129. doi:10.1038/nature06607

Jonzon, K. H., & Bindslev, L. (1991). [Acute severe respiratory insufficiency in adults as a complication of septic and traumatic shock]. *Lakartidningen, 88*(48), 4145-4148. Retrieved from http://www.ncbi.nlm.nih.gov/pubmed/1956254

Jorch, S. K., & Kubes, P. (2017). An emerging role for neutrophil extracellular traps in noninfectious disease. *Nat Med, 23*(3), 279-287. doi:10.1038/nm.4294

Kang, T., Yi, J., Guo, A., Wang, X., Overall, C. M., Jiang, W., . . . Pei, D. (2001). Subcellular distribution and cytokine- and chemokine-regulated secretion of leukolysin/MT6-MMP/MMP-25 in neutrophils. *J Biol Chem, 276*(24), 21960-21968. doi:10.1074/jbc.M007997200

Kanther, M., Sun, X., Muhlbauer, M., Mackey, L. C., Flynn, E. J., 3rd, Bagnat, M., . . . Rawls, J. F. (2011). Microbial colonization induces dynamic temporal and spatial patterns of NF-kappaB activation in the zebrafish digestive tract. *Gastroenterology, 141*(1), 197-207. doi:10.1053/j.gastro.2011.03.042

Kasashima, K., Nakamura, Y., & Kozu, T. (2004). Altered expression profiles of microRNAs during TPA-induced differentiation of HL-60 cells. *Biochem Biophys Res Commun, 322*(2), 403-410. doi:10.1016/j.bbrc.2004.07.130

Kasthuri, R. S., Wroblewski, M., Jilma, B., Key, N. S., & Nelsestuen, G. L. (2007). Potential biomarkers of an exaggerated response to endotoxemia. *Biomarkers, 12*(3), 287-302. doi:10.1080/13547500601160536

Kawakami, K. (2005). Transposon tools and methods in zebrafish. *Dev Dyn, 234*(2), 244-254. doi:10.1002/dvdy.20516

Kawasaki, H., & Taira, K. (2004). MicroRNA-196 inhibits HOXB8 expression in myeloid differentiation of HL60 cells. *Nucleic Acids Symp Ser (Oxf)*(48), 211-212. doi:10.1093/nass/48.1.211

Kennedy, A. D., & DeLeo, F. R. (2009). Neutrophil apoptosis and the resolution of infection. *Immunol Res, 43*(1-3), 25-61. doi:10.1007/s12026-008-8049-6

Kiers, D., Koch, R. M., Hamers, L., Gerretsen, J., Thijs, E. J., van Ede, L., . . . Pickkers, P. (2017). Characterization of a model of systemic inflammation in humans in vivo elicited by continuous infusion of endotoxin. *Sci Rep, 7*, 40149. doi:10.1038/srep40149

Kim, K., Vinayagam, A., & Perrimon, N. (2014). A Rapid Genome-wide MicroRNA Screen Identifies miR-14 as a Modulator of Hedgehog Signaling. *Cell Rep, 7*(6), 2066-2077. doi:10.1016/j.celrep.2014.05.025

Ko, H. J., Yang, J. Y., Shim, D. H., Yang, H., Park, S. M., Curtiss, R., 3rd, & Kweon, M. N. (2009). Innate immunity mediated by MyD88 signal is not essential for induction of lipopolysaccharide-specific B cell responses but is indispensable for protection against Salmonella enterica serovar Typhimurium infection. *J Immunol, 182*(4), 2305-2312. doi:10.4049/jimmunol.0801980

Kolaczkowska, E., & Kubes, P. (2013). Neutrophil recruitment and function in health and inflammation. *Nature Reviews Immunology, 13*(3), 159-175. doi:10.1038/nri3399

Koshizuka, K., Hanazawa, T., Kikkawa, N., Arai, T., Okato, A., Kurozumi, A., . . . Seki, N. (2017). Regulation of ITGA3 by the anti-tumor miR-199 family inhibits cancer cell migration and invasion in head and neck cancer. *Cancer Sci, 108*(8), 1681-1692. doi:10.1111/cas.13298

Kuwano, Y., Spelten, O., Zhang, H., Ley, K., & Zarbock, A. (2010). Rolling on E- or P-selectin induces the extended but not high-affinity conformation of LFA-1 in neutrophils. *Blood, 116*(4), 617-624. doi:10.1182/blood-2010-01-266122

Lacy, P. (2005). The role of Rho GTPases and SNAREs in mediator release from granulocytes. *Pharmacol Ther, 107*(3), 358-376. doi:10.1016/j.pharmthera.2005.03.008

Lahoz-Beneytez, J., Elemans, M., Zhang, Y., Ahmed, R., Salam, A., Block, M., . . . Macallan, D. (2016). Human neutrophil kinetics: modeling of stable isotope labeling data supports short blood neutrophil half-lives. *Blood, 127*(26), 3431-3438. doi:10.1182/blood-2016-03-700336

Lammermann, T., Bader, B. L., Monkley, S. J., Worbs, T., Wedlich-Soldner, R., Hirsch, K., . . . Sixt, M. (2008). Rapid leukocyte migration by integrin-independent flowing and squeezing. *Nature, 453*(7191), 51-55. doi:10.1038/nature06887

Landgraf, P., Rusu, M., Sheridan, R., Sewer, A., Iovino, N., Aravin, A., . . . Tuschl, T. (2007). A mammalian microRNA expression atlas based on small RNA library sequencing. *Cell, 129*(7), 1401-1414. doi:10.1016/j.cell.2007.04.040

Lanotte, M., Martin-Thouvenin, V., Najman, S., Balerini, P., Valensi, F., & Berger, R. (1991). NB4, a maturation inducible cell line with t(15;17) marker isolated from a human acute promyelocytic leukemia (M3). *Blood, 77*(5), 1080-1086. Retrieved from http://www.ncbi.nlm.nih.gov/pubmed/1995093

Laphanuwat, P., & Jirawatnotai, S. (2019). Immunomodulatory Roles of Cell Cycle Regulators. *Front Cell Dev Biol, 7*, 23. doi:10.3389/fcell.2019.00023

Larsen, M. T., Hother, C., Hager, M., Pedersen, C. C., Theilgaard-Monch, K., Borregaard, N., & Cowland, J. B. (2013). MicroRNA profiling in human neutrophils during bone marrow granulopoiesis and in vivo exudation. *PLoS One, 8*(3), e58454. doi:10.1371/journal.pone.0058454

Lauriol, J., Jaffre, F., & Kontaridis, M. I. (2015). The role of the protein tyrosine phosphatase SHP2 in cardiac development and disease. *Semin Cell Dev Biol, 37*, 73-81. doi:10.1016/j.semcdb.2014.09.013

Lauw, F. N., Simpson, A. J. H., Hack, C. E., Prins, J. M., Wolbink, A. M., van Deventer, S. J. H., . . . van der Poll, T. (2000). Soluble granzymes are released during human endotoxemia and in patients with severe infection due to gram-negative bacteria. *Journal of Infectious Diseases, 182*(1), 206-213. doi:Doi 10.1086/315642

Lehner, M. D., Ittner, J., Bundschuh, D. S., van Rooijen, N., Wendel, A., & Hartung, T. (2001). Improved innate immunity of endotoxin-tolerant mice increases resistance to Salmonella enterica serovar typhimurium infection despite attenuated cytokine response. *Infect Immun, 69*(1), 463-471. doi:10.1128/IAI.69.1.463-471.2001

Leitch, A. E., Lucas, C. D., Marwick, J. A., Duffin, R., Haslett, C., & Rossi, A. G. (2012). Cyclin-dependent kinases 7 and 9 specifically regulate neutrophil transcription and their inhibition drives apoptosis to promote resolution of inflammation. *Cell Death and Differentiation, 19*(12), 1950-1961. doi:10.1038/cdd.2012.80

Li, W., Zhang, Y., Han, B., Li, L., Li, M., Lu, X., . . . Zhang, B. (2019). One-step efficient generation of dual-function conditional knockout and geno-tagging alleles in zebrafish. *Elife, 8*. doi:10.7554/eLife.48081

Li, W. T., Wang, H., Zhang, J. B., Zhai, L. M., Chen, W. J., & Zhao, C. L. (2016). miR-199a-5p regulates beta 1 integrin through Ets-1 to suppress invasion in breast cancer. *Cancer Sci, 107*(7), 916-923. doi:10.1111/cas.12952

Li, X. J., Goodwin, C. B., Nabinger, S. C., Richine, B. M., Yang, Z., Hanenberg, H., . . . Chan, R. J. (2015). Protein-tyrosine phosphatase Shp2 positively regulates macrophage oxidative burst. *J Biol Chem, 290*(7), 3894-3909. doi:10.1074/jbc.M114.614057

Liamina, D., Sibirnyj, W., Khokhlova, A., Saenko, V., Rastorgueva, E., Fomin, A., & Saenko, Y. (2017). Radiation-Induced Changes of microRNA Expression Profiles in Radiosensitive and Radioresistant Leukemia Cell Lines with Different Levels of Chromosome Abnormalities. *Cancers, 9*(10). doi:Artn 136 10.3390/Cancers9100136

Liang, H., Dong, Z., Liu, J. F., Chuang, W., Gao, L. Z., & Ren, Y. G. (2017). Targeting miR-155 suppresses proliferation and induces apoptosis of HL-60 cells by targeting Slug/PUMA signal. *Histol Histopathol, 32*(9), 899-907. doi:10.14670/HH-11-837

Liao, Y., Smyth, G. K., & Shi, W. (2014). featureCounts: an efficient general purpose program for assigning sequence reads to genomic features. *Bioinformatics, 30*(7), 923-930. doi:10.1093/bioinformatics/btt656

Lieschke, G. J., & Currie, P. D. (2007). Animal models of human disease: zebrafish swim into view. *Nat Rev Genet, 8*(5), 353-367. doi:10.1038/nrg2091

Lightfoot, Y. L., & Kaplan, M. J. (2017). Disentangling the role of neutrophil extracellular traps in rheumatic diseases. *Curr Opin Rheumatol, 29*(1), 65-70. doi:10.1097/BOR.0000000000000357

Lim, K., Hyun, Y. M., Lambert-Emo, K., Capece, T., Bae, S., Miller, R., . . . Kim, M. (2015). Neutrophil trails guide influenza-specific CD8(+) T cells in the airways. *Science, 349*(6252), aaa4352. doi:10.1126/science.aaa4352

Lin, Y., Li, D., Liang, Q., Liu, S., Zuo, X., Li, L., . . . Huang, Z. (2015). miR-638 regulates differentiation and proliferation in leukemic cells by targeting cyclin-dependent kinase 2. *J Biol Chem, 290*(3), 1818-1828. doi:10.1074/jbc.M114.599191

Liongue, C., Hall, C. J., O'Connell, B. A., Crosier, P., & Ward, A. C. (2009). Zebrafish granulocyte colony-stimulating factor receptor signaling promotes myelopoiesis and myeloid cell migration. *Blood, 113*(11), 2535-2546. doi:10.1182/blood-2008-07-171967

Liu, T., Zhang, L. Y., Joo, D., & Sun, S. C. (2017). NF-kappa B signaling in inflammation. *Signal Transduction and Targeted Therapy, 2*. doi:UNSP e17023 10.1038/sigtrans.2017.23

Ma, F., Liu, X., Li, D., Wang, P., Li, N., Lu, L., & Cao, X. (2010). MicroRNA-466l upregulates IL-10 expression in TLR-triggered macrophages by antagonizing RNA-binding protein tristetraprolin-mediated IL-10 mRNA degradation. *J Immunol, 184*(11), 6053-6059. doi:10.4049/jimmunol.0902308

Malumbres, M., & Barbacid, M. (2009). Cell cycle, CDKs and cancer: a changing paradigm. *Nature Reviews Cancer, 9*(3), 153-166. doi:10.1038/nrc2602

Manz, M. G., & Boettcher, S. (2014). Emergency granulopoiesis. *Nat Rev Immunol, 14*(5), 302-314. doi:10.1038/nri3660

Mathias, J. R., Dodd, M. E., Walters, K. B., Yoo, S. K., Ranheim, E. A., & Huttenlocher, A. (2009). Characterization of zebrafish larval inflammatory macrophages. *Dev Comp Immunol, 33*(11), 1212-1217. doi:10.1016/j.dci.2009.07.003

Mazon-Moya, M. J., Willis, A. R., Torraca, V., Boucontet, L., Shenoy, A. R., Colucci-Guyon, E., & Mostowy, S. (2017). Septins restrict inflammation and protect zebrafish larvae from Shigella infection. *PLoS Pathog, 13*(6), e1006467. doi:10.1371/journal.ppat.1006467

McCarthy, D. J., Chen, Y., & Smyth, G. K. (2012). Differential expression analysis of multifactor RNA-Seq experiments with respect to biological variation. *Nucleic Acids Res, 40*(10), 4288-4297. doi:10.1093/nar/gks042

McGillicuddy, F. C., de la Llera Moya, M., Hinkle, C. C., Joshi, M. R., Chiquoine, E. H., Billheimer, J. T., . . . Reilly, M. P. (2009). Inflammation impairs reverse cholesterol transport in vivo. *Circulation, 119*(8), 1135-1145. doi:10.1161/CIRCULATIONAHA.108.810721

Meijering, E., Dzyubachyk, O., & Smal, I. (2012). Methods for cell and particle tracking. *Methods Enzymol, 504*, 183-200. doi:10.1016/B978-0-12-391857-4.00009-4

Mestas, J., & Hughes, C. C. (2004). Of mice and not men: differences between mouse and human immunology. *J Immunol, 172*(5), 2731-2738. doi:10.4049/jimmunol.172.5.2731

Mesureur, J., Feliciano, J. R., Wagner, N., Gomes, M. C., Zhang, L., Blanco-Gonzalez, M., . . . Vergunst, A. C. (2017). Macrophages, but not neutrophils, are critical for proliferation of Burkholderia cenocepacia and ensuing host-damaging inflammation. *PLoS Pathog, 13*(6), e1006437. doi:10.1371/journal.ppat.1006437

Mocsai, A. (2013). Diverse novel functions of neutrophils in immunity, inflammation, and beyond. *J Exp Med, 210*(7), 1283-1299. doi:10.1084/jem.20122220

Mocsai, A., Walzog, B., & Lowell, C. A. (2015). Intracellular signalling during neutrophil recruitment. *Cardiovasc Res, 107*(3), 373-385. doi:10.1093/cvr/cvv159

Moullan, N., Mouchiroud, L., Wang, X., Ryu, D., Williams, E. G., Mottis, A., . . . Auwerx, J. (2015). Tetracyclines Disturb Mitochondrial Function across Eukaryotic Models: A Call for Caution in Biomedical Research. *Cell Rep*. doi:10.1016/j.celrep.2015.02.034

Munford, R. S. (2016). Endotoxemia-menace, marker, or mistake? *J Leukoc Biol, 100*(4), 687-698. doi:10.1189/jlb.3RU0316-151R

Murray, P. J. (2006). STAT3-mediated anti-inflammatory signalling. *Biochem Soc Trans, 34*(Pt 6), 1028-1031. doi:10.1042/BST0341028

N, A. G., Bensinger, S. J., Hong, C., Beceiro, S., Bradley, M. N., Zelcer, N., . . . Castrillo, A. (2009). Apoptotic cells promote their own clearance and immune tolerance through activation of the nuclear receptor LXR. *Immunity, 31*(2), 245-258. doi:10.1016/j.immuni.2009.06.018

Nakazawa, D., Kumar, S. V., Marschner, J., Desai, J., Holderied, A., Rath, L., . . . Anders, H. J. (2017). Histones and Neutrophil Extracellular Traps Enhance Tubular Necrosis and Remote Organ Injury in Ischemic AKI. *J Am Soc Nephrol, 28*(6), 1753-1768. doi:10.1681/ASN.2016080925

Nathan, C. (2006). Neutrophils and immunity: challenges and opportunities. *Nat Rev Immunol, 6*(3), 173-182. doi:10.1038/nri1785

Noh, K. T., Park, Y. M., Cho, S. G., & Choi, E. J. (2011). GSK-3 beta-induced ASK1 stabilization is crucial in LPS-induced endotoxin shock. *Exp Cell Res, 317*(12), 1663-1668. doi:10.1016/j.yexcr.2011.03.022

Novoa, B., Bowman, T. V., Zon, L., & Figueras, A. (2009). LPS response and tolerance in the zebrafish (Danio rerio) *Fish Shellfish Immunol, 26*(2), 326-331. doi:10.1016/j.fsi.2008.12.004

Novoa, B., & Figueras, A. (2012). Zebrafish: model for the study of inflammation and the innate immune response to infectious diseases. *Adv Exp Med Biol, 946*, 253-275. doi:10.1007/978-1-4614-0106-3_15

Nusse, O., & Lindau, M. (1988). The dynamics of exocytosis in human neutrophils. *J Cell Biol, 107*(6 Pt 1), 2117-2123. Retrieved from https://www.ncbi.nlm.nih.gov/pubmed/3058717

O'Brien, X. M., Biron, B. M., & Reichner, J. S. (2017). Consequences of extracellular trap formation in sepsis. *Curr Opin Hematol, 24*(1), 66-71. doi:10.1097/MOH.0000000000000303

Okamoto, K., Tamura, T., & Sawatsubashi, Y. (2016). Sepsis and disseminated intravascular coagulation. *J Intensive Care, 4*, 23. doi:10.1186/s40560-016-0149-0

Olarerin-George, A. O., Anton, L., Hwang, Y. C., Elovitz, M. A., & Hogenesch, J. B. (2013). A functional genomics screen for microRNA regulators of NF-kappaB signaling. *BMC Biol, 11*, 19. doi:10.1186/1741-7007-11-19

Olszyna, D. P., Pajkrt, D., Lauw, F. N., van Deventer, S. J., & van Der Poll, T. (2000). Interleukin 10 inhibits the release of CC chemokines during human endotoxemia. *J Infect Dis, 181*(2), 613-620. doi:10.1086/315275

Otyepka, M., Bartova, I., Kriz, Z., & Koca, J. (2006). Different mechanisms of CDK5 and CDK2 activation as revealed by CDK5/p25 and CDK2/cyclin A dynamics. *Journal of Biological Chemistry, 281*(11), 7271-7281. doi:10.1074/jbc.M509699200

Palha, N., Guivel-Benhassine, F., Briolat, V., Lutfalla, G., Sourisseau, M., Ellett, F., . . . Levraud, J. P. (2013). Real-time whole-body visualization of Chikungunya Virus infection and host interferon response in zebrafish. *PLoS Pathog, 9*(9), e1003619. doi:10.1371/journal.ppat.1003619

Panopoulos, A. D., & Watowich, S. S. (2008). Granulocyte colony-stimulating factor: Molecular mechanisms of action during steady state and 'emergency' hematopoiesis. *Cytokine, 42*(3), 277-288. doi:10.1016/j.cyto.2008.03.002

Pazhakh, V., Clark, S., Keightley, M. C., & Lieschke, G. J. (2017). A GCSFR/CSF3R zebrafish mutant models the persistent basal neutrophil deficiency of severe congenital neutropenia. *Sci Rep, 7*, 44455. doi:10.1038/srep44455

Pedruzzi, E., Fay, M., Elbim, C., Gaudry, M., & Gougerot-Pocidalo, M. A. (2002). Differentiation of PLB-985 myeloid cells into mature neutrophils, shown by degranulation of terminally differentiated compartments in response to N-formyl peptide and priming of superoxide anion production by granulocyte-macrophage colony-stimulating factor. *British Journal of Haematology, 117*(3), 719-726. doi:DOI 10.1046/j.1365-2141.2002.03521.x

Pennati, M., Campbell, A. J., Curto, M., Binda, M., Cheng, Y., Wang, L. Z., . . . Newell, D. R. (2005). Potentiation of paclitaxel-induced apoptosis by the novel cyclin-dependent kinase inhibitor NU6140: a possible role for survivin down-regulation. *Mol Cancer Ther, 4*(9), 1328-1337. doi:10.1158/1535-7163.MCT-05-0022

Peters, N. C., Egen, J. G., Secundino, N., Debrabant, A., Kimblin, N., Kamhawi, S., . . . Sacks, D. (2008). In vivo imaging reveals an essential role for neutrophils in leishmaniasis transmitted by sand flies. *Science, 321*(5891), 970-974. doi:10.1126/science.1159194

Philip, A. M., Wang, Y., Mauro, A., El-Rass, S., Marshall, J. C., Lee, W. L., . . . Wen, X. Y. (2017). Development of a zebrafish sepsis model for high-throughput drug discovery. *Molecular Medicine, 23*. doi:10.2119/molmed.2016.00188

Philip, A. M., Wang, Y. D., Mauro, A., El-Rass, S., Marshall, J. C., Lee, W. L., . . . Wen, X. Y. (2017). Development of a Zebrafish Sepsis Model for High-Throughput Drug Discovery. *Molecular Medicine, 23*, 134-148. doi:10.2119/molmed.2016.00188

Phillipson, M., Kaur, J., Colarusso, P., Ballantyne, C. M., & Kubes, P. (2008). Endothelial domes encapsulate adherent neutrophils and minimize increases in vascular permeability in paracellular and transcellular emigration. *PLoS One, 3*(2), e1649. doi:10.1371/journal.pone.0001649

Pillay, J., den Braber, I., Vrisekoop, N., Kwast, L. M., de Boer, R. J., Borghans, J. A., . . . Koenderman, L. (2010). In vivo labeling with 2H2O reveals a human neutrophil lifespan of 5.4 days. *Blood, 116*(4), 625-627. doi:10.1182/blood-2010-01-259028

Pinsky, M. R., Vincent, J. L., Deviere, J., Alegre, M., Kahn, R. J., & Dupont, E. (1993). Serum cytokine levels in human septic shock. Relation to multiple-system organ failure and mortality. *Chest, 103*(2), 565-575. Retrieved from http://www.ncbi.nlm.nih.gov/pubmed/8432155

Pisharath, H., Rhee, J. M., Swanson, M. A., Leach, S. D., & Parsons, M. J. (2007). Targeted ablation of beta cells in the embryonic zebrafish pancreas using E. coli nitroreductase. *Mech Dev, 124*(3), 218-229. doi:10.1016/j.mod.2006.11.005

Pizzimenti, S., Ferracin, M., Sabbioni, S., Toaldo, C., Pettazzoni, P., Dianzani, M. U., . . . Barrera, G. (2009). MicroRNA expression changes during human leukemic HL-60 cell differentiation induced by 4-hydroxynonenal, a product of lipid peroxidation. *Free Radic Biol Med, 46*(2), 282-288. doi:10.1016/j.freeradbiomed.2008.10.035

Porcherie, A., Mathieu, C., Peronet, R., Schneider, E., Claver, J., Commere, P. H., . . . Mecheri, S. (2011). Critical role of the neutrophil-associated high-affinity receptor for IgE in the pathogenesis of experimental cerebral malaria. *J Exp Med, 208*(11), 2225-2236. doi:10.1084/jem.20110845

Pospieszalska, M. K., & Ley, K. (2009). Dynamics of Microvillus Extension and Tether Formation in Rolling Leukocytes. *Cell Mol Bioeng, 2*(2), 207-217. doi:10.1007/s12195-009-0063-9

Potera, R. M., Jensen, M. J., Hilkin, B. M., South, G. K., Hook, J. S., Gross, E. A., & Moreland, J. G. (2016). Neutrophil azurophilic granule exocytosis is primed by TNF-alpha and partially regulated by NADPH oxidase. *Innate Immun, 22*(8), 635-646. doi:10.1177/1753425916668980

Prajsnar, T. K., Hamilton, R., Garcia-Lara, J., McVicker, G., Williams, A., Boots, M., . . . Renshaw, S. A. (2012). A privileged intraphagocyte niche is responsible for disseminated infection of Staphylococcus aureus in a zebrafish model. *Cell Microbiol, 14*(10), 1600-1619. doi:10.1111/j.1462-5822.2012.01826.x

Qu, C. K. (2000). The SHP-2 tyrosine phosphatase: signaling mechanisms and biological functions. *Cell Res, 10*(4), 279-288. doi:10.1038/sj.cr.7290055

Raetz, C. R., & Whitfield, C. (2002). Lipopolysaccharide endotoxins. *Annu Rev Biochem, 71*, 635-700. doi:10.1146/annurev.biochem.71.110601.135414

Redl, H., Bahrami, S., Schlag, G., & Traber, D. L. (1993). Clinical detection of LPS and animal models of endotoxemia. *Immunobiology, 187*(3-5), 330-345. doi:10.1016/S0171-2985(11)80348-7

Reid, G., Kao, S. C., Pavlakis, N., Brahmbhatt, H., MacDiarmid, J., Clarke, S., . . . van Zandwijk, N. (2016). Clinical development of TargomiRs, a miRNA mimic-based treatment for patients with recurrent thoracic cancer. *Epigenomics, 8*(8), 1079-1085. doi:10.2217/epi-2016-0035

Remick, D. G., Green, L. B., Newcomb, D. E., Garg, S. J., Bolgos, G. L., & Call, D. R. (2001). CXC chemokine redundancy ensures local neutrophil recruitment during acute inflammation. *Am J Pathol, 159*(3), 1149-1157. doi:10.1016/S0002-9440(10)61791-9

Renshaw, S. A., & Trede, N. S. (2012). A model 450 million years in the making: zebrafish and vertebrate immunity. *Dis Model Mech, 5*(1), 38-47. doi:10.1242/dmm.007138

Roberts, A. W., Kim, C., Zhen, L., Lowe, J. B., Kapur, R., Petryniak, B., . . . Williams, D. A. (1999). Deficiency of the hematopoietic cell-specific Rho family GTPase Rac2 is characterized by abnormalities in neutrophil function and host defense. *Immunity, 10*(2), 183-196. doi:Doi 10.1016/S1074-7613(00)80019-9

Robinson, M. D., McCarthy, D. J., & Smyth, G. K. (2010). edgeR: a Bioconductor package for differential expression analysis of digital gene expression data. *Bioinformatics, 26*(1), 139-140. doi:10.1093/bioinformatics/btp616

Romani, L., Mencacci, A., Cenci, E., Spaccapelo, R., Del Sero, G., Nicoletti, I., . . . Puccetti, P. (1997). Neutrophil production of IL-12 and IL-10 in candidiasis and efficacy of IL-12 therapy in neutropenic mice. *J Immunol, 158*(11), 5349-5356. Retrieved from https://www.ncbi.nlm.nih.gov/pubmed/9164955

Rosales, C. (2018). Neutrophil: A Cell with Many Roles in Inflammation or Several Cell Types? *Front Physiol, 9*. doi:ARTN 11310.3389/fphys.2018.00113

Rosales, J. L., Ernst, J. D., Hallows, J., & Lee, K. Y. (2004). GTP-dependent secretion from neutrophils is regulated by Cdk5. *Journal of Biological Chemistry, 279*(52), 53932-53936. doi:10.1074/jbc.M408467200

Rosowski, E. E., Deng, Q., Keller, N. P., & Huttenlocher, A. (2016). Rac2 Functions in Both Neutrophils and Macrophages To Mediate Motility and Host Defense in Larval Zebrafish. *J Immunol*. doi:10.4049/jimmunol.1600928

Rossi, A. G., Sawatzky, D. A., Walker, A., Ward, C., Sheldrake, T. A., Riley, N. A., . . . Haslett, C. (2006a). Cyclin-dependent kinase inhibitors enhance the resolution of inflammation by promoting inflammatory cell apoptosis. *Nat Med, 12*(9), 1056-1064. doi:10.1038/nm1468

Rossi, A. G., Sawatzky, D. A., Walker, A., Ward, C., Sheldrake, T. A., Riley, N. A., . . . Haslett, C. (2006b). Cyclin-dependent kinase inhibitors enhance the resolution of inflammation by promoting inflammatory cell apoptosis. *Nat Med, 12*(9), 1056-1064. doi:10.1038/nm1468

Rossi, A. G., Sawatzky, D. A., Walker, A., Ward, C., Sheldrake, T. A., Riley, N. A., . . . Haslett, C. (2006c). Cyclin-dependent kinase inhibitors enhance the resolution of inflammation by promoting inflammatory cell apoptosis (vol 12, pg 1056, 2006). *Nat Med, 12*(12), 1434-1434. doi:Doi 10.1038/Nm1206-1434

Rupaimoole, R., & Slack, F. J. (2017). MicroRNA therapeutics: towards a new era for the management of cancer and other diseases. *Nature Reviews Drug Discovery, 16*(3), 203-221. doi:10.1038/nrd.2016246

Sadik, C. D., Kim, N. D., & Luster, A. D. (2011). Neutrophils cascading their way to inflammation. *Trends in Immunology, 32*(10), 452-460. doi:10.1016/j.it.2011.06.008

Sam, A. D., 2nd, Sharma, A. C., Law, W. R., & Ferguson, J. L. (1997). Splanchnic vascular control during sepsis and endotoxemia. *Front Biosci, 2*, e72-92. Retrieved from http://www.ncbi.nlm.nih.gov/pubmed/9307399

Scapini, P., Lapinet-Vera, J. A., Gasperini, S., Calzetti, F., Bazzoni, F., & Cassatella, M. A. (2000). The neutrophil as a cellular source of chemokines. *Immunol Rev, 177*, 195-203. Retrieved from https://www.ncbi.nlm.nih.gov/pubmed/11138776

Scapini, P., Laudanna, C., Pinardi, C., Allavena, P., Mantovani, A., Sozzani, S., & Cassatella, M. A. (2001). Neutrophils produce biologically active macrophage inflammatory protein-3alpha (MIP-3alpha)/CCL20 and MIP-3beta/CCL19. *Eur J Immunol, 31*(7), 1981-1988. doi:10.1002/1521-4141(200107)31:7<1981::AID-IMMU1981>3.0.CO;2-X

Seok, J., Warren, H. S., Cuenca, A. G., Mindrinos, M. N., Baker, H. V., Xu, W., . . . Host Response to Injury, L. S. C. R. P. (2013). Genomic responses in mouse models poorly mimic human inflammatory diseases. *Proc Natl Acad Sci U S A, 110*(9), 3507-3512. doi:10.1073/pnas.1222878110

Sepulcre, M. P., Alcaraz-Perez, F., Lopez-Munoz, A., Roca, F. J., Meseguer, J., Cayuela, M. L., & Mulero, V. (2009). Evolution of lipopolysaccharide (LPS) recognition and signaling: fish TLR4 does not recognize LPS and negatively regulates NF-kappaB activation. *J Immunol, 182*(4), 1836-1845. doi:10.4049/jimmunol.0801755

Sharifi, M., Salehi, R., Gheisari, Y., & Kazemi, M. (2014). Inhibition of microRNA miR-92a induces apoptosis and necrosis in human acute promyelocytic leukemia. *Adv Biomed Res, 3*, 61. doi:10.4103/2277-9175.125826

Shen, C., Chen, M. T., Zhang, X. H., Yin, X. L., Ning, H. M., Su, R., . . . Zhang, J. W. (2016). The PU.1-Modulated MicroRNA-22 Is a Regulator of Monocyte/Macrophage Differentiation and Acute Myeloid Leukemia. *PLoS Genet, 12*(9). doi:ARTN e1006259 10.1371/journal.pgen.1006259

Sica, A., Matsushima, K., Van Damme, J., Wang, J. M., Polentarutti, N., Dejana, E., . . . Mantovani, A. (1990). IL-1 transcriptionally activates the neutrophil chemotactic factor/IL-8 gene in endothelial cells. *Immunology, 69*(4), 548-553. Retrieved from https://www.ncbi.nlm.nih.gov/pubmed/2185985

Simopoulos, A. P. (1966). Diagnostic implications of cleft palate in the newborn. *J Am Med Womens Assoc, 21*(11), 921-923. Retrieved from http://www.ncbi.nlm.nih.gov/pubmed/4227677

Singh, N. N., & Ramji, D. P. (2008). Protein kinase CK2, an important regulator of the inflammatory response? *J Mol Med (Berl), 86*(8), 887-897. doi:10.1007/s00109-008-0352-0

Skirecki, T., Kawiak, J., Machaj, E., Pojda, Z., Wasilewska, D., Czubak, J., & Hoser, G. (2015). Early severe impairment of hematopoietic stem and progenitor cells from the bone marrow caused by CLP sepsis and endotoxemia in a humanized mice model. *Stem Cell Res Ther, 6*, 142. doi:10.1186/s13287-015-0135-9

Soehnlein, O., Steffens, S., Hidalgo, A., & Weber, C. (2017). Neutrophils as protagonists and targets in chronic inflammation. *Nature Reviews Immunology, 17*(4), 248-261. doi:10.1038/nri.2017.10

Sonego, F., Castanheira, F. V., Ferreira, R. G., Kanashiro, A., Leite, C. A., Nascimento, D. C., . . . Cunha, F. Q. (2016). Paradoxical Roles of the Neutrophil in Sepsis: Protective and Deleterious. *Front Immunol, 7*, 155. doi:10.3389/fimmu.2016.00155

Song, J., Gao, L., Yang, G., Tang, S., Xie, H., Wang, Y., . . . Fan, D. (2014). MiR-199a regulates cell proliferation and survival by targeting FZD7. *PLoS One, 9*(10), e110074. doi:10.1371/journal.pone.0110074

Sreeramkumar, V., Adrover, J. M., Ballesteros, I., Cuartero, M. I., Rossaint, J., Bilbao, I., . . . Hidalgo, A. (2014). Neutrophils scan for activated platelets to initiate inflammation. *Science, 346*(6214), 1234-1238. doi:10.1126/science.1256478

Srinivasan, S., Wang, F., Glavas, S., Ott, A., Hofmann, F., Aktories, K., . . . Bourne, H. R. (2003). Rac and Cdc42 play distinct roles in regulating PI(3,4,5)P3 and polarity during neutrophil chemotaxis. *J Cell Biol, 160*(3), 375-385. doi:10.1083/jcb.200208179

Steegmaier, M., Borges, E., Berger, J., Schwarz, H., & Vestweber, D. (1997). The E-selectin-ligand ESL-1 is located in the Golgi as well as on microvilli on the cell surface. *J Cell Sci, 110 ( Pt 6)*, 687-694. Retrieved from https://www.ncbi.nlm.nih.gov/pubmed/9099943

Stein, C., Caccamo, M., Laird, G., & Leptin, M. (2007). Conservation and divergence of gene families encoding components of innate immune response systems in zebrafish. *Genome Biol, 8*(11), R251. doi:10.1186/gb-2007-8-11-r251

Stoller, J. K. (2015). Murray & Nadel's Textbook of Respiratory Medicine, 6th Edition. *Annals of the American Thoracic Society, 12*(8), 1257-1258. doi:10.1513/AnnalsATS.201504-251OT

Sullivan, C., Charette, J., Catchen, J., Lage, C. R., Giasson, G., Postlethwait, J. H., . . . Kim, C. H. (2009). The gene history of zebrafish tlr4a and tlr4b is predictive of their divergent functions. *J Immunol, 183*(9), 5896-5908. doi:10.4049/jimmunol.0803285

Sullivan, C., & Kim, C. H. (2008). Zebrafish as a model for infectious disease and immune function. *Fish Shellfish Immunol, 25*(4), 341-350. doi:10.1016/j.fsi.2008.05.005

Surbatovic, M., Popovic, N., Vojvodic, D., Milosevic, I., Acimovic, G., Stojicic, M., . . . Radakovic, S. (2015). Cytokine profile in severe Gram-positive and Gram-negative abdominal sepsis. *Sci Rep, 5*, 11355. doi:10.1038/srep11355

Surmiak, M., Hubalewska-Mazgaj, M., Wawrzycka-Adamczyk, K., Musia, J., & Sanak, M. (2015). Neutrophil MiRNA-128-3p is Decreased During Active Phase of Granulomatosis with Polyangiitis. *Current Genomics, 16*(5), 359-365. doi:Doi 10.2174/1389202916666150707160434

Taganov, K. D., Boldin, M. P., Chang, K. J., & Baltimore, D. (2006). NF-kappa B-dependent induction of microRNA miR-146, an inhibitor targeted to signaling proteins of innate immune responses. *Proc Natl Acad Sci U S A, 103*(33), 12481-12486. doi:10.1073/pnas.0605298103

Tak, T., Tesselaar, K., Pillay, J., Borghans, J. A., & Koenderman, L. (2013). What's your age again? Determination of human neutrophil half-lives revisited. *J Leukoc Biol, 94*(4), 595-601. doi:10.1189/jlb.1112571

Takaki, K., Cosma, C. L., Troll, M. A., & Ramakrishnan, L. (2012). An in vivo platform for rapid high-throughput antitubercular drug discovery. *Cell Rep, 2*(1), 175-184. doi:10.1016/j.celrep.2012.06.008

Taniguchi, K., & Karin, M. (2018). NF-kappa B, inflammation, immunity and cancer: coming of age. *Nature Reviews Immunology, 18*(5), 309-324. doi:10.1038/nri.2017.142

Tao, B., Jin, W., Xu, J. Q., Liang, Z. Y., Yao, J. L., Zhang, Y., . . . Ke, Y. H. (2014). Myeloid-Specific Disruption of Tyrosine Phosphatase Shp2 Promotes Alternative Activation of Macrophages and Predisposes Mice to Pulmonary Fibrosis. *J Immunol, 193*(6), 2801-2811. doi:10.4049/jimmunol.1303463

Tucker, K. A., Lilly, M. B., Heck, L., & Rado, T. A. (1987). Characterization of a New Human-Diploid Myeloid-Leukemia Cell-Line (Plb-985) with Granulocytic and Monocytic Differentiating Capacity. *Blood, 70*(2), 372-378. Retrieved from <Go to ISI>://WOS:A1987J557200006

Urban, C. F., Ermert, D., Schmid, M., Abu-Abed, U., Goosmann, C., Nacken, W., . . . Zychlinsky, A. (2009). Neutrophil extracellular traps contain calprotectin, a cytosolic protein complex involved in host defense against Candida albicans. *PLoS Pathog, 5*(10), e1000639. doi:10.1371/journal.ppat.1000639

Vallieres, L., & Rivest, S. (1999). Interleukin-6 is a needed proinflammatory cytokine in the prolonged neural activity and transcriptional activation of corticotropin-releasing factor during endotoxemia. *Endocrinology, 140*(9), 3890-3903. doi:DOI 10.1210/en.140.9.3890

van Buul, J. D., Anthony, E. C., Fernandez-Borja, M., Burridge, K., & Hordijk, P. L. (2005). Proline-rich tyrosine kinase 2 (Pyk2) mediates vascular endothelial-cadherin-based cell-cell adhesion by regulating beta-catenin tyrosine phosphorylation. *J Biol Chem, 280*(22), 21129-21136. doi:10.1074/jbc.M500898200

van den Heuvel, S., & Harlow, E. (1993). Distinct roles for cyclin-dependent kinases in cell cycle control. *Science, 262*(5142), 2050-2054. Retrieved from http://www.ncbi.nlm.nih.gov/pubmed/8266103

van der Sar, A. M., Stockhammer, O. W., van der Laan, C., Spaink, H. P., Bitter, W., & Meijer, A. H. (2006). MyD88 innate immune function in a zebrafish embryo infection model. *Infect Immun, 74*(4), 2436-2441. doi:10.1128/IAI.74.4.2436-2441.2006

van der Vaart, M., Spaink, H. P., & Meijer, A. H. (2012). Pathogen recognition and activation of the innate immune response in zebrafish. *Adv Hematol, 2012*, 159807. doi:10.1155/2012/159807

van Ham, T. J., Mapes, J., Kokel, D., & Peterson, R. T. (2010). Live imaging of apoptotic cells in zebrafish. *FASEB J, 24*(11), 4336-4342. doi:10.1096/fj.10-161018

van Soest, J. J., Stockhammer, O. W., Ordas, A., Bloemberg, G. V., Spaink, H. P., & Meijer, A. H. (2011). Comparison of static immersion and intravenous injection systems for exposure of zebrafish embryos to the natural pathogen Edwardsiella tarda. *BMC Immunol, 12*, 58. doi:10.1186/1471-2172-12-58

Vidigal, J. A., & Ventura, A. (2015). The biological functions of miRNAs: lessons from in vivo studies. *Trends in Cell Biology, 25*(3), 137-147. doi:10.1016/j.tcb.2014.11.004

Vincent, P. C., Chanana, A. D., Cronkite, E. P., & Joel, D. D. (1974). The intravascular survival of neutrophils labeled in vivo. *Blood, 43*(3), 371-377. Retrieved from http://www.ncbi.nlm.nih.gov/pubmed/4590660

Walton, E. M., Cronan, M. R., Beerman, R. W., & Tobin, D. M. (2015). The Macrophage-Specific Promoter mfap4 Allows Live, Long-Term Analysis of Macrophage Behavior during Mycobacterial Infection in Zebrafish. *PLoS One, 10*(10), e0138949. doi:10.1371/journal.pone.0138949

Wang, H., Czura, C. J., & Tracey, K. J. (2004). Lipid unites disparate syndromes of sepsis. *Nat Med, 10*(2), 124-125. doi:10.1038/nm0204-124

Wang, J. (2018). Neutrophils in tissue injury and repair. *Cell Tissue Res, 371*(3), 531-539. doi:10.1007/s00441-017-2785-7

Wang, J., Mizui, M., Zeng, L. F., Bronson, R., Finnell, M., Terhorst, C., . . . Kontaridis, M. I. (2016). Inhibition of SHP2 ameliorates the pathogenesis of systemic lupus erythematosus. *J Clin Invest, 126*(6), 2077-2092. doi:10.1172/JCI87037

Wang, S. H., Zhou, J. D., He, Q. Y., Yin, Z. Q., Cao, K., & Luo, C. Q. (2014). MiR-199a inhibits the ability of proliferation and migration by regulating CD44-Ezrin signaling in cutaneous squamous cell carcinoma cells. *International Journal of Clinical and Experimental Pathology, 7*(10), 7131-7141. Retrieved from <Go to ISI>://WOS:000345135900090

Wang, S. L., Lv, J. F., & Cai, Y. H. (2016). Targeting miR-9 suppresses proliferation and induces apoptosis of HL-60 cells by PUMA upregulation in vitro. *International Journal of Clinical and Experimental Medicine, 9*(10), 19581-19587. Retrieved from <Go to ISI>://WOS:000391260400086

Wang, W., Jittikanont, S., Falk, S. A., Li, P., Feng, L. L., Gengaro, P. E., . . . Schrier, R. W. (2003). Interaction among nitric oxide, reactive oxygen species, and antioxidants during endotoxemia-related acute renal failure. *American Journal of Physiology-Renal Physiology, 284*(3), F532-F537. doi:10.1152/ajprenal.00323.2002

Wang, X., Qiu, L., Li, Z., Wang, X. Y., & Yi, H. (2018). Understanding the Multifaceted Role of Neutrophils in Cancer and Autoimmune Diseases. *Front Immunol, 9*, 2456. doi:10.3389/fimmu.2018.02456

Wang, X. S., Gong, J. N., Yu, J., Wang, F., Zhang, X. H., Yin, X. L., . . . Zhang, J. W. (2012). MicroRNA-29a and microRNA-142-3p are regulators of myeloid differentiation and acute myeloid leukemia. *Blood, 119*(21), 4992-5004. doi:10.1182/blood-2011-10-385716

Ward, J. R., Heath, P. R., Catto, J. W., Whyte, M. K., Milo, M., & Renshaw, S. A. (2011). Regulation of neutrophil senescence by microRNAs. *PLoS One, 6*(1), e15810. doi:10.1371/journal.pone.0015810

Warnatsch, A., Ioannou, M., Wang, Q., & Papayannopoulos, V. (2015). Neutrophil extracellular traps license macrophages for cytokine production in atherosclerosis. *Science, 349*(6245), 316-320. doi:10.1126/science.aaa8064

Weber, G. F., Chousterman, B. G., He, S., Fenn, A. M., Nairz, M., Anzai, A., . . . Swirski, F. K. (2016). Interleukin-3 amplifies acute inflammation and is a potential therapeutic target in sepsis. *Eur J Immunol, 46*, 83-83. Retrieved from <Go to ISI>://WOS:000383610400167

Weiss, S. J. (1989). Tissue destruction by neutrophils. *N Engl J Med, 320*(6), 365-376. doi:10.1056/NEJM198902093200606

Wen, A. Y., Sakamoto, K. M., & Miller, L. S. (2010). The role of the transcription factor CREB in immune function. *J Immunol, 185*(11), 6413-6419. doi:10.4049/jimmunol.1001829

Wewer, C., Seibt, A., Wolburg, H., Greune, L., Schmidt, M. A., Berger, J., . . . Tenenbaum, T. (2011). Transcellular migration of neutrophil granulocytes through the blood-cerebrospinal fluid barrier after infection with Streptococcus suis. *J Neuroinflammation, 8*. doi:Artn 51 10.1186/1742-2094-8-51

Williams, D. A., Tao, W., Yang, F. C., Kim, C., Gu, Y., Mansfield, P., . . . Boxer, L. (2000). Dominant negative mutation of the hematopoietic-specific Rho GTPase, Rac2, is associated with a human phagocyte immunodeficiency. *Blood, 96*(5), 1646-1654. Retrieved from <Go to ISI>://WOS:000089578300005

Williams, M. R., Azcutia, V., Newton, G., Alcaide, P., & Luscinskas, F. W. (2011a). Emerging mechanisms of neutrophil recruitment across endothelium. *Trends in Immunology, 32*(10), 461-469. doi:10.1016/j.it.2011.06.009

Williams, M. R., Azcutia, V., Newton, G., Alcaide, P., & Luscinskas, F. W. (2011b). Emerging mechanisms of neutrophil recruitment across endothelium. *Trends in Immunology, 32*(10), 461-469. doi:10.1016/j.it.2011.06.009

Winter, J., Jung, S., Keller, S., Gregory, R. I., & Diederichs, S. (2009). Many roads to maturity: microRNA biogenesis pathways and their regulation. *Nat Cell Biol, 11*(3), 228-234. doi:10.1038/ncb0309-228

Woodfin, A., Voisin, M. B., Beyrau, M., Colom, B., Caille, D., Diapouli, F. M., . . . Nourshargh, S. (2011). The junctional adhesion molecule JAM-C regulates polarized transendothelial migration of neutrophils in vivo. *Nature Immunology, 12*(8), 761-U145. doi:10.1038/ni.2062

Woodfin, A., Voisin, M. B., Imhof, B. A., Dejana, E., Engelhardt, B., & Nourshargh, S. (2009). Endothelial cell activation leads to neutrophil transmigration as supported by the sequential roles of ICAM-2, JAM-A, and PECAM-1. *Blood, 113*(24), 6246-6257. doi:10.1182/blood-2008-11-188375

Xu, J., Wang, F., Van Keymeulen, A., Herzmark, P., Straight, A., Kelly, K., . . . Bourne, H. R. (2003). Divergent signals and cytoskeletal assemblies regulate self-organizing polarity in neutrophils. *Cell, 114*(2), 201-214. doi:10.1016/s0092-8674(03)00555-5

Xu, X. M., & Zhang, H. J. (2016). miRNAs as new molecular insights into inflammatory bowel disease: crucial regulators in autoimmunity and inflammation. *World Journal of Gastroenterology, 22*(7), 2206-2218. doi:10.3748/wjg.v22.i7.2206

Yamahashi, Y., Cavnar, P. J., Hind, L. E., Berthier, E., Bennin, D. A., Beebe, D., & Huttenlocher, A. (2015). Integrin associated proteins differentially regulate neutrophil polarity and directed migration in 2D and 3D. *Biomed Microdevices, 17*(5), 100. doi:10.1007/s10544-015-9998-x

Yanai, H., Matsuda, A., An, J., Koshiba, R., Nishio, J., Negishi, H., . . . Taniguchi, T. (2013). Conditional ablation of HMGB1 in mice reveals its protective function against endotoxemia and bacterial infection. *Proc Natl Acad Sci U S A, 110*(51), 20699-20704. doi:10.1073/pnas.1320808110

Yang, L. L., Wang, G. Q., Yang, L. M., Huang, Z. B., Zhang, W. Q., & Yu, L. Z. (2014). Endotoxin molecule lipopolysaccharide-induced zebrafish inflammation model: a novel screening method for anti-inflammatory drugs *Molecules, 19*(2), 2390-2409. doi:10.3390/molecules19022390

Yang, Q., Ghose, P., & Ismail, N. (2013). Neutrophils Mediate Immunopathology and Negatively Regulate Protective Immune Responses during Fatal Bacterial Infection-Induced Toxic Shock. *Infect Immun, 81*(5), 1751-1763. doi:10.1128/Iai.01409-12

Yasui, K., & Baba, A. (2006). Therapeutic potential of superoxide dismutase (SOD) for resolution of inflammation.*Inflamm Res, 55*(9), 359-363. doi:10.1007/s00011-006-5195-y

Ye, H., Pang, L., Wu, Q., Zhu, Y., Guo, C., Deng, Y., & Zheng, X. (2015). A critical role of mir-199a in the cell biological behaviors of colorectal cancer. *Diagnostic Pathology, 10*, 65. doi:10.1186/s13000-015-0260-x

Yilmaz, Z., Eralp Inan, O., Kocaturk, M., Baykal, A. T., Hacariz, O., Hatipoglu, I., . . . Ulus, I. H. (2016). Changes in serum proteins after endotoxin administration in healthy and choline-treated calves. *BMC Vet Res, 12*, 210. doi:10.1186/s12917-016-0837-y

Yipp, B. G., Petri, B., Salina, D., Jenne, C. N., Scott, B. N., Zbytnuik, L. D., . . . Kubes, P. (2012). Infection-induced NETosis is a dynamic process involving neutrophil multitasking in vivo. *Nat Med, 18*(9), 1386-1393. doi:10.1038/nm.2847

Yokoyama, I., Gavaler, J. S., Todo, S., Miyata, T., Vanthiel, D. H., & Starzl, T. E. (1995). Endotoxemia Is Associated with Renal Dysfunction in Liver-Transplantation Recipients during the First Postoperative Week. *Hepato-Gastroenterology, 42*(3), 205-208. Retrieved from <Go to ISI>://WOS:A1995RM15800003

Yoo, S. K., Deng, Q., Cavnar, P. J., Wu, Y. I., Hahn, K. M., & Huttenlocher, A. (2010). Differential regulation of protrusion and polarity by PI3K during neutrophil motility in live zebrafish. *Dev Cell, 18*(2), 226-236. doi:10.1016/j.devcel.2009.11.015

Yoo, S. K., Deng, Q., Cavnar, P. J., Wu, Y. I., Hahn, K. M., & Huttenlocher, A. (2011). Differential Regulation of Protrusion and Polarity by PI(3)K during Neutrophil Motility in Live Zebrafish (vol 18, pg 226, 2010). *Dev Cell, 21*(2), 384-384. doi:10.1016/j.devcel.2011.08.006

Yoo, S. K., & Huttenlocher, A. (2011). Spatiotemporal photolabeling of neutrophil trafficking during inflammation in live zebrafish. *J Leukoc Biol, 89*(5), 661-667. doi:10.1189/jlb.1010567

Yoshimura, T., & Takahashi, M. (2007). IFN-gamma-mediated survival enables human neutrophils to produce MCP-1/CCL2 in response to activation by TLR ligands. *J Immunol, 179*(3), 1942-1949. Retrieved from https://www.ncbi.nlm.nih.gov/pubmed/17641061

Zang, Q. S., Martinez, B., Yao, X., Maass, D. L., Ma, L., Wolf, S. E., & Minei, J. P. (2012). Sepsis-induced cardiac mitochondrial dysfunction involves altered mitochondrial-localization of tyrosine kinase Src and tyrosine phosphatase SHP2. *PLoS One, 7*(8), e43424. doi:10.1371/journal.pone.0043424

Zarbock, A., Deem, T. L., Burcin, T. L., & Ley, K. (2007). Galphai2 is required for chemokine-induced neutrophil arrest. *Blood, 110*(10), 3773-3779. doi:10.1182/blood-2007-06-094565

Zdunek, M., Silbiger, S., Lei, J., & Neugarten, J. (2001). Protein kinase CK2 mediates TGF-beta 1-stimulated type IV collagen gene transcription and its reversal by estradiol. *Kidney Int, 60*(6), 2097-2108. doi:DOI 10.1046/j.1523-1755.2001.00041.x

Zenker, S., Panteleev-Ivlev, J., Wirtz, S., Kishimoto, T., Waldner, M. J., Ksionda, O., . . . Atreya, I. (2014). A key regulatory role for Vav1 in controlling lipopolysaccharide endotoxemia via macrophage-derived IL-6. *J Immunol, 192*(6), 2830-2836. doi:10.4049/jimmunol.1300157

Zeytun, A., Chaudhary, A., Pardington, P., Cary, R., & Gupta, G. (2010). Induction of cytokines and chemokines by Toll-like receptor signaling: strategies for control of inflammation. *Crit Rev Immunol, 30*(1), 53-67. Retrieved from https://www.ncbi.nlm.nih.gov/pubmed/20370620

Zhang, E. R., Liu, S., Wu, L. F., Altschuler, S. J., & Cobb, M. H. (2016). Chemoattractant concentration-dependent tuning of ERK signaling dynamics in migrating neutrophils. *Sci Signal, 9*(458), ra122. doi:10.1126/scisignal.aag0486

Zhang, H., Sun, C., Glogauer, M., & Bokoch, G. M. (2009). Human neutrophils coordinate chemotaxis by differential activation of Rac1 and Rac2. *J Immunol, 183*(4), 2718-2728. doi:10.4049/jimmunol.0900849

Zhang, L. X., Kendrick, C., Julich, D., & Holley, S. A. (2008). Cell cycle progression is required for zebrafish somite morphogenesis but not segmentation clock function. *Development, 135*(12), 2065-2070. doi:10.1242/dev.022673

Zhao, L., Xia, J., Li, T., Zhou, H., Ouyang, W., Hong, Z., . . . Xu, F. (2016). Shp2 Deficiency Impairs the Inflammatory Response Against Haemophilus influenzae by Regulating Macrophage Polarization. *J Infect Dis, 214*(4), 625-633. doi:10.1093/infdis/jiw205

Zhou, W., Cao, L., Jeffries, J., Zhu, X., Staiger, C. J., & Deng, Q. (2018). Neutrophil-specific knockout demonstrates a role for mitochondria in regulating neutrophil motility in zebrafish. *Dis Model Mech, 11*(3). doi:10.1242/dmm.033027

Zhou, W., Pal, A., Hsu, A. Y., Theodore Gurol, X. Z., 1 Sara E. Wirbisky-Hershberger,2, & Jennifer L. Freeman, 3 Andrea L. Kasinski,1,3 and Qing Deng1,3,4,5,*. (2018). MicroRNA-223 Suppresses the Canonical NF-kB Pathway in Basal Keratinocytes to Dampen Neutrophilic Inflammation. In.

Zhou, W. Q., Pal, A. S., Hsu, A. Y. H., Gurol, T., Zhu, X. G., Wirbisky-Hershberger, S. E., . . . Deng, Q. (2018). MicroRNA-223 Suppresses the Canonical NF-kappa B Pathway in Basal Keratinocytes to Dampen Neutrophilic Inflammation. *Cell Rep, 22*(7), 1810-1823. doi:10.1016/j.celrep.2018.01.058

# PUBLICATIONS


1. **Alan Yi-Hui Hsu**, Shang-Rung Wu, Jih-Jin Tsai, Po-Lin Chen, Ya-Ping Chen, Tsai-Yun Chen, Yu-Chih Lo, Tzu-Chuan Ho, Meed Lee, Min-Ting Chen, Yen-Chi Chiu & Guey Chuen Perng. (2015) Infectious Dengue Vesicles Derived from CD61+ Cells in Acute Patient Plasma Exhibited a Diaphanous Appearance. *Scientific Reports* 5: 17990. doi:10.1038/srep17990

2. **Alan Y. Hsu**, Decheng Wang, Theodore Gurol, Wenqing Zhou, Xiaoguang Zhu, Hsiu-Yi Lu, Qing Deng. (2017) Overexpression of microRNA-722 fine-tunes neutrophilic inflammation by inhibiting Rac2 in zebrafish. *Disease Models & Mechanisms 2017, 10(11):* 1323-1332. doi: 10.1242/dmm.030791

3. **Alan Y. Hsu**, Theodore Gurol, Tiago J. Sobreira, Sheng Zhang, Natalie Moore, Chufan Cai, Zhong-Yin Zhang and Qing Deng. (2018) Development and characterization of an endotoxemia model in zebrafish. *Front Immunol, 9*, 607. doi:10.3389/fimmu.2018.00607

4. **Alan Y. Hsu**, Sheng Liu, Kent A. Brasseale, Ramizah Sabri, Jun Wan, Qing Deng. Inducible overexpression of zebrafish microRNA-722 suppresses chemotaxis of human neutrophil like cells. *Mol Immunol, 112*, 206-214. doi:10.1016/j.molimm.2019.06.001

5. **Alan Y. Hsu**, Decheng Wang, Sheng Liu, Justice Lu, Ramizah Syahirah, David A. Bennin, Anna Huttenlocher, Jun Wan, Qing Deng. Phenotypical microRNA screen reveals a noncanonical role of CDK2 in regulating neutrophil migration. *Proc Natl Acad Sci USA, PNAS, 116(37)*, 18561-18570. doi:10.1073/pnas.1905221116

6. **Alan Y. Hsu**, Tzu-Chuan Ho, Mei-Ling Lai, Sia Seng Tan, Tsai-Yun Chen, Meed Lee, Yu-Wen Chien, Ya-Ping Chen, Guey Chuen Perng. (2019) Identification and characterization of permissive cells to dengue virus infection in human hematopoietic stem and progenitor cells. *Transfusion, 59(9),* 2938-2951. doi:10.1111/trf.15416

7. Tsai JJ, Chen PC, Liu LT, Chang K, Yao JH, Hsiao HM, Clark KB, Chen YH, **Hsu YH**, Perng GC. (2014) Pathogenic Parameters Derived from Activated Platelets in Dengue Patients. Trop Med Surg 1: 142.

8. Wenqing Zhou, Arpita S. Pal, **Alan Y. Hsu**, Theodore Gurol, Xiaoguang Zhu, Sarah E. Wirbisky, Jennifer L. Freeman, Andrea L. Kasinski, Qing Deng. (2018) MicroRNA-223 suppresses inflammation by down regulating NF-kB activation in epithelial cells. Cell Reports 22, 1810–1823

9. Jacob Jeffries, Wenqing Zhou, **Alan Y. Hsu**, and Qing Deng. (2019) miRNA-223 at the crossroads of inflammation and cancer. Cancer Letters, 451, 136-141

10. Jennifer N. Cash, Naincy R. Chandan, **Alan Y. Hsu**, Prateek V. Sharma, Qing Deng, Alan V. Smrcka, and John J.G. Tesmer. (2020) Discovery of small molecules that target the P-Rex1 PIP3-binding site and inhibit P-Rex1-dependent functions in human neutrophils. Molecular Pharmacology 2020, 97 (2) doi.org/10.1124/mol.119.117556